

Usama Al-Anbaki

Hydraulic Interaction of Soil and Nonwoven Geotextiles under
Unsaturated Conditions

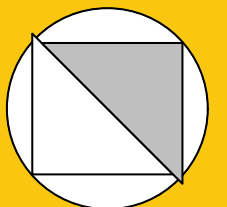
Bochum 2019

Heft 68

Schriftenreihe des Lehrstuhls für
Grundbau, Boden- und Felsmechanik

Herausgeber: Tom Schanz

ISSN 2190-3255



Ruhr-Universität Bochum

Schriftenreihe Grundbau, Boden- und Felsmechanik

Heft 68

Herausgeber:

Prof. Dr. -Ing. habil. Tom Schanz

Ruhr-Universität Bochum

Fakultät für Bau- und Umweltingenieurwissenschaften

Lehrstuhl für Grundbau, Boden- und Felsmechanik

44801 Bochum

Telefon: 0234/ 3226135

Telefax: 0234/ 3214236

Internet: www.gbf.ruhr-uni-bochum.de

ISSN 2190-3255

© 2019 der Herausgeber

Hydraulic Interaction of Soil and Nonwoven Geotextiles under Unsaturated Conditions

Dissertation

as a requirement of the degree of
Doktor-Ingenieur (Dr.-Ing.)

at the Faculty of
Civil and Environmental Engineering
Ruhr-Universität Bochum

submitted by
Usama Al-Anbaki
from Baghdad, Iraq

Reviewers
Prof. Dr.-Ing. habil. Markus Thewes
Prof. Dr.-Ing. habil. Eugen Perau
Dr. HDR Nathalie Touze

Bochum, 2019

This work is dedicated to my beloved parents Saeed and Nohida and for
my brother Samer and his lovely family

Vorwort des Herausgebers

Nichtgewebte Geotextilien werden u.a. als Teil von Drainagematten verwendet. Diese bestehen aus einem Kunststoffgerüst als Kern, welches an der Ober- und Unterseite mit den nichtgewebten Geotextilien besetzt ist. Während der Kern die eigentlich wasserleitende Funktion parallel zur Lage übernimmt, ist es die Aufgabe der Geotextilien anfallendes Sickerwasser senkrecht zur Lage passieren zu lassen, aber Bodenpartikel zurückzuhalten. Solche Drainagematten werden z.B. als Teil von Oberflächenabdichtungen von Deponien eingesetzt. Thema der vorliegenden Arbeit ist der Wasserfluss aus dem Boden in das nichtgewebte Geotextil.

Die Wasserdurchlässigkeiten von Böden und Geotextilien werden im Normalfall im gesättigten Zustand gemessen. In diesem Zustand ist die Durchlässigkeit des Geotextils deutlich größer als die der gewöhnlich als Deckschichten eingesetzten Böden. Das ändert sich, wenn der Porenraum des Bodens und des Geotextils teilweise mit Luft und teilweise mit Wasser gefüllt ist. In diesem teilgesättigten Zustand steht nur ein Teil des Porenraums für den Wasserfluss zur Verfügung und die Durchlässigkeit nimmt stark ab. Je geringer der Wassergehalt bzw. der Sättigungsgrad ist, desto geringer ist auch die Durchlässigkeit. Verknüpft mit dem Sättigungsgrad ist die Saugspannung des Bodens. Die Beziehung zwischen Sättigungsgrad und Saugspannung ist charakterisierend für einen Boden oder ein Geotextil, ebenso die Beziehung zwischen der Saugspannungen und der Durchlässigkeit. Bei geschichteten Systemen müssen die Saugspannungen an den Schichtgrenzen in beiden Materialien gleich sein. Daraus ergeben sich Sprünge im Sättigungsgrad und in der Durchlässigkeit. Da nichtgewebte Geotextilien bereits bei geringen Saugspannungen stark entwässern, kann sich die Situation ergeben, dass bei Zunahme der Saugspannung in den umgebenden Materialien die Durchlässigkeit des Geotextils unterhalb der des zu entwässernden Bodens fällt und die Drainagewirkung verloren geht. Solche Situationen wurden bereits für einzelne Kombinationen aus Geotextilien und Böden experimentell nachgewiesen.

An dieser Stelle setzt die Arbeit von Herrn Al-Anbaki an. Er untersucht dieses Phänomen erstmalig systematisch für unterschiedliche Böden, abgebildet durch Gemische aus Sand und

Kaolin mit unterschiedlichen Mischungsanteilen, und verschiedene Geotextilien. Er führt zum einen die Grundlagenuntersuchungen an den gewählten Materialien zum Zusammenhang Sättigungsgrad, Saugspannung und Durchlässigkeit aus, untersucht die hydraulische Interaktion Boden-Geotextil in Säulenversuchen und diskutiert deren Ergebnisse anhand der Ergebnisse aus den Grundlagenuntersuchungen. Zusätzlich führt er an den Bodenmaterialien Scherversuche zur teilgesättigten Scherfestigkeit aus und analysiert diese vor dem Hintergrund des Konzeptes der effektiven Spannungen. Die ausgeführten Experimente sind hoch anspruchsvoll und zeitaufwändig. Herr Al-Anbaki hat mit dieser Arbeit einen in dieser Form einmaligen sehr kompletten Datensatz zu verschiedenen Böden und Geotextilien geschaffen.

Bochum, November 2019

Diethard König

Acknowledgements

This research was carried out in the Chair of Foundation Engineering, Soil and Rock Mechanics, Ruhr-Universität Bochum. First and foremost, I would like to thank my supervisor Professor Tom Schanz who gave me a chance to start my study in RUB and provided me a lot of precious scientific support during my research work. His wisdom and personality deeply impressed me. I will be ever grateful for his support, and am sorry that he has not lived to see me graduate. His memory will be with me always.

I would like to thank Prof. Markus Thewes, Prof. Eugen Perau, Dr. Nathalie Touze, and Prof. Annette Hafner for reviewing my thesis. Their critical and constructive comments significantly improved this work.

I also would like to thank Professor Vanapallie, Professor Ning Lu, Professor Zornberg, Professor Tripathy, Professor Hettler, Professor Datcheva, Professor Aldamluji, Professor Razouki, Professor Belkhatir, and Professor Fattah for their valuable help and support during my research work. Also, I would like to thank all the Professors, doctors, and researchers who helped me with their results, publications and any scientific support.

My gratitude also is extended to my former colleagues from the Laboratory of Soil Mechanics at Ruhr-Universität Bochum including the research and laboratory staff.

My warm thanks for the laboratory staff at the company HUESKER Synthetic GmbH for thier kind help to perform specific tests at thier laborytory. My deep thanks to Dr. -Ing Oliver Detert for his support.

I would like to express my deep gratitude to the Deutsch Akademischer Austausch Dienst, DAAD (German Academic Exchange Service) for providing me the scholarship to achieve my doctoral study, your support and help were of great help to me.

I have special thanks to the Research School staff at the Ruhr-Universität Bochum. Your help, support, coaching, and assistance was really helpful.

I would like to appreciate the superb help of the library staff of the Ruhr-Universität Bochum, your extraordinary effort was of great help for me to get the literature I needed.

I acknowledge my deep thankfulness to my colleagues and friends, I am very proud and happy to work with. I appreciate your valuable help and support also the nice times we

shared together.

Last but not least, I would like to thank my family for all their love and encouragement.

For my parents who raised me with a love of science and supported me in all my pursuits.

For the endless support of my brother Samer and to his lovely family. Thank you. Köln,

November 2019

Usama Al-Anbaki

Abstract

Nonwoven geotextiles are widely used as component of drainage systems in geotechnical structures like landfills. These systems are generally located above ground water level and their hydraulic behavior is dominated by unsaturated conditions. Whereas the hydraulic conductivity of nonwoven geotextiles is a magnitude larger compared to the hydraulic conductivity of soils under saturated conditions, this relation is changing in case of unsaturated conditions. Depending on the characteristics of the geotextile and of the soil, unsaturated hydraulic conductivity of the nonwoven geotextile reaches values below the one of the soil. By this, the drainage function of the geotextile is limited.

During the last decades the behavior of soils under unsaturated conditions has been investigated. On the other side, investigations on the behavior of geotextiles under unsaturated conditions are limited. A number of references can be given to research related to the hydraulic interaction between soil and geotextile under unsaturated conditions but systematic studies taking into account different types of soils and different nonwoven geotextile products are rare.

The aim of this work is to get an insight into the complex hydraulic interaction between soil and geotextiles within drainage and infiltration processes in a system of a soil layer above a nonwoven geotextile. For this soils were selected with characteristics, which may be typical for cover soils of landfills above a drainage system, from a pure sand to sand kaolin mixtures with increasing fine content. Furthermore, a number of nonwoven geotextiles showing a bandwidth of apparent opening size has been chosen. First, the relevant properties of the materials have been determined experimentally, like grain size distribution and soil water characteristic curve (SWCC) for the soils and apparent opening size distribution (AOS) and geotextile water retention curve (GWCC) for the nonwoven geotextiles. Within this part of the work a method has been developed to derive the GWCC from the AOS and this method has been validated by the experimental results. Using existing models, the hydraulic conductivity curves for the soils and the geotextiles have been determined from the SWCC and GWCC, respectively.

Secondly, one dimensional column tests have been performed using one typical nonwoven

geotextile and four different soils with increasing fine content and due to that different SWCCs and hydraulic conductivity curves. The test results show that the hydraulic interaction and the drainage behavior are influenced by the soil type. In all cases the flow of water through the geotextile is disabled when degree of saturation of the soil above the geotextile is decreasing and the suction exceeds a certain value. The test results are analyzed and explained by the properties of the materials, which have been determined in the first part.

In addition, a separated part of the work is related to the unsaturated shear strength of the studied soils. Experimental data are compared to different theoretical approaches to describe unsaturated shear strength based on e.g. saturated shear strength and degree of saturation.

Zusammenfassung

Geotextilien, insbesondere nichtgewebte Geotextilien, werden häufig als Bestandteil von Drainagesystemen in der Geotechnik eingesetzt, so z.B. bei Deponien. Diese Systeme liegen allgemein oberhalb des Grundwasserspiegels und unterliegen teilgesättigten Verhältnissen. Während die gesättigte Durchlässigkeit des Geotextils um eine Größenordnung höher ist als die des Bodens, ändert sich dieses Verhältnis unter teilgesättigten Bedingungen. In Abhängigkeit der Eigenschaften des verwendeten Geotextils und des anstehenden Bodens kann die ungesättigte Durchlässigkeit des Geotextils Werte erreichen, die unterhalb der des Bodens liegen, wodurch die Drainagefunktion beeinträchtigt wird.

Das Verhalten von Böden bei Teilsättigung wurde in den letzten Jahrzehnten ausführlich untersucht. Dagegen liegen nur wenige Arbeiten zum Verhalten von Geotextilien unter teilgesättigten Bedingungen vor. Einzelne Arbeiten behandeln die hydraulische Interaktion zwischen Geotextil und Boden. Systematische Studien, welche die Wechselwirkung bei einer Bandbreite verschiedener Böden und Geotextilien behandeln, liegen nicht vor. Das Ziel dieser Arbeit ist es, hierzu einen Beitrag zu leisten, und einen Einblick in die komplexe hydraulische Wechselwirkung bei Drainage und Infiltrationsprozessen zwischen oberliegenden Boden und darunter befindlichem nichtgewebtem Geotextil zu erhalten.

Hierzu werden, ausgehend von reinem Sand, Mischungen aus Sand und Kaolin mit zunehmenden Feinanteil betrachtet, die Eigenschaften von Böden, welche in Deck- und Rekultivierungsschichten von Deponien verwendet werden, näherungsweise abbilden. Weiterhin werden verschiedene nichtgewebte Geotextilien mit einer Bandbreite von Öffnungsweitenverteilungen ausgewählt. An diesen Materialien werden zunächst die relevanten Eigenschaften, wie Kornverteilungen (Böden) bzw. Öffnungsweitenverteilungen (Geotextilien) und Saugspannungs-Sättigungsbeziehungen experimentell bestimmt. Dabei wird eine Vorgehensweise entwickelt und verifiziert, die Saugspannungs-Sättigungsbeziehung von Geotextilien aus der Öffnungsweitenverteilung abzuleiten. Für die Böden wie auch die Geotextilien wird die Wassergehalts-Durchlässigkeitsbeziehung unter Verwendung bekannter Modelle ermittelt.

In eindimensionalen Säulenversuchen wird das System aus Geotextil mit darüber liegen-

den Boden abgebildet und dessen hydraulisches Verhalten bei Drainage und Infiltration beobachtet. Eingesetzt werden ein typisches Geotextil und vier Böden mit unterschiedlichen Feinkornanteilen und damit abweichenden Saugspannungs-Sättigungsbeziehungen und Wassergehalts-Durchlässigkeitsbeziehungen. Die Versuchsergebnisse zeigen, dass die Eigenschaften des Bodens einen erheblichen Einfluss auf das hydraulische Verhalten des Systems haben. In allen Fällen wurde mit abnehmendem Wassergehalt des Geotextils der Abfluss des Wassers in das Geotextil behindert, welches sich anhand der zuvor ermittelten Materialeigenschaften erklären lässt.

Ein weiterer Teil der Arbeit beschäftigt sich mit der ungesättigten Scherfestigkeit der zuvor verwendeten Böden. Die experimentellen Ergebnisse dazu werden mit verschiedenen Ansätzen zur Beschreibung des Einflusses des Sättigungsgrades auf die Scherfestigkeit verglichen.

Contents

Vorwort des Herausgebers	i
Acknowledgements	iii
Abstract	v
Zusammenfassung	vii
Contents	ix
List of Figures	xvii
List of Tables	xxxii
List of symbols	xxxiii
List of abbreviations	xxxvii
1. Introduction	1
1.1. Background and motivation	1
1.2. Organization of the Dissertation	6
2. Geotextiles in landfill cover systems	9
2.1. Introduction	9
2.2. Geotextiles	10
2.3. Layout of typical capping system	12

2.4.	Filter geotextile mechanical and hydraulic stability	14
2.5.	Capillary barrier effect	15
2.6.	Case studies (Example from the field)	16
3.	Behavior of soils and geotextiles under unsaturated conditions	19
3.1.	Introduction	19
3.2.	Unsaturated soil	19
3.2.1.	Concept of suction	20
3.2.2.	Suction measurement	21
3.2.3.	Soil-water characteristics curve (SWCC)	21
3.2.4.	Hydraulic conductivity function	23
3.2.5.	Stress state variables for unsaturated soil	24
3.2.6.	Shear strength of unsaturated soil	27
3.2.7.	Experiments on the shear strength of unsaturated soil	30
3.2.8.	Suction stress	33
3.2.9.	Determination of the suction stress σ^s	36
3.3.	Unsaturated behavior of geotextiles	36
3.3.1.	Overview	36
3.3.2.	Definitions	37
3.3.3.	Capillary rise method	37
3.3.4.	Hanging column method	39
3.3.5.	Capillary pressure cell test	42
3.3.6.	Unsaturated hydraulic conductivity function of geotextile	43
3.3.7.	Laboratory measurement of 1-D flow of water through soil/geotextile interface	45
3.4.	Summary	48
4.	Materials used and experimental program	51
4.1.	General	51

- 4.2. Soils 51
 - 4.2.1. Hostun sand 51
 - 4.2.2. Silver sand 53
 - 4.2.3. Kaolin clay 54
 - 4.2.4. Hostun sand-kaolin mixtures 57
 - 4.2.5. Soil saturated permeability tests results 58
- 4.3. Nonwoven geotextiles 59
 - 4.3.1. Selected materials and basic properties 59
 - 4.3.2. Apparent opening size 61
- 4.4. Experimental program 62
- 4.5. Summary 65

- 5. Soil & geotextile water-characteristics and permeability relationships 67**
 - 5.1. Introduction 67
 - 5.2. Techniques and procedures used for SWCC/GWCC tests 68
 - 5.2.1. Overview 68
 - 5.2.2. Pressure plate apparatus following ATT 68
 - 5.2.3. Vapor equilibrium technique VET 69
 - 5.2.4. Chilled mirror hygrometer (AQUA LAB) 70
 - 5.2.5. Capillary rise method CRM 71
 - 5.2.6. Hanging column technique HCT 73
 - 5.3. Modified pressure plate (MPP) 74
 - 5.4. Performed experiments to determine soil-water characteristics curves . . . 75
 - 5.5. Experimental results of the SWCC 76
 - 5.5.1. SWCC experimental data 76
 - 5.5.2. SWCC experimental parameters 76
 - 5.5.3. SWCC fitting models 78

5.5.4.	Hydraulic conductivity function	80
5.5.5.	Influence of FC on SWCC and hydraulic conductivity function . . .	81
5.6.	Geotextile water characteristics curves	88
5.6.1.	Performance experiments to determine soil-water retention curves .	88
5.6.2.	Capillary rise tests	88
5.6.3.	Hanging column method	91
5.6.4.	GWCC for additional geotextiles products	93
5.6.5.	GWCC of geotextiles with intrusted soil	93
5.6.6.	Geotextile water characteristics curves under vertical stress	97
5.7.	Hydraulic conductivity function of unsaturated nonwoven geotextiles . . .	101
5.8.	GWCC derived from apparent opening size	101
5.9.	Summary	112
6.	Soil/geotextile column interaction	115
6.1.	Introduction	115
6.2.	Test equipment and test procedure	116
6.3.	Tensiometer Sensors	120
6.4.	Time Domain Reflectometry Sensors	121
6.5.	Testing program	121
6.6.	Tests results	122
6.6.1.	Hostun sand (without geotextile layer)	122
6.6.1.1.	Saturation stage	122
6.6.1.2.	Drainage stage	123
6.6.1.3.	Infiltration stage	127
6.6.1.4.	2nd drainage stage	129
6.6.1.5.	Main points from the test (HS)	129
6.6.2.	Hostun sand with geotextile	131
6.6.2.1.	Saturation stage	131

- 6.6.2.2. Drainage stage 132
- 6.6.2.3. Infiltration stage 134
- 6.6.2.4. 2nd drainage stage 138
- 6.6.2.5. Main points from the test (HS+G) 138
- 6.6.3. Mixture 10K 140
 - 6.6.3.1. Saturation stage 140
 - 6.6.3.2. Drainage stage 141
 - 6.6.3.3. Infiltration stage 142
 - 6.6.3.4. 2nd drainage stage 143
 - 6.6.3.5. Main points from the test (10K) 144
- 6.6.4. Mixture 15K 145
 - 6.6.4.1. Saturation stage 146
 - 6.6.4.2. Drainage stage 146
 - 6.6.4.3. Infiltration stage 147
 - 6.6.4.4. 2nd drainage stage 150
 - 6.6.4.5. Main points from the test (15K) 150
- 6.6.5. Mixture 20K 151
 - 6.6.5.1. Saturation stage 151
 - 6.6.5.2. Drainage stage 152
 - 6.6.5.3. Infiltration stage 153
 - 6.6.5.4. Main points from the test (20K) 154
- 6.7. Discussion of the column tests 156
- 7. Shear strength 167**
 - 7.1. Introduction 167
 - 7.2. Direct shear device 167
 - 7.2.1. General description 168

7.2.2.	Air pressure chamber	168
7.2.3.	Shear box	168
7.2.4.	Controlling suction	168
7.2.5.	Software and results monitoring	169
7.3.	Direct shear tests	169
7.3.1.	Validation tests	169
7.3.1.1.	Hostun sand	170
7.3.1.2.	Validation tests: Silver sand and kaolin	172
7.3.1.3.	Silver sand	172
7.3.1.4.	Silver sand-kaolin mixtures	173
7.3.2.	Partially saturated tests	176
7.3.2.1.	Hostun sand	176
7.3.2.2.	10K	177
7.3.2.3.	15K	178
7.3.2.4.	Fitting the results	179
7.4.	Discussion of shear tests results	179
7.4.1.	Hostun sand	180
7.4.2.	Sand-kaolin mixtures	183
7.5.	Suction stress	186
7.5.1.	Suction stress for Hostun sand	186
7.5.2.	10K	187
7.5.3.	15K	187
7.5.4.	Discussion of the results	189
7.6.	Summary	190
8.	Summary and Outlook	191
8.1.	Summary	191

- 8.2. Outlook 195

- A. Appendix A Measured and fitted SWCC 197**

- B. Appendix B (Direct shear tests under dry and saturated conditions) 203**

 - B.1. Hostun sand 203
 - B.1.1. Dense Hostun sand 203
 - B.2. Silver sand 204
 - B.2.1. Dense Silver sand 204
 - B.2.2. Meduim dense Silver sand 205
 - B.2.3. Loose Silver sand 205
 - B.3. 95% Silver sand + 5% kaolin clay 207
 - B.4. 93% Silver sand + 7% kaolin clay 207
 - B.5. 90% Silver sand + 10% kaolin clay 209
 - B.6. 80% Silver sand + 20% kaolin clay 209

- C. Appendix C (Direct shear tests under unsaturated saturated conditions) 211**

 - C.1. Hostun sand 211
 - C.2. 10K 215
 - C.3. 15K 219

- D. Appendix D (Fitting of direct shear tests results) 223**

 - D.1. HS 223
 - D.2. 10K 226
 - D.3. 15K 235

- Bibliography 245**

List of Figures

1.1. Schematic drawing shows the layers of a typical landfill after Bonaparte et al. (2002)	2
1.2. a) Final cover design for a landfill, b) typical seasonal moisture content fluctuations after (Zornberg & McCartney 2003; Zornberg & Christopher 2007).	3
1.3. Summery of the research activities of the current study	7
2.1. Construction of Valcros Dam downstream drain, after Giroud (2010).	11
2.2. Photographs for a) Woven structure, b) Nonwoven structure, after Ingold (1994)	11
2.3. Photographs for a) The needlepunching process, b) Typical barbed needle, after Ingold (1994).	12
2.4. Typical layers of a capping system of a landfill after Rowe (1998)	13
2.5. Slope failure for case 1, after Richardson & Zhao (2009).	17
2.6. Slope failure for case 2, after Richardson & Zhao (2009).	17
3.1. Typical SWCC after Leong & Rahardjo (1997).	23
3.2. Curves of parameter χ against degree of saturation for various soils after Jennings & Burland (1962a)	26
3.3. Relationship between the effective stress parameter χ and the suction ratio, (a) log-log scale, (b) liner scale after Khalili & Khabbaz (1998)	27
3.4. Extended Mohr-Coulomb failure envelope for unsaturated soils after Fredlund & Fredlund (2012)	29

3.5. Results of direct shear tests on sands under unsaturated condition, after Fredlund & Fredlund (2012)	31
3.6. Variation of shear strength with suction for different values of vertical stress after Escario & Juca (1989)	32
3.7. Change in angle of friction and shear strength with increasing suction after Gan et al. (1988)	32
3.8. Dimensions and directions for geotextiles after Koerner (2005)	38
3.9. Set-up of geotextile-water characteristic curve test after Krisdani et al. (2008 <i>a</i>)	39
3.10. Column drainage apparatus for geotextiles after Knight & Kotha (2001) . .	40
3.11. Schematic diagram of the inclined capillary rise technique after Handoko et al. (2012)	40
3.12. Hanging column test apparatus after Stormont et al. (1997)	42
3.13. GWCCs for polyester non-woven geotextiles with intruded soil after Stormont & Morris (2000).	42
3.14. Capillary pressure cell after Knight & Kotha (2001)	43
3.15. Relative hydraulic conductivity function for geotextiles (data from Stormont & Morris (2000) for curves No. 5 and 6; Morris (2000) for curves No. 7, 8 and 9; Lafleur et al. (2000) after Iryo & Rowe (2003) (in-plane direction) .	44
3.16. $k(\psi)$ -suction curves using the modified van Genuchten 1980 and Fredlund & Xing 1994 equations after Nahlawi et al. (2007 <i>b</i>)	45
3.17. 1-D test device & results after Bathurst et al. (2007) & Iryo & Rowe (2003)	46
3.18. 1-D test device & results after Krisdani et al. (2008 <i>a</i>)	47
4.1. Grain size distribution curves of Hostun sand and Silver sand	54
4.2. Structure of Kaolinite layer after Deer et al. (2013)	55
4.3. Unified soil classification system plasticity chart	56
4.4. Grain size distribution curves of Hostun sand and kaolin	57
4.5. Standard proctor compaction curves for soil mixtures	58
4.6. Saturated hydraulic conductivity	59

4.7. Apparent opening size curves for different nonwoven geotextiles (IRSTEA)	62
4.8. Apparent opening size curves for different nonwoven geotextiles (Huesker)	63
4.9. Grain size distribution curves for the soil mixtures within filter stability curves	63
5.1. Schematic sketch and a photograph of the pressure plate apparatus	69
5.2. Schematic sketch and a photograph of the desiccators	70
5.3. Chilled-mirror hygrometer (AQUA LAB)	71
5.4. Capillary rise test apparatus	72
5.5. Hanging column test apparatus	74
5.6. Modified pressure plate after Fredlund & Fredlund (2012)	75
5.7. ATT, Drying path	77
5.8. VET, Wetting path	77
5.9. SWCCs of the tested soils in term of mean drying (D) and mean wetting (W)	78
5.10. Idealized soil-water characteristics curve after Yang et al. (2004)	79
5.11. Relative permeability function vs suction for the soil mixtures (drying curves)	80
5.12. Relative permeability function vs suction for the soil mixtures (wetting curves)	81
5.13. Determination of the threshold value for Hostun sand-kaolin mixtures	82
5.14. SWCCs of the tested soils in term of mean drying curves	83
5.15. SWCCs of the tested soils in term of mean wetting curves	83
5.16. Inclination of the SWCC curves vs fines content	85
5.17. Saturated & 50% saturated hydraulic conductivity vs fines content	85
5.18. Inclination of the hydraulic conductivity curves vs fines content	86
5.19. Fines content vs. degree of saturation at residual suction	86
5.20. Scanning electron micrograph of discrete-particle kaolinite, scale bar = $4\mu\text{m}$ after Morris & Shepperd (1982)	87
5.21. Time-temperature curve	89

5.22. Drying curves - Capillary rise method	90
5.23. Wetting curves - Capillary rise method	90
5.24. Drying curves - Capillary rise method (repeated tests)	90
5.25. Comparison of drying curve of capillary rise method with Hanging column method	92
5.26. Comparison of wetting curve with Hanging column method	92
5.27. GWCC for 3 different geotextile samples (Terram)	94
5.28. GWCC for 2 geotextile samples (Naue)	94
5.29. GWCC for 5 geotextile samples from France	95
5.30. The grain size distribution curves for the soil mixtures and the AOS curve of the main geotextile (B)	96
5.31. GWCC for dirty geotextile samples (drying path)	96
5.32. GWCC under different vertical stresses	99
5.33. Change of height vs vertical stress for different suction values (Nonwoven geotextile)	100
5.34. stress-height curve for two geocomposite samples under saturated condition and 0.1 kPa suction	100
5.35. Hydraulic conductivity function of the main geotextile (B)	102
5.36. Hydraulic conductivity function of geotextiles	103
5.37. Relative hydraulic conductivity function of geotextiles	103
5.38. GWCC fitting for B	106
5.39. GWCC fitting for F1	107
5.40. GWCC fitting for F2	107
5.41. GWCC fitting for F3	108
5.42. GWCC fitting for F4	108
5.43. GWCC fitting for F5	109
5.44. GWCC fitting for N1	109
5.45. GWCC fitting for N2	110

5.46. GWCC fitting for T1	110
5.47. GWCC fitting for T2	111
5.48. GWCC fitting for T3	111
5.49. GWCC of geotextiles and SWCC of Hostun sand and kaolin	112
5.50. Hydraulic conductivity function of geotextiles and soils	113
6.1. Schematic sketch and a photograph of the column apparatus	118
6.2. Tensiometer Sensor, after Lins (2009)	120
6.3. Time Domain Reflectometry Sensor (TDR), after Lins (2009)	121
6.4. Saturation stage: Change of the readings vs time [HS]	123
6.5. Saturation stage: Tensiometer readings, location of the points on SWCC [HS]	123
6.6. Drainage stage: The readings of the tensiometers and TDRs [HS]	124
6.7. Drainage stage: Location of the points on the SWCC for different elevation [HS]	124
6.8. Drainage stage: Location on the points on the HC-suction function [HS] . .	125
6.9. Location of the points on the height - vol. WC relation	126
6.10. Readings of tensiometers and TDR sensors for drainage and imbibition SWCCs for column test I (loose specimen-left, dense specimen-right) after Lins (2009)	126
6.11. Infiltration stage: Readings of the tensiometers and TDRs [HS]	127
6.12. Infiltration stage: Location of the points on the SWCC for different elevation [HS]	128
6.13. Infiltration stage: Location on the points on the HC-suction function [HS] .	128
6.14. 2nd drainage stage: The readings of the tensiometers and TDRs [HS] . . .	129
6.15. Location of the points during the test stages for different elevation [HS] . .	130
6.16. Saturation stage: Tensiometer readings, location of the points on SWCC [HS+G]	131
6.17. Drainage stage: Sensors readings [HS+G]	133
6.18. Drainage stage: Sensors readings [HS+G]	133

6.19. Drainage stage: Location of the points on the SWCC [HS+G]	134
6.20. Hydraulic conductivity function of Hostun sand and geotextile and location of the points P1 and P5 at the end of the drainage stage on the function of Hostun sand [HS+G]	135
6.21. The state of the column at the end of the drainage stage	136
6.22. WC & pwp profiles from experiment & numerical simulation after Iryo & Rowe (2003)	136
6.23. Infiltration stage: The tensiometers and TDRs readings [HS+G]	137
6.24. Infiltration stage: Location of the points on the SWCC for different elevation [HS+G]	137
6.25. Infiltration stage: Hydraulic conductivity function of Hostun sand [HS+G]	138
6.26. 2nd drainage stage: The readings of the tensiometers and TDRs [HS+G]	139
6.27. Location of the points during the test stages for different elevation [HS+G]	140
6.28. Saturation stage: Readings of the tensiometers and the location of the points on the SWCC of 10K	141
6.29. Change of the reading during the drainage stage [10K]	141
6.30. Drainage stage: Location of the points on the SWCC for different elevation [10K]	142
6.31. Hydraulic conductivity function of 10K and geotextile	143
6.32. Infiltration stage [10K]	143
6.33. Infiltration stage: Location of the points on the SWCC for different elevation [10K]	144
6.34. 2nd drainage stage: The readings of the tensiometers and TDRs [10K] . . .	144
6.35. Location of the points during the test stages for different elevation [10K]	145
6.36. Saturation stage readings [15K]	146
6.37. Reading during the drainage stage [15K]	147
6.38. Drainage stage: Location of the points on the SWCC for different elevation [15K]	147
6.39. Hydraulic conductivity function of 15K and geotextile [15K]	148

6.40. The readings of the Tensiometers and TDRs during the infiltration stage [15K] 148

6.41. Location of the points on the SWCC for different elevation during the infiltration stage [15K] 149

6.42. Location of P3 and P4 on the hydraulic conductivity function of 15K at the end of the infiltration stage 149

6.43. The readings for after the infiltration stage [15K] 150

6.44. Location of the points during the test stages for different elevation [15K] . 151

6.45. Saturation stage: The pwp level and the location of the points on the SWCC [20K] 152

6.46. Drainage stage: Location of the points at different elevations [20K] 153

6.47. Drainage stage: Location of the points on the SWCC for different elevation [20K] 153

6.48. Hydraulic conductivity function of 20K and geotextile 154

6.49. Infiltration stage: The readings of the Tensiometers and TDRs [20K] . . . 154

6.50. Infiltration stage: Location of the points on SWCCs [20K] 155

6.51. Location of the points during the test stages for different elevation (20K) . 155

6.52. SWCCs of Hostun sand (test) and Silver sand (Model) 157

6.53. The PWP points during the test stages for different elevation (All tests) . . 159

6.54. Permeability function vs suction for the soil mixtures (Drying curves) . . . 160

6.55. Drainage stage: The readings of the tensiometers and TDRs (Sensors at level 1) 160

6.56. Drainage stage: The readings of the tensiometers and TDRs (Sensors at level 2) 161

6.57. Drainage stage: The readings of the tensiometers and TDRs (Sensors at level 3) 161

6.58. Drainage stage: The readings of the tensiometers and TDRs (Sensors at level 4) 162

6.59. Drainage stage: Degree of saturation and permeability versus suction, which is related to height. 162

6.60. infiltration stage: The readings of the tensiometers and TDRs (Sensors at level 1)	163
6.61. Infiltration stage: The readings of the tensiometers and TDRs (Sensors at level 2)	164
6.62. Infiltration stage: The readings of the tensiometers and TDRs (Sensors at level 3)	164
6.63. Infiltration stage: The readings of the tensiometers and TDRs (Sensors at level 4)	165
7.1. The new direct shear device	170
7.2. Dense Hostun sand (Dry) $e = 0.66$	171
7.3. Loose Hostun sand (Dry) $e=0.89$	171
7.4. Dense Silver sand	172
7.5. Meduim dense Silver sand	173
7.6. Loose Silver sand	173
7.7. Mixture 1	174
7.8. Mixture 2	174
7.9. Mixture 3	175
7.10. Mixture 4	175
7.11. Effect of suction on shear strength for Hostun sand	177
7.12. Effect of the matric suction on the maximum deviator stress after Alabdullah (2010)	177
7.13. Effect of suction on shear strength for 10K	178
7.14. Effect of suction on shear strength for 15K	178
7.15. Microscale Models-Schematic Representation: (a) Spherical Particles; (b) Forces Involved; (c) Disk Particles, after Cho & Santamarina (2001)	181
7.16. Compression and swelling index versus suction for Hostun sand after Lins (2009)	182
7.17. Effect of vertical stress on the maximum angle of dilatancy (HS)	183

7.18. Typical soil- water characteristic curve showing zones of desaturation Vana- palli & Fredlund (2000)	184
7.19. SSCC for Hostun sand	187
7.20. SSCC for 10K	188
7.21. SSCC for 15K	188
A.1. SWCC of Hostun sand	197
A.2. SWCC of 10K	198
A.3. SWCC of 15K	198
A.4. SWCC of 20K	198
A.5. SWCC of 25K	199
A.6. SWCC of 100K	199
A.7. SWCC of Silver sand based on fitting model by Fredlund (1997 <i>b</i>)	199
A.8. Hydraulic conductivity function vs suction for Hostun sand	200
A.9. Hydraulic conductivity function vs suction for 10K	200
A.10. Hydraulic conductivity function vs suction for 15K	201
A.11. Hydraulic conductivity function vs suction for 20K	201
A.12. Hydraulic conductivity function vs suction for 25K	201
A.13. Hydraulic conductivity function vs suction for 100K	202
B.1. Hostun sand: dry samples (new device)	203
B.2. Hostun sand: dry dense samples (traditional device)	204
B.3. Silver sand: dry dense samples (traditional device)	204
B.4. Silver sand: dry dense samples (new device)	205
B.5. Silver sand: dry medium dense samples (new device)	205
B.6. Silver sand: dry loose samples (traditional device)	206
B.7. Silver sand: dry loose samples (new device)	206
B.8. 95% Silver sand + 5% kaolin clay (traditional device)	207

B.9. 95% Silver sand + 5% kaolin clay (new device)	207
B.10.93% Silver sand + 7% kaolin clay (traditional device)	208
B.11.S93% Silver sand + 7% kaolin clay (new device)	208
B.12.90% Silver sand + 10% kaolin clay (traditional device)	209
B.13.90% Silver sand + 10% kaolin clay (new device)	209
B.14.80% Silver sand + 20% kaolin clay (traditional device)	210
B.15.80% Silver sand + 20% kaolin clay (new device)	210
C.1. Hostun sand: Suction = 1 kPa	211
C.2. Hostun sand: Suction = 2 kPa	212
C.3. Hostun sand: Suction = 3 kPa	212
C.4. Hostun sand: Suction = 4 kPa	212
C.5. Hostun sand: Suction = 8 kPa	213
C.6. Hostun sand: Suction = 14 kPa	213
C.7. Hostun sand: Vertical stress $\sigma'_v=60\text{kPa}$	213
C.8. Hostun sand: Vertical stress $\sigma'_v=80\text{kPa}$	214
C.9. Hostun sand: Vertical stress $\sigma'_v=120\text{kPa}$	214
C.10.Hostun sand: vertical stress $\sigma'_v=250\text{kPa}$	214
C.11.10K: Saturated samples	215
C.12.10K: Suction = 2 kPa	215
C.13.10K: Suction = 3 kPa	216
C.14.10K: Suction = 4 kPa	216
C.15.10K: Suction = 8 kPa	216
C.16.10K: Suction = 50 kPa	217
C.17.10K: Suction = 100 kPa	217
C.18.10K: Vertical stress $\sigma'_v=60\text{kPa}$	217
C.19.10K: Vertical stress $\sigma'_v=80\text{kPa}$	218

C.20. $\sigma'_v=120\text{kPa}$	218
C.21.10K: Vertical stress $\sigma'_v=250\text{kPa}$	218
C.22.15K: Saturated samples	219
C.23.15K: Suction = 2 kPa	219
C.24.15K: Suction = 3 kPa	220
C.25.15K: Suction = 4 kPa	220
C.26.15K: Suction = 8 kPa	220
C.27.15K: Suction = 50 kPa	221
C.28.15K: Suction = 100 kPa	221
C.29.15K: Vertical stress $\sigma'_v=60\text{kPa}$	221
C.30.15K: Vertical stress $\sigma'_v=80\text{kPa}$	222
C.31.15K: Vertical stress $\sigma'_v=120\text{kPa}$	222
C.32.15K: Vertical stress $\sigma'_v=250\text{kPa}$	222
D.1. Fitting the results of max. shear strength under $\sigma_v=60\text{kPa}$ for HS	223
D.2. Fitting the results of max. shear strength under $\sigma_v=80\text{kPa}$ for HS	224
D.3. Fitting the results of max. shear strength under $\sigma_v=120\text{kPa}$ for HS	224
D.4. Fitting the results of max. shear strength under $\sigma_v=250\text{kPa}$ for HS	225
D.5. Fitting the results of max. shear strength under $\sigma_v=60\text{kPa}$ for drying path (10K)	226
D.6. Fitting the results of max. shear strength under $\sigma_v=60\text{kPa}$ for wetting path (10K)	227
D.7. Fitting the results of max. shear strength under $\sigma_v=80\text{kPa}$ for drying path (10K)	227
D.8. Fitting the results of max. shear strength under $\sigma_v=80\text{kPa}$ for wetting path (10K)	228
D.9. Fitting the results of max. shear strength under $\sigma_v=120\text{kPa}$ for drying path (10K)	228

D.10.Fitting the results of max. shear strength under $\sigma_v=120\text{kPa}$ for wetting path (10K)	229
D.11.Fitting the results of max. shear strength under $\sigma_v=250\text{kPa}$ for drying path (10K)	229
D.12.Fitting the results of max. shear strength under $\sigma_v=250\text{kPa}$ for wetting path (10K)	230
D.13.Fitting the results of ϕ^b under $\sigma_v=60\text{kPa}$ for (10K)	230
D.14.Fitting the results of ϕ^b under $\sigma_v=80\text{kPa}$ for (10K)	231
D.15.Fitting the results of ϕ^b under $\sigma_v=120\text{kPa}$ for (10K)	231
D.16.Fitting the results of ϕ^b under $\sigma_v=250\text{kPa}$ for drying path (10K)	232
D.17.Fitting the results of app. cohesion strength under $\sigma_v=60\text{kPa}$ for (10K)	232
D.18.Fitting the results of app. cohesion under $\sigma_v=80\text{kPa}$ for (10K)	233
D.19.Fitting the results of app. cohesion under $\sigma_v=120\text{kPa}$ for (10K)	233
D.20.Fitting the results of app. cohesion under $\sigma_v=250\text{kPa}$ for (10K)	234
D.21.Fitting the results of max. shear strength under $\sigma_v=60\text{kPa}$ for drying path (15K)	235
D.22.Fitting the results of max. shear strength under $\sigma_v=60\text{kPa}$ for wetting path (15K)	236
D.23.Fitting the results of max. shear strength under $\sigma_v=80\text{kPa}$ for drying path (15K)	236
D.24.Fitting the results of max. shear strength under $\sigma_v=80\text{kPa}$ for wetting path (15K)	237
D.25.Fitting the results of max. shear strength under $\sigma_v=120\text{kPa}$ for drying path (15K)	237
D.26.Fitting the results of max. shear strength under $\sigma_v=120\text{kPa}$ for wetting path (15K)	238
D.27.Fitting the results of max. shear strength under $\sigma_v=250\text{kPa}$ for drying path (15K)	238
D.28.Fitting the results of max. shear strength under $\sigma_v=250\text{kPa}$ for wetting path (15K)	239

D.29.Fitting the results of ϕ^b under $\sigma_v=60\text{kPa}$ for (15K)	239
D.30.Fitting the results of ϕ^b under $\sigma_v=80\text{kPa}$ for (15K)	240
D.31.Fitting the results of ϕ^b under $\sigma_v=120\text{kPa}$ for (15K)	240
D.32.Fitting the results of ϕ^b under $\sigma_v=250\text{kPa}$ for (15K)	241
D.33.Fitting the results of app. cohesion under $\sigma_v=60\text{kPa}$ for (15K)	241
D.34.Fitting the results of app. cohesion under $\sigma_v=80\text{kPa}$ for (15K)	242
D.35.Fitting the results of app. cohesion under $\sigma_v=120\text{kPa}$ for (15K)	242
D.36.Fitting the results of app. cohesion under $\sigma_v=250\text{kPa}$ for (15K)	243

List of Tables

2.1.	The primary function for each type of geosynthetics, after Koerner (2005) .	10
3.1.	Some of the techniques introduced for measuring soil suction, modified after Toker (2007); Likos & Lu (2003); & Agus & Schanz (2005 <i>a</i>)	21
3.2.	Summery of shear tests performed under partially saturated condition . . .	34
3.3.	Summery of the empirical equation to determine the shear strength under unsaturated conditions	35
3.4.	Estimates of water entry suction heads after Stormont et al. (1997)	41
4.1.	Chemical composition of Hostun sand after Gay et al. (2003)	52
4.2.	Basic soil mechanic properties of Hostun sand (current study)	53
4.3.	Basic soil mechanic properties of Silver sand (current study)	53
4.4.	Chemical composition of Kaolin clay after (Dana & Dana 1892 and Anthony et al. 2001)	55
4.5.	Basic soil mechanic properties of the Kaolin clay (current study)	56
4.6.	Properties of the geocomposite drainage layer *	60
4.7.	Properties of the nonwoven geotextile layer specimens *	61
4.8.	Initial conditions of specimens for the tests	64
5.1.	75
5.2.	Review of the experimental parameters for the tested soils	78
5.3.	88
5.4.	Contact angles of textile fibers in water after Henry & Holtz (1998)	91

5.5. Fitting parameters of the GWCC curves for drying and wetting under vertical stresses	98
5.6. Input values to derive GWCC from AOS for each material	106
7.1.	167
7.2. Fitting parameters of model 1 and Model 2	179

List of symbols

$2s$	effective stress between two soil particles
b	fitting parameter
c	cohesion
c'	effective cohesion
C_c	coefficient of curvature
C_u	coefficient of uniformity
D_{10}	10% of the soil particles are finer than this size
D_{30}	30% of the soil particles are finer than this size
D_{50}	50% of the soil particles are finer than this size
D_{60}	60% of the soil particles are finer than this size
d_{eq}	equivalent hydraulic pore diameter
d_v	geotextile layer thickness [mm]
d_{15}	15% of the soil particles are finer than this size (filter material)
D_{15F}	D_{15} of filter material
D_{50F}	D_{50} of soil material
d_{15S}	D_{15} of filter material
d_{85S}	D_{85} of soil material
e	void ratio
(e_g)	intergranular void ratio
$(e_s)_{eq}$	equivalent void ratio
f_c	percentage by weight of the fines content
G_f	specific gravity of the fines content matrix
G_s	specific gravity of the coarse content matrix
g_t	gravitational constant [9.81 m/s ²]
h	height of the point [cm]
$k(\psi)$ or $k(\theta)$	unsaturated hydraulic conductivity
k_s	saturated hydraulic conductivity
k_n	coefficient of permeability normal to plane (geotextile)
$k_r(\psi)$ or $k_r(\theta)$	relative hydraulic conductivity
LL	Liquid limit [%]
M_A	geotextile mass per unit area [g/m ²]
MD	geotextile tensile strength [kN/m]

m	molar salt solution [mol/kg]
n	fitting parameter
O_{10}	Apparent opening size finer than 10%
O_{60}	Apparent opening size finer than 60%
O_{90}	Apparent opening size finer than 90%
O_{95}	Apparent opening size finer than 95%
p	water pressure [kN/m ²]
PI	Plasticity index [%]
PL	Plastic limit [%]
pwp	Pore-water pressure
R	radius
R	universal gas constant (i.e., 8.31432 J/mol.K)
R_1	radii of the curvature of the water bridge
R_2	radii of the curvature of the water bridge
R_{ks}	Relative hydraulic conductivity
s	matric suction
S_r	degree of saturation
s_{aev}	air entry value of the material
s_t	total suction [kPa]
T_s	surface tension of the water
T	absolute temperature in Kelvin
t	specimen thickness
u_a	pore-air pressure
u_w	pore-water pressure
V_{bridge}	volume of the water bridge

α	fitting parameter
β	half-filling angle
γ	soil density
ν	Biot's coefficient for Soil and Rock materials (also known as b and α)
κ	fitting parameter
λ	constant coefficient dependent on the criterion
μ	friction
π	osmotic suction
ρ	density of water [kN/m ³]
ρ_f	fibre density
ρ_w	density of water
σ	total stress
σ_s	effective stress
σ'	effective stress
σ^s	suction stress
τ, τ_{us}	shear stress
θ	contact angle
θ_r	volumetric water content at residual condition
θ_s	saturated volumetric water content
ϕ	osmotic coefficient
ϕ'	effective angle of friction
ϕ''	friction angle with respect to changes in suction
ϕ^a	friction angle with respect to changes in $(\sigma - u_w)$ when $(u_a - u_w)$ is held constant
ϕ^b	friction angle with respect to changes in $(u_a - u_w)$ when $(\sigma - u_w)$ is held constant
χ	effective stress parameter
ψ	suction value

List of abbreviations

<i>AEV</i>	air-entry value
<i>ASTM</i>	American Society for Testing and Materials
<i>ATT</i>	axis-translation technique
<i>DIN</i>	Deutsches Institut fuer Normung (German Institute for Standardization)
<i>EGME</i>	Ethylene Glycol Monoethyl Ether
<i>GDL</i>	Geocomposite drainage layer
<i>GWCC</i>	geotextile-water characteristic curve
<i>HC</i>	Hanging column method
<i>NCL</i>	normal consolidation line
<i>PWP</i>	Pore-water pressure
<i>SSA</i>	specific surface area [m ² /g]
<i>SP</i>	poorly graded sand
<i>SWCC</i>	soil-water characteristic curve
<i>VET</i>	vapor equilibrium technique
<i>VWC</i>	Volumetric water content
<i>USCS</i>	Unified Soil Classification System

1. Introduction

1.1. Background and motivation

In the last few decades, the use of nonwoven geotextiles [as a separate layer or as a part of the geocomposite drainage layer which is a rigid core sandwiched between two nonwoven geotextiles or any other materials (D4439-15a. 2015)] for filtration and/or drainage purposes to substitute the coarse grained soil layer became common and more attractive in several engineering applications such as paved and unpaved roads, landfill covers and liners, earth dams, embankments and retaining walls (Stormont & Morris 2000; Bouazza et al. 2006). This is due to the reduction in the cost (practically if the quantity and/or the quality of the appropriate soils are not available within acceptable distances from the location of the construction site), reduction in thickness in comparison to a thick soil layer (in case of a landfill the effective space for depositing waste may increase), the quality of industrially manufactured geocomposite drainage layer is more uniform than that of a natural soil, the possibility to produce the geosynthetic materials following certain criteria to follow the design aspects also with special shape, and geosynthetic products are easy to handle and require less effort and may also decrease the air and noise pollution also when considering the manufacturing and transportation pollution (low CO₂ emission) (Ingold 1994; Koerner 2005).

The current study focuses on the nonwoven geotextile used for drainage and filtration purposes as part of the final capping system of a landfill under partially saturated condition. However, the outcome of this study may shed the light on the performance of this material (or any possible similar material) in the other applications under partially saturated condition.

The geocomposite drainage layer consists of a geonet (core) sandwiched between two layers of nonwoven geotextiles, the upper one works for drainage, filtration, and separation while the bottom one works for separation purposes. The liquid enters through the top geotextile and travels horizontally through the space of geonet until it reaches a suitable drainage system (Figure 1.1). Such system might be used to intercept and convey leachate

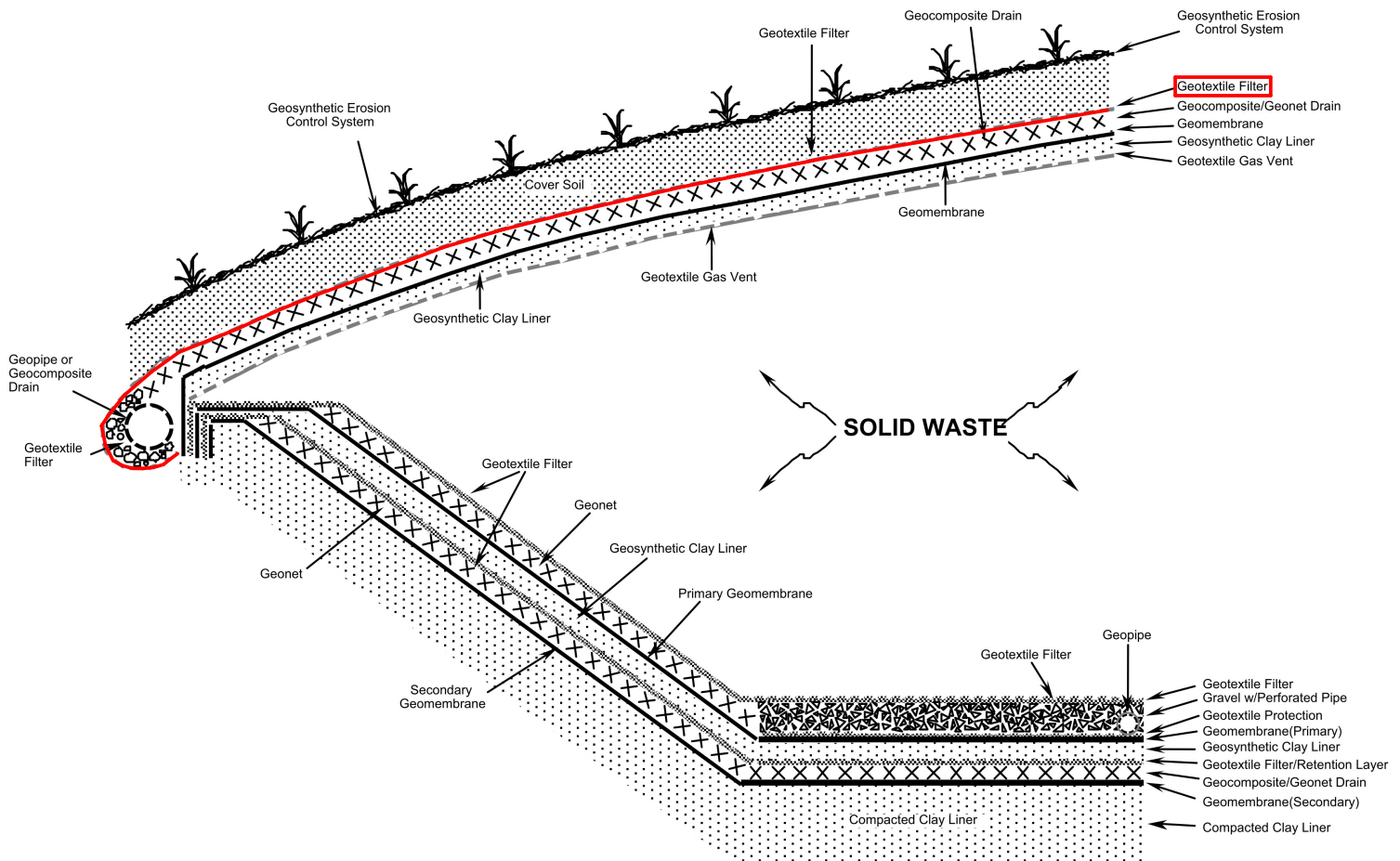


Figure 1.1.: Schematic drawing shows the layers of a typical landfill after Bonaparte et al. (2002)

in landfill liner or percolating water in landfill cover systems and to conduct vapor or water beneath pond liners of various types (Koerner 2005). The design procedures related to the flow of water through drainage system can guarantee a high drainage performance of the geotextile material by considering during the design stage that both the top soil and the geotextile are fully saturated during their lifetime. In this case the hydraulic conductivity of the geotextile is several orders higher than that for the top soil layer and thus a smooth flow of water will be insured from the top soil through the geotextile (e.g. Holtz & Berg 1997; Fannin & Palmeira 2002; Koerner 2005). However, the engineering applications in which geotextiles are commonly used are under partially saturated conditions for the majority of their design life. Figure 1.2. shows the change in the water content in a soil layer near the surface at different climatic conditions where a drainage layer could be placed beneath it. The thickness of cover soil layer in landfill capping systems is about 1 to 5 meters (Koerner 2012).

However, the waste material may contain toxicity, acidity, mobility, or volume of hazardous waste (Rushbrook & Pugh 1999; Tammemagi 1999; Shukla & Yin 2006; Hauser 2008), therefore, the regulations are insisting to place the waste materials above the water table in order to ensure there will be no contact between the water and the waste material. As a result, the landfill body and its layers should be placed above the groundwater table.

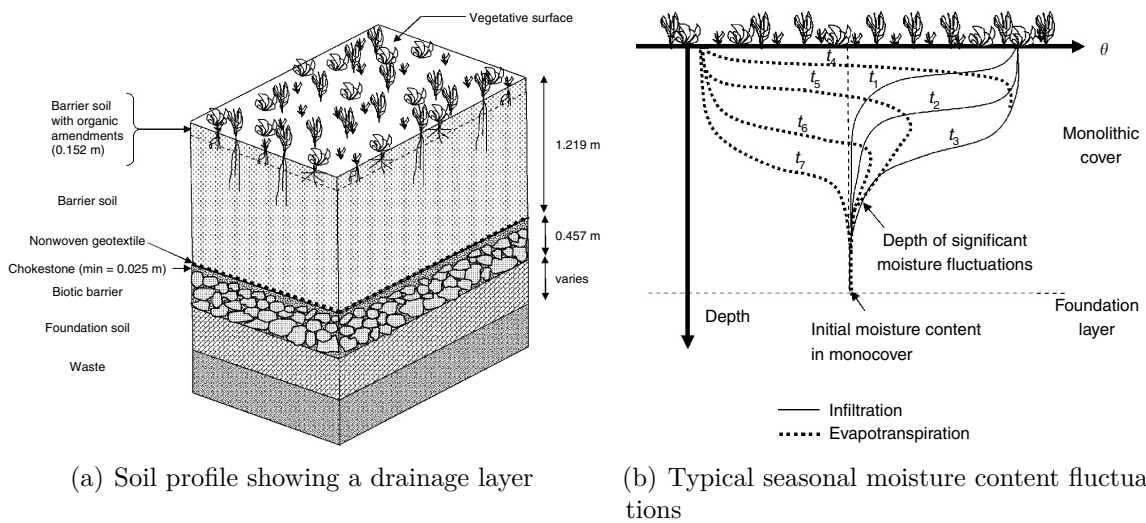


Figure 1.2.: a) Final cover design for a landfill, b) typical seasonal moisture content fluctuations after (Zornberg & McCartney 2003; Zornberg & Christopher 2007).

In that case, the pores of the soil and the geotextile will be, mostly, filled with water and air (i.e. under partially saturated conditions) and consequently a drop in the hydraulic conductivity of the soil and geotextile will occur with small increase in the suction value. The drop of that for the geotextile will be rapid and faster compared to the soil which has a relatively higher air-entry value. As a result, the product may fail to drain the water coming from the top soil layer which may lead to store the water in the soil layer and thus weakening the soil layer (due to its limited storage capacity) and causes severe problems like reduction in the shear strength of the soil and/or may reduce the shear strength at the interface between the soil and geotextile (which could be weaker than that in the soil) and as a result lowering the factor of safety and failure.

Such effect can be defined as a *capillary barrier* phenomena, which is known from two layers system where a fine to coarse sand overlies a coarse sand to fine gravel (Khire et al. 2000). Under partially saturated conditions, water flow from above into the lower layer is held within it against gravity due to capillary forces and water flow into the capillary block is prevented (Steinert et al. 1997). While there are some applications which may

benefit from the capillary barriers effect, there are also other applications in which an increase in moisture storage from a capillary barrier effect can be detrimental (Zornberg & Christopher 2007).

Such condition may urge the need to consider the partially saturated conditions parameters in order to have a better understanding to the behavior and efficiency of such systems, in which such parameters are still not widely used in the design procedures for landfills or other applications.

Besides numerous studies on the capillary barrier effect at soil-soil systems, a number of studies exists on hydraulic interaction between soil and geotextile under unsaturated conditions. These studies are showing that the relation between water content, suction and hydraulic conductivity of both soil and geotextile is dominating the hydraulic behavior of the soil geotextile system. Systematic studies on the hydraulic interaction of soil and geotextile for various type of soils with increasing fines content and various types of nonwoven geotextiles are rare.

For understanding the hydraulic interaction between soil and geotextile it is necessary to determine the relationship between water content and suction and between hydraulic conductivity and suction for both soils and geotextile. The relationship between water content and suction for soils is usually described by the soil-water characteristics curve (SWCC). Experimental procedures to measure this relationship are nowadays well established and for a wide range of soils empirical data are available (Nemes et al. 2018). The experimental determination of the relationship between suction and hydraulic conductivity is time consuming and complex equipment is needed. Due to this several approaches exist to derive this relationship from SWCC.

The experimental determination of the relationship between water content and suction for geotextiles (GWCC) are less established compared to the procedures for soils. Up to now, no approach exists to derive the GWCC from apparent opening size (AOS), which is widely used to characterize nonwoven geotextiles. Such procedure could be developed analogues to the once for soils where SWCC is derived from grain size distribution.

However, for geotextiles, the experimental determination of the relationship between hydraulic conductivity and suction is still unusual and there are rare number of studies on that topic which show that this experimental test is time consuming and error-prone. Due to these reasons, the relationship is derived from GWCC similar to soils, where the relationship between hydraulic conductivity and suction is derived from SWCC.

The type of soils which are overlying a drainage layer may vary. As example the soils used for top soil layer of landfills are varying from silty sands to silts with sand and clay fractions (Koerner 2005). Also different nonwoven geotextiles with different AOS are avail-

able. Therefore, the water content-suction relationships and hydraulic conductivity-suction relationships for a variety of soils and nonwoven geotextiles have to be investigated.

The hydraulic interaction between the soil and the geotextile can influence the water content in the cover soil layer, e.g. in case of a capillary barrier effect, and therefore the shear strength will be affected. Consequently, the influence of degree of saturation and suction on the shear strength of the investigated soils is of interest. From this following objectives of this work are defined:

1. Experimental determination of SWCC for soils with increasing fines content
2. Determination of hydraulic conductivity - suction relationship for the selected soils
3. Experimental determination of GWCC for different types of nonwoven geotextiles
4. Development of an approach to determine GWCC of nonwoven geotextile from AOS
5. Determination of hydraulic conductivity - suction relationship for nonwoven geotextiles
6. Performance and analysis of one-dimensional flow experiments on studying the hydraulic interaction of soil- geotextile and interpretation of the observations of the column tests by using the results of the studies on the material
7. Studying the effect of suction on the shear strength and on the shear strength parameters for the selected soil mixtures

In order to study these properties, the current study consists the following parts:

- **Experimental part** which is divided into four categories of tests:
 - *Soil tests (hydraulic)*: Determining the physical properties, saturated hydraulic conductivity, soil-water characteristics curve of the top soil layer SWCC. In this purpose, five types of soils: Hostun sand, kaolin clay, and three different mixtures of adding kaolin clay to Hostun sand (by weight) 10%, 15%, and 20% are investigated.
 - *Geotextile tests*: Determining the physical, mechanical and hydraulic properties of a wide range of nonwovens geotextile including the effect of suction.
 - *Soil-geotextile tests*: Evaluate the performance of one geotextile at drainage and filtration conditions by conducting column tests on one-dimensional flow of water through various types of soils overlying nonwoven geotextile

- *Shear strength*: The shear strength parameters of Hostun sand and soil mixtures 10% and 15% under saturated and unsaturated conditions are determined in direct shear tests.
- **Theoretical part** Determining the fitting parameters of the water-retention curves for soils and geotextile. Also, since the testing techniques to determine the water-retention curve for the geotextile are complicated, not popular or available in every laboratory, and also could be time consuming or require hard work to achieve accuracy (Fredlund & Fredlund 2012), an attempt is made to develop a model to determine the water-retention curve of nonwoven geotextile based on its physical properties (pore size) based on the data from the apparent opening size curve or AOS. The idea behind this model is based on the concept of determining the water retention curve of the soil based on the grain size distribution curve by Fredlund & Xing (1994). The tests results from the laboratory are compared with the developed model in order to check the accuracy. The results of the 1-D column tests are discussed taking into account the measured soil-water retention curves and geotextile-water retention curve.

Finally, for measured SWCC of the soil materials, the suction stress and by this the shear strength are derived independent of the degree of saturation using existing models. The results are compared to measured shear strength saturation relationships.

The objective of this research can be summarized by having a better understanding to the performance of the nonwoven geotextile by considering partially saturated conditions.

Figure 1.3 summarizes the research activities of the current study.

1.2. Organization of the Dissertation

This dissertation contains eight chapters. **Chapter one** presents the background, objectives and motivations, scope of the study, and the organization of the thesis. **Chapter two** defines geotextiles as special type of geosynthetics materials, describes the outline of typical landfill cover systems and the use of geotextiles within these systems, and reviews two case studies of failure at the interface between top soil layer and geotextile due to partially saturated conditions.

In **chapter three**, a literature review is given on the basics of unsaturated soil mechanics,

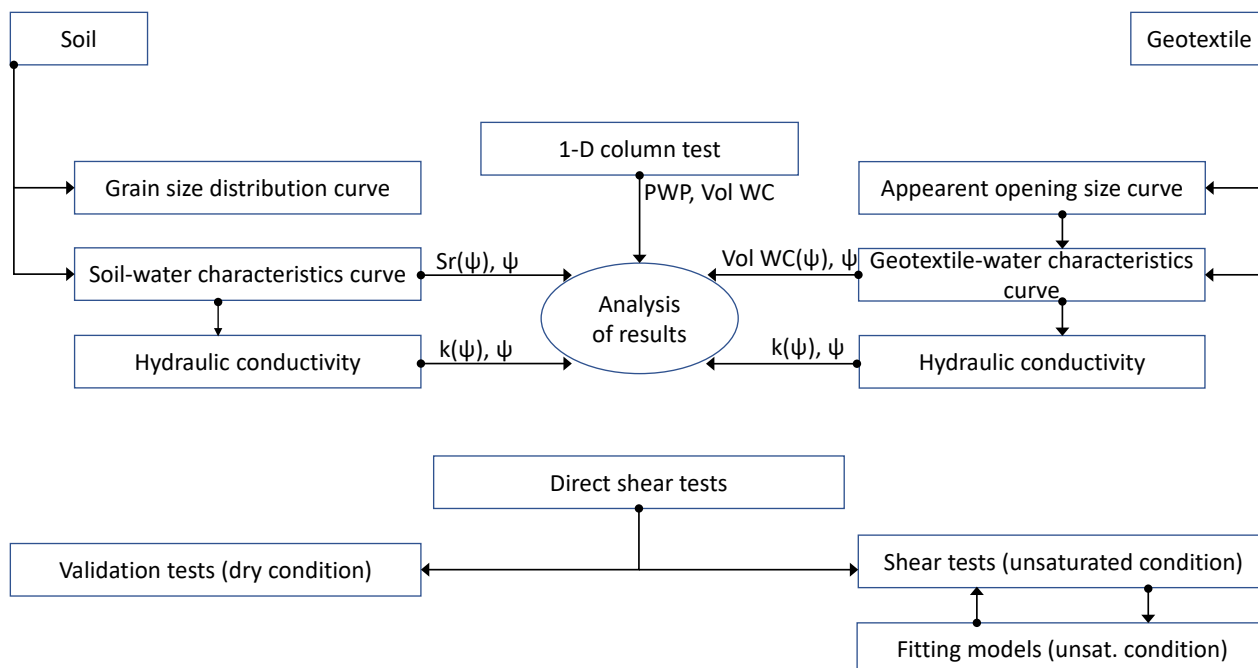


Figure 1.3.: Summary of the research activities of the current study

direct shear test results under partially saturated conditions, and the theoretical models to determine the change of shear strength with suction. Also a state of art is included on the previous studies to determine the water-retention curve of nonwoven geotextiles using different methods, and the experimental and the numerical studies on the one-dimensional flow of water through soil and geotextile.

In **chapter four**, the materials used for the experimental studies are introduced, also the initial and boundary conditions are presented. **Chapter five**, presents the experimental techniques, equipments, and the results on the selected soil and geotextile materials under partially saturated conditions such as water-retention curves and the hydraulic conductivity versus suction curves. Also the development and validation of a method to predict the GWCC from AOS is described. In **Chapter six**, a description to the column device is followed by review of the results of one-dimensional filtration test through soil and geotextile. The observations of the column tests are analyzed and explained using the results of chapter five. **Chapter seven** presents the direct shear device for partially saturated conditions and the results of the experiments which were performed on sand and soil mixtures. The shear strength and water content relationships derived from SWCC are shown and discussed together with the experimental results. Finally, **chapter eight** summarizes the main results and provides related conclusions and recommendations, and

propounds an outlook for future studies in this field.

2. Geotextiles in landfill cover systems

2.1. Introduction

In this chapter, an attempt is presented to define the geosynthetics materials with focusing on the nonwoven geotextile material used for drainage and filtration purposes, and the applications of the different products. As stated earlier in chapter 1, the drainage geotextile material is used for many applications however, in the current study there will be a focus on the function of these geotextiles under partially-saturated conditions in the landfill cover systems. Such projects are considered massive and any damage or failure could be costly and probably some environmental consequences Koerner (2012). A definition to the landfill and its cross-section is reviewed. At the end of this chapter, two case studies for failure at the interface between the top soil layer and the drainage geotextile layer occurred due to unsaturated conditions are presented.

Geotextiles are types of geosynthetics products. *Geosynthetic* is a generic term describing thin, flexible, planar products in which at least one of whose components is/are made from synthetic or natural polymer generally derived from crude petroleum oils, although rubber, fiberglass, and other materials. They are formed as a sheet, a strip or a three dimensional structure. Geosynthetics are used in contact with soil, or rock, and/or other materials in geotechnical and civil engineering applications as an integral part of a human-made project, structure, or system (Ingold 1994; Koerner 2005; Shukla & Yin (2006)).

There are, mainly, eight types of geosynthetics materials; (1) geotextiles, (2) geogrids, (3) geonets, (4) geomembranes, (5) geosynthetics clay liners, (6) geopipe, (7) geofoam, and (8) geocomposites (Koerner 2012). Table 2.1 presents the primary function of each type of the geosynthetic products (Koerner 2005). However, there are some other functions of the geosynthetics materials such as protection, absorption, cushioning, insulation, screening, surface stabilization, vegetative reinforcement Shukla & Yin (2006). In this study, a short review for geotextiles will be presented focusing on the drainage and filtration applications.

Table 2.1.: The primary function for each type of geosynthetics, after Koerner (2005)

Type of geosynthetics (GS)	Primary function				
	Separation	Reinforcement	Filtration	Drainage	Containment
Geotextile GT	✓	✓	✓	✓	-
Geogrid GG	-	✓	-	-	-
Geonet GN	-	-	-	✓	-
Geomembrane GM	-	-	-	-	✓
Geosynthetic clay liners GCL	-	-	-	-	✓
Geopipe GP	-	-	-	✓	-
Geofoam GF	✓	-	-	-	-
Geocomposite GC	✓	✓	✓	✓	✓

2.2. Geotextiles

Geotextiles are permeable geosynthetic comprised solely of textile which, when used in association with soil, rock, or any other geotechnical engineering-related material. It has the ability to separate, filter, reinforce, protect, or drain. Typically it is made from polypropylene ($\approx 85\%$), polyester ($\approx 12\%$), polyethylene ($\approx 2\%$), polyamide (nylon) ($\approx 1\%$), polyvinylidene-chloride, and fiberglass. Sewing thread for geotextiles is made from KevlarL or any of the above polymers (ASTM D4439; Koerner 2005). It has been reported that the earliest use for geotextile materials as filters had began in the 1950s behind precast concrete seawalls, under precast concrete erosion control blocks, beneath large stone riprap, and in other erosion control situations (Barrett 1966). However, Giroud was the first to use nonwoven geotextile as a filter in a dam, Valcros Dam, in France in 1970 as shown in Figure 2.1 (Giroud 2010).

Geotextiles can be classified into four main types:

- **Woven geotextile:** a geotextile produced by interlacing, usually at right angles, two or more sets of yarns (made of one or several fibers) or other elements using a conventional weaving process with a weaving loom (Figure 2.2a).
- **Nonwoven geotextile:** a geotextile produced from directionally or randomly oriented fibres into a loose web by bonding with partial melting, needle-punching, or chemical binding agents (glue, rubber, latex, cellulose derivative, etc.) (Figure 2.2b).

- **Knitted geotextile:** a geotextile produced by interlooping one or more yarns (or other elements) together with a knitting machine, instead of a weaving loom.
- **Stitched geotextile:** a geotextile in which fibres or yarns or both are interlocked/bonded by stitching or sewing.

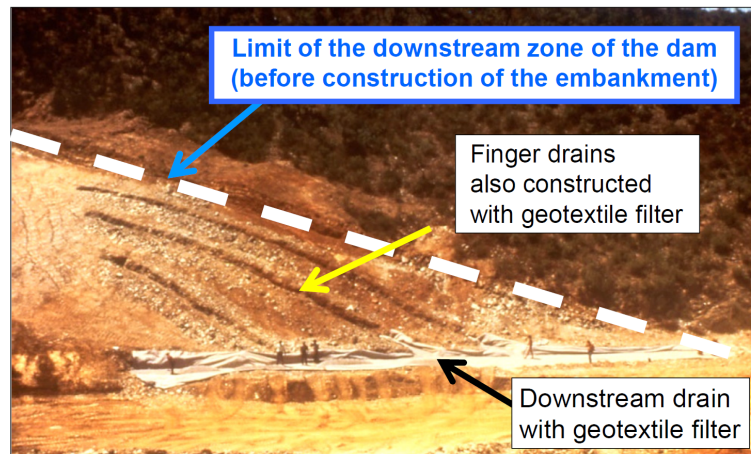
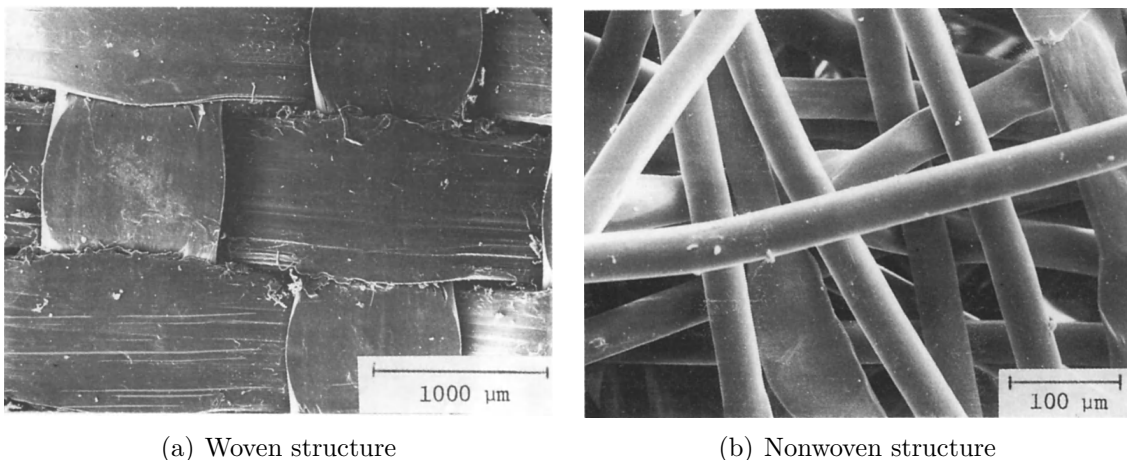


Figure 2.1.: Construction of Valcros Dam downstream drain, after Giroud (2010).

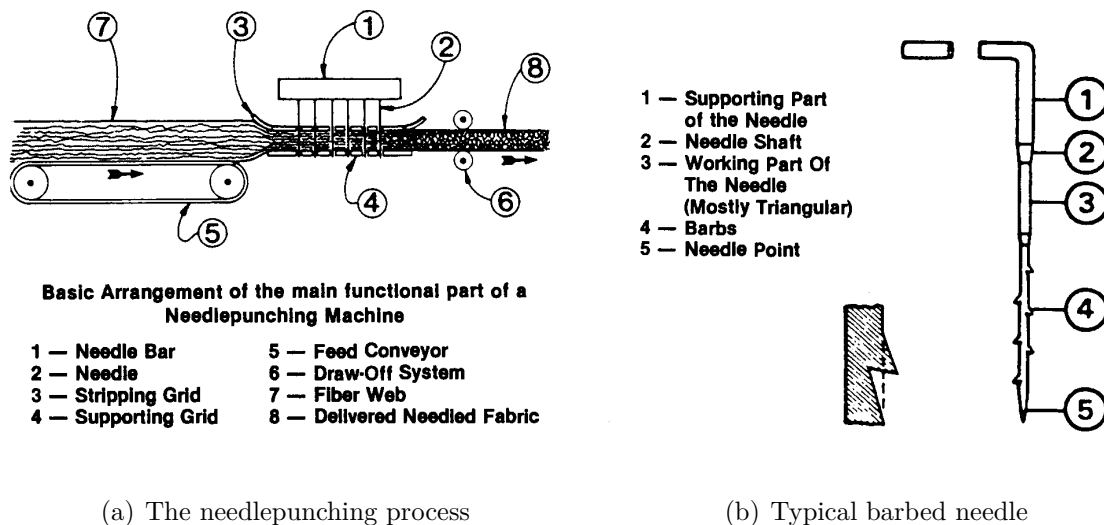


(a) Woven structure

(b) Nonwoven structure

Figure 2.2.: Photographs for a) Woven structure, b) Nonwoven structure, after Ingold (1994)

As the name implies, woven geotextiles are made by traditional methods in which two orthogonal sets of elements are woven together. In contrast nonwoven geotextiles are made from much finer elements, usually circular in cross-section, which are laid down in a loose web and then bonded, usually by heat or mechanical entanglement, to produce a coherent fabric. Figure 2.3 shows the diagrammatic representation of the production of needle-punched geotextiles.



(a) The needlepunching process

(b) Typical barbed needle

Figure 2.3.: Photographs for a) The needlepunching process, b) Typical barbed needle, after Ingold (1994).

2.3. Layout of typical capping system

There are fundamental scientific and technical aspects for placing a cover on a landfill. Regulations (e.g. in Germany DepV 2009) control the selection and design of landfill covers; however, they are based on specific environmental concerns and have a technical basis. Landfill covers provide several environmental benefits, but they have three primary goals (Hauser 2009):

- Minimize infiltration into the waste and percolation from the waste to groundwater
- Isolate the wastes from receptors and control their movement by wind and water
- Control landfill gases

The main objective of the capping system is to prevent physical contact and exposure to waste, prevent humans or animals from digging into waste, reduce (or almost eliminate) precipitation and infiltration, and reduces/prevents transport of contaminants to ground water by infiltrating water. A layout of a typical capping system of a landfill is shown in Figure 2.4.

- Cap layers: Vegetation

The purposes of this layer is to control erosion and reduce water infiltration by evapotranspiration.

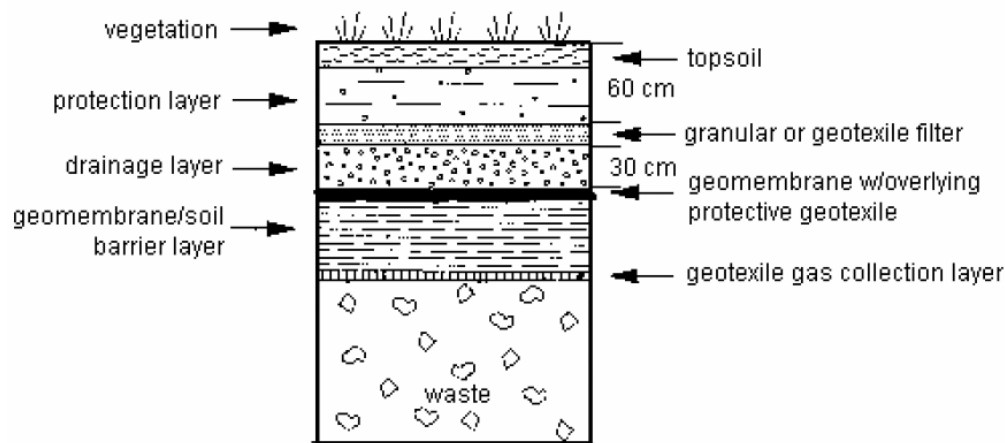


Figure 2.4.: Typical layers of a capping system of a landfill after Rowe (1998)

The characteristics of the vegetative supporting layer consists of shallow rooted plants, low nutrient needs, and drought and heat resistant.

- Cap layers: top soil layer
this layer is supporting the vegetative supporting layer, used to store the water or transfer it to the drainage layer, and protect the underlying layers.
- Cap layers: Protection layer
layer of cobbles to stop burrowing animals and deep roots (Not always included).
- Filter layer/ drainage layer
Minimizes contact between infiltrated water and low k_s -layers below, prevents ponding of water on geomembrane liner, and drains by gravity to toe.
- Cap layers: Low K layer
Composite liner: both geomembrane and low- k_s soil (clay). Low k_s prevents infiltration of water into waste: hydraulic barrier
Geomembrane: at least 0.5 mm thick
compacted clay: at least 60 cm with $k_s \leq 10^{-7}$ cm/s
- Cap layers: Gas vent layer
Needed if waste will generate methane (explosive) or toxic gas
Similar to drainage layer: 30 cm of sand or equivalent geosynthetic
Connected to horizontal venting pipes (minimal number to maintain cap integrity)

2.4. Filter geotextile mechanical and hydraulic stability

Design criteria in current engineering practice are mostly based on empirical relationships derived from tests carried out on different combinations of base and filter materials. A typical Terzaghi relationship (USACE 1953) describing effective filters made for soils, later extended by Sherard & Talbot (1984), is as follows:

$$D_{15F}/d_{85S} \leq 4 \quad (2.1)$$

,

$$D_{15F}/d_{15S} \geq 4 \quad (2.2)$$

and

$$D_{50F}/d_{85S} \leq 10 \quad (2.3)$$

where $D_{15F} = d_{15}$ of the filter; $D_{50F} = d_{50}$ of the filter; and $d_{85S} = d_{85}$ of the soil.

Equation 2.1 means that the d_{15} of the filter must be not too small to fulfill the hydraulic criterion that the permeability is high enough. Equation 2.2 means that the d_{15} of the filter must be not too large to fulfill the retention or mechanical criterion ensuring that no grains of the overlying soil entering the pores of the filter material.

The uniformity coefficient C_u is most commonly used as 2 which indicates that there is a filtering between two materials.

In case of nonwoven geotextiles there is no grain size distribution. The apparent opening size curve AOS is used to describe the pore structure of the nonwoven geotextile.

The filtration function of a geotextile consists of allowing the liquid (water) to move through it (hydraulic criteria) at the same time the geotextile must retain the soil on its upstream side (mechanical criteria). A third factor is the long-term soil-to-geotextile flow compatibility which prevent clogging the geotextile fabric during the lifetime of the system is necessary.

The permeability of a geotextile is the property to transmit or flow the water in the cross-plane of the geotextile (perpendicular to the plane of the geotextile).

The mechanical criterion is commonly expressed as (Mizkowska et al. (2017))

$$O_n \leq x \cdot D_n \quad (2.4)$$

where O_n percent opening size of geotextile (usually O_{90}) (Giroud 2010); x retention ratio parameter; D_n diameter, for which n [%] in mass of the remaining soil particles are smaller than that diameter (usually D_{85}).

The design parameters considered by different authors are variable, chiefly with regard to the indicative diameter of the base soil, the soil relative density, the geotextile opening size, and the type of the geotextile. Therefore, the use of dissimilar retention design criteria must be cautiously evaluated referring to the real in-situ design parameters.

The permeability criterion includes flow rate and pore pressure requirements. The flow rate requirement consists of comparing the flow rate in a two-layered filter soil filtering system and flow rate in the same soil layer without a filter. The pore pressure requirement means that the presence of the geotextile filter should not increase the pore water pressure in the soil in comparison to the case performed without a filter. Furthermore, the permeability criterion takes into account the blinding and clogging limit states.

The permeability criterion is commonly expressed as Giroud (2010) and Miskowska et al. (2017)

$$k_n = \lambda \cdot k_s \quad (2.5)$$

where k_n coefficient of permeability normal to the plane of geotextile (cross-plane); λ constant coefficient (usually 10-100); k_s coefficient of soil permeability; k_n coefficient of geotextile permeability.

2.5. Capillary barrier effect

Capillary barrier is based on the a principle in which two soil layers, high permeable in a water-saturated state, juxtaposed (side to side) in the order by capillary layer (fine to coarse sand) overlies a capillary block (coarse sand to gravel). Under partially saturated conditions, water flowing from above into the capillary layer is held within it against gravity due to capillary forces and prevented from flowing into the capillary block (Steinert et al. 1997; Khire et al. 2000).

Nonwoven geotextile underlying a soil layer can also act as capillary block (Lima et al. 2016).

It is necessary to distinguish from those applications which the capillary break condition is an aim to block the water to move from conductive porous layer to a higher conductivity layer due to the action of the capillary forces e.g. the capillary barrier.

2.6. Case studies (Example from the field)

The use of geotextiles for drainage purposes in several projects to replace the use of soils specially when the suitable soil for the application can be found faraway from the site and transport and preparation of the soil is too expensive. The use of the geotextile as drainage material has been examined in the laboratory by several researchers, Tan et al. (2001) performed a two-dimensional flow of water test using a horizontal nonwoven geotextile beneath a residual soil. The results showed that the geotextile was effective as a drainage material to relieve excess pore pressure caused by loading at the soil surface. Giroud (1983) concluded that the use of geotextiles was accepted to drain the water from saturated soil during consolidation.

However, there have been several cover soil stability problems reported in the literature, varying from being relatively small (which can be easily repaired), to very large (involving litigation and financial judgments against the parties involved), Koerner & Soong (1998). The sliding of relatively thin cover soil layers (called veneer above both geosynthetic and natural soil liners, i.e., geomembranes (GM), geosynthetic clay liners (GCL)) and compacted clay liners (CCL) are the particular materials of concern.

Dierickx (1996) observed after a heavy rainfall, water ponded to a depth of 0.1 m above a geotextile used at a sports ground and showed that an excess of 10 mm of pressure head was required to cause water percolation across several geotextiles. Richardson (1997); Richardson & Zhao (2009) reported a slide failure in the sealing cover system of a landfill due to capillary block developed over the geotextile beneath the top soil layer (case study 1). This failure occurred on a relatively gentle slope ($\beta = 8.5^\circ$) as shown in Figure D.16. The vegetative supporting soil was washed to slope base. Investigation to the failed cover indicated that the soil was saturated (15 cm top soil, 45 cm silty sands). Thus the flow of water into the geocomposite was not continuous.

Richardson & Zhao (2009) described a massive sliding of cover soils occurring after a major storm dropped 120 mm of rain on an East Coast municipal solid waste landfill cap construction project (case study 2). The rainfall occurred within a span of 5 to 6 hours and damaged approximately 14 hectares of cover. Figure 2.6a shows massive cover soil loss along the slope, and Figure 2.6b demonstrates landfill gas pressure built-up under the geomembrane.

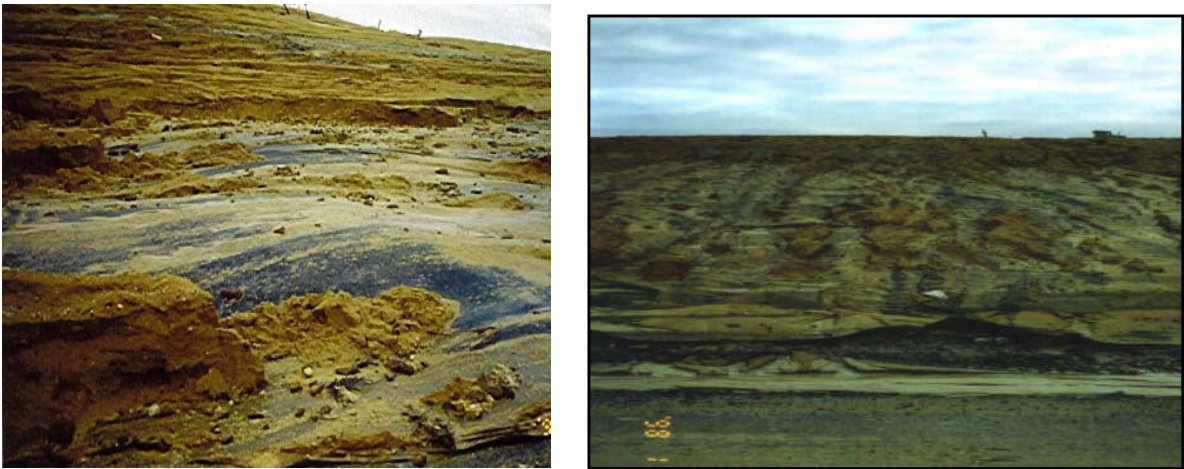
Field observations and laboratory testing indicated that the in-place soil was saturated. This soil was composed of fine sugar sand containing a high percentage of silt fines. The Unified Classification for this soil is SP-SM. The soil was to function as a vegetative support layer immediately above the final cover geomembrane and drainage geocomposite.



(a) Cracks widening between sliding blocks (b) Vegetative support soils washed to slope base

Figure 2.5.: Slope failure for case 1, after Richardson & Zhao (2009).

The vegetative support layer was to be covered with 150 mm of topsoil supporting grass. Failure occurred before the topsoil layer and associated grass could be placed. This failure



(a) LFG buildup under the geomembrane (b) Massive Soils Loss on Slopes

Figure 2.6.: Slope failure for case 2, after Richardson & Zhao (2009).

showed similar characteristics like the one described in case study 1 and might be also initiated by a capillary block phenomena restraining the flow of water into the drainage geocomposite.

However, the links between soil-geotextile interaction at unsaturated conditions (capillary block), increasing water content in the soil above the drainage layer and slope failure by increasing seepage force or decreasing shear strength was not discovered, finally.

3. Behavior of soils and geotextiles under unsaturated conditions

3.1. Introduction

This chapter provides a review of the concept of soil suction, summary of the different methods to determine the soil-water retention curve, the effective stress and shear strength of soil under partially saturated condition, direct shear equipments and state of arts of the published results, and the theoretical approaches to determine the shear strength of the soil under unsaturated condition. This review will be useful to explain and discuss the results of the shear tests under partially saturated conditions.

Also, this chapter summarizes the different methods and techniques to determine the water-retention curve of nonwoven geotextiles. A review of the tests results for one-dimensional flow of water through a column of soil and geotextile with different flow conditions is presented.

Finally, the existing investigations on hydraulic interaction between soil and nonwoven geotextile are discussed, and limitations are identified.

3.2. Unsaturated soil

The soil near the ground surface, especially in the arid or semi-arid regions which has deep ground water table or which receives precipitation below potential evapotranspiration, is comprised of notoriously hazardous geomaterials called *unsaturated soils* (Fredlund & Rahardjo 1993; & Fredlund & Fredlund 2012). Compacting, excavating, and remoulding soil processes used in several engineering constructions, such as earth dams, highways, embankments, and airport runways, result in unsaturated soils. These soils are hazard to slopes, earth structures and earth-supported structures because on wetting by rain or any other means, they can expand or collapse; on drying by evaporation or by any other

means, they can desiccate and crack with serious consequences for safety and high costs (Ng & Chen 2008).

A partially saturated soil, unlike saturated soils, has more than two phases; solid skeleton, pore-water, and pore-air, however, more correct to recognize the existence of a fourth phase, namely, the air-water interface or the contractile skin because this interface affects volume change and shear strength (Fredlund & Morgenstern 1977). It can be described as a thin membrane interwoven throughout the voids of the soil, forming a partition between the air and water phases. However, as this interface is directly linked to the air, water, and solid phases, unsaturated soil is simplified as a three-phase system. The pore-water pressure is negative due to the pore-air pressure (Fredlund & Fredlund 2012).

3.2.1. Concept of suction

The concept of suction was developed by several researches (e.g., Buckingham 1907; Edlefsen & Anderson 1943; Bolt & Miller 1958; & Aitchison 1965). Soil suction, generally, consists, primarily, of two components: matric component and osmotic component (Fredlund & Rahardjo 1993). The sum of these two components (i.e., matric suction, s , and osmotic suction, π) is called the total suction s_t ,

$$s_t = s + \pi \quad (3.1)$$

The matric component is related to the difference between pore-air pressure u_a and pore-water pressure u_w in the soil (the air-water interface or surface tension) giving rise to the capillary phenomenon. The matric component of soil suction comes from the hydration forces and capillary component effects (Pusch & Yong 2003; Arifin 2008 & Arifin & Schanz 2009). Therefore the matric suction is the sum of the hydration forces and the capillary forces. The osmotic suction component is related to the dissolved salts and other solutes in bulk water which is defined as the *free water* (Fredlund & Fredlund 2012).

Many of the engineering problems involving unsaturated soils are a result of changes in the surrounding environment. For example, a slope may become unstable due to the reduction of matric suction caused by an increase in pore-water pressure from water infiltrating into the soil (Nelson & Miller 1992; & Rowe 2000).

3.2.2. Suction measurement

Soil suction is measured by direct and indirect methods. Different tension measurement devices are cataloged frequently in the literature (Fredlund & Rahardjo 1993; Fredlund & Fredlund 2012; Lee & Wray 1995; Ridley & Wray 1996; Toker 2002; Toker 2002; Toker et al. 2004; Vanapalli 2008, Murray 2010, Toker 2002; Baille 2014) as presented in Table 3.1. Among the variety of the available techniques, only tensiometers can measure the suction directly. All other techniques measure other parameters, which indirectly correspond to a suction value through predetermined calibrations (Toker 2007).

Table 3.1.: Some of the techniques introduced for measuring soil suction, modified after Toker (2007); Likos & Lu (2003); & Agus & Schanz (2005*a*)

Technique (Reference)	Suction type	Parameter measured	Suction range [kPa]
Axis Translation Technique (Southworth 1980)	Matric	u_a & u_w are controlled	0-1500
Porous Plate (D2325-68)	Matric	u_a & u_w are controlled	10-100
Pressure Membrane (D3152-72)	Matric	u_a & u_w are controlled	0-1500
Filter Paper (D5298-94)	Matric	contacting paper water content	30-100000
Filter Paper (D5298-94)	Total	nearby paper water content	400-100000
Time Domain Reflectometry (Conciani et al. 1996)	Matric	dielectric constant of device	entire range
Tensiometer (Agus & Schanz 2005 <i>a</i>)	Matric	water tension	0-100
Tensiometer (by IC, MIT, Sasktch.)	Matric	water tension	0-1500
Centrifuge (D425-88)	Matric	capillarity	0-3000
Psychrometers (Fredlund & Fredlund 2012)	Total	temperature at evaporation	100-8000
Humidity Chamber (Fredlund & Fredlund 2012)	Total	relative humidity of air	100-1000000
Gypsum Porous Block (Toker 2007)	Matric	electrical conductivity of device	10-3000
Heat Dissipation Sensor (Matile et al. 2013)	Matric	thermal conductivity of device	0-700
Osmotic technique (Fredlund & Fredlund 2012)	Matric	thermal conductivity of device	30-1500
Hanging column method (Vanapalli 2008)	Matric	u_a & u_w are controlled	0-30
Vacuum control technique (Vanapalli 2008)	Matric	u_a & u_w are controlled	0-40
high-suction tensiometer (Tarantino et al. 2008)	Matric	water tension	up to 1100

3.2.3. Soil-water characteristics curve (SWCC)

The relationship between the amount of the water or moist between the soil grains and the associated suction in the pore water could be described by the Soil-Water Characteristic Curve (SWCC). This curve or relationship represents the ability of soil to retain (hold) water at different suctions.

The amount of the retained water or moist can be expressed by any of the parameters showing the wetness of soil (i.e. degree of saturation, volumetric water content, or gravimetric water content). The corresponding suction (negative pore-water pressure) can be expressed as stress or height.

SWCC is one of the most useful characteristics in the unsaturated soil mechanics and

related to many geotechnical and hydro-mechanical properties of a soil such as hydraulic conductivity, effective stress, and volume change Fredlund & Fredlund 2012.

A typical SWCC of a non-expansive soil is drawn in Figure 3.1 which represents the relationship between degree of saturation and suction (Leong & Rahardjo 1997). SWCC shows different paths for imbibition (absorption) and drainage conditions. If a specimen of saturated soil undergoes suctions, increasing a little at a time, starting from a very low suction, it loses its water content and follows the drainage path which is also called desorption or the drying path. The increase in suction starting from the saturated condition can be performed under zero net applied stress (unconfined) or under any specific net stress (isotropic or one-dimensional compression). The reverse (i.e. wetting path) is the process where the water content of soil increases with a decrease in suction. If an oven-dried specimen experiences suctions decreasing stepwise starting from very high suction, the soil starts absorbing water.

Usually the drying path ends in the oven-dried condition (105 °C). The suction corresponding to the oven-dried condition is about 1000 MPa as found by Croney & Coleman 1961. Fredlund & Rahardjo (1993) also found from the gravimetric water content versus suction relationship for various sand and clay soils that at zero water content the suction approaches a value of approximately 980 MPa. This value is also supported by thermodynamic considerations Richards 1966.

The SWCC is influenced by type, texture, and mineralogy of soil. The behavior of fine grained soils can be indicated by the consistency or Atterberg limits Sridharan & Nagaraj 1999.

In order to determine the SWCC, the amount of water in the soil specimen with respect to the applied suction is required. Several testing procedures with different types of equipment have been established to apply a certain suction to a soil specimen and by measuring the water content related to the applied suction to determine the SWCC. The most common laboratory technique is the axis translation technique (ATT), which utilizes high-air-entry ceramic disks in a pressure plate device. This method can cover matric suctions reaching 1500 kPa. However, when a higher range of suction is required, a controlled relative humidity environment (i.e. vapour equilibrium technique, VET) is used to apply total suction. This technique provides a total suction up to more than 250,000 kPa depending on the type and concentration of salt used (Agus 2005; Lins 2009; Al-Badran 2011; Fredlund & Fredlund 2012).

The SWCC consist of two main paths (i.e. the drying path and the wetting path). To determine the drying path, the applied suction is increased incrementally for an initially fully saturated prepared soil specimen under zero net vertical stress (i.e. unconfined,

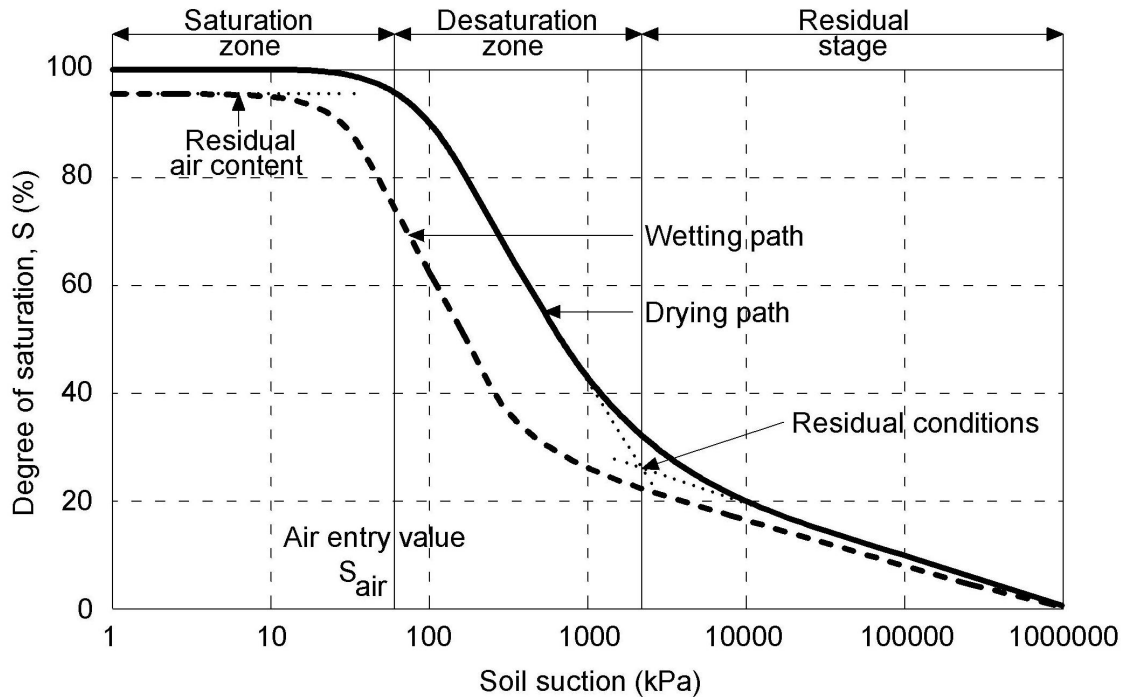


Figure 3.1.: Typical SWCC after Leong & Rahardjo (1997).

such as using the pressure plate apparatus), or under any specific net vertical stress (i.e. isotropic, or one-dimensional compression, such as using a Oedometer-suction controlled cell). The volume and the amount of water in the saturated specimen are slightly decreased as the suction increases until the air-entry value suction is reached AEV (i.e. the saturation zone). With further increase in the suction, the volume and the amount of water significantly decrease along a drying path (i.e. transition zone) until the residual suction RES is reached. After that, the increase in applied suction cause insignificant no change in the volume or amount of water of the soil specimen (i.e. the residual zone).

3.2.4. Hydraulic conductivity function

The unsaturated hydraulic conductivity describes the ability of the fluid to flow through the partially saturated soil pores under a specified hydraulic gradient and is essential for dealing with pollutant transport or the modeling of flow through earth structures. Whereas the saturated hydraulic conductivity of granular materials is a function of void ratio and the type of pore fluid, the unsaturated hydraulic conductivity is also a function of water content or degree of saturation, volumetric water content or suction Leong &

Rahardjo (1997). The shape of the hydraulic conductivity function is influenced by the void ratio, the amount of fluid (e.g. water content) and the type of fluid (e.g. viscosity) in the pores.

The magnitude of the conductivity for different soil types also vary from high values as for gravel and very low values as for clay. The suction-water content drainage path of the SWCC, that is directly related to the unsaturated hydraulic conductivity, the unsaturated hydraulic conductivity function and the relative conductivity function are characteristic for each type of soil at a given state (e.g. density). The relative conductivity function relates the relative conductivity to the effective degree of saturation.

In saturated soil, the permeability coefficient of soil specimens can be determined by direct experimental measurements (i.e. the constant head test or the falling head test) using Darcy's law to analyze the flow through the soil media as follows:

$$k_s = \frac{q}{iA} \quad (3.2)$$

where: k_s = the permeability coefficient for saturated soil, q the flow rate, A the cross-sectional area of the specimen normal to the direction of flow, and i the hydraulic gradient. In unsaturated soil, determining the permeability coefficient is difficult and time consuming. Brooks & Corey 1964; van Genuchten 1980; Fredlund & Xing 1994; Leong & Rahardjo 1997 proposed statistical models for geotechnical engineering applications.

Fredlund & Xing (1994) presented the following relative conductivity function for unsaturated soils using the soil water characteristic curve:

$$k_r(\theta) = \frac{\int_{\ln(\psi)}^b \frac{\theta(e^y) - \theta(\psi)}{e^y} \cdot \theta'(e^y) \cdot dy}{\int_{\ln(\psi_{AEV})}^b \frac{\theta(e^y) - \theta(s)}{e^y} \cdot \theta'(e^y) \cdot dy} \quad (3.3)$$

where: b is equal to $\ln(1,000,000)$, y presents the logarithm of suction, θ' is the time derivative of Equation (3.3) and e is the base of the natural logarithm. This equation requires the functional relation between suction and water content using Fredlund & Xing (1994) model.

3.2.5. Stress state variables for unsaturated soil

The mechanical behavior of soils (i.e., the volume change and shear strength behavior) can be described in terms of state of stresses in the soil. They are called *stress state variables* and they are independent of the physical and chemical properties of the soil. The number of stress state variables needed to fully describe the state of the soil depends on

the number of phases involved (Coussy 1995).

For saturated porous media, one stress state variable represented by the *effective stress*, σ' is very neat to fully describe the mechanical behavior. The stress variable then can be defined as (Biot 1941; Terzaghi 1943):

$$\sigma' = \sigma - \nu \cdot u_w \quad (3.4)$$

where σ' is the effective stress, σ is the total stress, u_w is the pore-water pressure, and ν is Biot's coefficient for soil and rock materials which is the fraction of the pore-water pressure that gives the effective stress, (also known as b and α). Several expression are proposed to determine ν . For incompressible fluid and solid particles, ν becomes equal to 1, thus the effective stress equation return to the equation defined by Terzaghi (1943):

$$\sigma' = \sigma - u_w \quad (3.5)$$

Terzaghi suggested that $\nu = 1$. For real soils, Biot coefficient is close to unity, ranging from ≈ 0.998 for dense sand to 0.999 for normally consolidated clay NC-clay (Mitchell 1993). As a conclusion, Terzaghi's assumption provides an excellent approximation to the effective stress.

One of the early attempts to study unsaturated soils was made by Croney et al. (1958), Bishop (1959), Aitchison (1960), and Bishop & Blight (1963) which modified the Terzaghi's principle of effective stresses for saturated soils to unsaturated soils for two-phase nature of the pore fluid in the unsaturated soil:

$$\sigma' = (\sigma - u_a) + \chi(u_a - u_w) \quad (3.6)$$

where u_a is the pore air pressure, $(\sigma - u_a)$ is the net normal stress, and χ is effective stress parameter, equals to 1 for saturated soil, and 0 for dry soil.

Due to difficulties to find a single effective stress equation, illustrated in the works of (Aitchison & Donald 1956; Bishop & Donald 1961; Jennings & Burland 1962*b*; Bishop & Blight 1963; Burland 1965), progressively led to the acceptance of the two independent stress state variables fields as a necessary framework to describe the observed features of unsaturated soil behavior under paths involving the variation of total stress and pore-water pressure deficiency (or suction).

Thus $(u_a - u_w)$ was introduced as an additional stress variable. Experimental evidence showed that a change in the value of $(u_a - u_w)$ does not coincide directly to a change in neutral stress (pore-water pressure), as defined by Terzaghi, since the term represents a

pressure difference due to surface tension acting in general over only a part of the surface area of the soil particles. Furthermore the presence of large surface tension forces within the soil leads to differences in soil structure in specimens following an apparently similar effective stress path.

Many attempts have been made to determine the effective stress parameter χ . Some studies relate it to the degree of saturation S_r (Aitchison & Donald 1956; Aitchison 1960; Bishop 1959; Bishop & Donald 1961; Jennings & Burland 1962*b*; Croney & Coleman 1961; Bishop & Blight 1963; and Burland 1965).

Jennings & Burland (1962*b*) used the same equation of Bishop 1959 to determine the parameter χ which is equal to the ratio of net normal stress to the effective stress on the normal consolidation line (NCL), at the same void ratio of unsaturated condition, as shown in Figure (3.2).

Khalili & Khabbaz (1998) presented a relationship between the effective stress parameter χ and the suction ratio $(u_a - u_w)/(u_a - u_w)_b$, Figure (3.3). The term $(u_a - u_w)_b$ represents the air-entry value of soil, s_{aev} . They showed that the effective stress parameter χ can be calculated as $[(u_a - u_w)/(u_a - u_w)_b]^{\kappa}$ and the best-fit value of the exponent $\kappa = -0.55$ is appropriate to represent the behavior of different soil types. The parameter χ can therefore be considered as a material-independent constant. The air-entry value, s_{aev} depends on the soil type and on the void ratio, though in the original formulation it was considered, for simplicity, as void ratio independent constant.

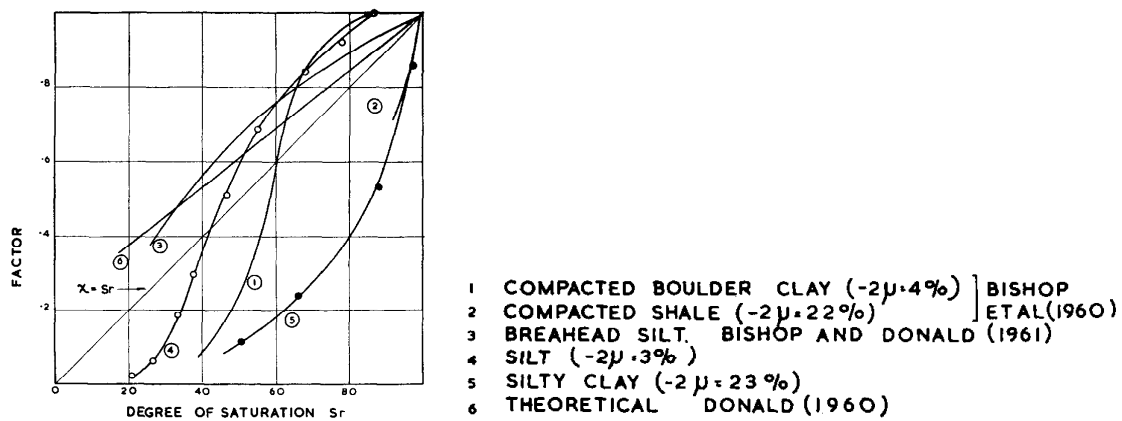


Figure 3.2.: Curves of parameter χ against degree of saturation for various soils after Jennings & Burland (1962*a*)

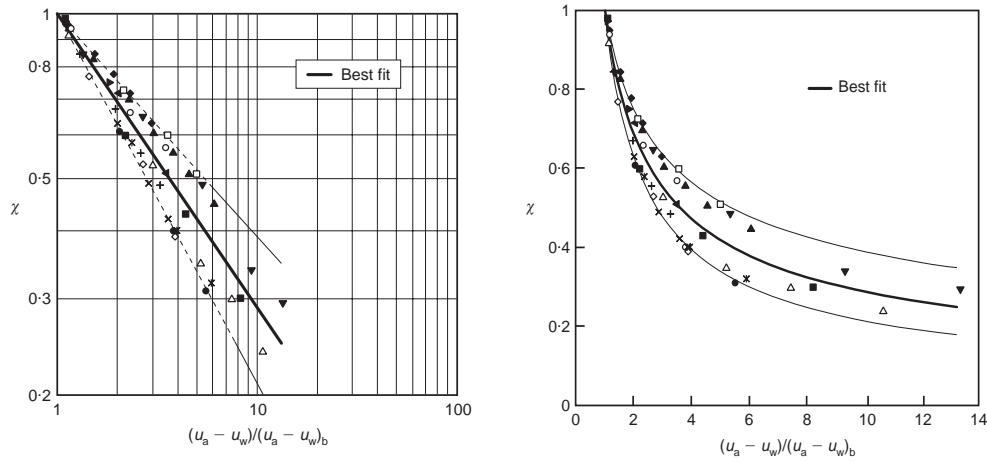


Figure 3.3.: Relationship between the effective stress parameter χ and the suction ratio, (a) log-log scale, (b) linear scale after Khalili & Khabbaz (1998)

3.2.6. Shear strength of unsaturated soil

Mohr (1900) introduced a theory for rupture in materials which contended that a material fails because of a critical combination of normal stress and shear stress:

$$\tau_f = f(\sigma) \quad (3.7)$$

Coulomb (1776) was the first one who expressed a failure criterion for soil by assuming that the resistance to sliding in a plane through a soil mass is a sum of a cohesion (c), being constant, and a friction ($\sigma \mu$) which increases proportional to the normal pressure

$$\tau_f = c + \sigma \mu \quad (3.8)$$

where μ is the coefficient of internal friction.

Based on Coulomb's empirical equation (as stated by Terzaghi 1943), Bishop (1959) proposed an equation to determine the shear strength for unsaturated soil using the effective stress concept:

$$\tau_f = c' + (\sigma - u_a) \tan(\phi') + \chi(u_a - u_w) \tan(\phi') \quad (3.9)$$

where τ is the shear strength of the soil, c' is the effective cohesion, $(\sigma - u_w)$ is the effective stress, and ϕ' is the effective angle of friction.

By considering Terzaghi's effective stress under partially saturated condition as developed by Bishop (1959) (7.2) and Mohr-Coulomb failure criterion (3.9), shear strength equation

for partially saturated soils becomes:

$$\tau_f = c' + [(\sigma - u_w) + \chi(u_a - u_w)] \tan(\phi') \quad (3.10)$$

Fredlund & Morgenstern (1977) and Fredlund et al. (1978) presented two formulations for the shear strength modeling using two sets of independent stress state variables. One set of stress state variables was defined using the water pressure as reference and one set was defined using the air pressure as reference. The formulations with the two sets of stress state variables are:

$$\tau_f = c' + (\sigma - u_w) \tan(\phi') + (u_a - u_w) \tan(\phi'') \quad (3.11)$$

The advantage of this combination of variables is that it provides a readily visualized transition from the unsaturated to the saturated case. The disadvantage arises in that, when the pore-water pressure is changed, two stress state variables are being affected (Fredlund et al. 1978).

ϕ' friction angle with respect to changes in $(\sigma - u_w)$ when $(u_a - u_w)$ is held constant.

ϕ'' friction angle with respect to changes in $(u_a - u_w)$ when $(\sigma - u_w)$ is held constant.

$$\tau_f = c'' + (\sigma - u_a) \tan(\phi^a) + (u_a - u_w) \tan(\phi^b) \quad (3.12)$$

The advantage of this combination is that only one stress variable is affected when the pore-water pressure is changed and therefore, it is considered more suitable for engineering practice.

ϕ^a friction angle with respect to changes in $(\sigma - u_w)$ when $(u_a - u_w)$ is held constant.

ϕ^b friction angle with respect to changes in $(u_a - u_w)$ when $(\sigma - u_w)$ is held constant.

Regardless of the combination of stress variables used to define the shear strength, the value of shear strength obtained for a particular soil with certain values of σ , u_a and u_w must be the same (Fredlund et al. 1978).

The final expression of the shear strength is (Figure 3.4):

$$\tau_f = c' + (\sigma - u_a) \tan(\phi') + (u_a - u_w) \tan(\phi^b) \quad (3.13)$$

$\phi' = \phi^a$ which represents the angle of friction at saturated condition and $c' = c''$.

ϕ^b friction angle corresponding to suctions below the air-entry value of the soil. It decreases because water no longer covers the entire void space on the failure plane.

Fredlund & Barbour (1996) and Vanapalli (1996b) proposed several models for predicting

the shear strength of an unsaturated soil using the soil-water characteristic curve and the saturated shear strength parameters:

$$\tau_f = c' + (\sigma - u_a) \tan(\phi') + (u_a - u_w) \tan(\phi') \cdot \left[\frac{\theta - \theta_r}{\theta_s - \theta_r} \right]^\kappa \quad (3.14)$$

where: θ_s is the saturated volumetric water content, θ_r is the volumetric water content at residual condition, and κ is fitting parameter depends on the soil type. The second term of the equation is the shear strength contribution due to suction. It can be also expressed as

$$\tau_{us} = (u_a - u_w) \tan(\phi') \cdot \left[\frac{\theta - \theta_r}{\theta_s - \theta_r} \right]^\kappa \quad (3.15)$$

where τ_{us} is suction strength. It indicates that the soil water characteristic curve can be used to compute soil property functions for unsaturated soils approximately.

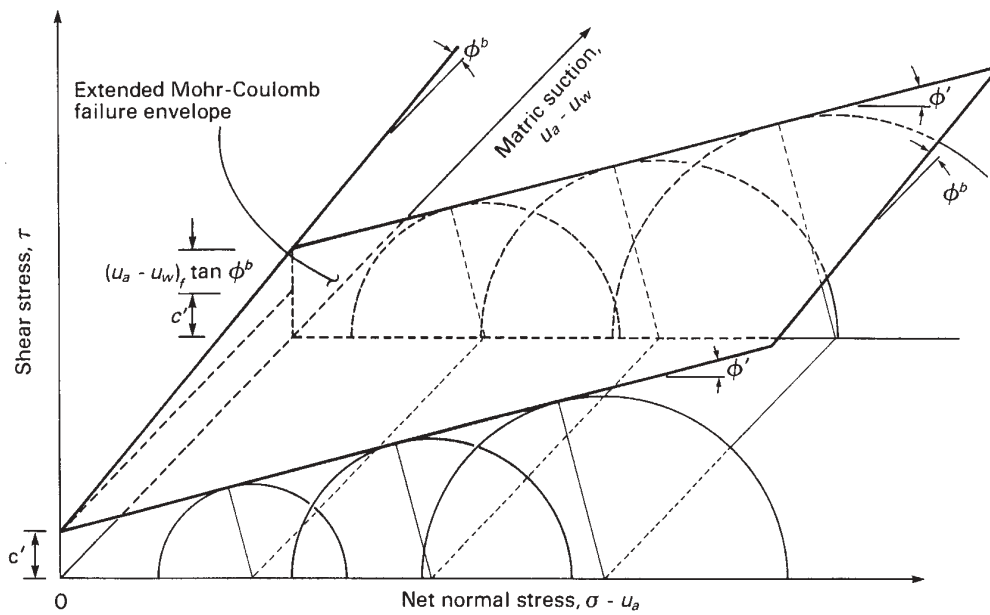


Figure 3.4.: Extended Mohr-Coulomb failure envelope for unsaturated soils after Fredlund & Fredlund (2012)

3.2.7. Experiments on the shear strength of unsaturated soil

A detailed background on the methods, techniques and equipments which are used to determine the parameters of the shear strength under partially saturated condition, including direct shear box, was presented by Fredlund & Rahardjo (1993) and Fredlund & Fredlund (2012). Alabdullah (2010) and Fard (2014) presented state of arts on the equipments and studies carried out under plane-strain conditions. In the next section, a short review for the main studies on the shear strength characteristics under partially saturated conditions using the direct shear device is given.

Prior to the 1960's, partially saturated soils were tested almost similar to saturated soils using conventional testing equipments. The control of the suction was limited and the strain rates were relatively high (Fredlund & Fredlund 2012). Several triaxial test techniques for measuring the shear strength of an unsaturated soil were proposed by Bishop et al. (1960). As the axis-translation technique was introduced for the first time in triaxial shear testing by Hilf (1956), this technique is commonly used for testing unsaturated soils at matric suctions higher than the atmospheric pressure (101.325 kPa). The acceptability of the axis-translation technique was verified by Bishop & Blight (1963).

Wilson (1902), Haines (1925) and Haines (1927) were, probably, the earliest investigators to study the shear strength behavior of soils under unsaturated condition. Their studies reported an increase in cohesion with an increase in negative pore-water pressure. Haines (1925) attempted to estimate the intergranular stresses due to pressure deformation in the pore-water in the partially saturated soil. Fisher (1926) extended the theoretical approach of Haines and assumed that the soil consisted of homogeneous spherical particles arranged in a known systematic packing.

Terzaghi (1943) referred to an increase in the cohesion due to a reduction in water content. He suggested a better understanding to the shear strength under unsaturated condition could be achieved by studying the distribution of the pore-water of the soil.

Rutledge (1947) stated that four variable may affect the shearing resistance of clays under unsaturated condition when testing soil specimens with controlled water content, namely: minor principal stress; dry soil density; water content; and degree of saturation.

Donald (1956) performed series of direct shear tests on fine sands and coarse silts under unsaturated conditions. The results for four types of sand are presented in Figure 3.5. As the matric suction is increased, the shear strength increases to a peak value and then decreases to a fairly constant value.

Escario (1980) performed series of drained direct shear and triaxial tests on unsaturated Madrid Grey clay. The suction was controlled using the axis-translation technique (ATT).

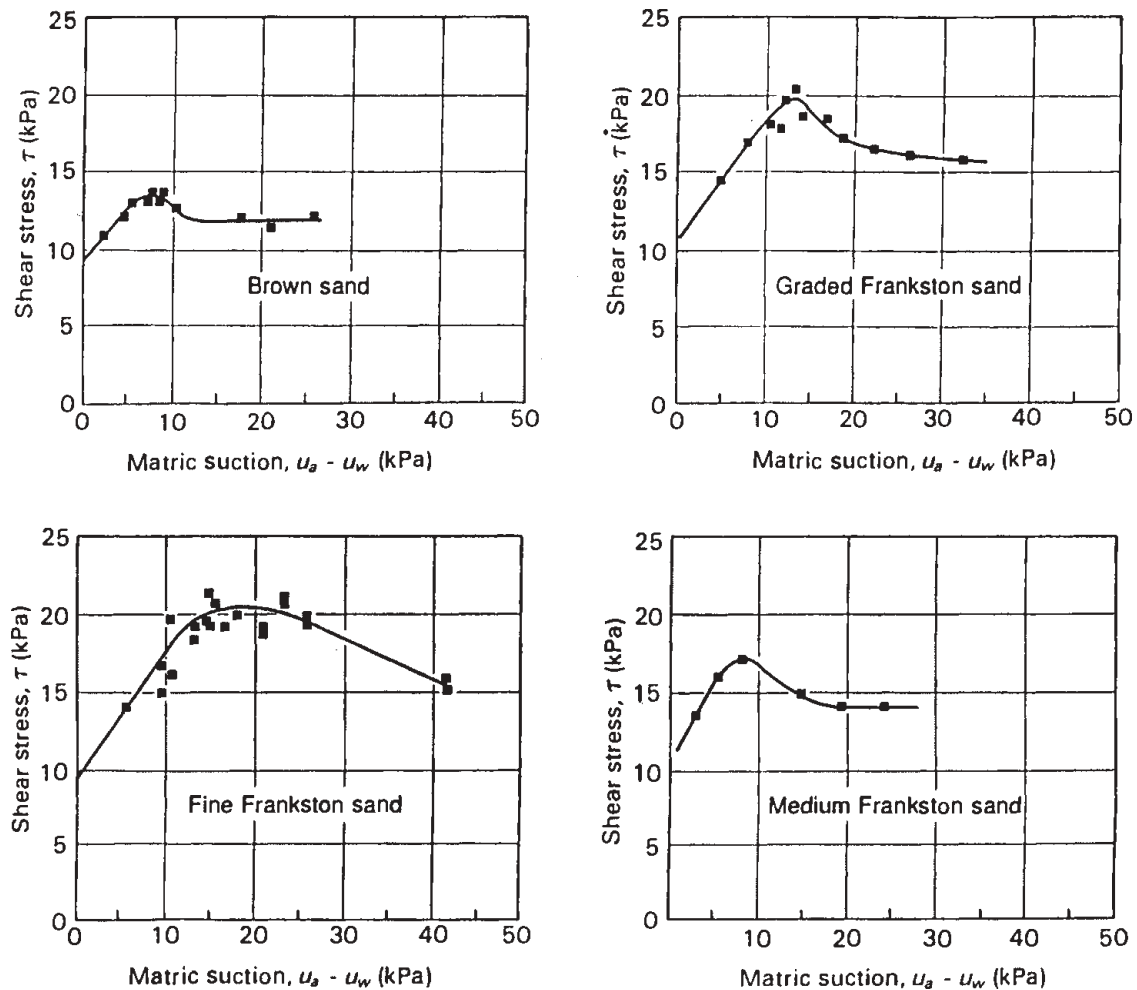


Figure 3.5.: Results of direct shear tests on sands under unsaturated condition, after Fredlund & Fredlund (2012)

Escario & Saez (1986) and Escario & Juca (1989) performed direct shear tests on three soils using a modified direct shear box and the procedure described by Escario (1980) on three different soils. The results exhibited an increase in the shear strength as the matric suction was increased. They also found that the results of the soils followed an empirical formulation using a (2.5°) degree elliptical curve as shown in Figure (3.6).

Gan (1986) and Gan et al. (1988) performed multistage direct shear tests on compacted glacial till under unsaturated condition. Suction was applied using the axis-translation technique in a range between 0 to 500 kPa. The displacement rate was 1.7×10^{-4} mm/sec. Figure (3.7a & b) shows the change of angle of friction and shear strength with suction, respectively. Similar multistage and also single stage direct shear tests were carried out on ash-tuff and decomposed granite by Gan & Fredlund (1994), Gan & Fredlund (1995), and

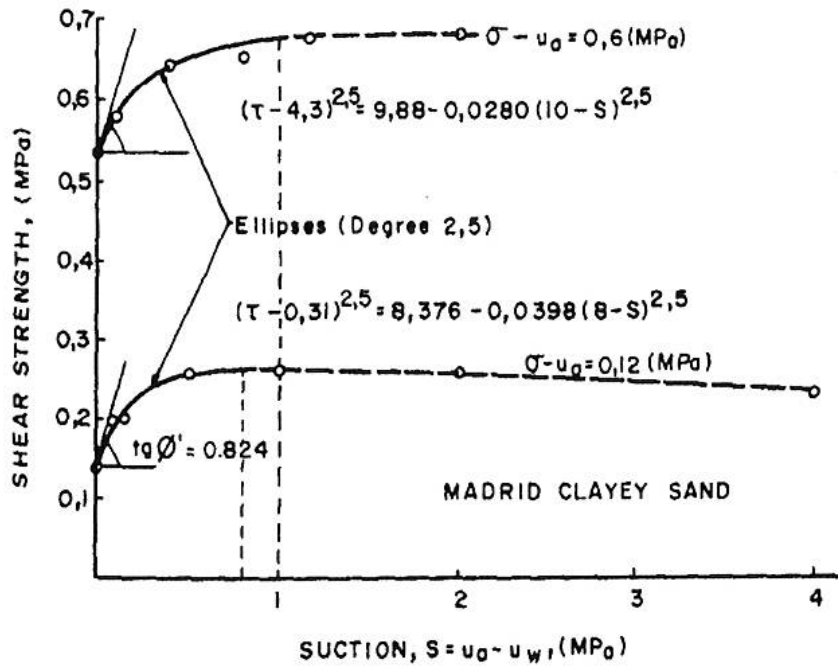


Figure 3.6.: Variation of shear strength with suction for different values of vertical stress after Escario & Juca (1989)

Gan & Fredlund (1996).

Vanapalli (1996b) have shown that for drained direct shear tests in unsaturated conditions,

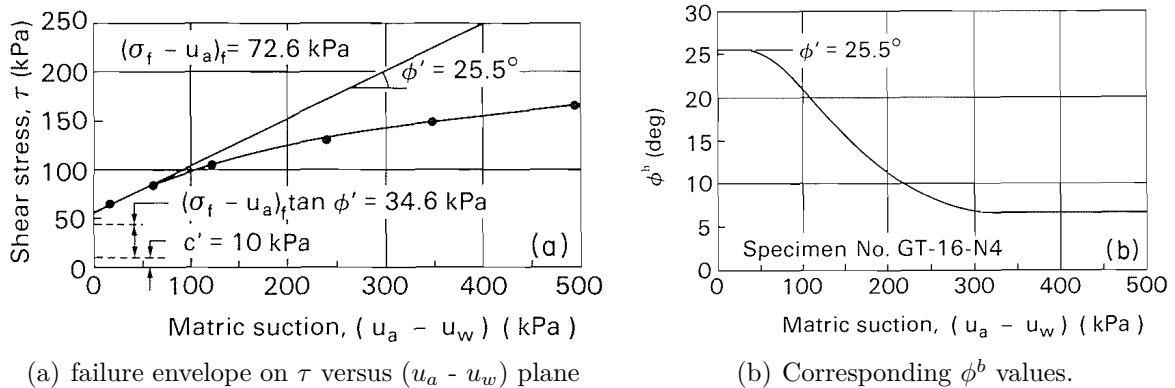


Figure 3.7.: Change in angle of friction and shear strength with increasing suction after Gan et al. (1988)

the soil suction has no influence on the angle of shearing resistance, ϕ^b . Thus, the difference between the shear strength at failure conditions and the strength contribution due to net normal stress. Vanapalli & Lane (2002) found a reasonably good comparison between experimental results on Head till using conventional direct shear equipment under partially

saturated initial conditions with the once using a modified direct shear device presented by Vanapalli (1996*a*). A semi-empirical procedure for predicting the shear strength of an unsaturated soil using the soil-water characteristic curve and the saturated shear strength parameters proposed by Vanapalli (1996*b*).

Sridharan (1968) provided an understanding of undrained shear strength of unsaturated using soil mineralogy concepts. He concluded that the soil type and soil structure affect the pore-water tension.

Satija (1978) proposed a statistical analysis approach for shear strength of unsaturated soils. Karube (1988), Toll (1990), and Wheeler & Kumar (1992) have used the concepts of critical state soil mechanics to the shear strength of unsaturated soils.

Borana et al. (2015) fabricated a direct shear equipment to test the shear strength at the interface between soil and steel plate under unsaturated condition. The matric suction in the test specimens was controlled using axis translation technique. The results showed that the shear strength and dilatancy increases with an increase in matric suction. The rate and degree of gain in shear strength due to matric suction is more for soil as compared to interfaces.

Table (3.2) summarizes some shear tests which were performed under partially saturated condition for several soils. Table (3.3) summarizes some of the existing equations to fit the shear strength.

3.2.8. Suction stress

Suction stress is a stress state variable established on the representative elementary volume of unsaturated soil, It describes the contribution of matric suction to effective stress. Because suction stress takes into account of all the possible inter-particle stress mechanisms (i.e., physicochemical forces, surface tension, and capillarity) it can realistically describe effective stress variation due to changes in soil saturation in all types of soil (Lu & Likos 2006; Lu & Godt 2008; Lu et al. 2010).

Suction stress characteristically depends on degree of saturation, water content, or matric suction through the SSCC, thus paralleling well-established concepts of the soil-water characteristic curve and hydraulic conductivity function for unsaturated soils.

Table 3.2.: Summary of shear tests performed under partially saturated condition

Author(s)	Soil type	Shear apparatus	Shearing stage	Shearing rate [mm/min]	Suction method
Escario (1980)	Clay	Modified	Single	0.0083	ATT
Escario & Juca (1989)	Clay & Clayey sand	Modified	Single	0.0016	ATT
Abramento & Carvalho (1989)	Clayey sand				
Shimada (1998)	River sand	Simple shear	Single	0.002	ATT
Vaunat et al. (2002)	Silty soils				
Huat et al. (2005)	Residual soils	Modified	Single	x0.006	ATT
Zhan & Ng (2006)	Expansive clay	Modified	Single	0.0019	ATT
Ampadu (2007)	Sandy clay	Conventional	Single	0.048	Constant WC
Sun & Xu (2007)	Sandy silt	Modified	Single	0.0096	Hanging column
Kulkarni (2008)	Grey clay	Modified	Single	0.0005	Constant WC
Asadzadeh & Soroush (2009)	Rockfill	Conventional	Multi	0.5	Constant WC
Ajdari et al. (2010)	Silt-bentonite	Conventional	Single	0.1 - 0.036	Osmotic & VET
Gallage & Uchimura (2010)	Silty soils	Modified	Single	0.048	ATT
Casini et al. (2011)	Silty sand	Conventional	Single	0.033	Constant WC
Hamidi et al. (2011)	Silty clay	Modified	Single	0.003	Osmotic
Nam et al. (2011)	Deposite	Modified	Multi	0.005 - 0.008	ATT
Jotisankasa et al. (2012)	Silt-kaolin	Modified	Single	0.05	Constant WC
Heitor et al. (2013)	Silty sand	Conventional	Single	0.01	Constant WC
Kim et al. (2013)	Jumunjin sands	Modified	Single	0.002	ATT
Purwana & Nikraz (2013)	Sand-Kaolin	Modified	Single	0.122	Constant WC
Nishimura et al. (2007)	Silt	Modified	Single	0.05	ATT
Caruso & A. Tarantino (2004)	clayey silt	Modified	Single	0.005	Constant WC
Caruso & A. Tarantino (2004)		Modified	Single		Osmotic & VET
Villar et al. (2011)	sand/silt	Modified	Single	0.001	ATT
Caruso & A. Tarantino (2004)	Clayey silt	Modified	Single	0.0055	Constant WC
de Campos & Carillo (1995)	Residual soils	Modified	Single	-	ATT
Chen et al. (2013)	Silty soil	Conventional	Single	0.8	Constant WC
Feuerharmel et al. (2006)	Colluvium soil	Modified	Single	0.000203	ATT
Hossain & Yin (2010)	CDG soil	Modified	Single	0.005	ATT
Horndee et al. (2005)	collapsible soil	Modified	Single	0.2	ATT
Vanapalli & Lane (2002)	sandy-clay till	Conventional	Single	1.25	Constant WC

Table 3.3.: Summary of the empirical equation to determine the shear strength under unsaturated conditions

Author(s)	Equation	
Bishop (1959)	$\tau_f = c' + (\sigma - u_a) + \chi(u_a - u_w) \tan(\phi')$	(3.16)
Fredlund & Widger (1978)	$\tau = c' + (\sigma - u_a) \tan(\phi') + (u_a - u_w) \tan(\phi^b)$	(3.17)
Lamborn (1986)	$\tau = c' + (\sigma - u_a) \tan(\phi') + (u_a - u_w) \theta_w \tan(\phi^b)$	(3.18)
Peterson (1988)	$\tau_f = c' + (\sigma - u_a) \tan(\phi') + C_\psi$	(3.19)
Escario & Juca (1989)	$(\tau_m + \tau_b)^{2.5} - (\tau_o + \tau_b)^{2.5} = (\tau_o + \tau_b)^{1.5} \cdot (u_a - u_w)_m \cdot \tan(\phi')$	(3.20)
Abramanto & Carvalho (1989)	$\tau_f = c' + (\sigma - u_a) \cdot \tan(\phi') + \alpha \cdot (u_a - u_w)^\beta$	(3.21)
Lytton (1995)	$\tau = c' + (\sigma - u_a) + (u_a - u_w) \cdot \theta_w \cdot \tan(\phi')$	(3.22)
Öberg & Sällfors (1995)	$\tau = c' + (\sigma - u_a) \cdot \tan(\phi') + S \cdot (u_a - u_w) \cdot \tan(\phi')$	(3.23)
Rohm & Vilar (1995)	$q = c^{\wedge''} + (p-u \cdot a) \cdot \tan(\alpha)$	(3.24)
Shen (1996)	$\tau_f = c' + (\sigma - u_a) \tan(\phi') + (u_a - u_w) \frac{1}{1+d(u_a-u_w)} \cdot \tan(\phi')$	(3.25)
Vanapalli (1996b) & Fredlund & Barbour (1996)	$\tau_f = c' + (\sigma - u_a) \tan(\phi') + (u_a - u_w) \tan(\phi') \cdot (\Theta)^\kappa$	(3.26)
Bao et al. (1998)	$\tau_f = c' + (\sigma - u_a) \tan(\phi') + (u_a - u_w) \left[\frac{\log(u_a - u_w)^r - \log(u_a - u_w)}{\log(u_a - u_w)^r - \log(u_a - u_w)_b} \right] \tan(\phi')$	(3.27)
Khalili & Khabbaz (1998)	$\tau_f = c' + [(\sigma - u_a) + \left[\frac{(u_a - u_w)}{(u_a - u_w)_b} \right]^\eta (u_a - u_w)] \cdot \tan(\phi')$	(3.28)
Rassam & Williams (1999)	$\tau_f = \alpha + (\sigma - u_a) \tan(\phi') - \varphi [(u_a - u_w) - (u_a - u_w)_b]^\beta$	(3.29)
Yü (2000)	$\tau_f = c' + (\sigma - u_a) \cdot \tan(\phi') + (u_a - u_w) \frac{1}{\tan(\alpha')} \frac{(u_a - u_w)}{\beta}$	(3.30)
Lee et al. (2003)	$\tau_f = c' + \frac{(u_a - u_w)}{a+b(u_a - u_w)}$	(3.31)
Schick (2004)	$\tau_f = c' + (\sigma - u_a) \cdot \tan(\phi') + \frac{(u_a - u_w)}{a_2 + b_2(u_a - u_w)}$	(3.32)
Xu & Sun (2001)	$\tau_f = c' + (\sigma - u_a) \tan(\phi') + m^{1-\zeta} \cdot (u_a - u_w)^\zeta \tan(\phi')$	(3.33)
Rassam (2002)	$\tau_f = (u_a - u_w) \tan(\phi') - \left[\frac{\psi_r \cdot \tan(\phi' - s_r)}{(\psi_r - \psi_e)_b} \right]^\beta [(u_a - u_w) - (u_a - u_w)]^f$	(3.34)
Miao et al. (2002)	$\tau_{us} = \frac{a_2 u_s}{1 + \frac{1-a_2}{P_{at}} u_s}$	(3.35)
Aubeny & Lytton (2004)	$\tau_f = c' + (\sigma - u_a) \tan(\phi') + f_1 \cdot (u_a - u_w) \cdot \theta \cdot \tan(\phi')$	(3.36)
	$\tau_{us} = f_1 \cdot (u_a - u_w) \cdot \theta \cdot \sin(\phi') \cdot 1 - \sin(\phi')$	(3.37)
Tekinsoy et al. (2004)	$\tau_f = c' + (\sigma - u_a) \tan(\phi') + \tan(\phi') [(u_a - u_w)_b + P_{at}] \cdot Ln \left[\frac{(u_a - u_w) + P_{at}}{P_{at}} \right]$	(3.38)
Xu (2004)	$\tau_f = c' + (\sigma - u_a) \tan(\phi') + (u_a - u_w)_b^{1-\zeta_2} \cdot (u_a - u_w)^\zeta \cdot \tan(\phi')$	(3.39)
Lee et al. (2005)	$\tau_{us} = AEV \tan(\phi') + [(u_a - u_w) - AEV] \theta^\kappa [1 + ((u_a - u_w))] \tan(\phi')$	(3.40)
Vilar (2006)	$\tau_f = c' + (\sigma - u_a) \cdot \tan(\phi') + \frac{(u_a - u_w)}{\tan(\phi') + \left[\frac{1}{\tau_{us-max}} \frac{1}{(u_a - u_w) \tan(\phi')} \right]}$	(3.41)
Lu et al. (2010)	$\tau_f = c' + (\sigma - u_a) \tan(\phi') + P_s \tan(\phi')$	(3.42)

3.2.9. Determination of the suction stress σ^s

Lu et al. 2010 derived the following equation to determine the suction stress from SWCC using the fitting parameters n and α of van Genuchten 1980 model:

$$\sigma^s = -(u_a - u_w), \text{ when } (u_a - u_w) \leq 0. \quad (3.43)$$

$$\sigma^s = -\frac{(u_a - u_w)}{1 + [\alpha(u_a - u_w)]^{\frac{n-1}{n}}}, \text{ when } (u_a - u_w) \geq 0. \quad (3.44)$$

If the suction value is less than the air-entry value of the soil, the magnitude of the suction stress equals to the suction value. However, for higher suction range, the suction stress can be calculated from the equation. In case of direct shear test condition, the suction stress can be calculated following the equation (Lu et al. 2010):

$$\sigma^s = -\frac{c^s}{\tan \phi'} = \frac{\tau - c' - (\sigma - u_a) \tan \phi'}{\tan \phi'} \quad (3.45)$$

3.3. Unsaturated behavior of geotextiles

3.3.1. Overview

Recently, the geotextile for drainage and filtration purposes is widely used in many engineering application. However, since the mid of the 90s of the past century, several studies were started to investigate the effect of suction on the hydraulic properties of the woven and nonwoven geotextiles. It has been found that these polymer materials have similar behavior compare to coarse granular materials (Stormont et al. 1997). In the following section, a review of the published techniques and methods which are used to determine the water-retention curve for geotextiles is given.

There are several methods and techniques used to determine the geotextile water characteristic curve (GWCC). Two methods have been used in the current study; the capillary rise method, and the hanging column method. Some modifications were made to these methods in order to control the boundary conditions of the tests. Discussion of the results from the current study are made with the current literature and some remarks will be mentioned in the following chapter.

3.3.2. Definitions

Herein, a short definition of some terms that will be used in the following parts of the thesis.

- **Cross-plane flow:** occurs when the water flow cross the geotextile layer. In this case the geotextile will perform for filtration function. Figure 3.8
- **In-plane flow:** occurs when the water flows through the geotextile layer (drainage function).
- **As-new geotextile:** a geotextile layer as received from the manufacturer.
- **Cleaned geotextile:** occurred by rinsing (cleaning) the geotextile specimen with water, squeezed by hand and then left to dry by air. It is observed that by cleaning the geotextile, some of the coating layer might be removed.
- **Dirty geotextile:** occurred by introducing soil fines into the geotextile layer.
- **Cleaned dirty geotextile:** occurred by rinsing (cleaning) the geotextile specimen with water, the geotextile specimen has already introduced by fine soil layer.
- **Machine direction:** which coincides with the direction in which the geotextile is produced on the conveyor belt.
- **Cross direction (Cross-machine direction):** coincides with the opposite direction in which the geotextile is produced on the conveyor belt.

Figure 3.8 shows the different directions of geotextile material.

These conditions are presented in the literature of the drainage and filtration geotextiles in order to investigate the possible real conditions these materials may face during their working life.

3.3.3. Capillary rise method

The idea of the capillary rise method is to observe the rise of water due to the capillary forces within a strip, in-plane (Figure 3.9a) or a stack of geotextile specimens, cross-plane (Figure 3.10). The lower end of the geotextile strip or stack is submerged inside a water reservoir. The water content within the stack is measured after reaching equilibrium at different heights. By linking the measured water content to the hydrostatic height the GWCC is determined. The test can be performed from saturated or dry condition. Henry & Holtz (1997), Henry & Holtz (2001), and Bouazza & Nahlawi (2006) observed the

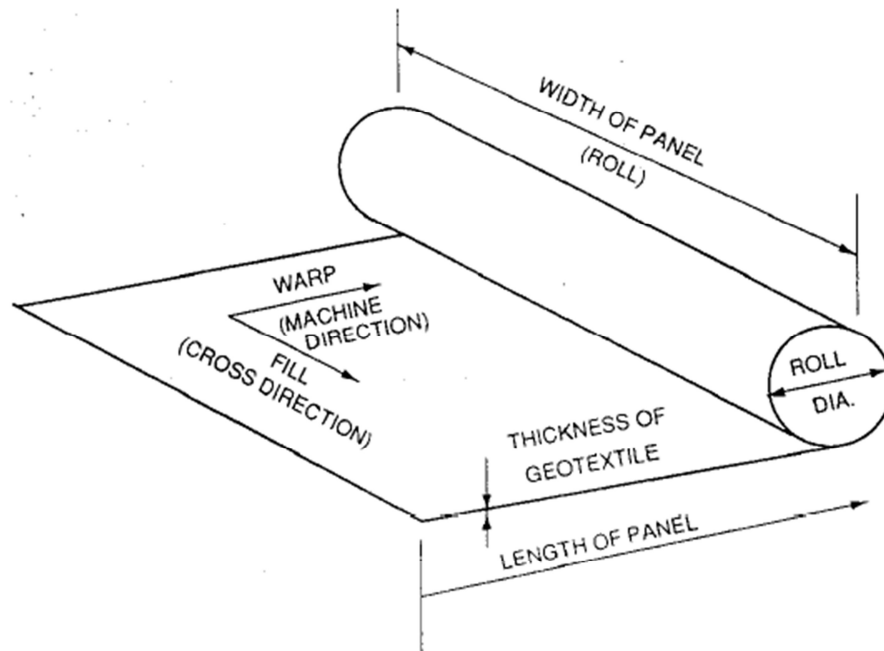


Figure 3.8.: Dimensions and directions for geotextiles after Koerner (2005)

capillary rise of water through a layer of geotextile. Henry & Holtz (1997) performed tests on different types of nonwoven geotextile and in four different conditions: new, cleaned, dirty, and cleaned dirty. Results showed that the rise of water through dirty geotextiles was higher than that which was found in the as-new geotextiles. Cleaning the geotextile specimen will cause no capillary rise or capillary depression. Tests were also performed in the machine direction and in the cross-machine direction which showed no significant difference in the results. Bouazza & Nahlawi (2006) performed a test for a duration of 72 hours to measure the in-plane drying water retention for two specimen of nonwoven geotextiles under two conditions; as received from the manufacturer (as new) which absorbed no water at suctions greater than zero, and warped with plastic film to prevent evaporation, the wetting appeared took place at suction less than 0.09 and 0.13 kPa. A different behavior was found when measuring the water retention curve in cross-plane direction of the same geotextile using the hanging column method. They concluded that the tested geotextiles were more hydrophobic in the in-plane than in the cross-plane direction during wetting.

Lafleur et al. (2000), Stormont & Ramos (2004), Krisdani et al. (2006), Krisdani et al. (2008b), Nahlawi et al. (2008), and Handoko et al. (2012) determined the water-retention

curve of the geotextile using the capillary rise test. A (300)mm length and (50)mm width strip of geotextile was hanged in a chamber with (20)mm length submerged inside the water as shown in (Figure 3.9a). Small specimens of (10×50)mm were taken at different heights [represent the suction] and the gravitational water content was measured to determine the volumetric water content. Knight & Kotha (2001) performed a cross-plane capillary rise test through 18 vertically stacked geotextile specimen layers using a column drainage experiment apparatus as shown in Figure 3.10.

Stormont & Ramos (2004) compared the results of the capillary rise test with those obtained from hanging column method which will be presented later.

Handoko et al. (2012) performed their tests with similar procedure to the previous once but the geosynthetic specimens were inclined in different angles as shown in Figure 3.11.

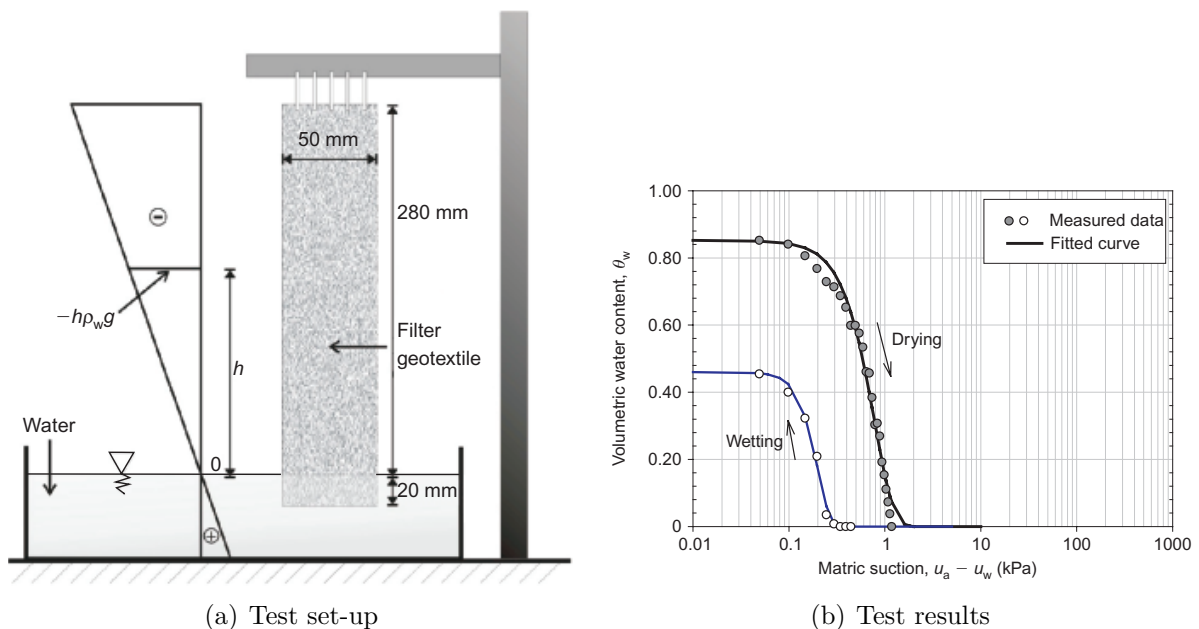


Figure 3.9.: Set-up of geotextile-water characteristic curve test after Krisdani et al. (2008a)

3.3.4. Hanging column method

The concept of hanging column method applied to determine the GWCC is shown in Figure 3.12a (Klute 1986). A stack of geotextile specimen is placed inside a cell. The water saturated ceramic plate is connected to a water reservoir below lower-end of a geotextile. The suction in the geotextile specimen is controlled by the height of the water level h .

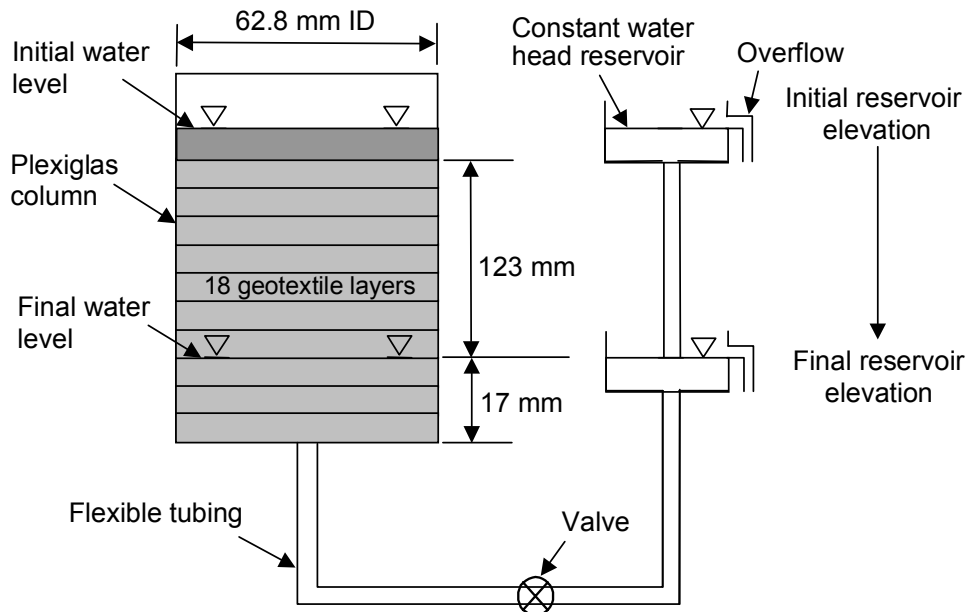


Figure 3.10.: Column drainage apparatus for geotextiles after Knight & Kotha (2001)

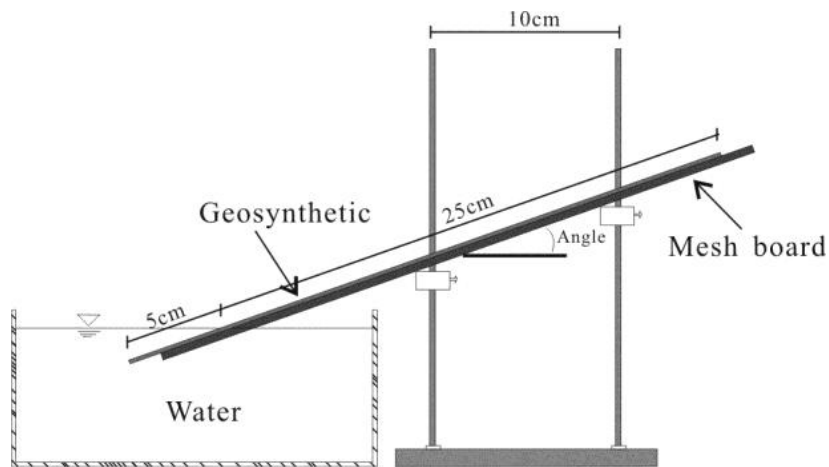


Figure 3.11.: Schematic diagram of the inclined capillary rise technique after Handoko et al. (2012)

The water content of the geotextile specimen is determined by weighting the specimen or by measuring the magnitude of water entering or leaving the geotextile specimen.

Stormont et al. (1997) measured, for the first time, the water retention function for four nonwoven, needle-punched, polypropylene geotextiles using the hanging column method in the cross-plane direction. The testing device is similar to the hanging column apparatus used for testing the water retention curve of soils as presented by Klute (1986) and shown in Figure 3.12a. The tested specimens were in two conditions: new and cleaned in order to

study the effect of the surfactants used in geotextile manufacturing on geotextile wetting behavior. The new geotextile specimens always contained more water at comparable suction heads than the cleaned geotextile specimens. The minimum equilibrium period of 24 hours was chosen for each suction head after performing preliminary tests which were used to refine the experimental procedure. Typical preliminary test results for a cleaned specimen at suction head being increased from 100 to 150 mm are shown in (Figure 3.12b). Results were compared with the once obtained by Henry & Holtz (1997) for the same geotextiles using in-plane from capillary rise measurements as shown in Table (3.4). It can be seen that water entry suction head values are different between the in-plane and cross-plane testing procedures which concludes that the tested geotextiles are anisotropic. Similar testing procedure was also followed by other researches such as Morris (2000), Stormont & Morris (2000), Henry et al. (2002), McCartney et al. (2005), Bouazza & Delage (2006), Bouazza & Nahlawi (2006), Bouazza et al. (2006), Park & Fleming (2006), Garcia et al. (2007), and McCartney et al. (2008b).

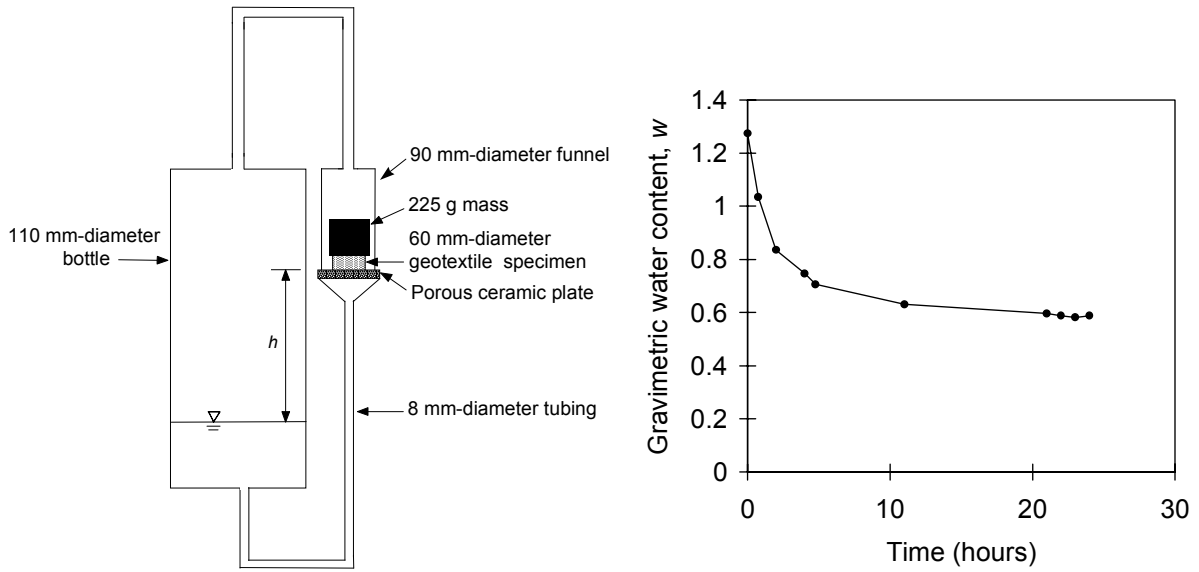
Stormont & Morris (2000) studied the influence of the intrusion of soil particles on the wetting performance of polyester non-woven geotextiles (dirty geotextile) following the procedure used by Henry (1998). The intruder of soil caused the geotextile specimens to be wetted-up at higher suction heads as shown in (Figure 3.13). It was noticed that the water entry suction heads for silt and sand-contaminated specimens were not noticeably different.

Hanson et al. (2001) presented an apparatus to measure the shear strength for interfaces containing nonwoven geotextiles under unsaturated conditions. The apparatus consisting of a ceramic disk which allows to measure the water retention curve of nonwoven geotextiles.

Table 3.4.: Estimates of water entry suction heads after Stormont et al. (1997)

specimen	Cross-plane [mm]	Cross-plane [mm]	In-plane [mm]
	Hanging column test Stormont et al. (1997)	Hanging column test Henry & Holtz (1997)	Capillary rise test Henry & Holtz (1997)
A1	0 - 20	60 - 69	50 [9]*
A2	0 - 20	60 - 70	75 [6]*
B1	0 - 10	60 - 70	25 [9]*
B2	0 - 30	41 - 48	36 [15]*

* the standard deviation value



(a) The test apparatus used to measure the water retention functions of geotextile (b) Gravimetric water content versus time for a cleaned specimen

Figure 3.12.: Hanging column test apparatus after Stormont et al. (1997)

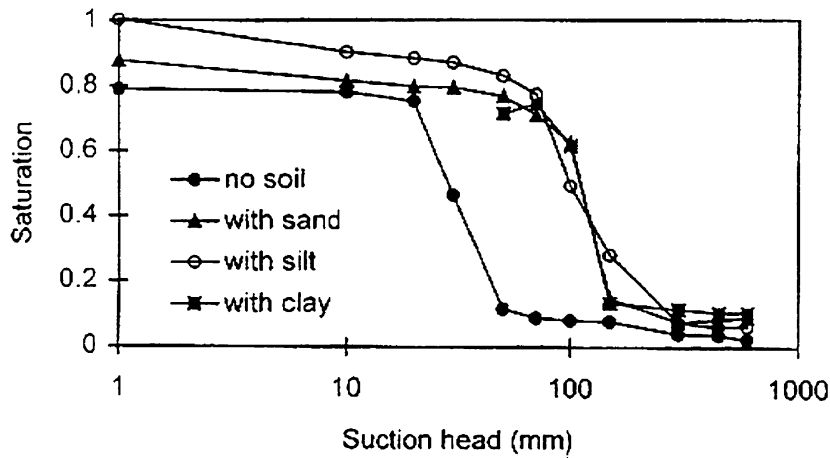


Figure 3.13.: GWCCs for polyester non-woven geotextiles with intruded soil after Stormont & Morris (2000).

3.3.5. Capillary pressure cell test

Knight & Kotha (2001) and Nahlawi et al. (2007a) used a controlled outflow cell to determine the water-retention curve of nonwoven geotextile based on the information presented by Lorentz et al. (1993). The schematic features of this apparatus and the testing assembly are shown in Figure 3.14. The main features of the modified capillary cell are the ability to accommodate a specimen of 150 mm in diameter and the possibility

of achieving an accurate control of air pressure through a computer controlled pneumatic pressure controller (accuracy of 0.001 kPa).

Nahlawi et al. (2007a) compared their results with the results established from the hanging column method and the results found to be comparable.

The presented methods and techniques show an ability to determine the geotextile-water

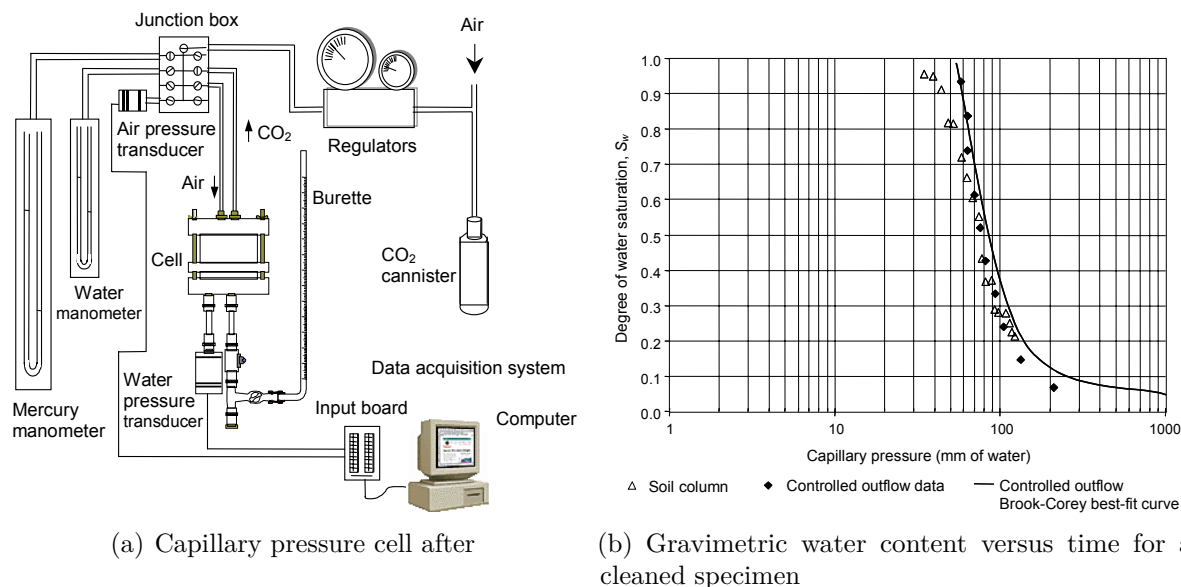


Figure 3.14.: Capillary pressure cell after Knight & Kotha (2001)

retention curve of the geotextile in the laboratory. However, these techniques require special equipments and testing procedures which may need a control to the test continuously and high control to prevent evaporation. However, there is no approach to determine the GWCC using the physical properties of the geotextile specimen such as the distribution of the pores of the specimen. These methods were known and widely used for soils and showed reliable results.

3.3.6. Unsaturated hydraulic conductivity function of geotextile

Due to the low air-entry value and the narrow suction range of the GWCC (ranging between 1 to 5 kPa for many tested materials in the literature) of the geotextile material used for drainage and filtration purposes, the determination of the hydraulic conductivity-suction function is difficult in the laboratory and studies on this topic are rare.

The hydraulic conductivity functions in the in-plane direction (transitivity) measured by Stormont & Morris (2000), Morris (2000) and Lafleur et al. (2000) in both drying and wetting paths are shown in Figure 3.15.

It is very likely to determine the relationship using well-known existing models which are developed originally for soils such as van Genuchten (1980) and Fredlund & Xing (1994) who proposed an empirical approach in order to obtain the coefficient of hydraulic conductivity functions from volumetric water content for unsaturated soils. The theoretical basis for the hydraulic conductivity function is the entire soil suction range.

The proposed models can provide good prediction to the hydraulic conductivity function - suction which are acceptable in the field of the unsaturated soil mechanics. Figure 3.16 shows the hydraulic conductivity function - suction fitted from the GWCC tests results performed by Nahlawi et al. (2007b) using both models presented by van Genuchten (1980) and Fredlund & Xing (1994). The generated curves are similar for both models until the air-entry value AEV. After the AEV, the fittings are showing more and more differences. The characteristics of the hydraulic conductivity function using van Genuchten (1980) model are closer to the measured once in Figure 3.16 and more related to the shape of the GWCC.

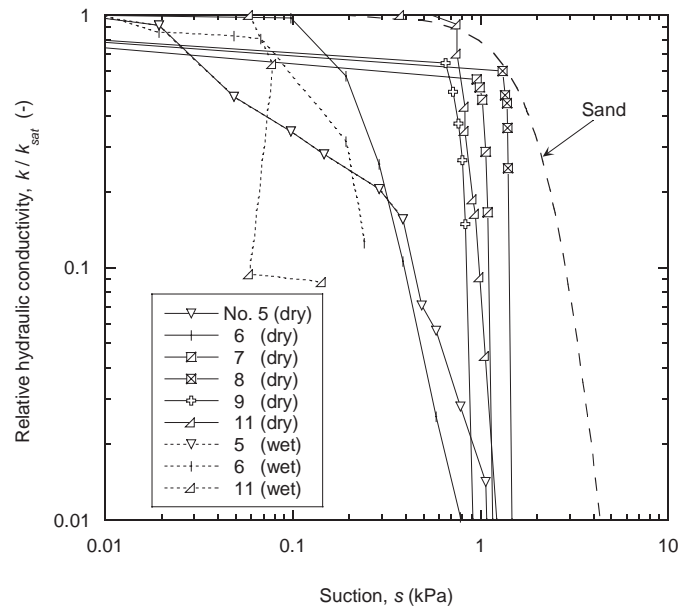


Figure 3.15.: Relative hydraulic conductivity function for geotextiles (data from Stormont & Morris (2000) for curves No. 5 and 6; Morris (2000) for curves No. 7, 8 and 9; Lafleur et al. (2000) after Iryo & Rowe (2003) (in-plane direction)

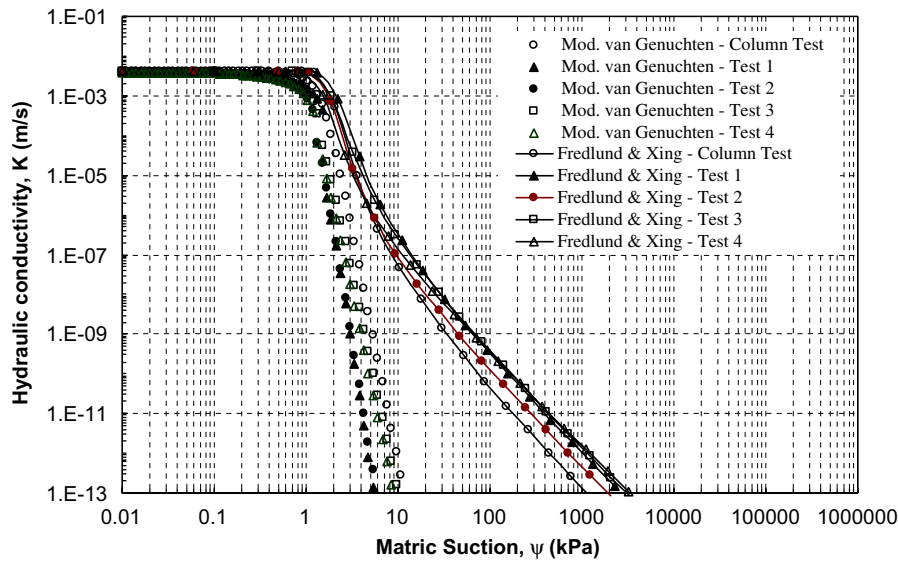
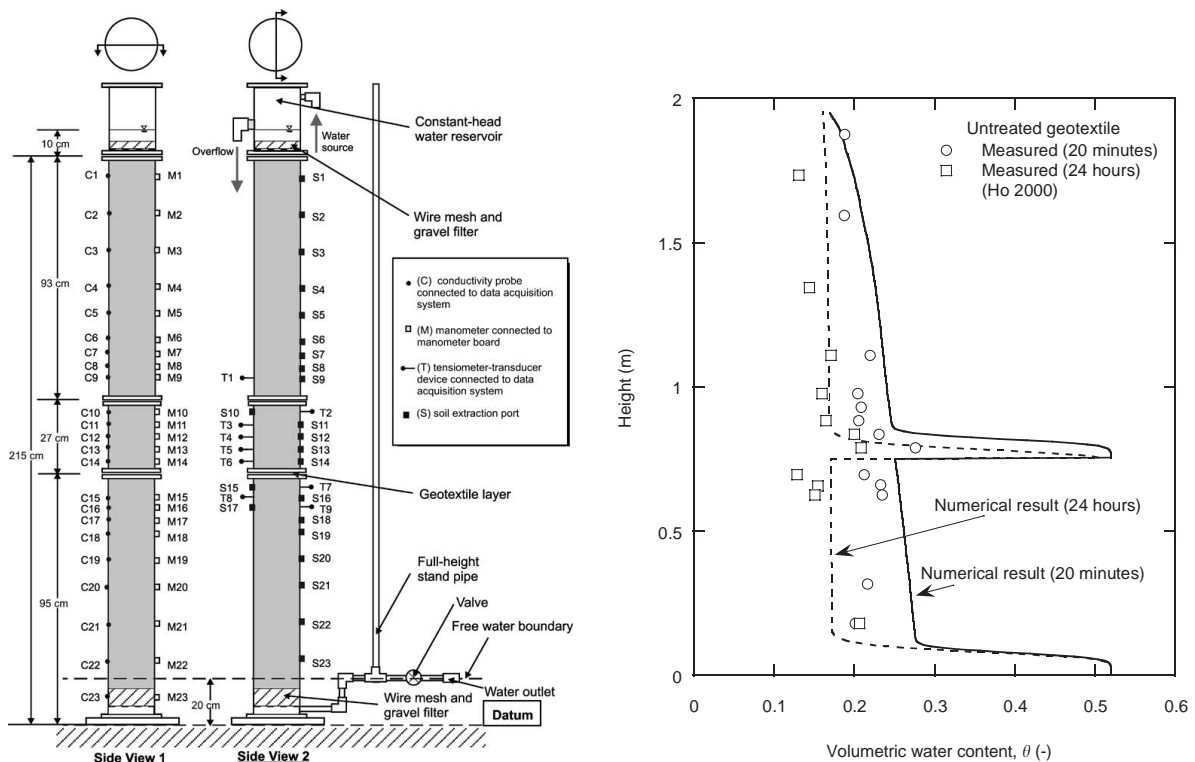


Figure 3.16.: $k(\psi)$ -suction curves using the modified van Genuchten 1980 and Fredlund & Xing 1994 equations after Nahlawi et al. (2007b)

3.3.7. Laboratory measurement of 1-D flow of water through soil/geotextile interface

Ho (2000) which also reported in Iryo & Rowe (2003), Bathurst et al. (2007), Bathurst et al. (2009), and McCartney & Znidarcic (2010) performed a one-dimensional flow of water through a cylindrical column consisting of a horizontal layer of nonwoven geotextile sandwiched between two layers of sand as shown in Figure (3.17a). The column was initially filled with water and then drained from the bottom up to create an initial condition for the subsequent infiltration test. The column was initially filled with water and then drained from the bottom to create an initial condition for the subsequent infiltration test. The water content profile following the drainage was measured at 20 min and 24 h following initiation of drainage as shown in Figure (3.17b). The test has been repeated in which the geotextile was rubbed with kaolin paste before it was installed in the sand column. The treatment by kaolin paste was found to reduce the porosity and saturated hydraulic conductivity of the geotextile relative to the untreated specimen.

McCartney et al. (2005) (also reported by Bouazza et al. (2006) performed a water flow through a column of clayey soil and soil/geotextile profiles. The values of the water content in which the flow of water was blocked through the geotextile layer is evaluated on the water retention and hydraulic conductivity curves of the soil and geotextile without any information on pore-water pressure measurements of water. The results indicated that similar behavior can be expected from both conventional granular drains and geosynthetic



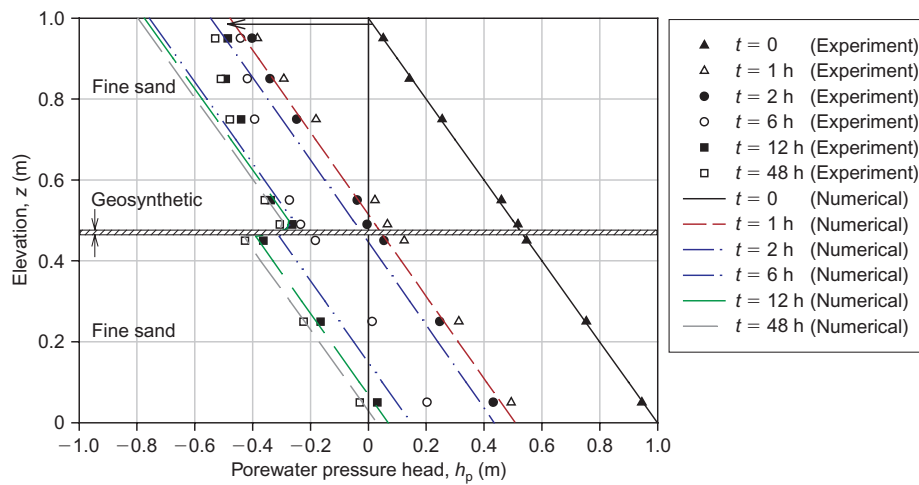
(a) Column test apparatus and instrumentation (b) Water content profile from experiment and numerical results

Figure 3.17.: 1-D test device & results after Bathurst et al. (2007) & Iryo & Rowe (2003)

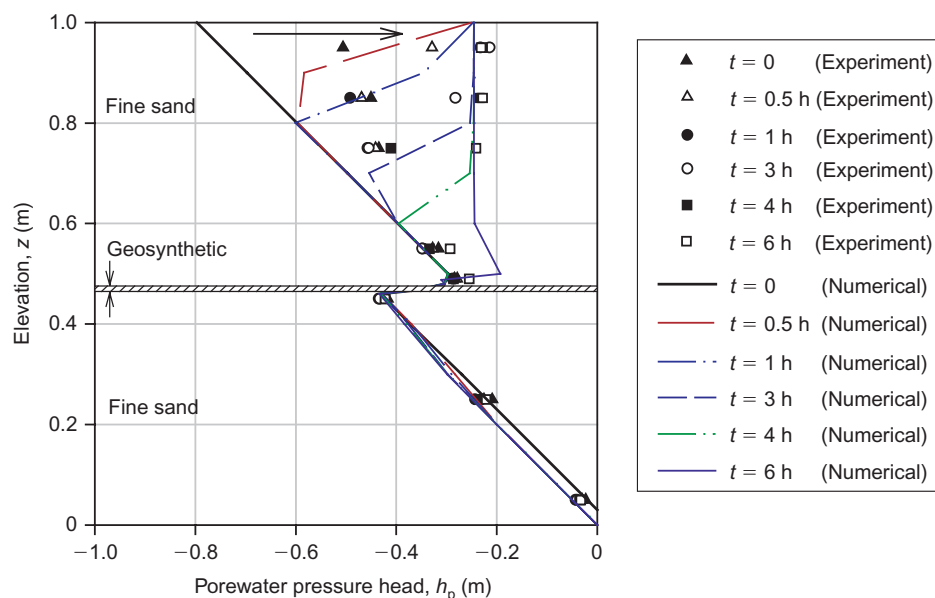
drainage layers overlain by unsaturated soil. The moisture front advance was indicated by an increase in volumetric moisture content within the profile.

Krisdani et al. (2006) and Krisdani et al. (2008a) studied flow of water through a column consists of a 0.51 m thick layer of fine sand overlying a geosynthetics drainage product consisting of nonwoven geotextile which was placed on 0.49 m layer of fine sand. Small-tip tensiometer and TDR waveguide were installed. Two types of test were applied to the soil column model: a drawdown test, which was conducted by lowering the water table from the top of the soil column to the bottom of the soil column and a second type of test, which was a rainfall test. Results of rainfall tests with an intensity of 5.8 mm/h for 6 h duration are presented in Figure (3.18b).

Nahlawi et al. (2007b) studied the one-dimensional unsaturated hydraulic behavior of a layered sand-geotextile using clear Perspex cylinder of 138.7 mm in diameter and 1,600 mm in height. A set of volumetric water content probes, pore water pressure sensors, and air pressure sensors, were used in this test apparatus. Two tests were performed: initially dry sand and initially saturated sand. When the infiltration test was conducted with a dry soil, the wetting fronts become unstable and preferential flow occurred. Whereas when



(a) Experimental and numerical results of pore-water pressure during drawdown test



(b) Experimental and numerical results of pore-water pressure during rainfall test

Figure 3.18.: 1-D test device & results after Krisdani et al. (2008a)

the infiltration test was conducted with gravity-drained soil, preferential flow of water (fingering) did not develop in the soil profile. Test results showed that the wetting fronts advanced uniformly and the total head gradient was stable throughout the column height. Iryo & Rowe 2003 and Iryo & Rowe 2004 carried out numerical simulation of the column tests described earlier using a commercially available finite element code.

Siemens & Bathurst 2010 performed numerical modeling using to investigate the influence of geotextile and soil hydraulic conductivity and height of ponded water at the surface on wetting front advance below the geotextile and potential ponding of water above the

geotextile due to a capillary break mechanism.

The presented column tests were performed for one type of soil material, mostly sand or clayey soil, which a lot of intermediate soils with different amounts of fines content are used in landfills cover systems.

The tests were performed starting from initial water content or from dry condition. However, starting from fully saturated condition is important to avoid any hysteresis which could occur if the test has been started from certain initial condition which will cause some error when explaining the results using the SWCC of the soil.

Most tests were carried out by measuring the volumetric water content or positive and negative pore-water pressure. However, measuring both components will provide valuable data which can be used to adopt the results coming from the SWCC, GWCC, soil permeability vs suction, and geotextile permeability vs suction at different stages of the test.

McCartney & Zornberg (2010) and Zornberg et al. (2010) performed an experimental investigation of the transient movement of water in unsaturated soil layers underlain by a geocomposite drainage layer (GDL) during cycles of infiltration and evaporation. The capillary break was observed to have re-established itself after infiltration was stopped and the soil near the interface dried. The suction and volumetric water content measured in the soil at breakthrough were consistent after multiple cycles of wetting and drying. The conditions in the soil after each breakthrough event corresponded to the point on the drying-path water retention curve of the nonwoven geotextile where it transitioned from residual to saturated conditions.

3.4. Summary

The reviewed literature shows different methods to determine the water retention curve of the soil specimen based on the soil type and the suction range. These methods have been used for decades in different laboratories for unsaturated soil mechanics. An existing model is described to predict the hydraulic conductivity of the soil based on mathematical models to determine the permeability for wide range of suction.

The development of the effective stress equation to consider the effect of the suction was reviewed and also the expansion of the relationships to describe the shear strength to consider the influence of the suction.

Existing publications present different methods to determine the water retention curve for the geotextile material. These methods are developed basically for soils and are varying

from relatively simple methods (i.e. hanging column method) to more advanced methods (i.e. capillary pressure cell). However, some notes can be highlighted from these methods:

- In most publications, the geotextile specimen is taken out of the cell, weighted and then returned back to the cell to continue the test. This process may cause some errors due to losing water during the sampling or due to evaporation.
- Determining the GWCC for a tilted specimen might be affected by the board in which the geotextile specimen is lying on. The contact angle between the board and the specimen could affect the water rises through the geotextile layer. Also, no differences in the results due to changing the inclination angle were observed.
- The capillary rise test for some types of geotextiles was unable to determine the GWCC and therefore more investigation is needed to understand the factors controlling the test.
- The laboratory tests used to determine the water-retention curve for geotextile demand special equipment and setup, level of control to make sure the tests are running correctly, and time and additional costs if the objective is to study several materials. There are no studies focusing on predicting the GWCC of the geotextile material based on its pore structure which can be determined using the apparent opening size curve (AOS curve).
- There are few geotextile materials which are tested and presented in the literature. However, it is necessary to test wide range of geotextile material with different curves of AOS in order to compare between the hydraulic properties, the range of AEV and residual suction, of these material under partially saturated conditions to study the range of the AEV and residual suction for different geotextile material.
- Most the selected soil material used in the literature are sand or soil with high fines content. Normally these soils are not ideal to be used as top soil layer above the drainage layer. In the current study, three soil mixtures were selected for the testing program which are suitable from mechanical and hydraulic perspective to be used as top soil material. Such systematic study provides valuable information on the performance of such systems.
- Studying the shear strength parameters of the selected soils will provide important information on the behavior of these soils at different suction values. These information can shed the light on the range of the shear strength for the measured suction range from the column device results.

In term of 1-D flow of water through a soil/geosynthetics system, it is concluded:

- there are only a few studies which presents pore-water pressures and volumetric water content measured along the height of the column profile at different flow conditions with time. The measurements of both pore-water pressure (suction) and water content is necessary to analyze the results using SWCC and GWCC.
- Adopting the water retention curves of the soil and the geotextile material will be important to explain the hydraulic interaction of soil and geotextile under unsaturated condition.
- Most of the column tests were performed on soil which are initially fully dry or with defined initial water content. However, the initial degree of saturation influences the hydraulic behavior of the system due to the hysteresis.
- Most of the tests were performed on sand. Mostly soils with different amount of fine content are used as cover soils for landfills for different reasons (i.e. the stability of the slope, the mechanical and hydraulic stability of the filter layer, the water storage capacity to support vegetation layer).

4. Materials used and experimental program

4.1. General

Physical, mechanical, and hydraulic properties of the soil and geotextile materials used in the current study are presented in this chapter. These properties were determined following the ASTM (American Society for Testing and Materials) and DIN (Deutscher Institut für Normung) standards and testing methods. The presented properties of the nonwoven geotextiles are provided by the manufacturer using specialized equipments for geosynthetic products. These parameters are standard and may not be precisely to the tested samples in the current study. However, these parameters will be also presented in this chapter. At the end of this chapter, a review to the testing program of the current study and the boundary conditions of the samples for each test.

4.2. Soils

The basic physical and chemical properties of Hostun sand and Kaolin clay are reviewed. Also the Hostun sand and Kaolin clay mixtures will be presented which will be used in the testing program. The following sections will discuss each material.

4.2.1. Hostun sand

Hostun Sand has been well studied and investigated by many researchers (Desrues 1984; Biarez et al. 1989; Flavigny et al. 1990; Hammad 1991; Mokni 1992; di Prisco & Posimato 1996; Schanz & Vermeer 1996; Dubujet & Doanh 1997; Doanh et al. 1997; Tatsuoka et al. 1997; Mokni & Desrues 1998; Shahrour & Rezaie 1997; Schanz 1998; Foray et al. 1998; Mokni & Desrue 1999; Lins et al. 2002; De Gennaro et al. 2004; Desrues & Viggiani 2004;

Gennaro et al. 2004; Avci & Ehlers 2006; Doanh et al. 2006; Lancelot et al. 2006; Amat 2007; Bouferra et al. 2007; Andrade & Ellison 2008; Jafarzadeh & Javaheri 2008; Ezaoui & Di Benedetto 2009; Lins 2009; Alabdullah 2010; Doanh et al. 2010; Doanh et al. 2012; Hareb & Doanh 2012; Ping et al. 2014).

Hostun sand is originally obtained from a place called Hostun in the area of Drôme in the southeast part of France. The color of Hostun sand may vary between the gray-white to the rosy-beige. The chemical components consist of high siliceous amount ($\text{SiO}_2 > 98\%$) and the grain shape varies from angular to sub-angular (Amat 2007). Table 4.1 illustrates the mineralogy of Hostun sand after Gay et al. (2003).

Hostun Sand is poorly-graded sand with grain sizes range from 0.1 mm to 1.0 mm in diameter. According to the United Soil Classification System (USCS), it is classified as poorly graded sand (SP). It has a coefficient of uniformity value, $C_u = 1.72$ and coefficient of curvature value, $C_c = 1.05$. Table 4.2 summarizes the soil mechanics properties of Hostun sand.

The saturated hydraulic conductivity of the sand is required for the experimental testing program and to compute the unsaturated hydraulic conductivity curve from the soil-water characteristic curve using the indirect method. The saturated hydraulic conductivity was determined using the constant head permeability test (Lins et al. 2002; Lins & Schanz 2005). The saturated hydraulic conductivity for a loose specimen ($e = 0.89$) is $k_s = 2.75 \times 10^{-4}$ m/s and for a dense specimen ($e = 0.66$) $k_s = 2.03 \times 10^{-4}$ m/s.

Table 4.1.: Chemical composition of Hostun sand after Gay et al. (2003)

Material	Percentage [%]
SiO_2	99.17
Flammable compounds	0.55
Al_2O_3	0.25
TiO_2	0.01
Fe_2O_3	0.17
CaO	0.14
MgO	0.14
K_2O	0.02
Na_2O	0.05

Table 4.2.: Basic soil mechanic properties of Hostun sand (current study)

Property	Value
e_{\max} [-]	0.66
e_{\min} [-]	0.89
Specific gravity G_s [-]	2.65
D_{10} [mm]	0.21
D_{30} [mm]	0.29
D_{50} [mm]	0.36
D_{60} [mm]	0.4
C_u [-]	1.72
C_c [-]	1.05
Classification (USCS)	SP

4.2.2. Silver sand

The name of the silver sand originated from its mining area, close to the lake "Silbersee" near Haltern, Germany. It is a Quartz sand with rounded grains in a grain size range of 0.06 mm to 0.71 mm. Table 4.3 shows the parameters for silver sand (Röchter 2011). Figure 4.1 shows the grain size distribution curve of both Hostun sand and Silver sand.

Table 4.3.: Basic soil mechanic properties of Silver sand (current study)

Property	Value
e_{\max} [-]	0.901
e_{\min} [-]	0.556
Specific gravity G_s [-]	2.65
D_{10} [mm]	0.16
D_{30} [mm]	0.2
D_{50} [mm]	0.23
D_{60} [mm]	0.25
C_u [-]	1.8
C_c [-]	1.0
Classification (USCS)	SP

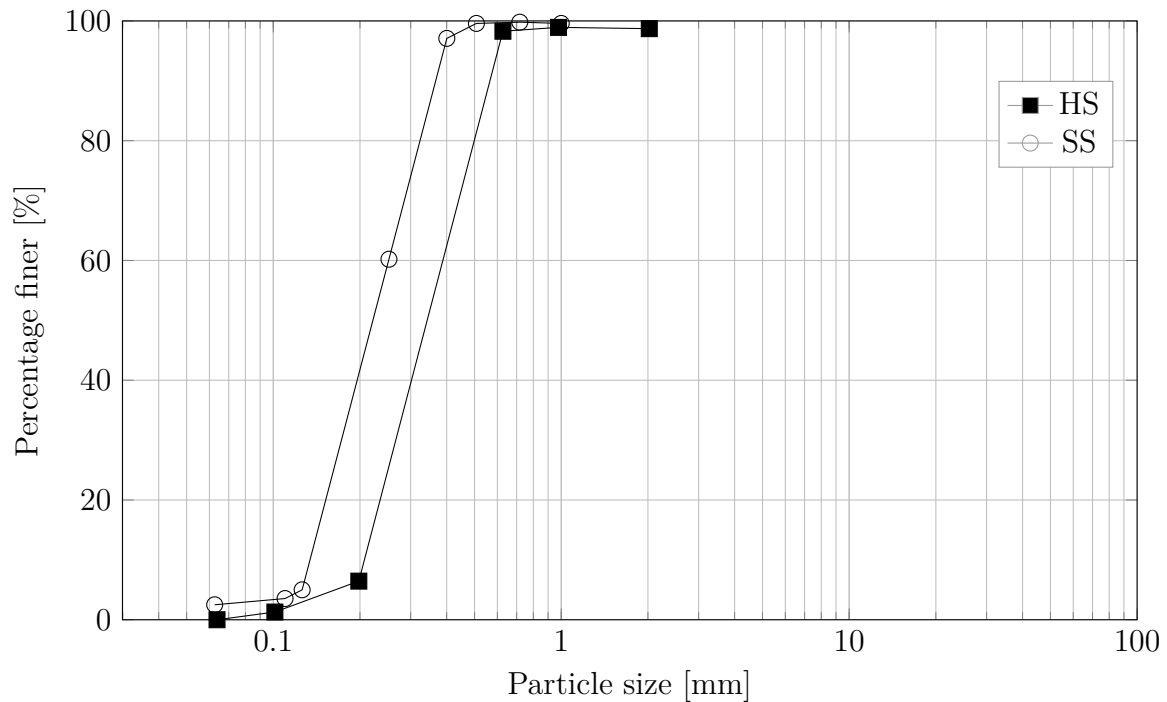


Figure 4.1.: Grain size distribution curves of Hostun sand and Silver sand

4.2.3. Kaolin clay

Kaolinite is a fine-grained clay mineral. It is part of the group of industrial minerals and has the chemical composition $\text{Al}_2\text{Si}_2\text{O}_5(\text{OH})_4$. It is formed when the anhydrous aluminum silicates which are found in feldspar rich rocks, like granite, are altered by weathering or hydrothermal processes.

Kaolinite is a layered silicate mineral, with one tetrahedral layers linked through oxygen atoms to one octahedral sheet of alumina octahedra as shown in Figure 4.2 (Deer et al. (2013)). Table (4.4) summarizes the chemical properties of Kaolin clay.

The Kaolin clay is obtained from the west side of Germany, it has a liquid limit of 49.5% and plastic limit of 32.1% which has a small differences compare to the Spergauer Kaolin studied by Alabdullah 2010; Baille 2014. It is classified according to USCS (Unified Soil Classification System) as (ML & OL) as shown in Figure 4.3. According to ASSHTO soil classification system, the soil classification is A-7-5 (22).

Fine-grained soils with liquid limit equal or less than 50% are considered low to medium compressible soil material (Punmia & Jain 2005).

An investigation to the basic properties of the used material includes the determination of specific gravity, plastic and liquid limits, grain-size distribution, specific surface area, and

compaction characteristics. Table (4.5) summarizes the physical properties of Kaolin clay. The specific surface area (SSA) is the surface area of the soil particles measured in $[\text{m}^2/\text{g}]$. It is also an indicator of the retention and sorption capacity of clays. The SSA was determined using the Ethylene Glycol Monoethyl Ether (EGME) adsorption method (Eltantawy & Arnold 1973, Cerato & Lutenegeger 2002, Yukselen & Kaya 2006, and Jotisankasa et al. 2009). The stepwise instruction is provided in the above-mentioned references. The SSA of the soil presented in this chapter is $17.8 [\text{m}^2/\text{g}]$ which is the average of the three measurements.

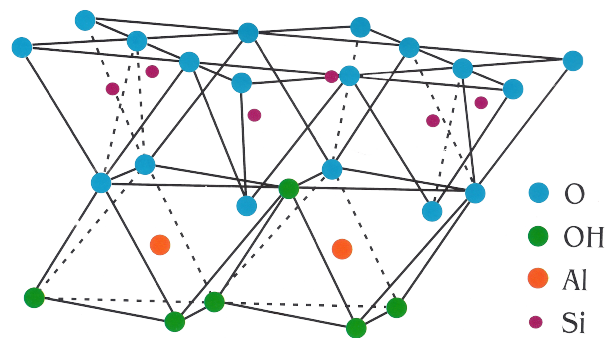


Figure 4.2.: Structure of Kaolinite layer after Deer et al. (2013)

Table 4.4.: Chemical composition of Kaolin clay after (Dana & Dana 1892 and Anthony et al. 2001)

Material	Percentage [%]
SiO_2	45.80
Al_2O_3	39.55
Fe_2O_3	0.57
FeO	0.18
CaO	0.41
MgO	0.14
K_2O	0.03
H_2O^+	13.92
H_2O^-	0.17

Table 4.5.: Basic soil mechanic properties of the Kaolin clay (current study)

Property	Value
Specific gravity G_s [-]	2.72
Liquid limit LL [%]	49.5
Plastic limit PL [%]	32.1
Plasticity index PI [%]	17.4
Specific surface area SSA m^2/g	17.8
Saturated Permeability k_s [m/s]	$1 \times 10^{-9*}$

* Permeability measured at 95% Proctor density.

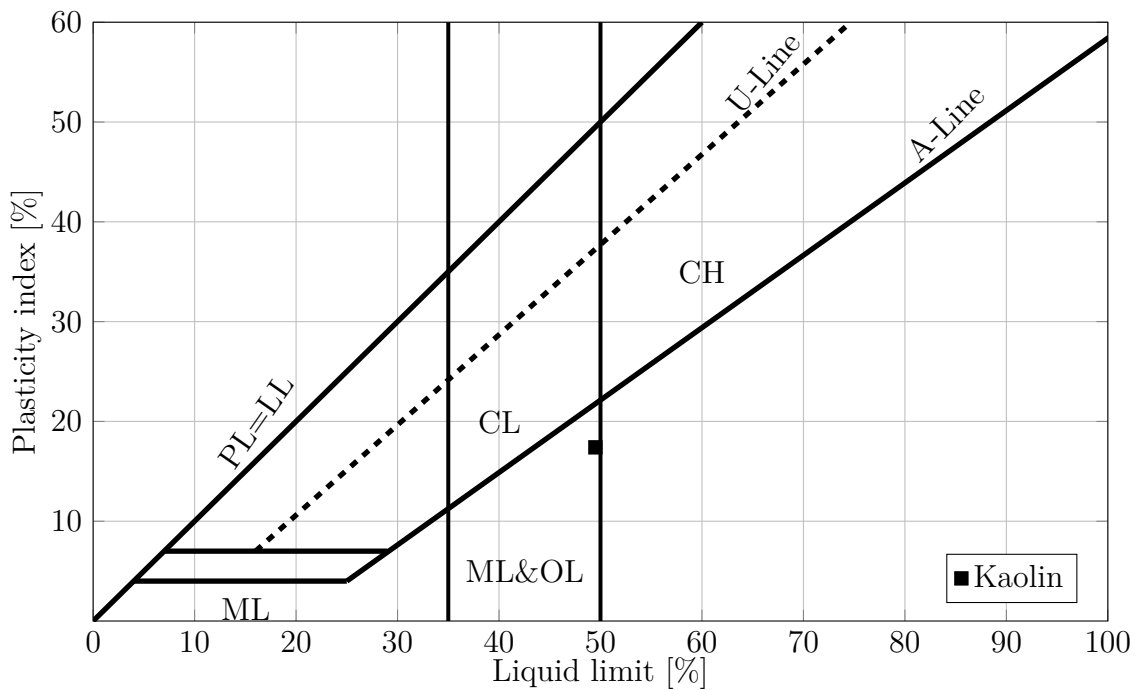


Figure 4.3.: Unified soil classification system plasticity chart

4.2.4. Hostun sand-kaolin mixtures

Three Hostun sand-kaolin mixtures were used in the current study, namely; 90% Hostun sand + 10% Kaolin (10K), 85% Hostun sand + 15% Kaolin (15K), 80% Hostun sand + 20% Kaolin (20K), and 75% Hostun sand + 25% Kaolin (25K).

Figure 4.4 shows the grain size distribution curves for Hostun sand and Kaolin clay determined using the grain size analysis test (ASTM 2006). The standard compaction tests were conducted according to (ASTM D698) using an effort of $600 \text{ kN}\cdot\text{m}/\text{m}^3$ ($594.8 \text{ KJ}/\text{m}^3$). Figure 4.5 illustrates the compaction curves for Hostun sand HS, the soil mixtures 10K, 15K, 20K, and pure Kaolin 100K. The test results show an increase in the maximum dry density with increasing the fines content up to the soil mixture 25%. The fines are filling the void between the soil grains which leads to increasing the density of the soil mixture. Compaction is a process that increases the soil density, accompanied by a decrease in air volume. There is usually no change in water content. The degree of compaction is measured by dry unit weight and depends on the water content and compactive effort (weight of hammer, number of impacts, number of passes). For a given compactive effort, the maximum dry unit weight occurs at an optimum water content. However, in practice, compaction cannot completely eradicate air fraction, only reduces it to a minimum.

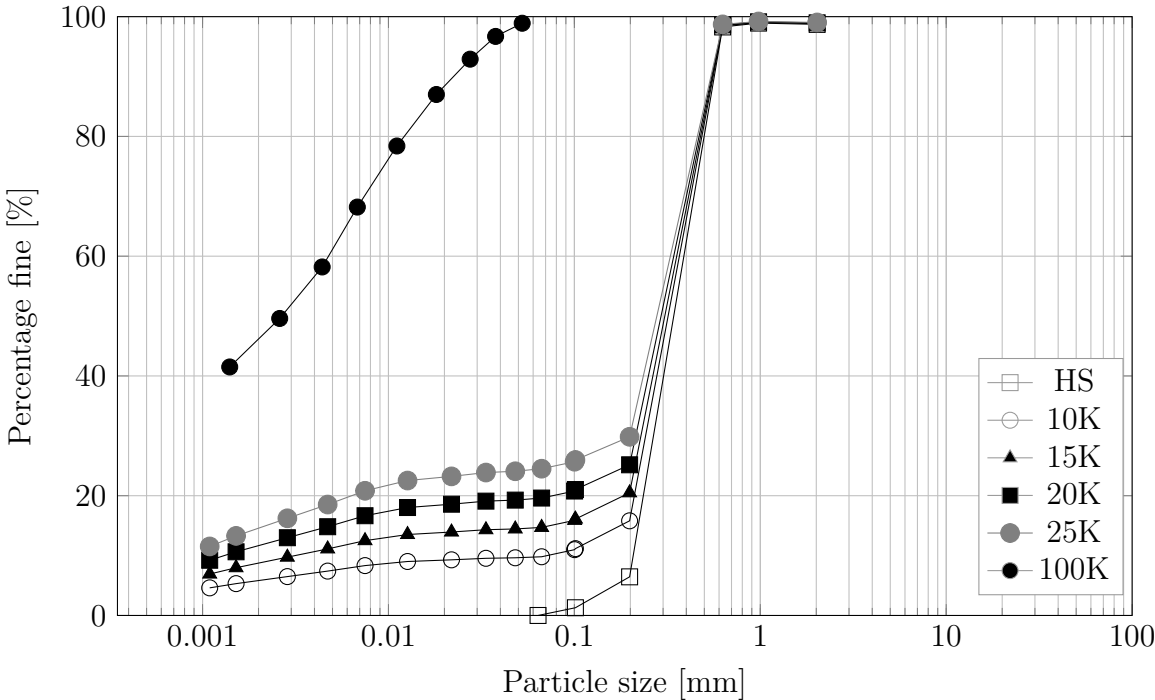


Figure 4.4.: Grain size distribution curves of Hostun sand and kaolin

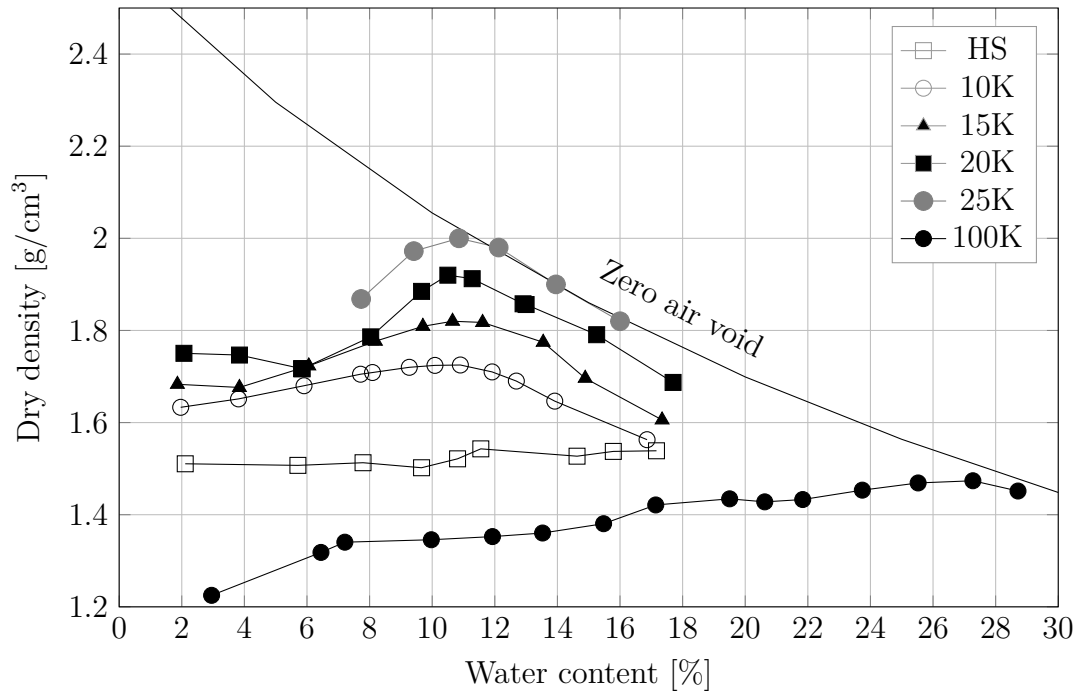


Figure 4.5.: Standard proctor compaction curves for soil mixtures

4.2.5. Soil saturated permeability tests results

In order to define the suitable value of the flow of water in the one-dimensional flow tests and to derive the unsaturated hydraulic conductivity function of the soil mixtures, the constant head permeability test was carried out following the ASTM D2434. Figure 4.6 shows the results of soil HS, 10K, 15K, 20K, 25K, and 100K with other soil mixtures 30K, 40K, 50K, and 60K which were prepared on the maximum dry density and optimum water content as shown in Figure Figure 4.5.

Tests results show that the permeability decreases with increasing the Kaolin content. The fine particles of the Kaolin will fill the voids between the sand coarse particle which lead to reduce the porosity of the soil mixture and thus reduce the hydraulic conductivity.

As stated in Table 4.5 the saturated hydraulic conductivity for Kaolin clay at 95% proctor density is 1×10^{-9} m/s.

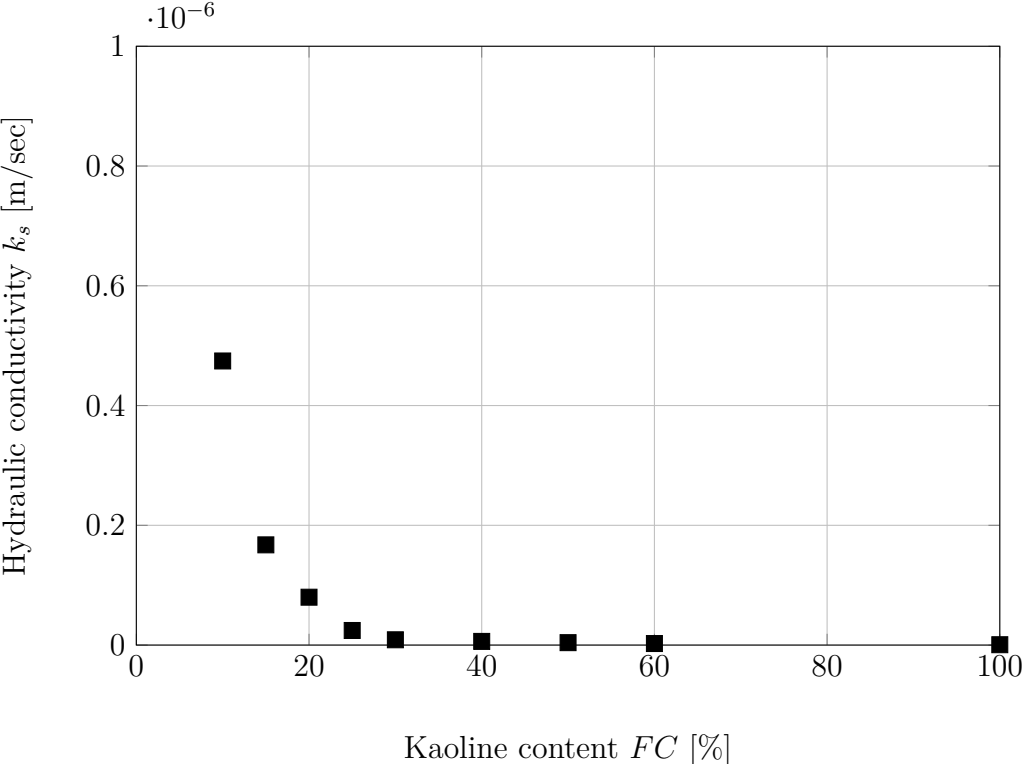


Figure 4.6.: Saturated hydraulic conductivity

4.3. Nonwoven geotextiles

4.3.1. Selected materials and basic properties

The nonwoven geotextile which is mainly used in this study is part of the geocomposite drainage material (geocomposite) produced by company Bonar (the name of this material in the current research will be referred as B). Its commercial name is Enkadrain[®] ZB which consists of geonet (drainage core), which is used to allow the water to flow through it, sandwiched between two polypropylene nonwoven needle-punched geotextiles, one used to drain the water and layers separation while the other is used for separation purposes. The hydraulic properties of the products (Nonwoven geotextile, drainage core, and Enkadrain ZB) are shown in Table 4.6. The geotextile specimens used in the current study were manufactured using polypropylene material. The specific gravity of the polypropylene material as provided by the manufacturer was equal to 0.91. This value is consistent with the specific gravity for polypropylene reported by Koerner (2005) and Ingold (1994). However, three tests were performed to determine the specific gravity of the geotextile following the (ASTM D854) within this study. The average specific gravity of the geotextile was found to be 0.91.

In the current study, the hydraulic interaction between the nonwoven geotextile and soil is studied. Due to this the further investigation of the properties of the other parts of the geocomposite is not needed.

For discussing the variation of GWCC with changing AOS and hydraulic conductivity function of different nonwoven geotextiles additional nonwoven geotextiles are used in this study. The properties of these materials are given in Table 4.7. Tables 4.7 presents the

Table 4.6.: Properties of the geocomposite drainage layer *

<i>Parameter</i>	<i>Symbol</i>	<i>Unit</i>	<i>Average</i>	<i>Minimum value</i>
Nonwoven Geotextile				
Layer thickness	d_v	mm	2.0	1.8
Mass per unit area	M_A	g/m ²	200	190
Tensile strength (MD)	-	kN/m	11	9.5
Elongation (MD)	-	%	60	75 (max)
Apparent opening size	O_{90}	μm	80	110 (max)
Water permeability	K_s	mm/s	80	60
Drainage Core				
Layer thickness	d_{DK}	mm	5.7	5.4
Mass per unit area	M_{DK}	g/m ²	500	492
Enkadrain[®] ZB				
Layer thickness	d	mm	8.7	8.0
Mass per unit area	m	g/m ²	900	870

* All parameters are provided by the manufacturer (Bonar©)

hydraulic properties of other nonwoven geotextile products which are tested in the current study to determine the geotextile-water retention curve.

Table 4.7.: Properties of the nonwoven geotextile layer specimens *

Material	Thickness	Mass per unit area	Tensile strength	AOS	Permeability
Symbol	d_v	M_A	-	O_{90}	k_s
Unit	mm	g/m^2	kN/m	μm	mm/s
N1	0.7	130	16	90	90
N2	2.2	180	20.7	120	10
T1	0.6	90	16	180	130
T2	0.72	120	20.7	150	100
T3	1.4	330	20.7	85	85
F1	0.7	85	16	180	130
F2	0.72	93	15.5	150	100
F3	0.8	105	17.4	110	85
F4	0.93	112	21	90	88
F5	1.1	112	22	85	95

* All parameters are provided by the manufacturers

4.3.2. Apparent opening size

Apparent opening size (AOS) is a geotextile property, which indicates the diameter of the approximate largest particle that would effectively pass through the geotextile. At least 95% of the openings apparently have that diameter, or are smaller, as measured by the dry sieve test (ASTM D-4751).

The test uses known-diameter glass beads or soil particles of a wide particle size. The test can be performed dry or by flowing water to ensure a better distribution of the beads/soil particles around the geotextile sample.

Figures 4.7 and 4.8 present the apparent opening size curves for different nonwoven geotextiles. The curves were compared with the material used in the current study as main material (Bonar). The tests were performed at the laboratories IRSTEA (France) and Huesker (Germany).

There is an objective in the current study to select geotextile specimens which have different AOS values (O_{90}), these materials will be compared between each other to verify the approach to determine the GWCC of the geotextile using the properties of the geotextile material.

Figure 4.9 shows the grain size distribution curves of the three selected mixtures and Hostun sand together with the boundaries given by the supplier of the geotextile product

(B), which is used later in the column tests. In case the grain size distribution of the soils are between the given boundaries, the hydraulic (permeability) and mechanical (retain) stability of the system are assured. Also, criteria presented in Equations 2.4 and 2.5 are fulfilled.

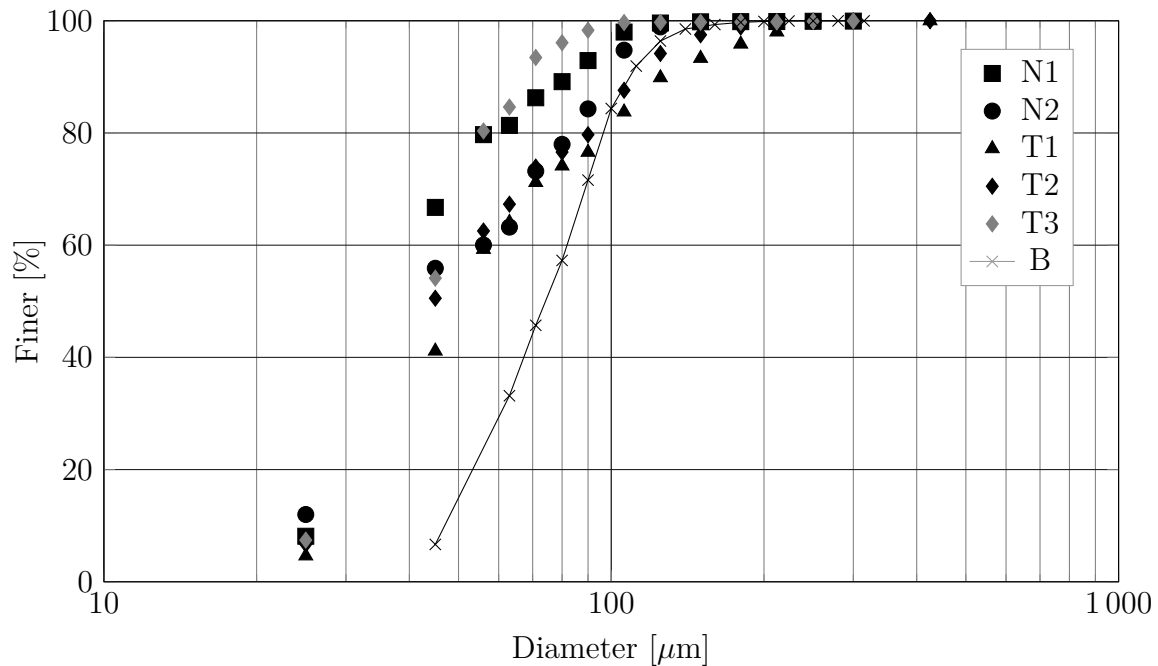


Figure 4.7.: Apparent opening size curves for different nonwoven geotextiles (IRSTEA)

4.4. Experimental program

As it has been described earlier, in order to understand the effect of the partially saturated condition on the hydraulic flow of water through the nonwoven geotextile and the change in shear strength with different water contents, an experimental testing program is needed to be established so that adequate parameters are collected and the phenomena of the capillary break can be observed.

Aside from the the primary and prerequisite tests and observations explained above, the laboratory testing program consists of investigating the effect of capillary forces on soil mixtures, geotextile, and soil/geotextile specimens. The determination of soil-water retention curves, the shear strength parameters using modified direct shear device for Hostun sand, soil mixtures 10K and 15K. The compressibility of geotextile sample under unsaturated conditions was also investigated. The results will help to understand the behavior of the nonwoven geotextile material under vertical stresses (overburden pressure) with different saturation conditions.

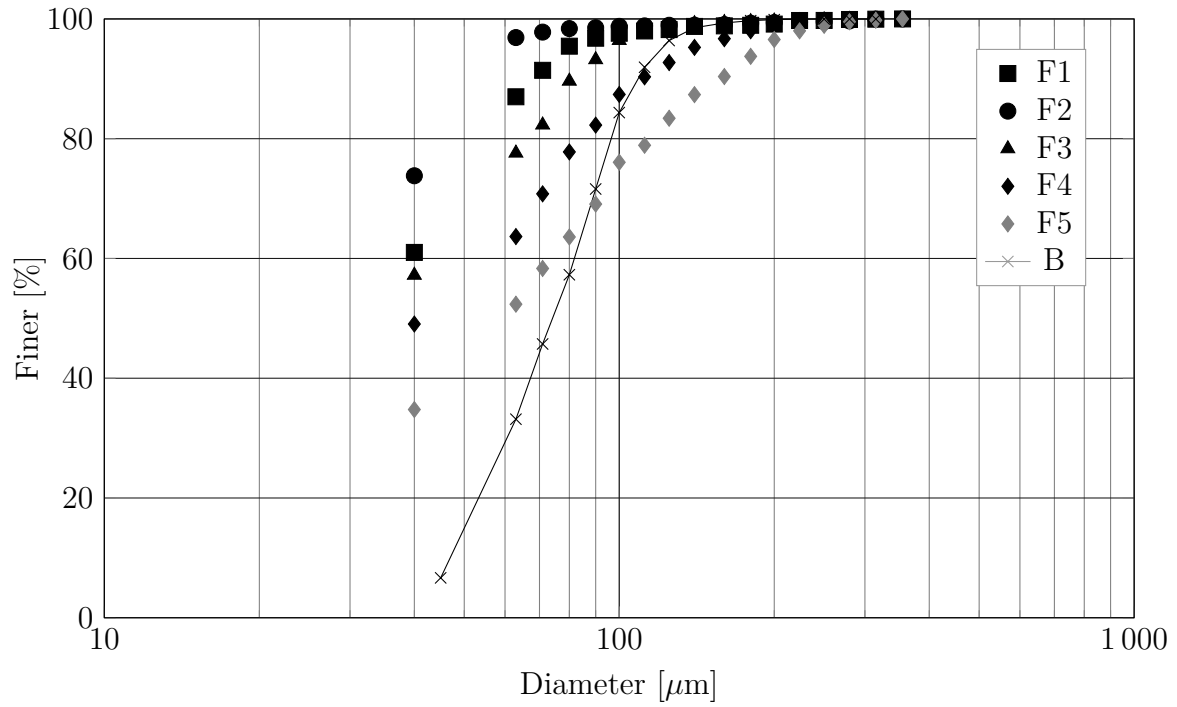


Figure 4.8.: Apparent opening size curves for different nonwoven geotextiles (Huesker)

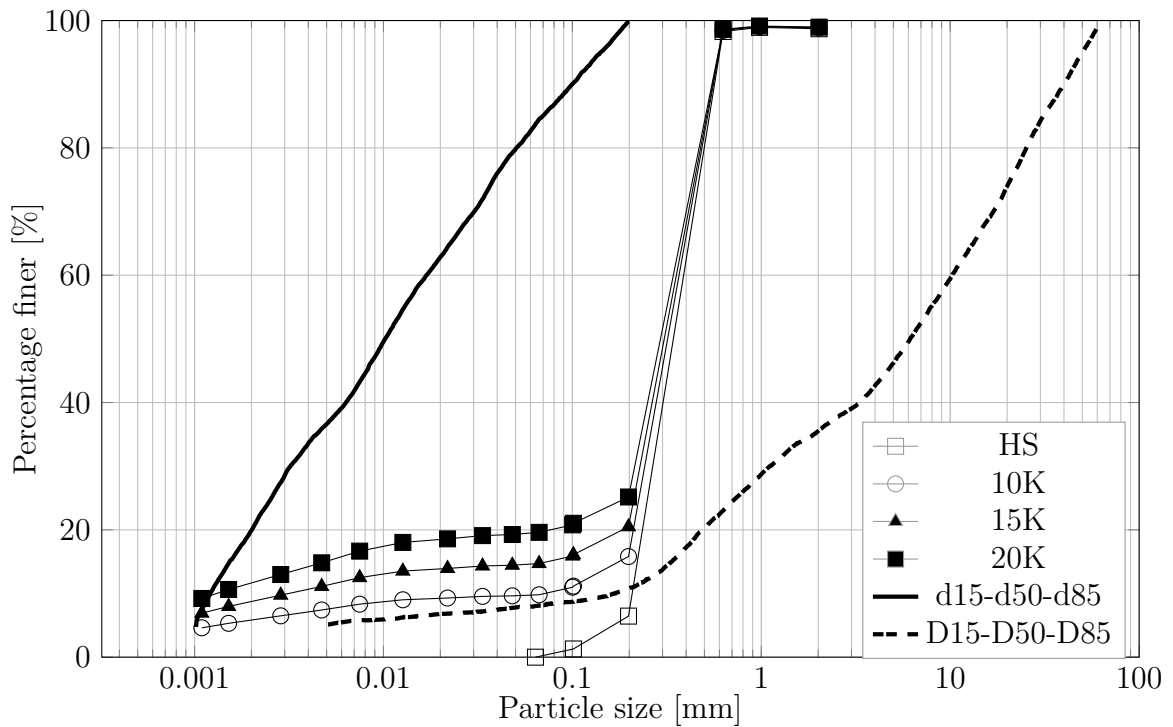


Figure 4.9.: Grain size distribution curves for the soil mixtures within filter stability curves

Finally, one-dimensional flow of water tests through a column of soil and a horizontal layer of geotextile have been performed for different mixtures.

In all tests, the soil specimens were prepared initially with void ratio and water content as summarized in Table 4.8. The soil specimens, later, were saturated and then desaturated to reach the target suction for the SWCC or direct shear tests. To make sure that the samples were fully saturated, they were placed over saturated porous stones and covered with nylon foil. After a few days in these conditions the samples reached constant weights. These weights were supposed to be equal to the pre-calculated weight of saturated samples, and as such they were assumed to be fully saturated.

SWCC is the most essential and important parameter to study the soils under partially saturated conditions (Fredlund & Fredlund 2012). Series of tests were performed using three different techniques to establish the SWCC; hanging column method, axis-translation technique; and vapor-equilibrium method.

For the soil/geotextile column tests, different sample preparations were examined first; dry pluviation was used method in which the dry mixed sand and kaolin were added to the column and compacted carefully to the desire density as shown in Table 4.7 and later the water was added from the bottom to saturate the soil. The procedure was not useful when increasing the fines content. Because a fully saturated soil was not reached specially near the geotextile layer due to trapped air. In the second method the dry sand and kaolin were mixed in small amounts (≈ 5 kg) and mixed with the optimum water content and then added to the column, which was filled with an amount of water before, in small portions with considering that the water level inside the column should be higher then the soil elevation to ensure a saturated condition. A careful compaction of the soil is necessary to achieve the required density without damaging the electrical equipments connected to the column by this method saturated specimens with the desired density were prepared and this method was used in all column tests.

Table 4.8.: Initial conditions of specimens for the tests

Nr.	mixture	Symbol	e_o	γ_d	wc_i
1	100H:0K	HS	0.66		0.0
2	90H:10K	10K	0.545	1.72	10.9
3	85H:15K	15K	0.462	1.82	10.65
4	80H:20K	20K	0.388	1.92	10.5
5	75H:25K	25K	0.334	2.00	12.0
6	0H:100K	100K	0.86	1.466	27.3

4.5. Summary

In this chapter, the basic properties of the soil materials used in this study were presented, the properties of the nonwoven geotextile material, and the design qualifications proposed to determine the suitable type of soil for certain nonwoven geotextile which can assure a hydraulic and mechanical stability for filter materials. The initial properties (void ratio and water content) of the soil mixtures were presented.

5. Soil & geotextile water-characteristics and permeability relationships

5.1. Introduction

In this chapter the techniques and equipments which are used to determine the water characteristics curve of the soils and geotextile are presented. The oedometer device to determine the water characteristics curve of the geotextile material under vertical loads is also presented. The soil-water characteristics curves results, which are a function of volumetric change during mean drying and wetting of sand HS and soil mixtures 10K, 15K, 20K, 25K and 100K are presented. The details of the SWCC are presented in appendix A. The water characteristics curves of geotextiles in different conditions and under applied vertical stresses are illustrated and discussed.

The objective of this chapter is to determine the SWCC and GWCC which will be used to analyze the one-dimensional infiltration tests in the next chapter and to explain the change in the shear strength parameters with changing the suction. Studying the effect of suction on geotextiles used for drainage and infiltration have been started since about 20 years. However, a complete understanding to the behavior of such materials is still needed in order to improve their performance in the field under different conditions specially that a small amount of applied suction may significantly affect their hydraulic behavior as it will be discussed in this chapter.

5.2. Techniques and procedures used for SWCC/GWCC tests

5.2.1. Overview

There are several techniques to control the suction for soil and geotextile which have been used in this study depending on the suction range; the hanging column technique HCT (i.e., suction 0-30 kPa, head difference up to approximately 3 meter high), the axis-translation technique ATT (i.e., suction 0-1500 kPa); the vapor equilibrium technique VET (suction \geq 2000 kPa). The ATT is particularly useful for testing specimens with suction values greater than 100 kPa avoiding problems associated with cavitation (Richards 1931; Vanapalli 2008). Also, in this study, the capillary rise method CRM (suction \leq 15 kPa) was used in addition to the hanging column method to determine the water-characteristics curve of the nonwoven geotextile.

The limitation of using the hanging column and the capillary rise methods may be associated to the effect to the difficulties to test a sample longer than 1 meters inside the laboratory.

5.2.2. Pressure plate apparatus following ATT

The pressure plate apparatus as shown in Figure 5.9 following ASTM 2015 consists of an air-tight chamber enclosing a water-saturated porous plate (high-air entry ceramic disk, HAEV), which allows water but not air to flow through its pores. The testing technique was introduced for the first time by Hilf (1956).

The soil sample is placed on the top of the saturated ceramic plate. Three types of ceramic plates were used with different air-entry values AEV, namely; 100, 500, and 1500 kPa depending on the applied air pressure. The use of ceramic plate with a high AEV is not desirable when lower matric suction value is to be applied (Agus 2005). This is due to the fact that the test can run for longer time duration.

The tests started initially from fully saturation of the ceramic disc by placing it under desired water. Afterwards, in order to remove all the air bubbles from inside the ceramic disc, it was subjected to water pressure less than its air-entry value in the pressure plate apparatus. In this way the water followed through the ceramic disc and brought the air bubbles out. This water pressure lasted until no bubbles were seen in the out-flow pipe. Prepared soil specimen were placed on the saturated ceramic disk inside the pressure

apparatus and the tests had been started by creating suction pressure by making a difference between the air pressure and the water pressure. The specimens were weighed frequently until equilibrium occurred. A precision balance with an accuracy of 0.0001 g was used to weigh the specimens. Regular flushing to the water below the ceramic disk is necessary to remove the diffused air bubbles which may cause discontinuity between the water phase in the specimen and the water source.

In this study, the pressure plate apparatus is used to control the suction between 20-800 kPa.

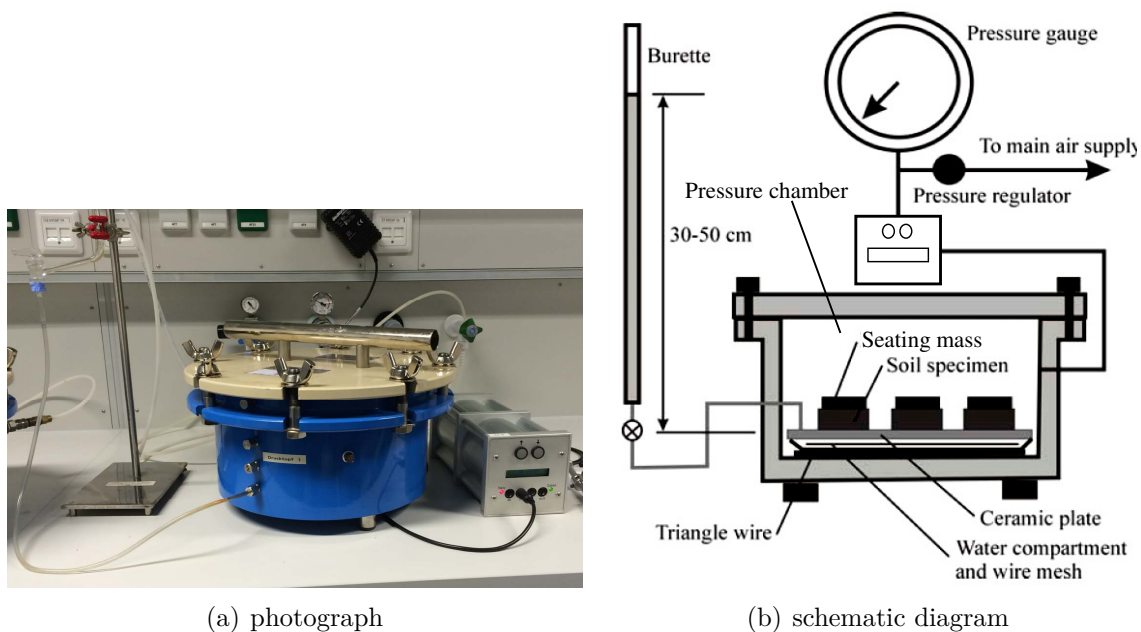


Figure 5.1.: Schematic sketch and a photograph of the pressure plate apparatus

5.2.3. Vapor equilibrium technique VET

The vapour equilibrium technique (VET) has been used by several researchers to control total suction during unsaturated tests (e.g., Cuisinier & Masrouri 2002; Lloret et al. 2003; Blatz & Graham 2003) and to determine the soil-water characteristic curve (e.g., Croney et al. 1952; Agus et al. 2001; Schanz et al. 2004; Alabdullah 2010; Al-Badran 2011; Nguyen-Tuan 2014; Fard 2014).

Figure 5.2 shows the desiccators which were used to apply the vapour equilibrium technique. Group of six large desiccators were used each for different suction value. The desiccators were placed in a temperature-controlled room in which the temperature was kept constant at $22^{\circ}\text{C} \pm 0.5^{\circ}\text{C}$. Aqueous and molal salt solutions using NaCl were prepared according

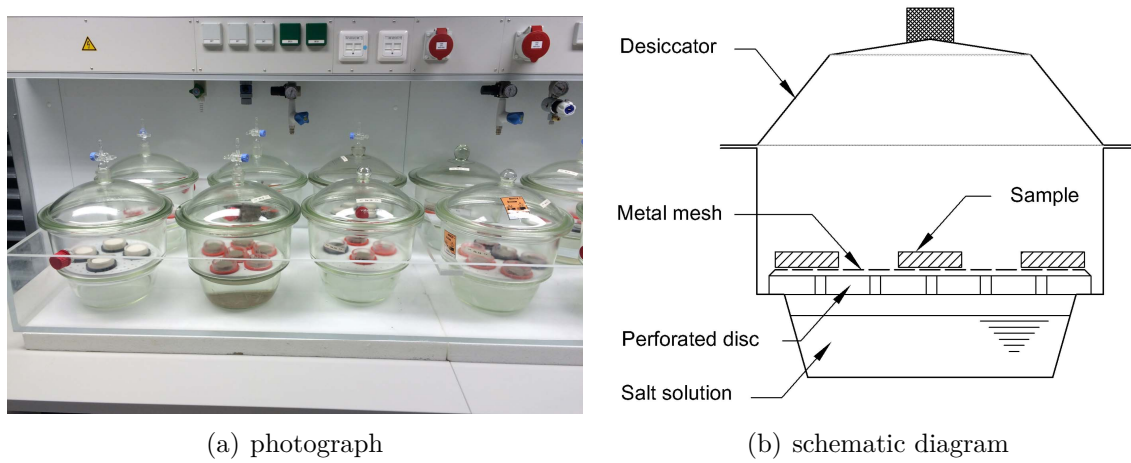


Figure 5.2.: Schematic sketch and a photograph of the desiccators

to equation 5.1 given by Lang (1967) and the data reported by Pitzer & Pelper (1984) with different relative humidity of the vapor space in order to apply different total suction to the soil specimens. The concentrations were verified using chilled-mirror hygrometer technique.

$$s_t = 2 \cdot m \cdot R \cdot T \cdot \phi \quad (5.1)$$

where s_t is total suction [kPa], m molar salt solution [mol/kg], R is the universal gas constant (i.e., 8.31432 J/mol.K), T is absolute temperature in Kelvin, and ϕ is osmotic coefficient.

At the end of each test, the relative humidity of the solution was measured using the chilled mirror technique to compute the final total suction applied to the specimens.

5.2.4. Chilled mirror hygrometer (AQUA LAB)

In this study, the chilled mirror technique was used to determine the total suction of soil specimens and to verify the salt solution which is used in the vapor equilibrium technique. The chilled-mirror used was a water activity meter type 3TE produced by AQUA LAB device, as shown in Figure 5.3. The equipment has a sealed chamber of about 12 cc in volume, where the soil specimen is placed. The sensors in Chilled Mirror apparatus measure the relative humidity of the air in the sealed chamber at a given temperature. The components and principal working of the equipment were described by Leong et al. (2003); Albrecht et al. (2003); and Agus & Schanz (2005b). Agus & Schanz (2007) stated that the technique can be used for suction measurement as low as 1500 kPa if the maximum measurement error is limited to 30%.

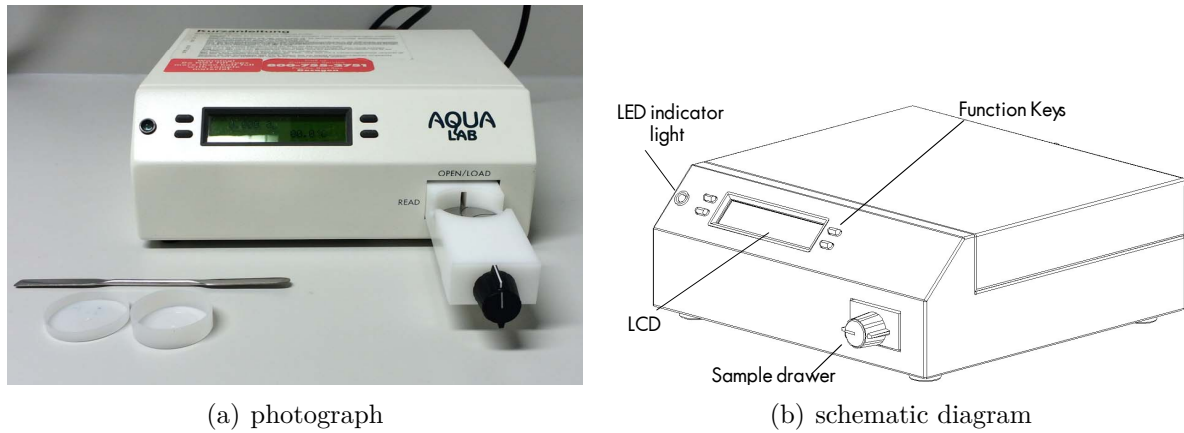


Figure 5.3.: Chilled-mirror hygrometer (AQUA LAB)

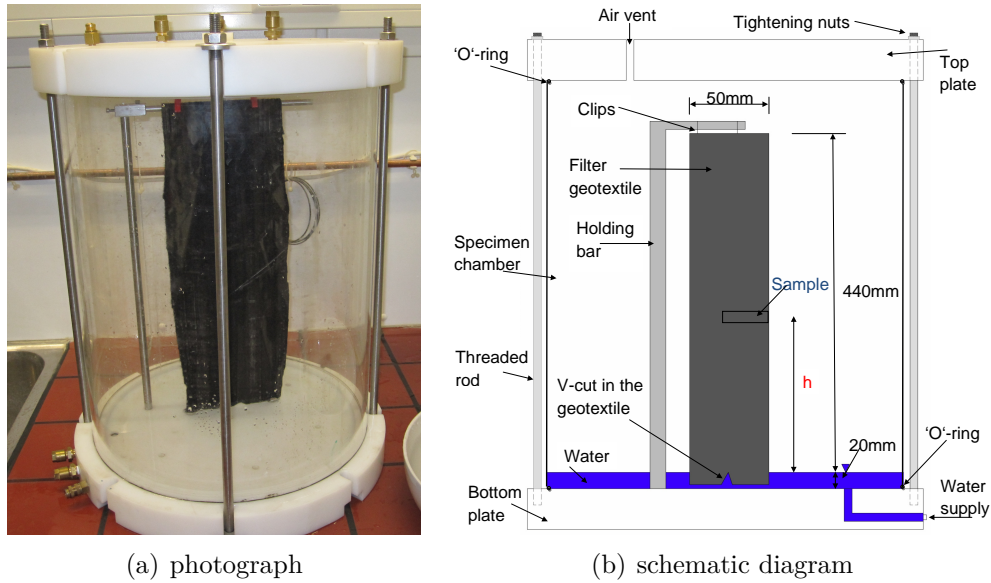
The total suction in the chilled-mirror technique can be calculated using Kelvin equation (Thomson 1871) that is the thermodynamic relationship between total suction and relative humidity of the vapor space in the soil (Sposito 1981):

$$s_t = \frac{R \cdot T}{M_w(1/\rho_w)} \ln\left[\frac{RH}{100}\right] \quad (5.2)$$

where s_t is total suction in kPa, R is the universal gas constant (8.31432 J/mol K), T is absolute temperature in Kelvin, M_w is the molecular weight of water (18.016 kg/kmol), ρ_w is the unit weight of water in kg/m^3 as a function of temperature, and RH is the relative humidity.

5.2.5. Capillary rise method CRM

The capillary rise method is used to determine the GWCC. Figure 5.4 shows the setup for the capillary rise experimental cell. A Plexiglas cell in 500 mm in height and 390 mm in inner diameter contains a holder to hang the geotextile specimen. The cell has a valve to apply water from the bottom and a valve at the top used for air ventilating. Eight tightening nuts are used to lock the cell with the top and the bottom plate. A geotextile specimen 440 mm long and 50 mm wide was used and hanged using plastic clips. About 20 mm of the sample length was submerged inside the water. To determine the drying path of the geotextile-water characteristics curve, the geotextile specimen was saturated prior to the test for 48 hours, while for the wetting curve, an initially saturated and then oven-dried sample at temperature 60 degrees and for 12 hours was prepared. The distribution of gravimetric water content of the geotextile over the height of the sample



(a) photograph

(b) schematic diagram

Figure 5.4.: Capillary rise test apparatus

was measured at the end of each test. The geotextile specimens were cut into small strips 5-10 mm and then placed in the oven at temperature 105° for 24 hours to obtain the water contents. The drying and wetting water characteristics curves were obtained by plotting the volumetric water contents of each strip at different heights against the corresponding matric suctions determined from the elevation of the specimen above the water table. In order to calculate the suction value (for capillary rise test), the suction (ψ) at different heights can be determined from the equation:

$$\psi = h \cdot \rho_w \cdot g \quad (5.3)$$

where (h) is the height of the geotextile sample from the water surface, (ρ_w), water density, and (g) is the gravitational acceleration. For a geotextile, the volumetric water content (θ) can be determined using the following expression:

$$\theta = S \cdot n \quad (5.4)$$

where (S) is the degree of saturation, and (n) is the porosity. The degree of saturation (S) and porosity (n) of the geotextile can be computed using the below equations:

$$n = 1 - \frac{M_A}{t \cdot \rho_f} \quad (5.5)$$

and

$$S = \frac{\omega \cdot M_A}{t \cdot n \cdot \rho_w} \quad (5.6)$$

where (M_A) is the mass per unit area, (ρ_f) is the fibre density, (t) is the specimen thickness, (ω) is the water content, and (ρ_w) is the density of water.

5.2.6. Hanging column technique HCT

Perhaps Buckingham (1907) was one of the earliest researchers who used the hanging column technique (i.e., negative water column) by studying the relationship capillary potential and water content (Barbour 1998; Narasimhan 2005).

The hanging column method is used to apply suction in the range 0 - 80 kPa (ASTM 2002). It was used in this study to determine the water retention function of the nonwoven geotextile in the cross-plane direction and also of the soils for suction range between 0-30 kPa.

The salient features of the apparatus and the testing assembly are schematically shown in Figure 5.5. The cell can accommodate a sample of 60 mm diameter and maximum height of 20 mm. The cell consists of three layers built from Plexiglas. Three screws are joining the three parts to each other and the joints are sealed by O-rings. A high-flow ceramic porous stone (60 mm in diameter and 7.14 mm in thickness), having a saturated permeability, K_s , of 7.56×10^{-7} m/s with an air entry pressure value of 100 kPa, is seated on the lower part which is attached to two connections to control the water pressure in the specimen. Figure 5.5 shows a cross-section through the cell layout.

A 25 ml burette acting as a constant head reservoir was connected by 8 mm tubing to the cell from the top and bottom. Prior the test, the porous ceramic disk was saturated and flushed to remove the air bubbles and connected to the water reservoir in the burette. A geotextile specimen with diameter 60 mm (weighting between 0.5-0.7 g) was first saturated for 48 hours and then seated on the saturated porous ceramic disk. A stainless steel mass of 117 g containing holes, to allow the air to pass through, was placed above the geotextile specimen to achieve hydraulic contact between the geotextile specimen and the ceramic porous plate (Stormont et al. 1997). After saturating the geotextile sample, suction will be changed by lowering the water level in the burette in increments of 0.02 kPa until reaching the equilibrium in each step. In order to prevent any loss in the volumetric water content due to weighting the specimen on a balance, the volume of water coming out from the sample towards the burette was measured. As the mass of the water at initial state is known as well as the weight of the dry sample.

Plexiglas cells used to determine the water retention curve of the geotextile. Geotextile specimens were prepared inside the cell which has 1-bar ceramic disk. After saturating the sample suction was applied by lowering the water level in the burette until reaching equilibrium. Suction was applied to the sample using hanging column method (Haines 1930).

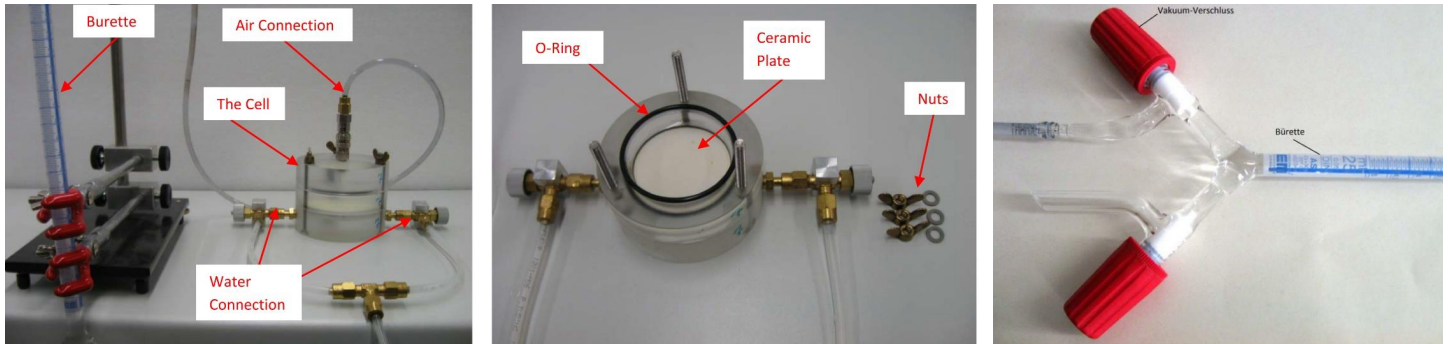


Figure 5.5.: Hanging column test apparatus

5.3. Modified pressure plate (MPP)

The modified pressure plate apparatus, also known as black cell (due to its color), was used to determine the stress-strain curve for nonwoven geotextile under controlled suction. It has been used by Lins (2009); and Al-Badran (2011).

A detailed scheme of the cross section of the apparatus is given in Figure 7.1. It has a specimen ring with diameter of 70 mm and height of 20 mm. A coarse porous stone is placed on the top of the soil specimen and a ceramic disk is placed at the bottom of the specimen. The ceramic disk used below the soil specimen in this study has an air-entry value of 100 kPa. There is the possibility to replace this ceramic disk by a ceramic disk with an air-entry pressure of 500 kPa or a porous stone for performing conventional saturated tests (Lins 2009). Below the ceramic disc a water reservoir is located. A burette with a capacity of 25 cc and a least count of 0.05 cc is connected to this water reservoir. Net stress is applied to the specimen by placing the cell in an oedometer loading frame. Volume changes of the specimens are measured by an attached dial gauge.

In order to fill the specimen room inside the cell, ten layers of geotextiles were placed over each other. The geotextiles were saturated outside the cell and then again inside the cell to ensure no air bubbles were trapped between the layers.

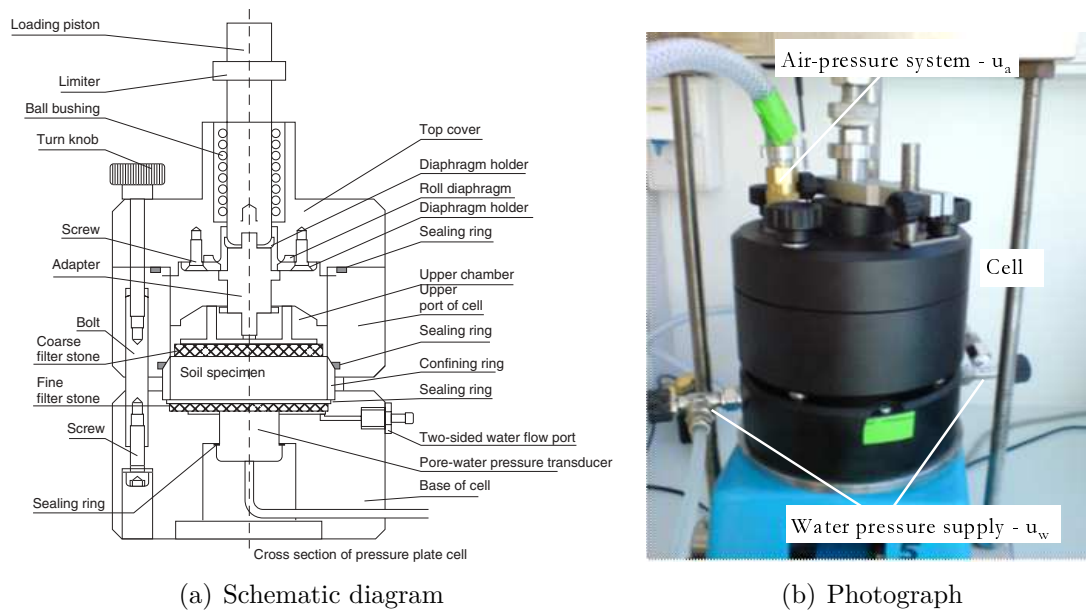


Figure 5.6.: Modified pressure plate after Fredlund & Fredlund (2012)

5.4. Performed experiments to determine soil-water characteristics curves

In the next section, SWCCs of the different mixtures are presented which determined by the experimental procedures described previously.

The water-retention curves were fitted using the empirical model proposed by Fredlund & Xing (1994). This model is also used to establish the hydraulic conductivity-suction relationship based on the saturated hydraulic conductivity of the soil. Table 5.1 presents the tests of the SWCC for each soil mixture.

Table 5.1.

Suction range to determine SWCC				
Nr.	Test	Symbol	Material(s)	Suction range [kPa]
1	Hanging column method	HC	Soil*	0.0 - 15
2	Axis-translation technique	ATT	Soil*	20-800
3	Vapor-equilibrium technique	VET	Soil*	1000-60000

* Soil includes the soil mixtures 10K, 15K, 20K, 25K, and 100K

5.5. Experimental results of the SWCC

5.5.1. SWCC experimental data

Soil water characteristic curves were determined by performing the mean drying and mean wetting paths for four soil mixtures 10K, 15K, 20K, 25K, and 100K. The change of specimen mass with time of selected specimens for drying and wetting paths are shown in Figure 5.7 & 5.8 for different samples tested using the ATT and VET methods, respectively. The soil sample 10K needed less time to reach the equilibrium state and the weight of the sample became stable compare to the soil sample 15K in which the air needs to replace the water in the small inter-particle pores which are relatively larger in the 10K and therefore the time duration needed is longer. In case of the wetting path, the soil sample 15K also needed longer time period to reach an equilibrium state because the water needs longer time to replace the air in the small voids between the soil particles.

Figure 5.9 shows the curves for the different soil mixtures used in this study in term of suction ψ [kPa] versus degree of saturation S_r [%]. The water retention curves for dense Hostun sand were determined by Lins (2009) and were also used in the study by Alabdullah (2010). A details review of the water-retention curves for the soils are shown in Appendix A.

The results show that the SWCC of Hostun sand is steep and covers narrow range of suction (poor graded sand). The SWCC of kaolin covers wide range of suction and has a more curved shape. By increasing the amount of fines content (kaolin), the SWCC of the soil mixtures start to cover the range between Hostun sand and the pure kaolin.

The majority of the pores of Huston sand are drained at a narrow range of suction and show tendency to desaturated with further increase in suction. The pores of pure kaolin are smaller and high suction values are needed to push the water away.

In the next step, an analysis to determine the characteristic parameters of the SWCC such as air-entry value, water-entry value will be presented, and residual suction. Also, the hydraulic conductivity versus suction function will be derived based on existing models.

5.5.2. SWCC experimental parameters

The SWCC parameters were determined following the methods suggested by Fredlund & Xing (1994) (see Figure 5.10):

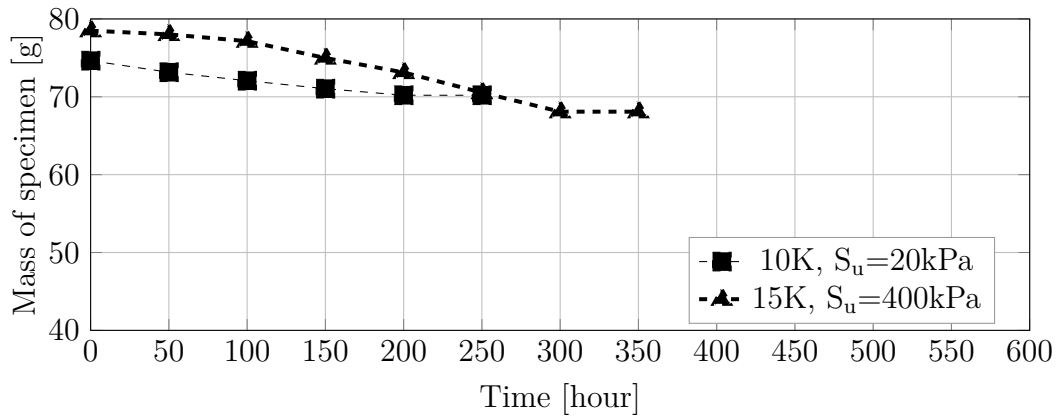


Figure 5.7.: ATT, Drying path

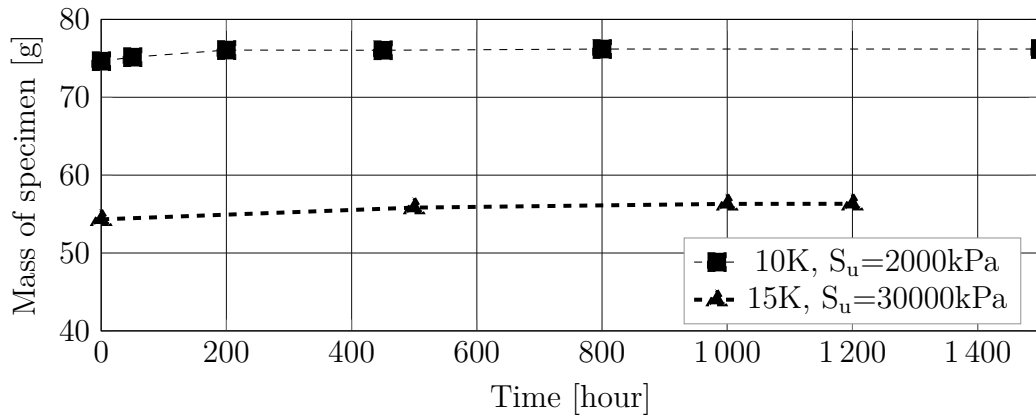


Figure 5.8.: VET, Wetting path

- i **Air-entry value** (ψ_{AEV}) is the value of suction at which air starts to enter the largest pores of the soil during the drainage process. before AEV the soil is assumed to be saturated (e.g. Vanapalli 1996b and Khalili & Khabbaz 1998).
- ii **Residual suction** (ψ_r) is the suction at which the water starts to be held in the soil by adsorption forces (Sillers 1996).
- iii **Water-entry value** (ψ_{WEV}) is the suction at which water starts to enter the smallest pores during the wetting process. The water-entry value corresponds to the suction at which the water content of the soil starts to increase significantly during the wetting process (Yang et al. 2004).

The SWCC parameters of mixtures can be determined from Figure 5.9. Table 5.2 presents the SWCC parameters defined above for the materials used in this research.

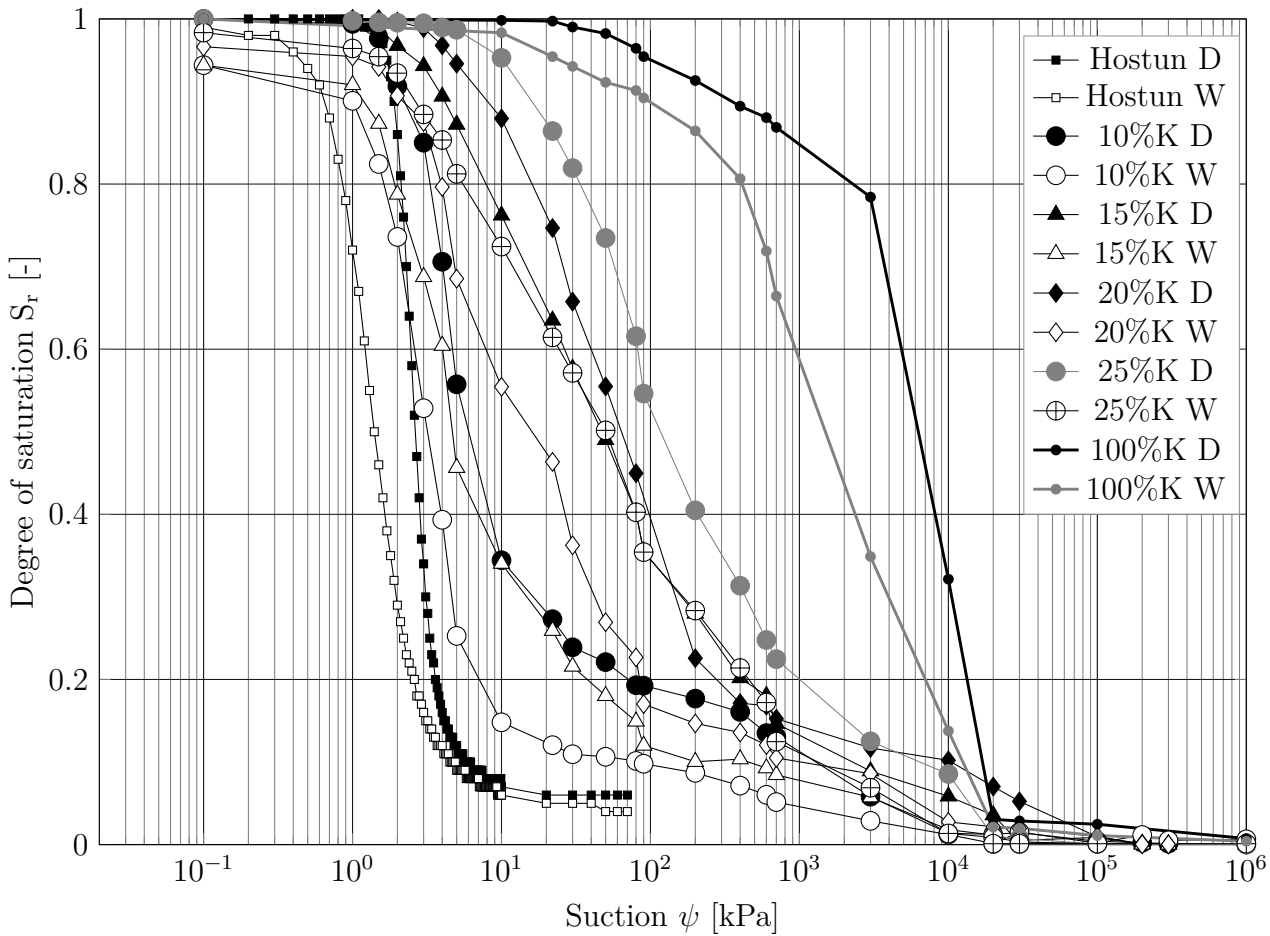


Figure 5.9.: SWCCs of the tested soils in term of mean drying (D) and mean wetting (W)

Table 5.2.: Review of the experimental parameters for the tested soils

Soil type	ψ_{AEV}	S_{rAEV}	ψ_r	S_{rr}	ψ_w	S_{rw}
HS	1.5	98	4.5	13	4.1	9.7
10K	2	97.6	22	25.3	10.3	14.8
15K	3.1	97.1	50	27.45	30	21.8
20K	5.5	96.57	90	33.2	87	22.5
25K	11.2	95.5	600	34.7	200	28.8
100K	3300	78	20000	8	19000	4

5.5.3. SWCC fitting models

Several fitting models or equations have been suggested and developed to simulate the soil-water characteristics curve. Most of the models are based on a best fit to the experimental data. Other models were made based on the soil properties, grain-size distribution curve, pore-size distribution curve.

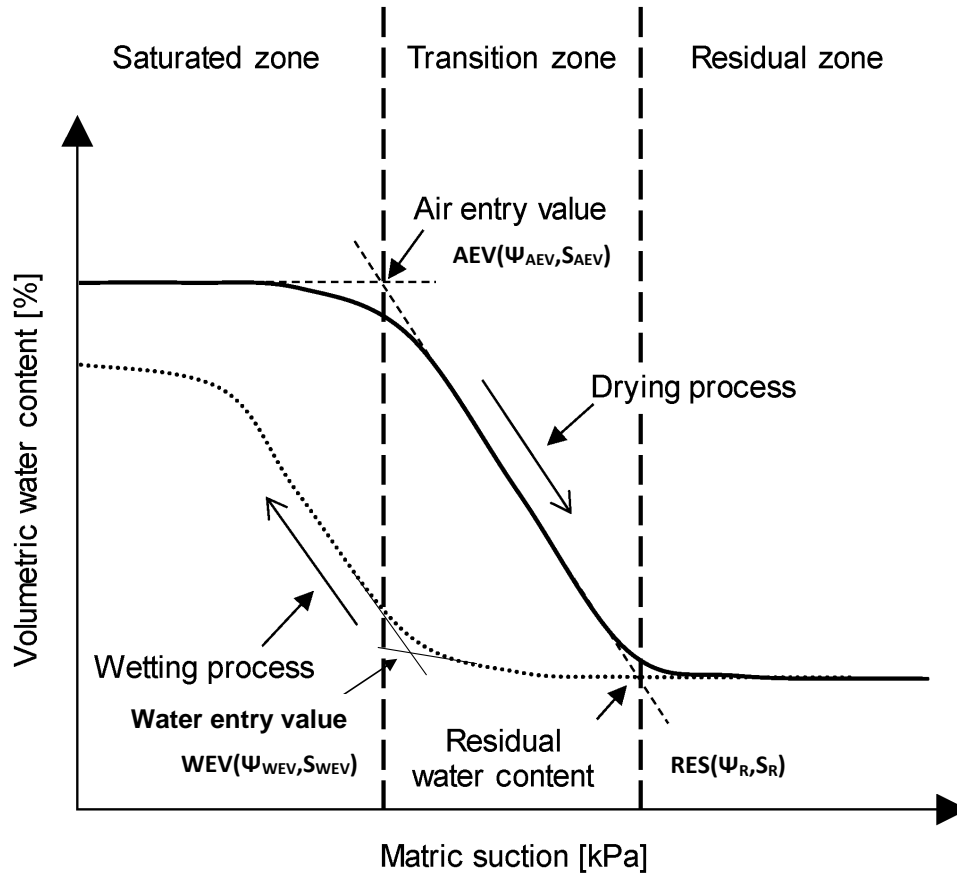


Figure 5.10.: Idealized soil-water characteristics curve after Yang et al. (2004)

The model derived by Fredlund & Xing (1994) is considering the pore-size distribution of the soil. It can assess a reliable closeness to fit many experimental data sets (Leong & Rahardjo 1997; Sillers 1996; Sillers & Fredlund 2001; Fredlund & Fredlund 2012):

$$S_c = C(S) \frac{1}{\left(\ln\left[e + \left(\frac{\psi}{\alpha}\right)^m\right]\right)^n} \quad (5.7)$$

$$C(S) = 1 - \frac{\ln\left(1 + \frac{\psi}{\psi_r}\right)}{\ln\left(1 + \frac{1000000}{\psi_r}\right)} \quad (5.8)$$

The coefficient $C(S)$ is used in the equation to give a zero volumetric water content at a suction of 1000 MPa which approximately corresponds to the oven-dried condition of the soil. The fitting of the SWCCs are used later to derive the hydraulic conductivity - suction relationships. The measured and fitted SWCCs are presented in Appendix A.

5.5.4. Hydraulic conductivity function

Several indirect methods (Fredlund & Xing 1994, Leong & Rahardjo 1997, Agus et al. 2003) can be used to determine the unsaturated hydraulic conductivity function. These methods may be based on empirical models, macroscopic models, and statistical models (Mualem 1986). In this study, the model by Fredlund & Xing (1994) is used to determine the hydraulic conductivity function based on the saturated hydraulic conductivity of the soil as shown in Appendix A.

The hydraulic conductivity becomes smaller with increasing the fines content however, the continuous phase stills for higher suction value and thus the the soil mixture is still more permeable compare to the mixtures with smaller fines content.

Figure 5.11 presents the fitted relative hydraulic conductivity curves for HS, 10K, 15K, 20K, 25K, and 100K using the model based on Fredlund & Xing (1994).

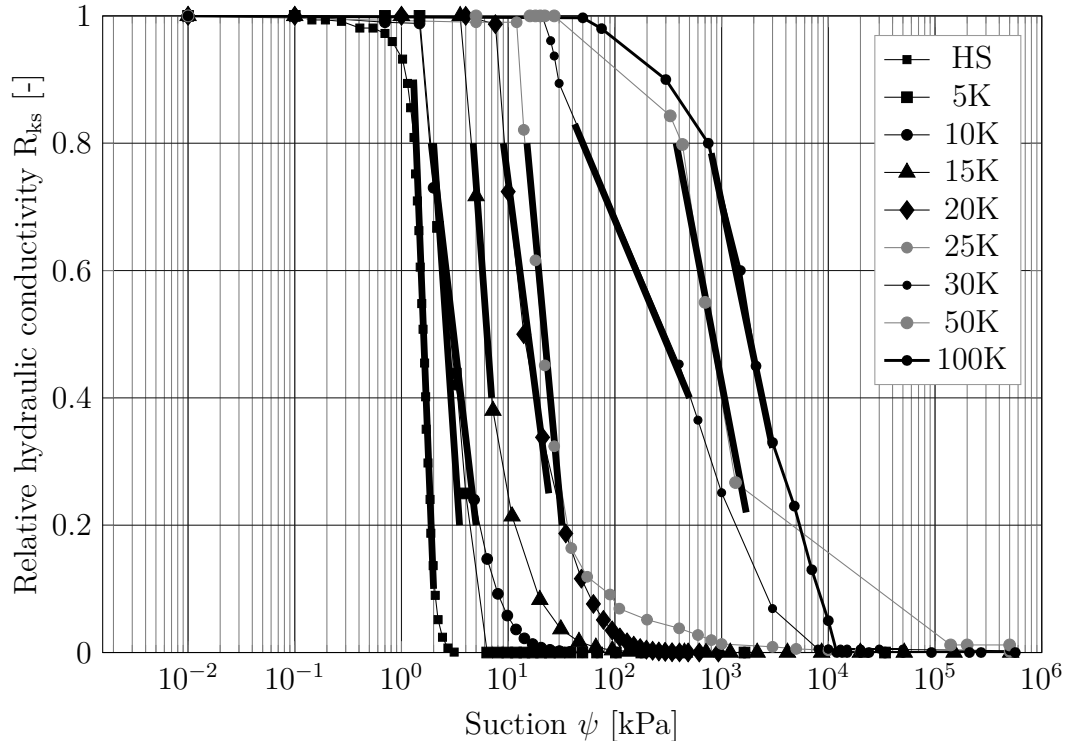


Figure 5.11.: Relative permeability function vs suction for the soil mixtures (drying curves)

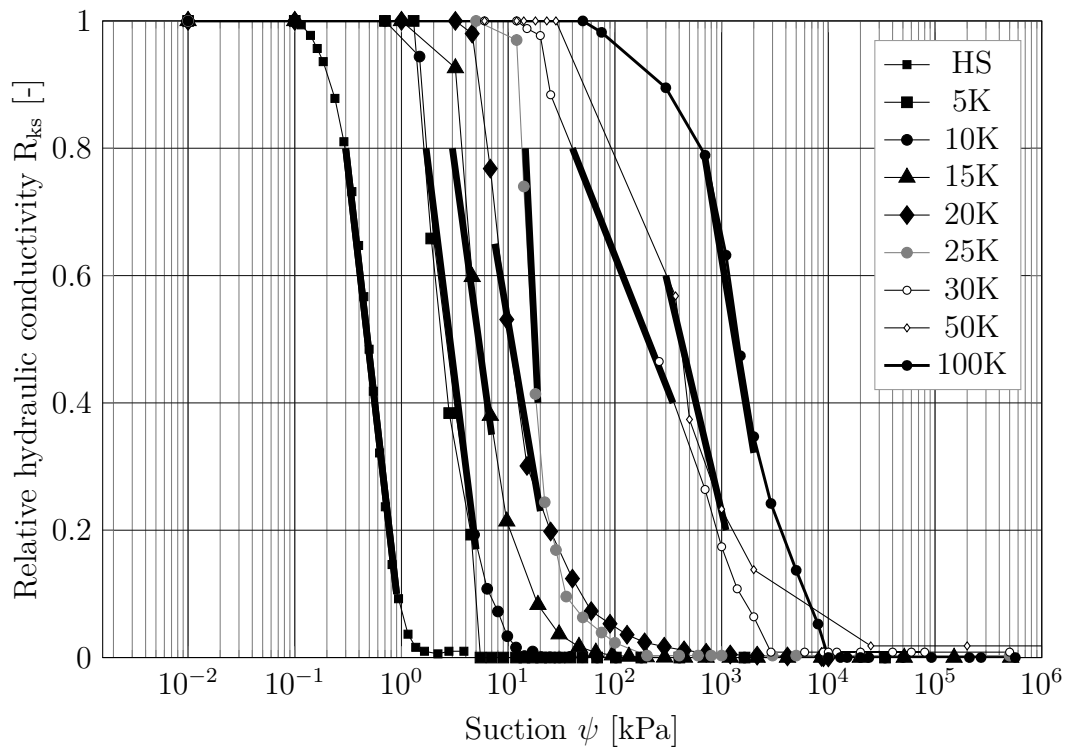


Figure 5.12.: Relative permeability function vs suction for the soil mixtures (wetting curves)

5.5.5. Influence of FC on SWCC and hydraulic conductivity function

Figure 5.9 shows the SWCCs of the pure sand HS, sand-kaolin (10K, 15K, 20K, 25K) mixtures and 100K. The curves cover wide range of suction values. Test results presented by Stoicescu et al. (1998) on sand-Bentonite mixtures performed using multiple apparatuses to measure the soil-water characteristic curves showed no effect on the results.

It can be seen that with increasing the kaolin content, the SWCC curves are shifted to the right direction (to the direction of pure kaolin), also an increase in water retention capacity is significantly observed (increasing the air-entry value AEV and residual suction values). This is due to the presence of smaller pore size developed as a result of filling the small pores between sand grains with with smaller kaolin grains. It is also observed, that adding kaolin to Hostun sand causes the pore-water to remain within the sand mass until increasing in the suction values (Stoicescu et al. 1998). When small increase in the suction value, water can be spilled out from the larger voids between sand grains. With further increase in the suction, the water can be pushed from the smaller voids. With increasing the fines content, the kaolin grains will effect on the ability of the soil to hold water with higher suction compare with the soil mixtures with fewer fines content. In case of pure

sand, one pore size is dominating, also for pure kaolin, while for soil mixtures, a double porosity material will exist.

When adding water to the soil during the wetting path, an the fine material will hinder the water from flowing through the small pores which will lead to a delay to reach the water-entry value for soil mixtures with higher kaolin content.

The SWCCs have a gradual sloping curve at low suction values (0.1 to 10-100kPa) and then a sharp dropping curve at higher suction values. The pore-water was trapped in the inter-aggregate and intra-aggregate pores.

Following the concept of fines content by Thevanayagam (1998), the threshold value of the current mixture is determined from maximum void ratio tests and proctor tests to 25% as shown in Figure 5.13. It is predicted with increasing the kaolin content more than 25%, the SWCC will change in the shape to look similar to the one of pure kaolin.

In Figures 5.14 and 5.15 show the SWCC curves for both drying and wetting curves, respectively including the tests results performed by Alabdullah (2010) for the soil mixtures 30K and 50K. In the figures the tangents of the measured SWCC are marked.

Figure 5.16 summarizes the inclinations of the SWCCs of soil mixtures (inclinations of the tangents marked in Figures 5.14 and 5.15). It is observed that with increasing the fines content, the inclination of the SWCC (tangential) is reducing until reaching 25% fines content which is the threshold value of this soil mixture. The inclinations of the SWCCs for the drying and wetting paths are similar. After the threshold value, the inclination of the SWCC stays nearly constant with increasing the fines content.

Figure 5.17 and 5.18 show the values of the saturated hydraulic conductivity and the

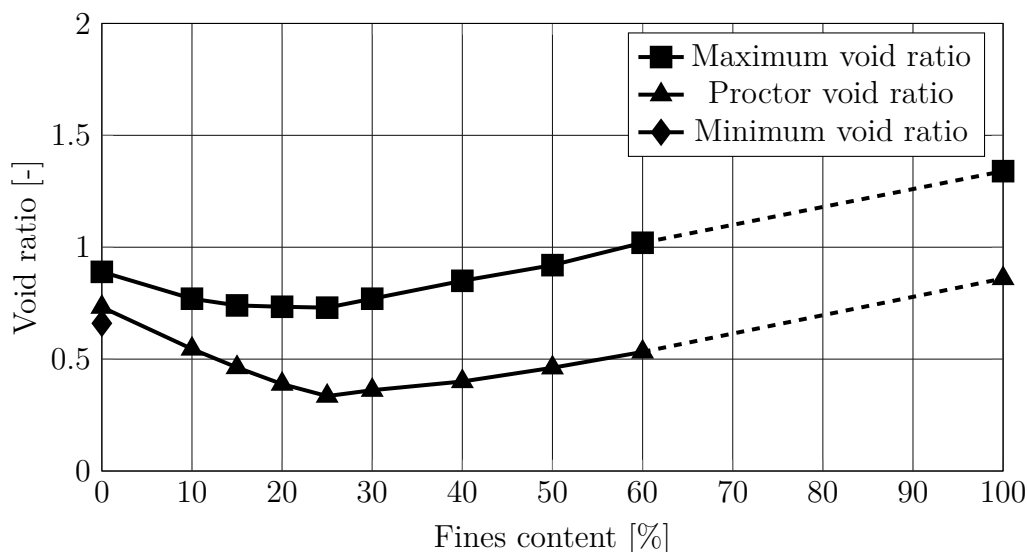


Figure 5.13.: Determination of the threshold value for Hostun sand-kaolin mixtures

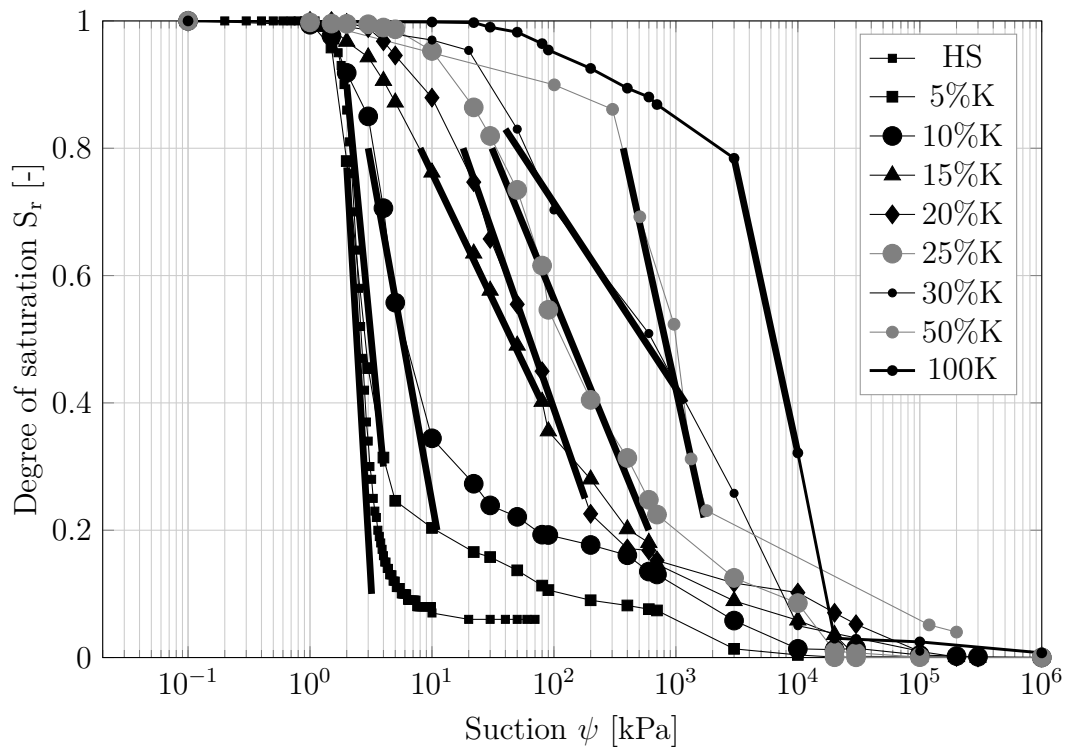


Figure 5.14.: SWCCs of the tested soils in term of mean drying curves

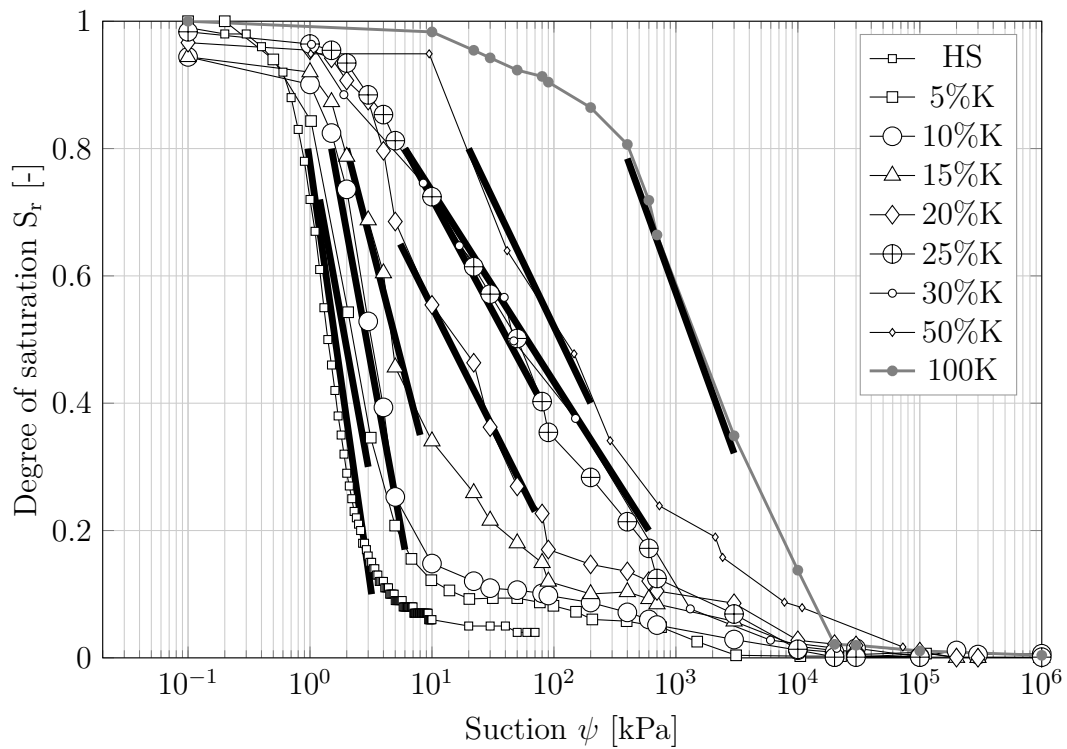


Figure 5.15.: SWCCs of the tested soils in term of mean wetting curves

hydraulic conductivity at 50% of the degree of saturation vs fines content and the tangential of the hydraulic conductivity curve for different fines contents, respectively. It is to be noted that with increasing the fines content, the tangential of the curves starts to increase up to the threshold value, and then the increase in the tangential will reduce.

Based on the concept of the fines content, the values of the degree of saturation at the residual suction, and water entry value are plotted versus suction for the tested soils as shown in Figure 5.19. As the fines contents increases, the air residual suction values will increase as the fines grains of the kaolin will fill the small voids between the sand particles and thus the suction value needed to expel the water will be higher.

With increasing the fines content above the threshold value (25%), the value of the degree of saturation at the residual suction will tend to reduce. This is because the SWCC of these soil mixtures will occur at lower moist content compare to sand dominant mixtures. kaolinite occurs largely as discrete soil grains and mostly as pseudo-hexagonal, subidiomorphic platy crystals loosely attached to pore walls, or as an intergranular pore fill (Figure 5.20a & b). kaolinite crystals can reduce the intergranular pore volume (Wilson & Pittman 1977) but more importantly can act as migrating fines in the pore system (Neasham 1977). The "discrete particle" kaolinite acts as if they are another sand grain and has little effect on the permeability and the capillary pressure curve.

A large AEV is required for a soil with small pores and micro-scale structure dominated. The difference between drying and wetting narrows with an increase of kaolin content.

The pore-size distribution parameter (n) controls the slope of SWCC. As shown in Figure 5.14, n tends to decrease as the kaolin content of the mixtures increases. The average values for both drying and wetting have close values to each other, so a single trend line for both states was drawn.

The average residual volumetric water contents resulting from these test results are plotted versus kaolin content. As expected, residual volumetric water content increases with kaolin content. As shown in Figure 5.19, a tremendous difference is noted between the samples with 0% kaolin content (pure sand) and 100% kaolin content. Also, the slope of trend line decreases with increasing kaolin content.

The experimental results indicate that an increase in kaolin content results in an increase of residual volumetric water content, and a decrease in the fitting parameters (α and n).

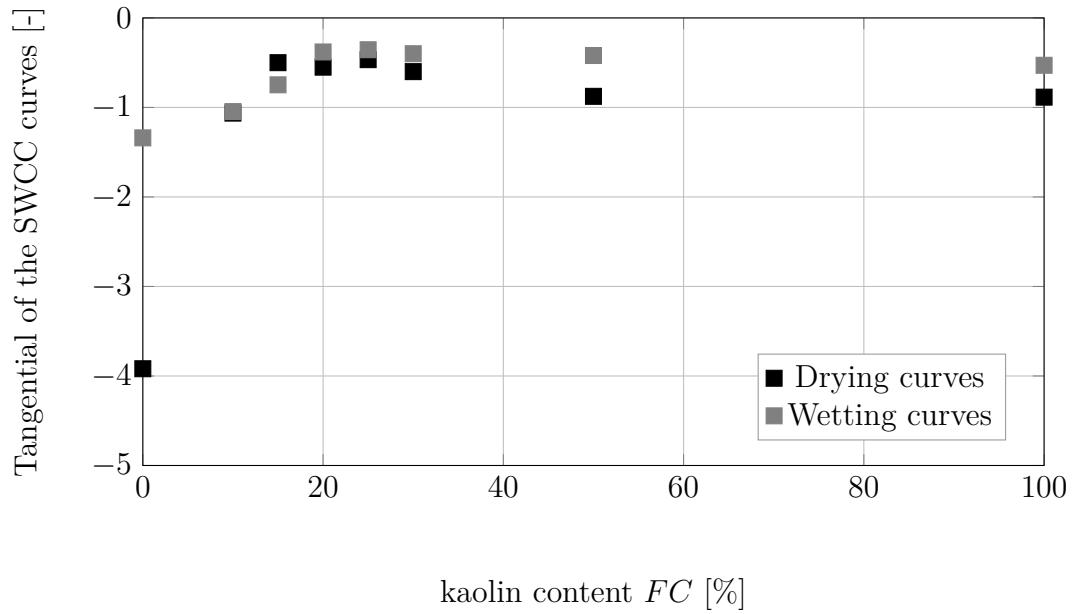


Figure 5.16.: Inclination of the SWCC curves vs fines content

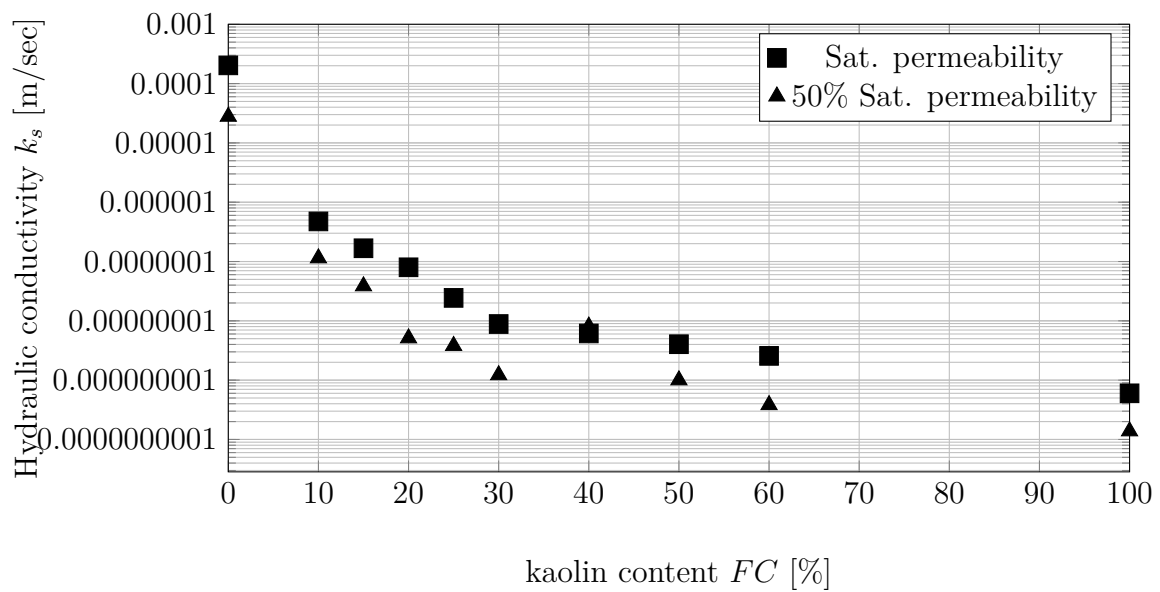


Figure 5.17.: Saturated & 50% saturated hydraulic conductivity vs fines content

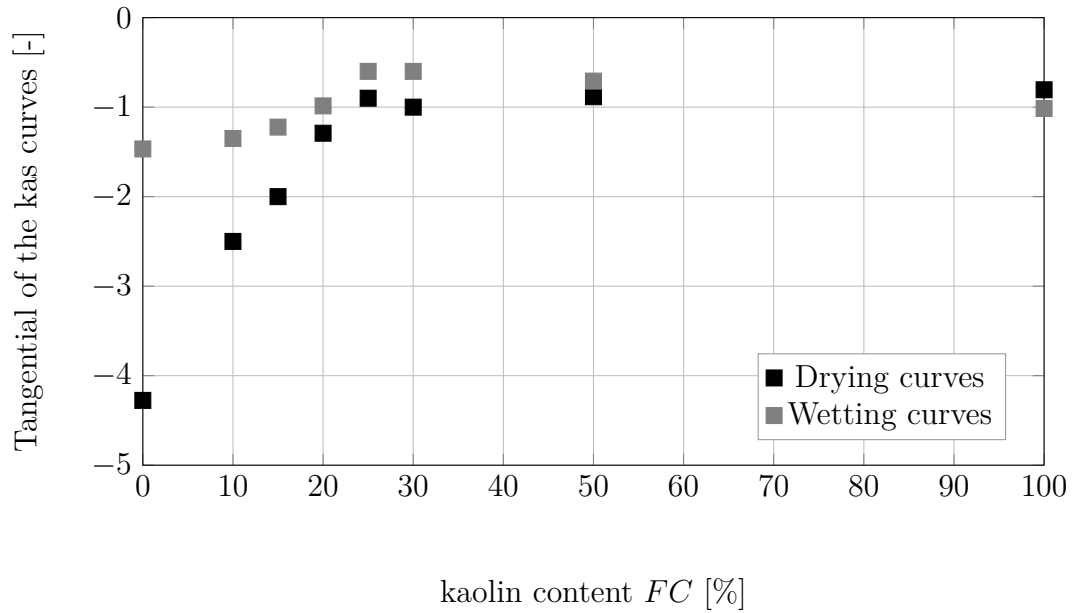


Figure 5.18.: Inclination of the hydraulic conductivity curves vs fines content

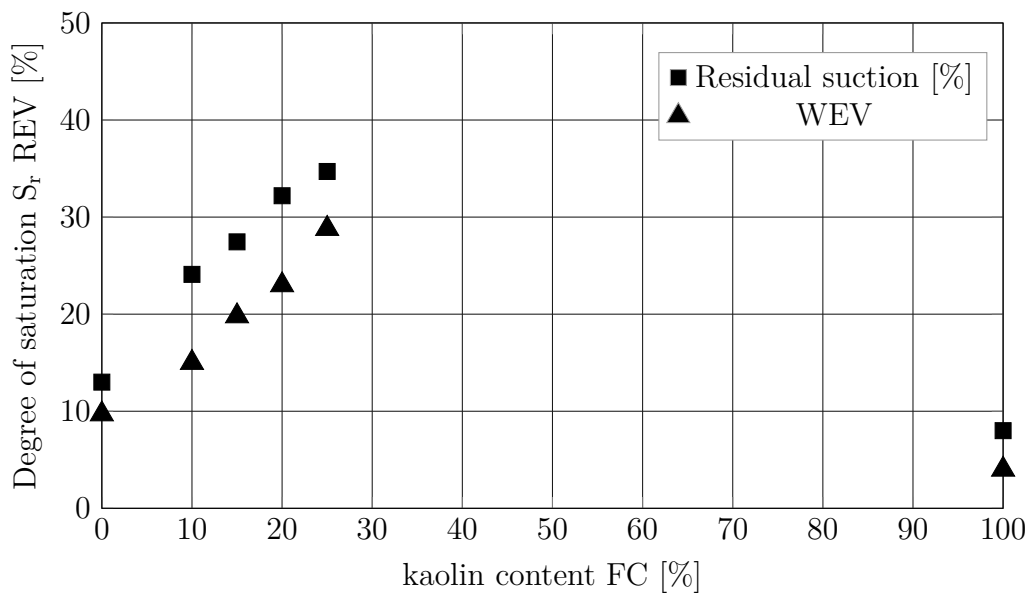
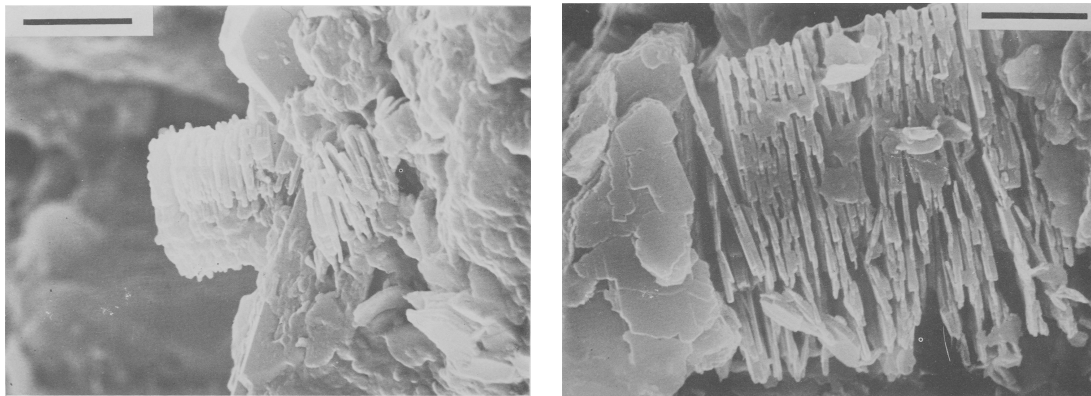


Figure 5.19.: Fines content vs. degree of saturation at residual suction



(a) Discrete-particle kaolinite crystal aggregates attached to a pore wall (b) Loose basal plane stacking arrangement of pseudo-hexagonal crystal

Figure 5.20.: Scanning electron micrograph of discrete-particle kaolinite, scale bar = $4\mu\text{m}$ after Morris & Shepperd (1982)

5.6. Geotextile water characteristics curves

5.6.1. Performance experiments to determine soil-water retention curves

In this section, the results of the water-retention curves for the nonwoven geotextiles used in the current study will be presented. The geotextiles are B (from Bonar) which is the main material that used in the column tests, N1, and N2 (from Naue), T1, T2, and T3 (from Terram) and F1, F2, F3, F4, and F5 (from France). The properties of the products are presented in chapter 4. The characteristics of the retention curves will be discussed and compared with data from literature.

Table 5.3 summarizes the tests performed on the geotextile samples.

Table 5.3.

Suction range to determine GWCC			
Nr.	Test	Symbol	Material(s)
1	Hanging column method	HC	B, T, N, F
2	Capillary rise method	CR	B
3	Hanging column method (Dirty Geotextile)	HCD	B
4	GWCC under vertical stress	BC	B

5.6.2. Capillary rise tests

This test was performed by several researchers in the literature (subsection 3.3.3), however, some of the testing setups were performed using a follie to cover the geotextile sample and to prevent evaporation. However, some results showed no capillary rise of water through the geotextile, this could be due to the testing conditions and the evaporation control and/or the temperature inside the testing chamber.

To assure a reliable results using the capillary rise cell, it is important to control the temperature inside the cell and make sure a constant temperature during the test, a thermometer has been attached to the Plexiglas cylinder from inside. Figure 5.21 shows the change in the temperature during 1-day test drying path and 3-days test wetting path. Figure 5.24 shows the capillary rise test repeated for 4 times in order to check the accuracy and reliability of the test.

The drying and wetting paths of nonwoven geotextile (G1) for different time durations

(1-day, 2-days, 3-days, and 4-days) are shown in Figures (5.22) and (5.23) respectively.

The results of capillary rise tests performed with different time durations. The differences between the tests results are small and there is small bandwidth which could happen due to the testing conditions. It can be concluded that 1-day test is sufficient to determine the water-retention curve of the geotextile as shown in Figures 5.22 and 5.23. The water retention curves determined from the tests with different durations are located within a cognizable band width and show no systematic tendency. Comparing this bandwidth with the scattering of 1-day test result (which is selected as a reference test), this is might be due to the testing conditions in which the geotextile sample has to be taken from the cell, cut into small pieces, reassuming the weight and then taken to the oven. For lighter color geotextiles, probably, pre-defining the height in which the small sample will be cut would reduce the time of the cutting process.

Similar observations are reported by Krisdani et al. (2006). They had performed the capillary rise test with different duration and suggested that the tests results after one day are sufficient. However, Bouazza & Nahlawi (2006) tested two geotextile materials using the capillary rise method. They noticed that the nonwoven polyester geotextile was able to observe small amount of water in the in-plane direction in compare to the cross-plane that could be due to the fact that the geotextile is more hydrophobic in the in-plane than the cross-plane direction and also to the testing condition as the geotextile was not protected from losing the water due to the evaporation or maybe the warping technique was used was lowering the contact angle. The eye observations were achieved based on the highest level reached by the water (which was blue dyed) and this may not be an accurate method to prove that the water did not rise higher.

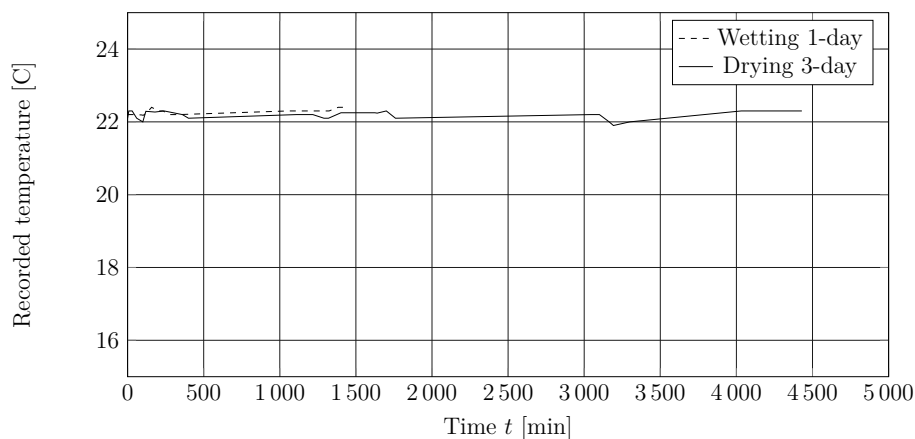


Figure 5.21.: Time-temperature curve

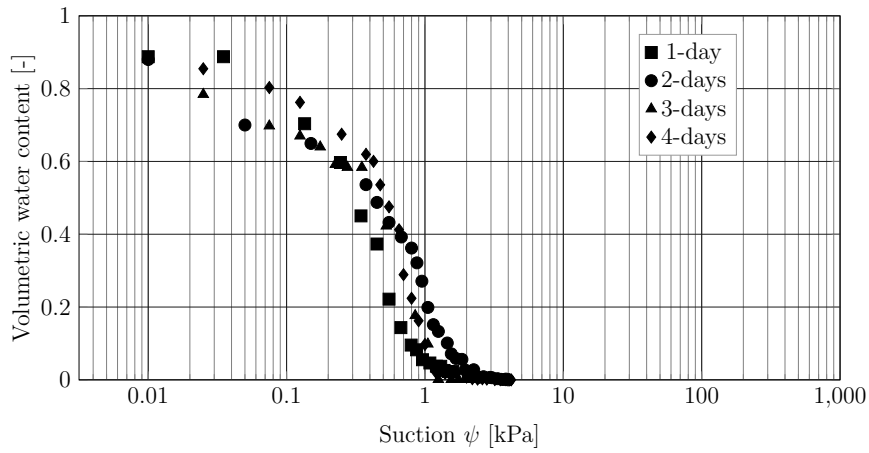


Figure 5.22.: Drying curves - Capillary rise method

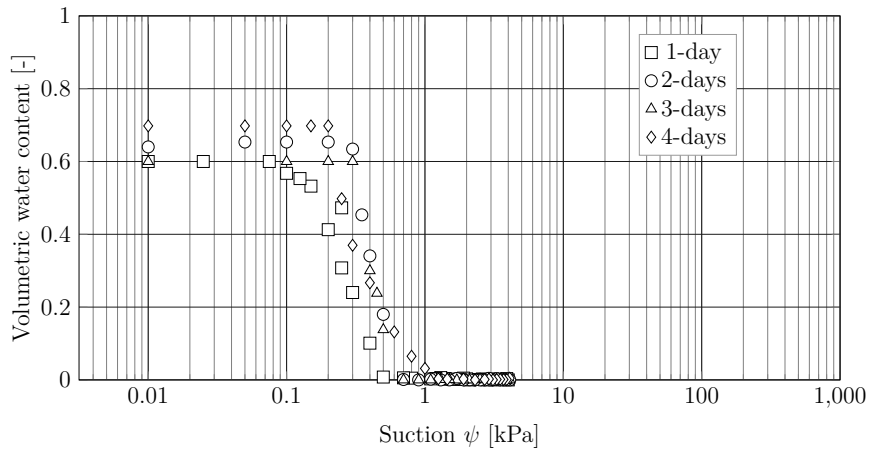


Figure 5.23.: Wetting curves - Capillary rise method

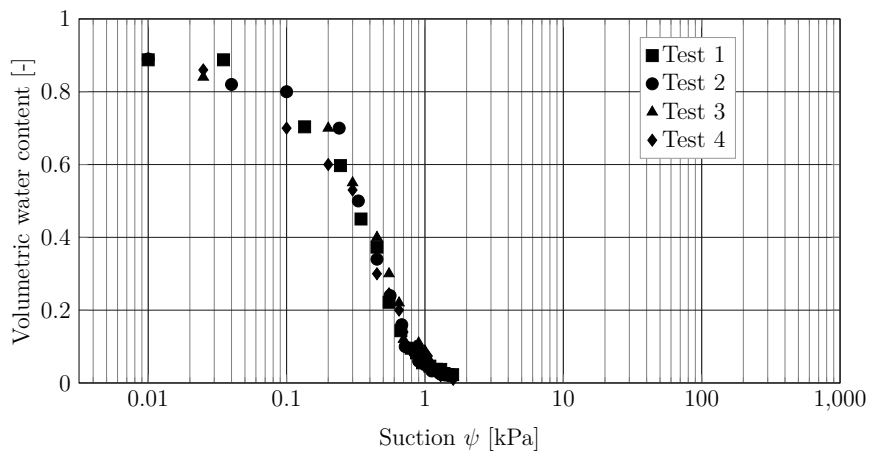


Figure 5.24.: Drying curves - Capillary rise method (repeated tests)

Holtz & Kovacs (1981a) reported that the contact angle of water and soil particles is assumed to be 0° , however, the contact angle of water with most plastics is ranging between 0° and 90° . This difference is due to chemical composition used, trace contamination of fiber surfaces, and surface roughness (Berg 1989). Table 5.4 shows that the contact angle for Polypropylene is higher than that for Polyester on the advancing cycle but less for receding cycle (Miller 1977; Kamath et al. 1987; Henry & Holtz 1998). The method

Table 5.4.: Contact angles of textile fibers in water after Henry & Holtz (1998)

Fiber type	Advancing $\theta [^\circ]$	Receding $\cos\theta, \theta$
Polyester	76-79	63-65
Polypropylene	86	54

described by Knight & Kotha (2001) is considered easy and to assess. However, the nonwoven geotextile used in this study has a waved surface and the points of contact between the geotextiles could be weak and may not allow the water to rise smoothly specially to measure the wetting path.

5.6.3. Hanging column method

Figures (5.25 and 5.26) presents the drying and wetting curves for nonwoven geotextile (G1). The test duration was 15 days for both drying and wetting paths.

The test results for both drying and wetting paths were compared with the results of 1-day test using the capillary rise test. A good agreement between the tests results is observed which can lead to the conclusion that the capillary rise test is capable to establish reliable results using less time and relatively cheaper set-up.

The tests results show that the GWCC of the nonwoven geotextile is similar to the basic shape of the SWCC (as can be idealized in Figure 5.10). The air entry value is small (0.2 kPa). Reported results from the literature show that most geotextile air entry values are between 0.2 and 1.2kPa (Iryo & Rowe 2003) which is similar to granular materials (Stormont et al. 1997).

The coarser materials (sand and geotextile) show highly nonlinear behavior, with a significant decrease in volumetric water content (or degree of saturation) within a significant narrow range of suction. The fine-grained soils (sand-silt mixtures and clayey materials) show instead a more gradual decrease in water content with increasing suction.

The nonlinearity observed in these relationships is caused partly by the range of pore size distributions in these materials. During initial drying of a fully saturated geomaterial, the

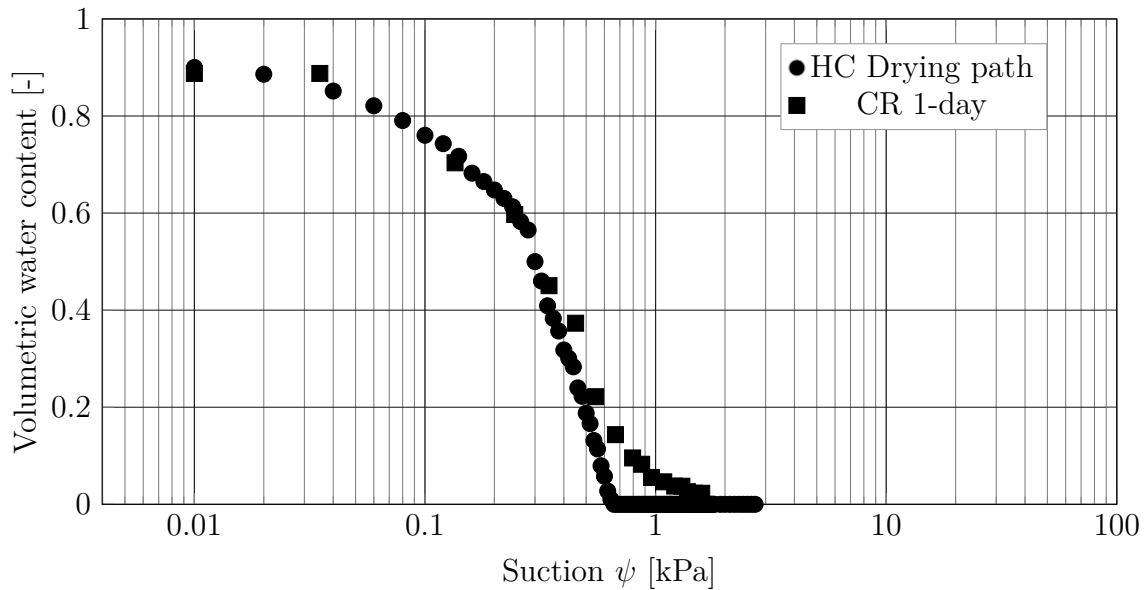


Figure 5.25.: Comparison of drying curve of capillary rise method with Hanging column method

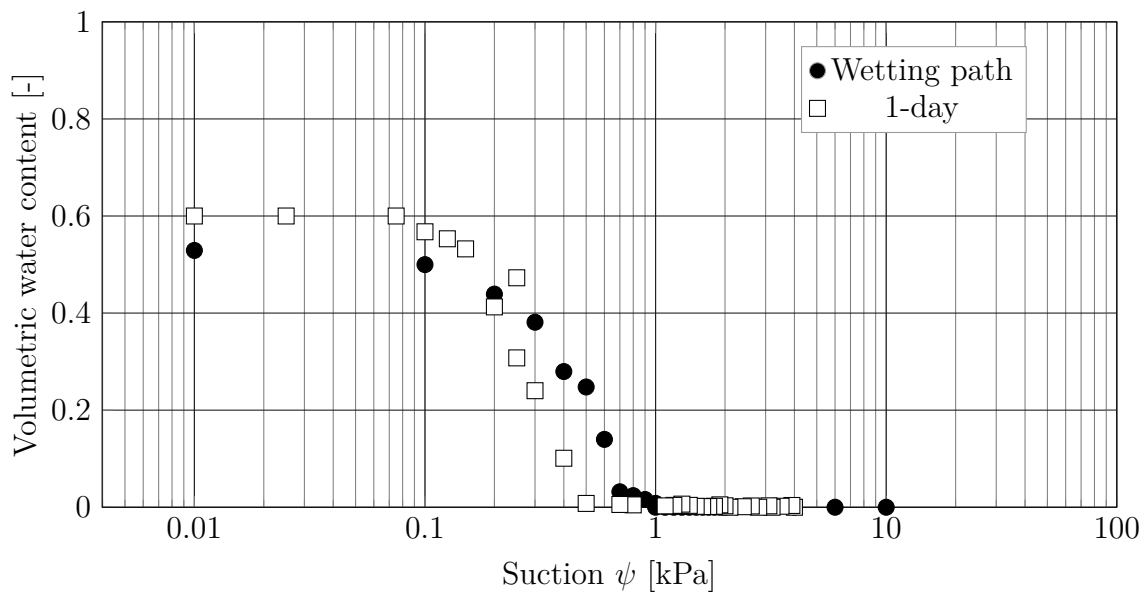


Figure 5.26.: Comparison of wetting curve with Hanging column method

negative pressure in the water increases, but water does not flow from the geomaterial until the value of suction corresponding to the air entry value is reached. When this suction value is reached, air enters the specimen and the water content decreases. The residual condition occurs because the water becomes occluded (or disconnected) within the soil pores, with no available pathways for water to flow.

The water characteristic curve WCC for a given material is sensitive not only to the

pore size distribution, but also to the soil mineralogy (for soils), polymeric material (for geosynthetics), density, and pore structure (Hillel 1998). The water characteristic curve can show significantly different wetting and drying paths.

During drying, the largest pores drain first, followed by the smaller pores. During wetting, the smaller pores fill first, but the presence of large pores may prevent some of the small pores from filling. Also, wetting of a dry geomaterial often leads to entrapment of air in the larger pores of the nonwoven geotextile, preventing saturation of the medium unless positive pressure is applied to the water. Air entrapment causes the wetting path to be relatively flat for high suction, with a steep increase in volumetric water content at lower suctions.

5.6.4. GWCC for additional geotextiles products

In this section, water-retention tests results for additional nonwoven geotextile materials are presented. The objectives from these tests are to distinguish the range of the air entry values of these products (Chapter 4), also they will be used in the theoretical analysis later.

Figure 5.27, 5.28, and 5.29 shows tests results for the samples donated by TERRAM (T1, T2, T3), Naue (N1, N2), and other 5 samples donated from France (F1, F2, F3, f4, F5), respectively.

The tests results show that for the selected samples the GWCCs are similar to or in the range close to the previous tested samples and to the other samples from the literature. The air entry value of these samples is within the range of the previous tested geotextile samples also. The selected samples from France have different AOS values and the GWCC results show an influence of the AOS curve on the shape and air-entry value also.

5.6.5. GWCC of geotextiles with intrusted soil

As geotextiles are placed in soil, soil particles may adhere to geotextile fibers and may affect the characteristics of the water-retention curve of the geotextiles. Henry & Holtz (1997) investigated the influence of the intrusion of soil particles on the wetting performance of two polyester non-woven geotextiles. Results showed that the intruded soil caused the geotextile specimens to be wetted-up at higher suction heads (i.e., higher water-entry suction head). The water-entry suction heads for silt and sand-contaminated specimens were not noticeably different.

Figure 5.30 shows the grain size distribution curves for 6 soil mixtures (HS, 10K, 15K, 20K,

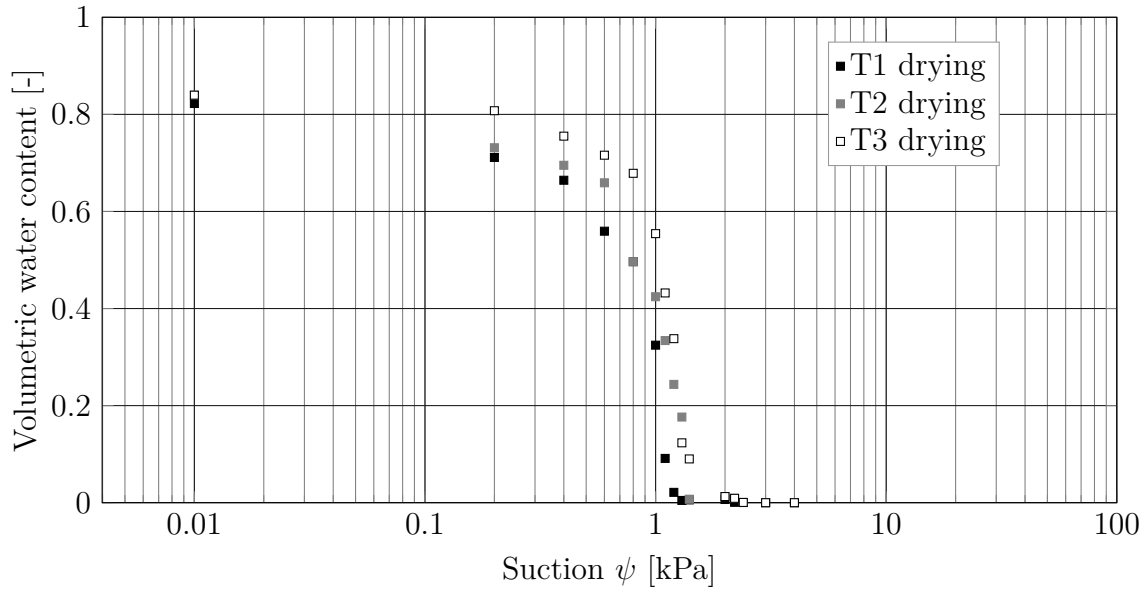


Figure 5.27.: GWCC for 3 different geotextile samples (Terram)

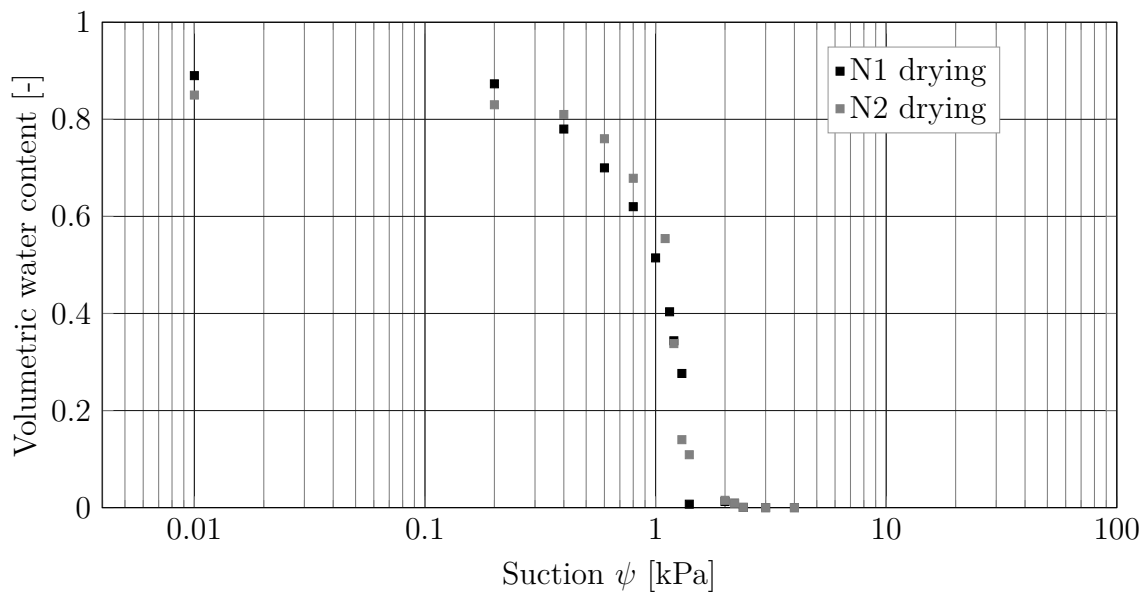


Figure 5.28.: GWCC for 2 geotextile samples (Naue)

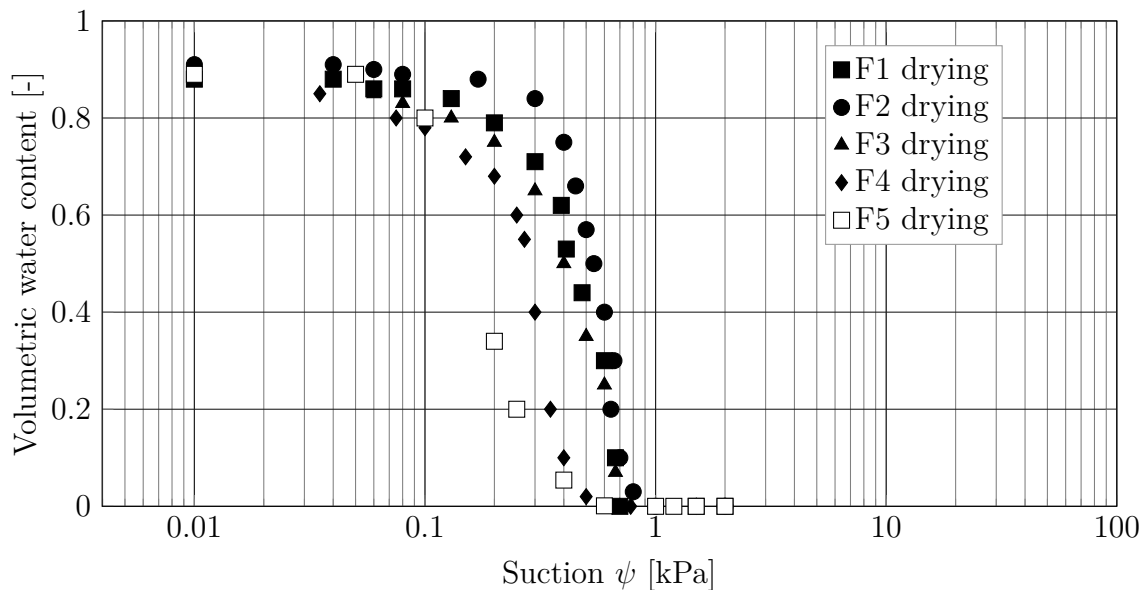


Figure 5.29.: GWCC for 5 geotextile samples from France

25K, and K) together with the geotextile opening size curve AOS of the main geotextile material (B). The curves show that for pure Hostun sand, the sand particles are larger than the openings of the geotextile material. However, with the increase of the fines content, the amount of the retained soil particles above the geotextile will decrease from 90% for 10K to 77% for 25K. In case of pure kaolin material, the openings of the geotextile are larger than the biggest particle of the kaolin. Due to this an intrusion of finer grains into the geotextile may be possible. In the following the influence of intruded grains on the GWCC is investigated.

The test procedure was performed by pouring soil material of each mixture on the geotextile sample, covering the geotextile layer with a folio and then hammering it gently using rubber-hammer to allow the soil particles to pass through the pores of the geotextile. Then the soil/geotextile sample was saturated and tested using the hanging column method to determine the GWCC using the previous procedure to determine the GWCC in the current study.

Figure 5.31 shows the tests results for the tested geotextile after poring 6 different type of soil mixtures. It can be seen that the geotextile retention curve was not be affected by the soils HS, and 10K, but the AEV has been shifted with further increase in the kaolin content for the mixtures 15K, 20K, 25K, and pure kaolin 100K. Henry & Holtz (1997) found that dirty geotextiles had larger capillary rises than cleaned or new specimens because soil fines coated the fibers and thereby increased the wettability of the fibers. To have a better understanding to this topic, it is important to classify the soil particles into

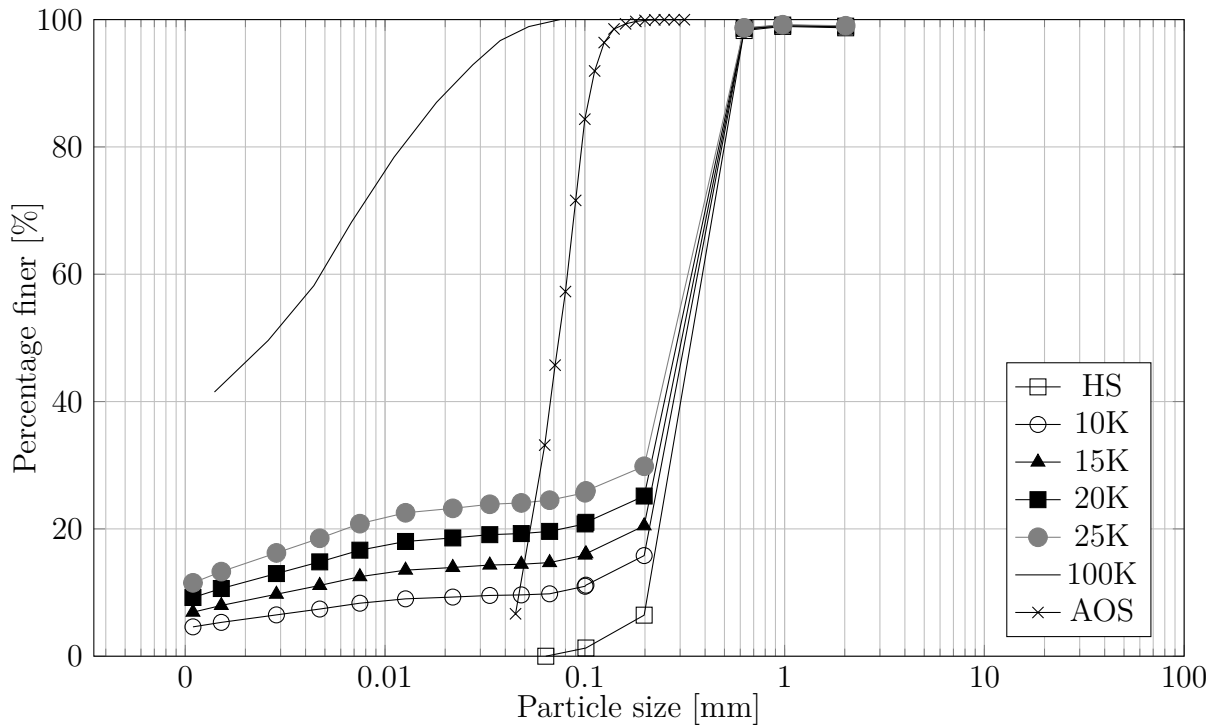


Figure 5.30.: The grain size distribution curves for the soil mixtures and the AOS curve of the main geotextile (B)

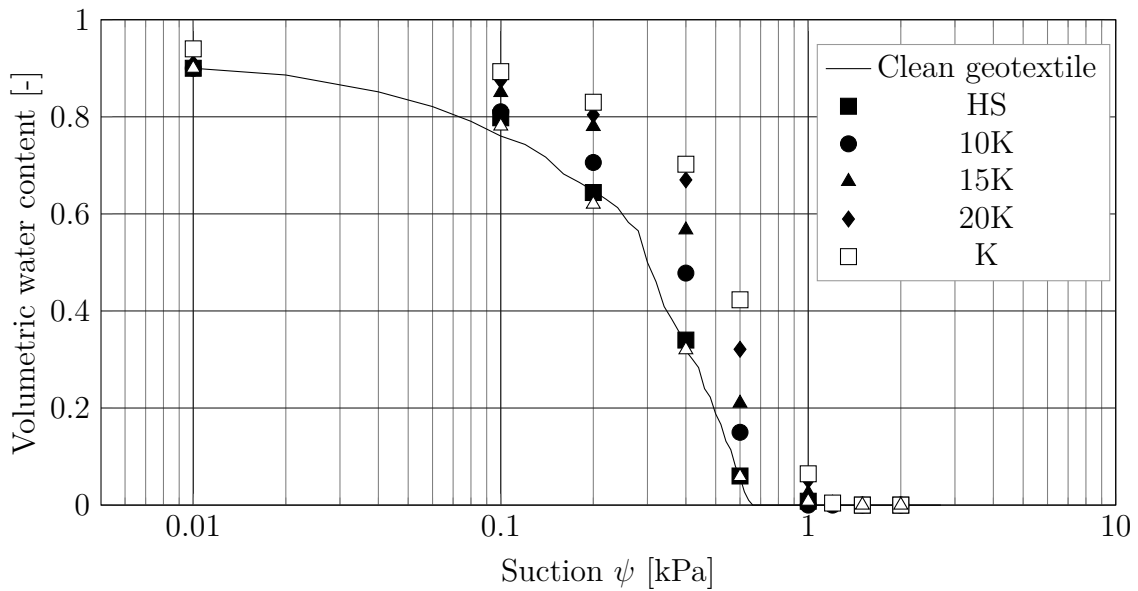


Figure 5.31.: GWCC for dirty geotextile samples (drying path)

three types; soil particles which are larger than the openings of the geotextile and will be located above the geotextile layer, soil particles smaller than the openings of the geotextile

and may be washed away by the water, and the soil particles which are in a size close to the openings of the geotextiles and can be held by the openings. It is most likely that the third type of the soil particles may cause an increase in the wettability of the geotextile.

5.6.6. Geotextile water characteristics curves under vertical stress

The nonwoven geotextile as part of the cover layer in the landfill is placed in a depth between 1 m to 5 m under the ground surface. A thick soil layer above the geotextile layer applies an overburden pressure which could compress it and therefore reduce the pores of the material which affects the properties of the geotextile layer.

Few studies had been published to study the effect of vertical stress on the hydraulic performance of a nonwoven geotextile. Ho (2000) studied the effect of the compressibility on the woven and nonwoven geotextiles using a modified oedometer device. Gourc et al. (1982), McGown et al. (1982), and Palmeira & Gardoni (2000) studied the influence of stress on the physical and hydraulic properties of nonwoven geotextile. The results showed an effect of confinement on geotextile properties, with special reference to pore size diameters.

The increase of geotextile retention capacity caused by increasing stress levels and geotextile partial clogging was also evaluated, as well as the accuracy of equations for the estimate of geotextile permeability. The results obtained showed a marked effect of confinement on geotextile properties, with special reference to pore size diameters, with implications to current filter criteria for non-woven geotextiles.

Ten geotextile samples were cut to the desired diameter (70 mm) and weighted to determine the dry weight of each sample. The samples were later saturated using a container filled with distilled water. After 24 hours, the geotextile samples were tested again to determine the saturated weight and then were set in the sample room inside the cell. To avoid any possibility of existing air trapped inside the cell and to make sure the ceramic disc is fully saturated, a flushing process was performed by allowing distilled water to flow from the top valves towards the lower valves through the geotextile samples and the ceramic disc. The test was started by applying the target vertical stress with small increments to avoid increasing the porewater pressure inside the geotextile sample. After reaching the target vertical stress, the reduction in the height of the geotextile was monitored and recorded until reaching a stable reading. The suction was started to be reduced by lowering the water inside the burette. The water inside the burette was further reduced to measure several points on the GWCC for the drying and wetting paths. After finishing the test, the samples were taken from the cell and the weight was again measured to re-check the

gravimetric water content at the end of the test. The test was repeated with new vertical stress to cover a range of different vertical stresses namely; 5, 10, 20, 50 and 100 kPa. To measure the height of one geotextile sample, the recorded reduction in the height of the ten samples was divided by 10.

Figures 5.32(a) and 5.32(b) present the drying and wetting GWCCs under different vertical stresses. The drying and wetting paths for the material under unconfined vertical stress were also presented to compare the results. Table 5.5 presents the fitting parameters of the GWCCs using the models van Genuchten (1980) and Fredlund and Xing (1994).

Figure 5.33 shows the change in the height of the geotextile sample with the increase in the vertical stress. Each curve was determined by measuring the height from different test under different vertical stress with the same suction value.

Two tests were performed on the whole geocomposite material presented in Figure 5.34. The first test was for a saturated sample while the other test was performed under 0.1 kPa suction. The tests were highly influenced by the compressibility of the geonet material between the two geotextile layers.

Table 5.5.: Fitting parameters of the GWCC curves for drying and wetting under vertical stresses

Model	Van Genuchten (1980)		Fredlund & Xing (1994)			
	Fitting parameter	α [1/m]	n	α_f [kPa]	n_f	m_f
Drying 5 kPa		0.45	0.0012	1.2	2.8	4.3
Wetting 5 kPa		0.43	0.0014	1.1	2.7	4.2
Drying 10 kPa		0.466	0.002	1.33	3.0	4.0
Wetting 10 kPa		0.44	0.0012	1.2	2.9	3.8
Drying 20 kPa		0.88	0.002	2.4	3.2	4.3
Wetting 20 kPa		0.80	0.0013	2.2	3.1	4.1
Drying 50 kPa		1.5	0.13	3.0	3.2	2.0
Wetting 50 kPa		1.4	0.10	2.8	3.0	1.9
Drying 100 kPa		2.4	0.21	3.5	3.3	1.0
Wetting 100 kPa		2.2	0.20	3.4	3.1	0.9

The results of tests on packs of geotextiles will provide average values of geotextile properties, because of the number of layers being simultaneously tested.

The tests results show an increase in the storage capacity for curves with increasing the vertical stress as the air-entry value for both drying and wetting paths. This shifting of the air-entry values is related to the reduction of the pores of the geotextile sample due to

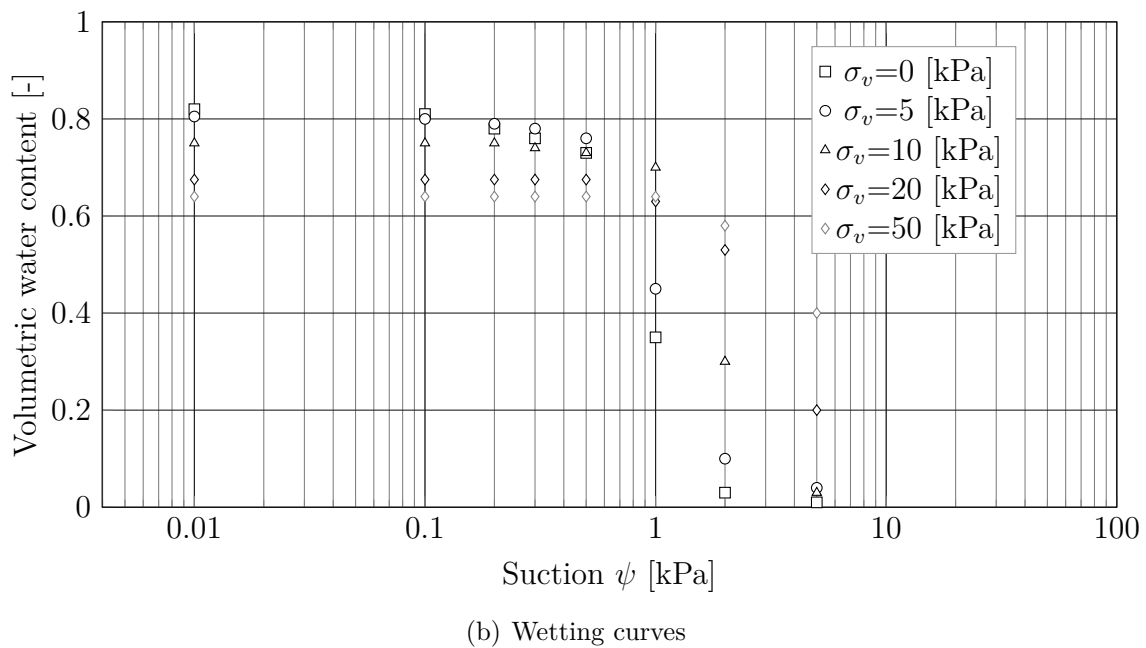
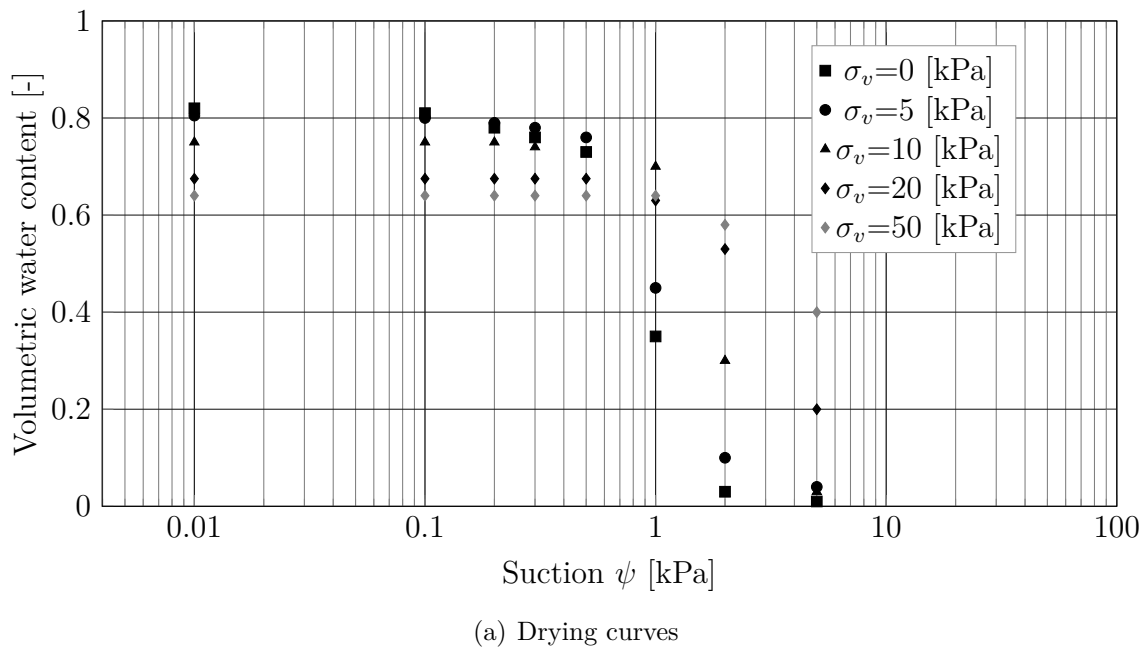


Figure 5.32.: GWCC under different vertical stresses

the applied stress. This reduction in the pores will need a higher suction value to expel the water from the geotextile sample in comparison to less or no vertical stress. The influence of the vertical stress on the GWCC is almost negligible after an applied vertical stress higher than 20 kPa. A reason for that could be that the most significant reduction in the pores of the geotextile will occur at stresses around 50-100 kPa. It is also expected to reduce the conductivity of the water with increasing the vertical stress as a result from

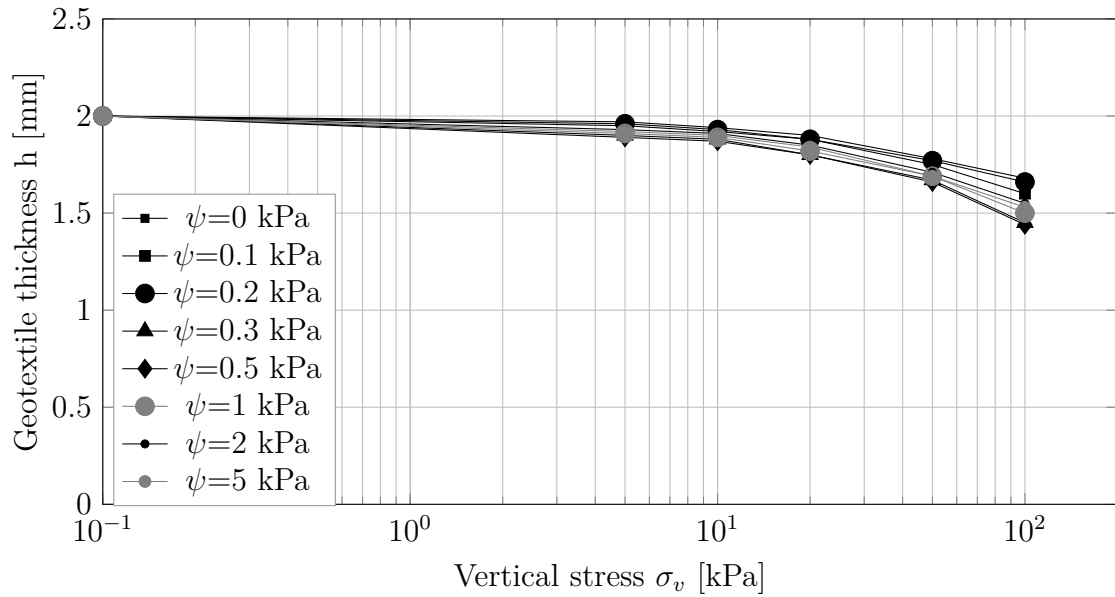


Figure 5.33.: Change of height vs vertical stress for different suction values (Nonwoven geotextile)

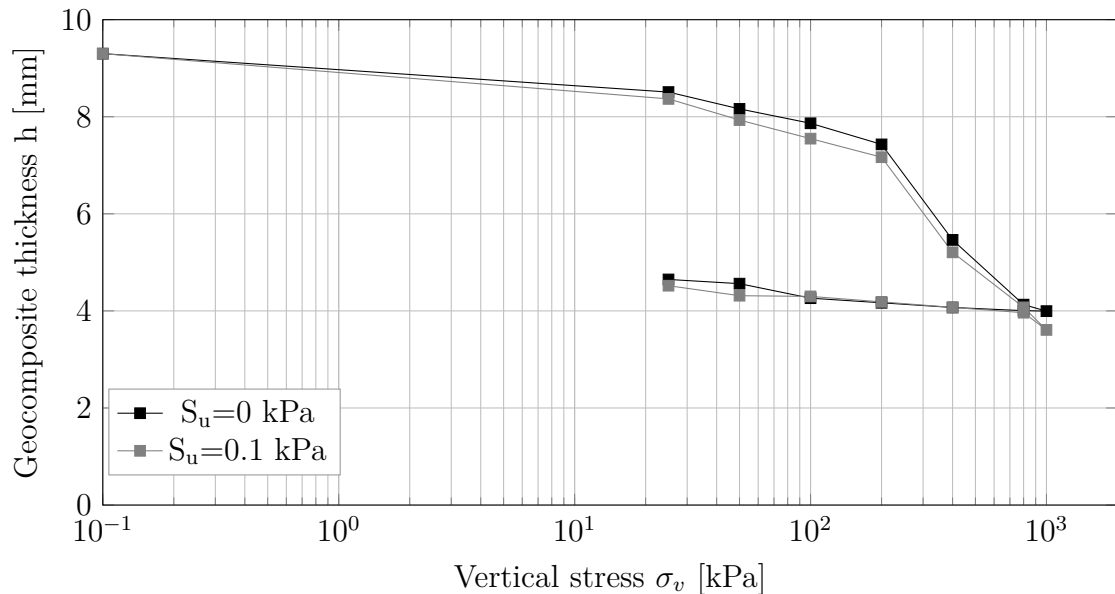


Figure 5.34.: stress-height curve for two geocomposite samples under saturated condition and 0.1 kPa suction

reducing the pores of the material.

The change in the suction values shows no clear influence on the height-vertical stress curves. The structure of the geotextile pores is different from the pores between the soil grains which could change and re-mold due to the applied vertical stress. The water-geotextile interaction due to the applied vertical stress may not be affecting the height of

the geotextile sample.

5.7. Hydraulic conductivity function of unsaturated nonwoven geotextiles

The relationship between hydraulic conductivity versus suction provides a measure of the increased impedance to water flow with increasing suction. It is difficult to determine the hydraulic conductivity function in the laboratory due to the low air-entry value of the nonwoven geotextiles therefore it is more practical to determine the function using a proposed model from the literature which has been used by several others to determine the hydraulic conductivity for geosynthetic products (Chapter 3).

Figure 5.35 shows the $k(\psi)$ -functions of the nonwoven geotextile B using the model proposed by Fredlund & Xing (1994).

Figures 5.36 5.37 show the $k(\psi)$ -functions of the tested nonwoven geotextile for the different specimen selected in the current study. The curves show similar trend for wide range of nonwoven geotextiles and the curves are located in a narrow bandwidth within a relatively small suction range.

5.8. GWCC derived from apparent opening size

Predicting the water retention curve from the apparent opening size curve (AOS) for geotextiles using the model to predict the SWCC from basic geotechnical properties (Aubertin et al. 2003)

This model is established based on the original by Kovács (1981) which uses parameter defined as the equivalent capillary rise h_{co} in the porous medium. This parameter is derived from the well known expression used for the rise h_c of water in a capillary tube having a diameter d . The value of h_c is given by (Smith 1990; Chin 2000):

$$h_{co} = \frac{4\sigma_w \cdot \cos \beta_w}{d \cdot \gamma_w} \quad (5.9)$$

where

σ_w : surface tension of water, $\sigma_w = 0.073 \text{ N/m}$ at 20°C

β_w : contact angle between water and the tube surface ($^\circ$) for polypropylene β_w is 86°

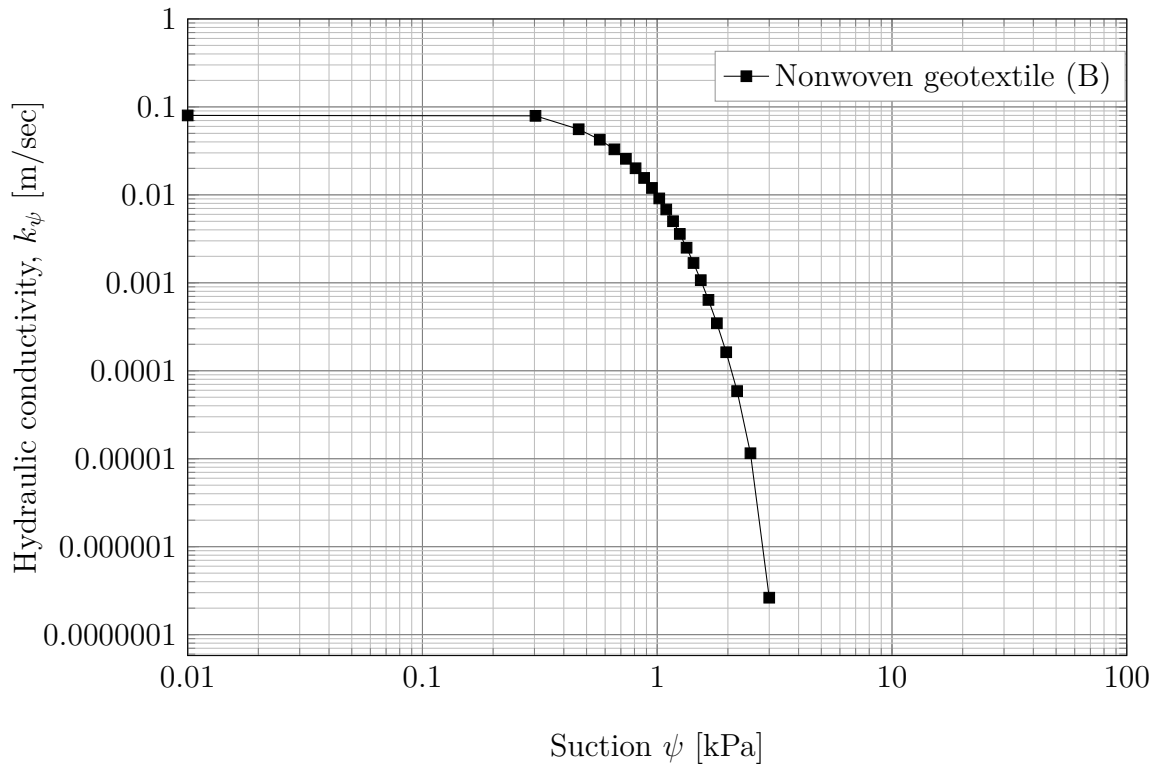


Figure 5.35.: Hydraulic conductivity function of the main geotextile (B)

γ_w : unit weight of water [N/m^3]

d : pore diameter [m]

Equation 5.9 indicates that capillary rise is proportional inversely to the diameter of the tube.

Geotextiles are similar to soils, in which, the pore size is not uniform as shown in Figures 4.7 and 4.8, hence, h_c is not easily defined with equation 5.9.

This pore system can be substituted by a system of regular channels with a diameter expressed as the equivalent hydraulic pore diameter d_{eq} , defined as (Bear 1972; Kovács 1981):

$$d_{eq} = 4 \frac{V_v}{A_v} \quad (5.10)$$

where V_v and A_v are respectively the volume and surface of the voids. In practice, A_v approximately corresponds to the surface area ASS of the solid grains. By relating ASS to the massic specific surface area S_m , equation (5.10) can be transformed as Scheidegger 1974:

$$d_{eq} = 4 \frac{e}{\rho_s \cdot S_m} \quad (5.11)$$

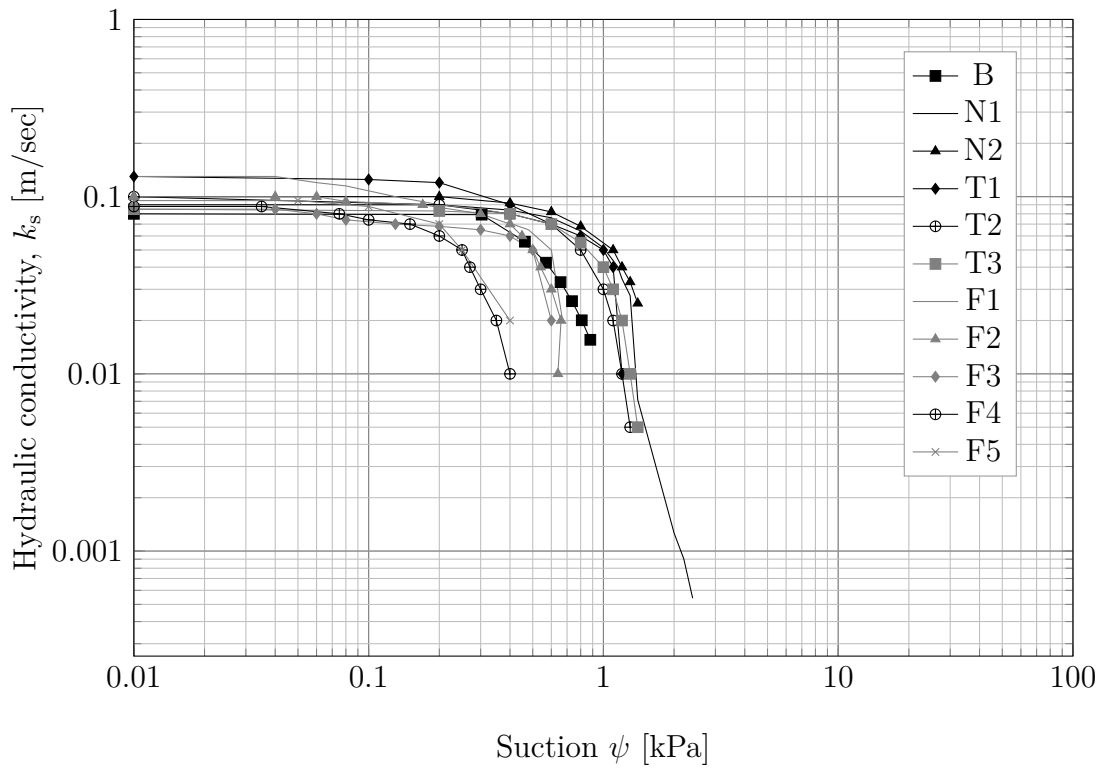


Figure 5.36.: Hydraulic conductivity function of geotextiles

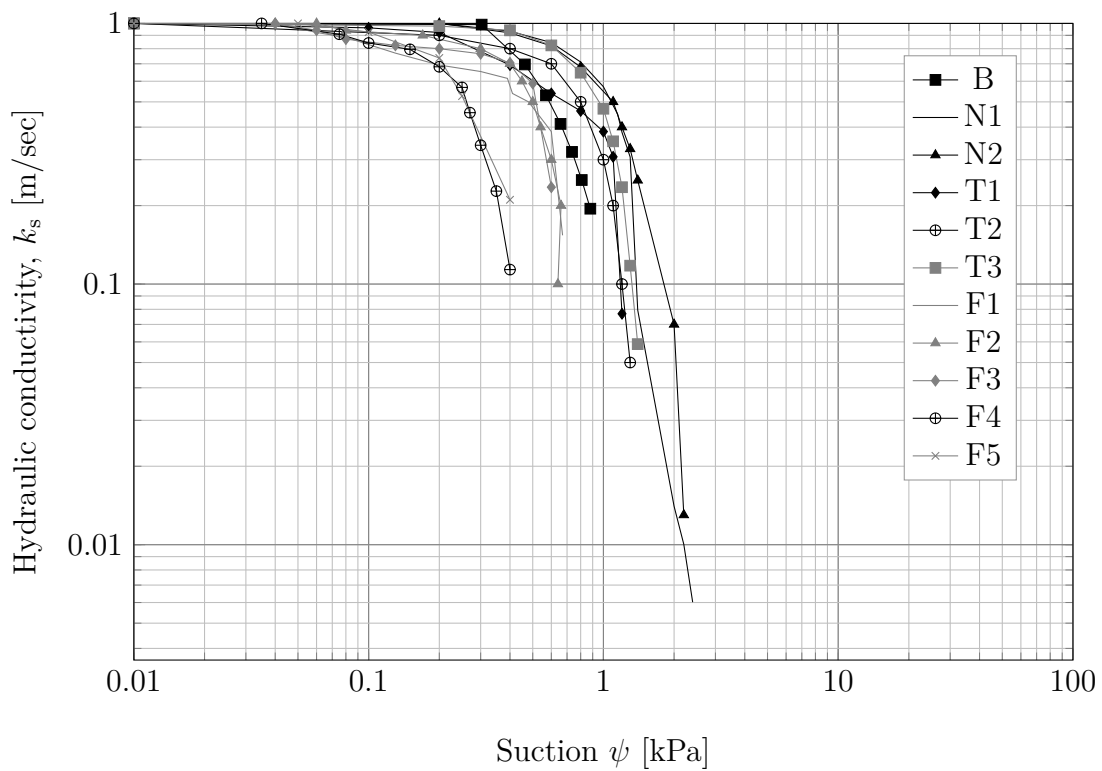


Figure 5.37.: Relative hydraulic conductivity function of geotextiles

In this equation, e is the void ratio and ρ_s is the solid grain density for polypropylene is $146.76 \text{ m}^2/\text{kg}$.

The equivalent capillary rise h_{co} is obtained by replacing diameter d (in equation 5.9) by the equivalent hydraulic pore diameter d_{eq} , and can therefore be expressed as:

$$h_{co} = \frac{\sigma_w \cdot \cos \beta_w}{\gamma_w} \frac{\rho_s \cdot S_m}{e} \quad (5.12)$$

This is one of the fundamental equations from which the MK model is built. As it will be indicated below, h_{co} is somewhat equivalent (at least for granular soils) to the height of the capillary fringe above the still water table in a homogeneous deposit, as defined in many geotechnique textbooks (e.g., Lambe & Whitman 1969; Bowles 1984).

Although S_m can be directly measured by various techniques (e.g., Lowell & Shields 1984), in most practical cases, the value of S_m is not readily available to apply equation (5.12). For coarse-grained soils, the specific surface area can nevertheless be estimated from the grain size distribution using the following expression Holtz & Kovacs 1981*b*:

$$S_m = 4 \frac{\alpha}{\rho_s \cdot D_H} \quad (5.13)$$

where α is a shape factor ($6 \leq \alpha \leq 18$; $\alpha = 10$ is used here as in the Kovacs original model), and D_H is an equivalent particle diameter for a heterogeneous mixture. The equivalent diameter D_H for a heterogeneous mix of particles theoretically represents the diameter of a homogeneous mix (with a single size) that has the same specific surface area as the heterogeneous one.

$$h_{co,G} = \frac{\sigma_w \cdot \cos \beta_w}{\gamma_w} \frac{\alpha}{e \cdot D_H} \quad (5.14)$$

where subscript G stands for granular (low plasticity, low cohesion) materials, as opposed to clayey (plastic/cohesive) materials (which will be discussed below). In this equation, the contact angle β_w will be taken as zero (e.g., Marshall et al. 1996).

In granular soils, S_m and D_H can be evaluated by subdividing the grain size curve based on standard mesh sizes Chapuis & Legare 1992. For practical geotechnical applications, the value of D_H can also be approximated using the following function (Aubertin & Chapuis 1998; Mbonimpa et al. 2002):

$$D_H = [1 + 1.17 \log(C_U)] D_{10} \quad (5.15)$$

where O^{10} is the diameter corresponding to 10% passing on the cumulative grain-size distribution curve, and C_U is the coefficient of uniformity ($C_U = O_{60}/O_{10}$). For the equivalent

capillary rise in granular soils, equation (5.14) is then expressed as follows:

$$h_{co} = \frac{b}{e \cdot D_{10}} \quad (5.16)$$

with

$$b = \frac{\alpha \cdot \sigma_w \cdot \cos \beta_w}{[1.17 \log(C_U) + 1] \gamma_w} \quad (5.17)$$

To determine the residual suction ψ_r , the following relationship provides an adequate estimate of the residual suction:

$$\psi_r = \frac{0.42}{(eD_h)^{1.26}} \quad (5.18)$$

A simple relationship was established between ψ_r and the equivalent capillary rise, h_{co} :

$$\psi_r = 0.86 h_{co}^{1.2} \quad (5.19)$$

The value of h_{co} could be used to define the relationship between the degree of saturation, S_r (or volumetric water content, θ), and suction. The capillary saturation, S_c , and by adhesive forces, causing saturation by adhesion, S_a .

$$S_r = S_c + S_a^*(1 - S_c) \quad (5.20)$$

The contributions of the capillary and adhesion components to the total degree of saturation are defined as functions of h_{co} and ψ using the following equations:

$$S_c = 1 - [(h_{co}/\psi)^2]^m \exp[-m(h_{co}/\psi)^2] \quad (5.21)$$

$$S_a = a_c C_\psi \frac{h_{co}/\psi^{2/3}}{e^{1/3}(\psi/\psi_n)^{1/6}} \quad (5.22)$$

in which

$$C_\psi = 1 - \frac{\ln(1 + \psi/\psi_r)}{\ln(1 + \psi_0/\psi_r)} \quad (5.23)$$

Figures 5.38 to 5.48 present GWCCs for the selected geotextile materials AOS method, which are compared with the experimental results using the hanging column method. The results show that the method is capable to predict the geotextile-water characteristics curves based on the apparent opening size of the geotextiles.

The input data for each material are presented in Table 5.6. The small differences in the comparison could be related to several factors; testing conditions of the GWCC, testing condition of the selected sample for the AOS, and the value of the angle of contact of between the geotextile and the water which can vary from a product to the other. However,

the method could be very suitable to predict the GWCC without performing a laboratory test to determine the GWCC which could be expensive, time consuming, and may require special equipments which are not available in every laboratory.

Table 5.6.: Input values to derive GWCC from AOS for each material

Material	O10 [mm]	O60 [mm]
B	0.0475	0.082
N1	0.026	0.041
N2	0.0245	0.056
T1	0.029	0.056
T2	0.0265	0.0535
T3	0.027	0.047
F1	0.009	0.039
F2	0.005	0.031
F3	0.007	0.043
F4	0.005	0.058
F5	0.009	0.074

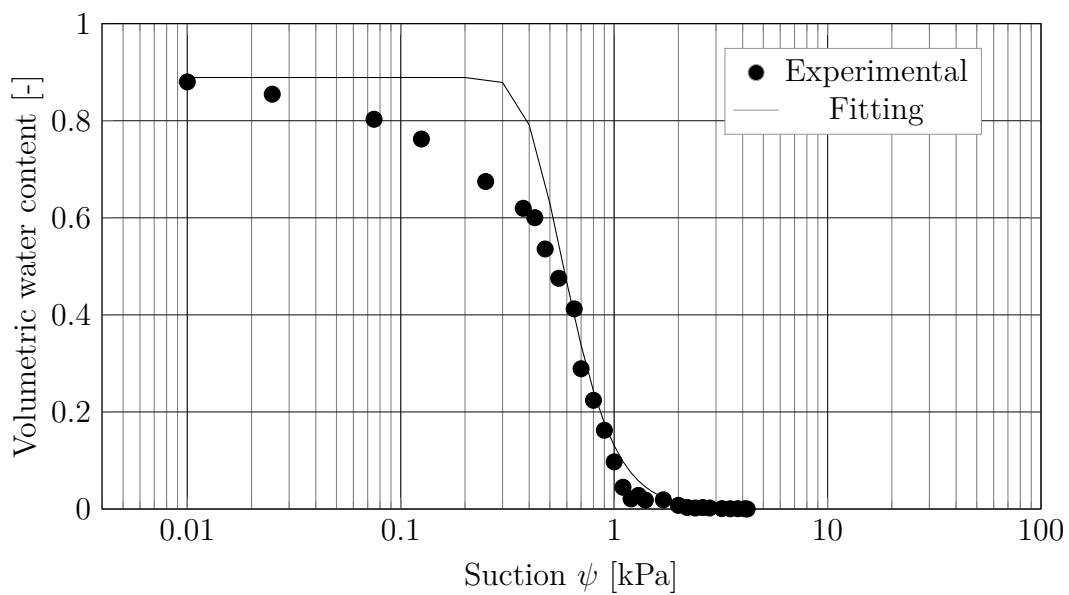


Figure 5.38.: GWCC fitting for B

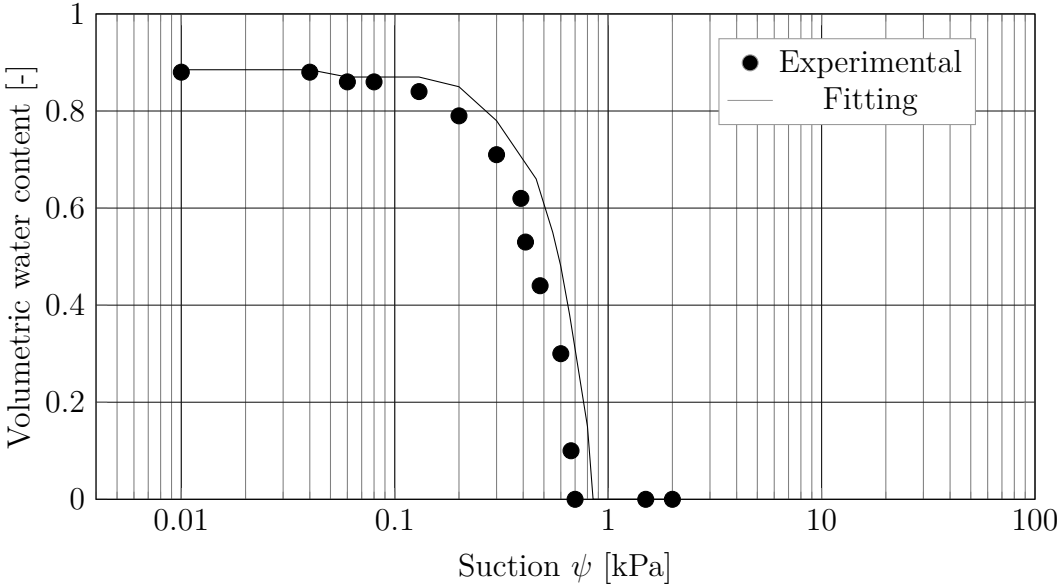


Figure 5.39.: GWCC fitting for F1

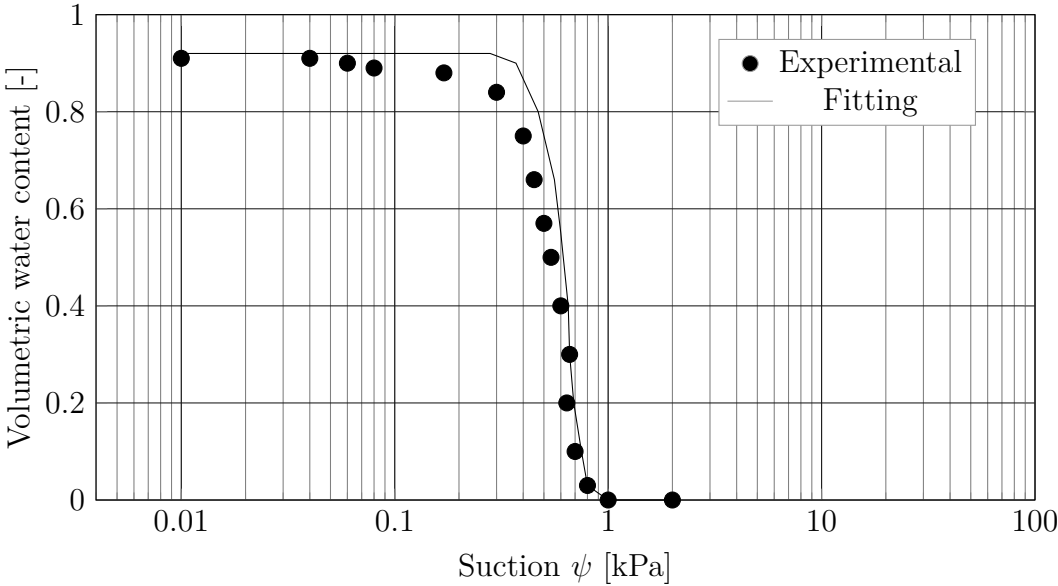


Figure 5.40.: GWCC fitting for F2

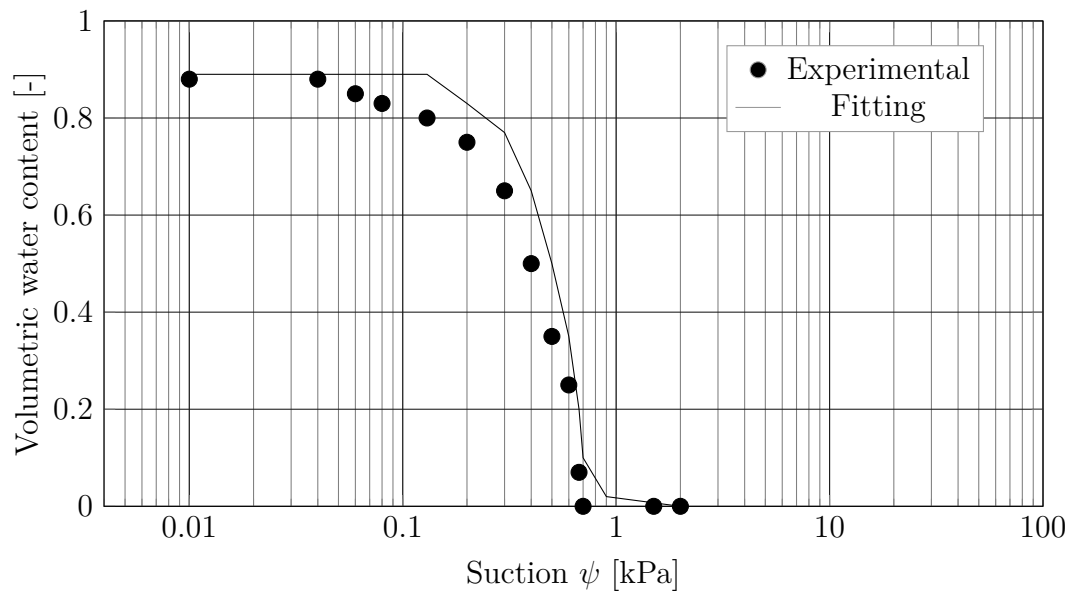


Figure 5.41.: GWCC fitting for F3

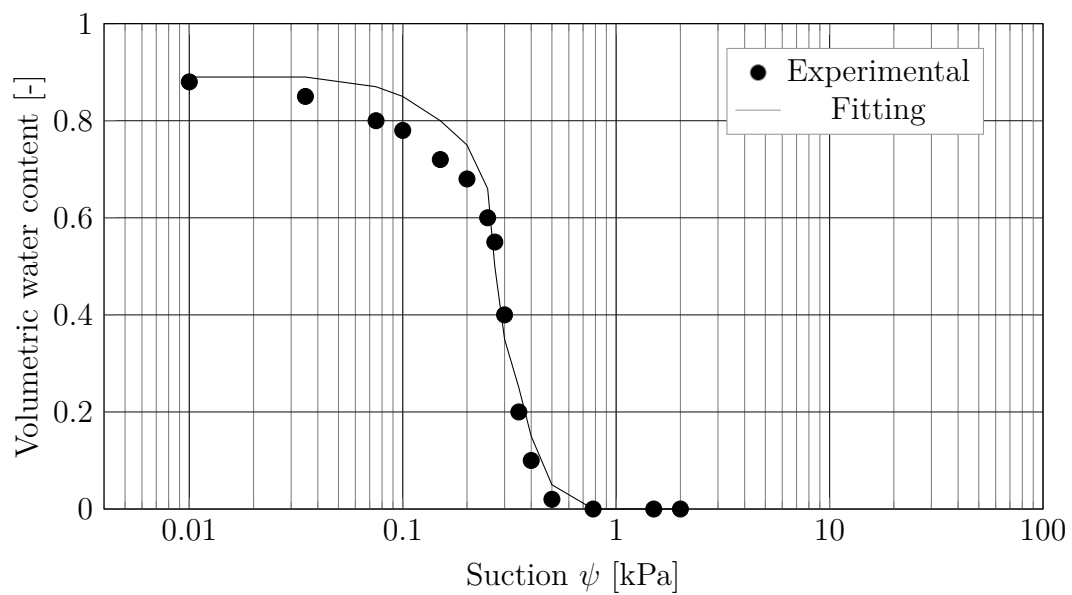


Figure 5.42.: GWCC fitting for F4

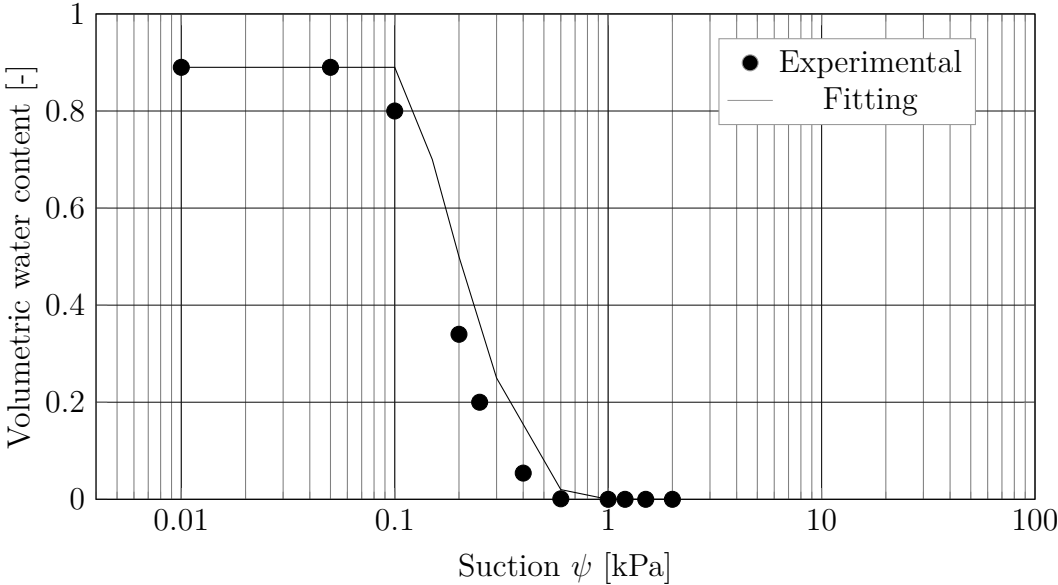


Figure 5.43.: GWCC fitting for F5

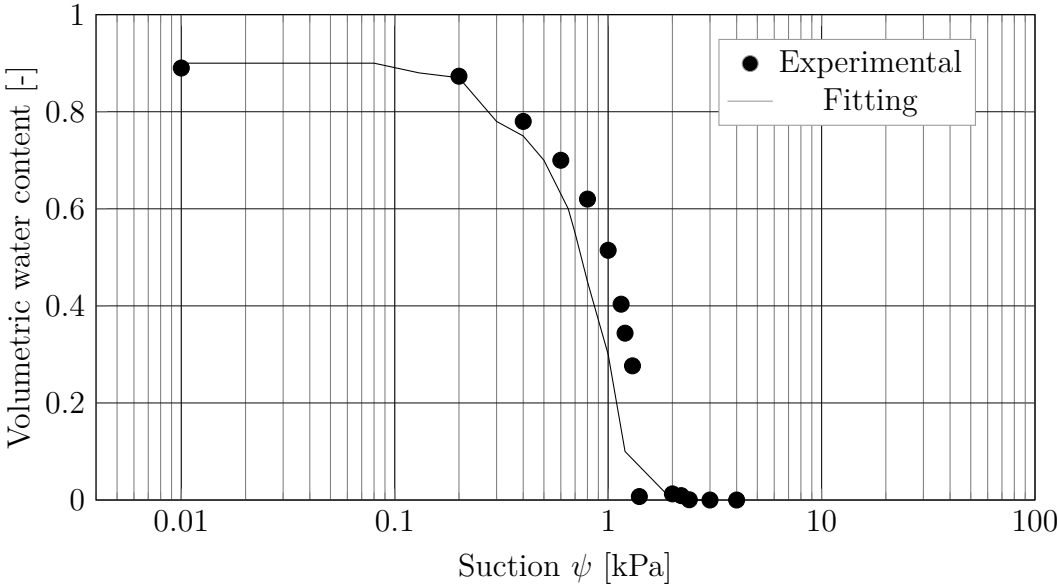


Figure 5.44.: GWCC fitting for N1

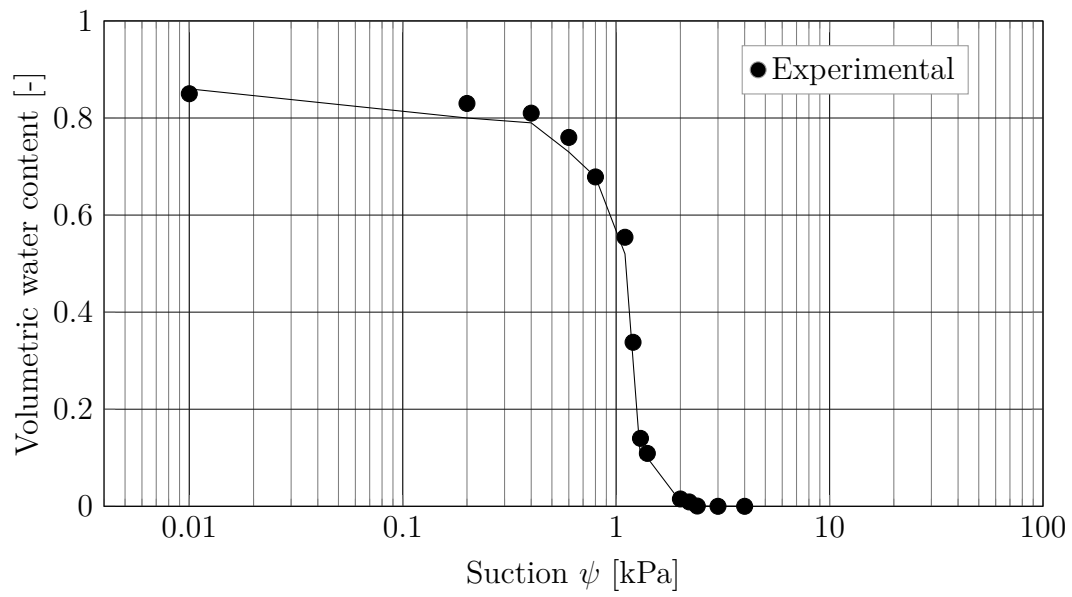


Figure 5.45.: GWCC fitting for N2

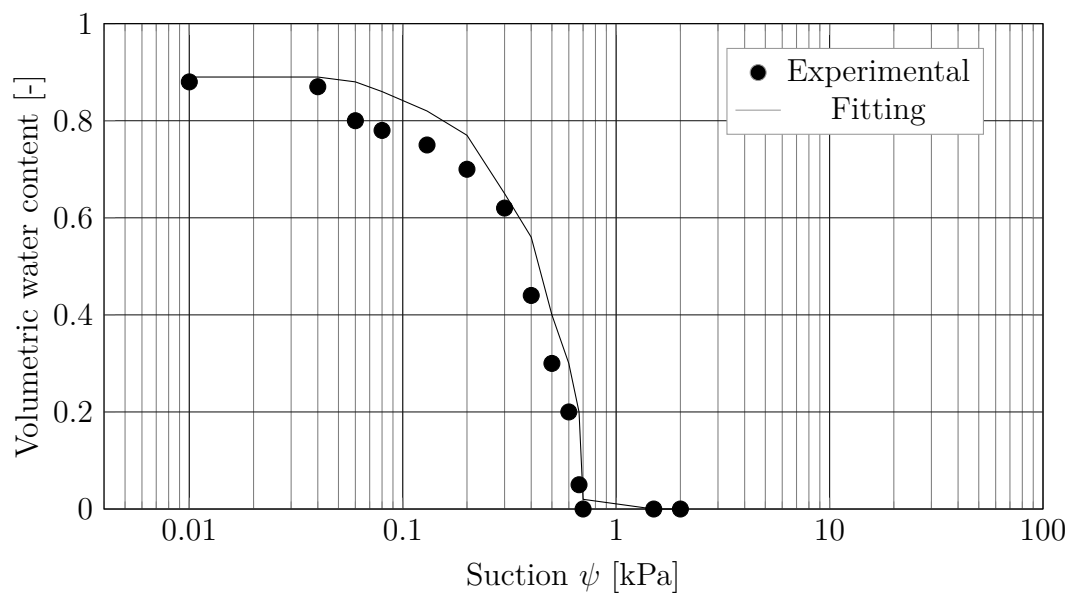


Figure 5.46.: GWCC fitting for T1

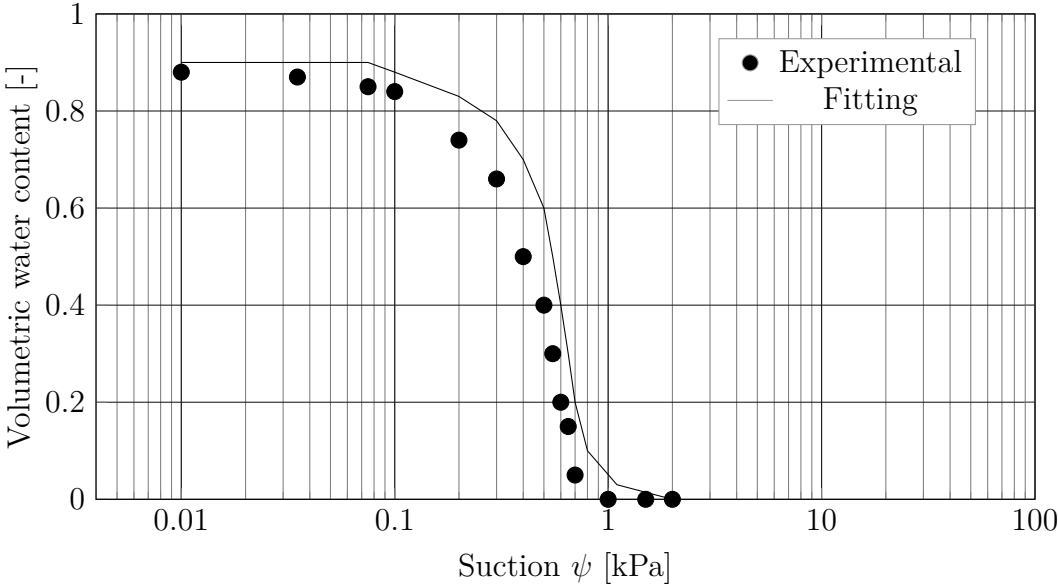


Figure 5.47.: GWCC fitting for T2

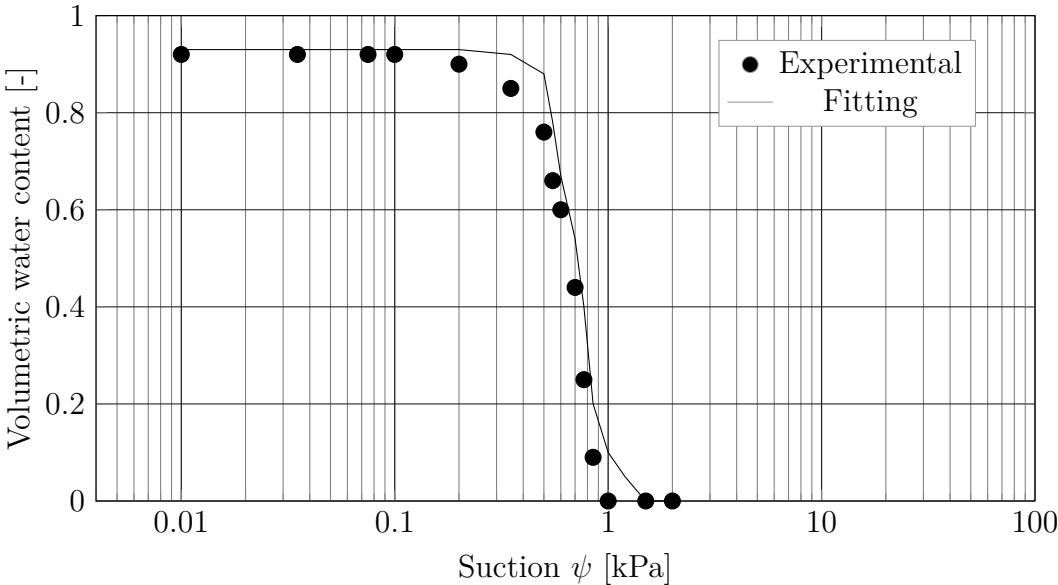


Figure 5.48.: GWCC fitting for T3

5.9. Summary

In this chapter, the experimental results of the SWCCs and GWCCs tests are presented. The hydraulic conductivity functions are derived from these curves using an existing model from the literature which were found to be suitable for geotextiles. Water-characteristic curves are very important since to understand the attitude of the material due to shearing, compression, and infiltration under partially saturated condition. In this chapter also, a method to determine the water-characteristic curve of the geotextile based on the AOS has been presented. Measured GWCCs were compared to the GWCCs derived by the proposed method. Good agreement was found. Figures 5.49 and 5.50 presents the water-characteristic curves and hydraulic conductivity curves of the geotextiles, Hostun sand and kaolin. It can be seen that the geotextile curves are presented by small bandwidth at small suction range compared to the SWCCs. The GWCC curves tested for several geotextile materials show that for wide range of geotextiles the curves are close to each other in case of the values of the AEV and the residual suction. The hydraulic conductivity curves vs suction derived from the GWCC curves show also similarities. Therefore, one nonwoven geotextile sample (B) will be taken to perform the column tests in the following chapter to study the soil-geotextile interaction with one-dimensional flow of water.

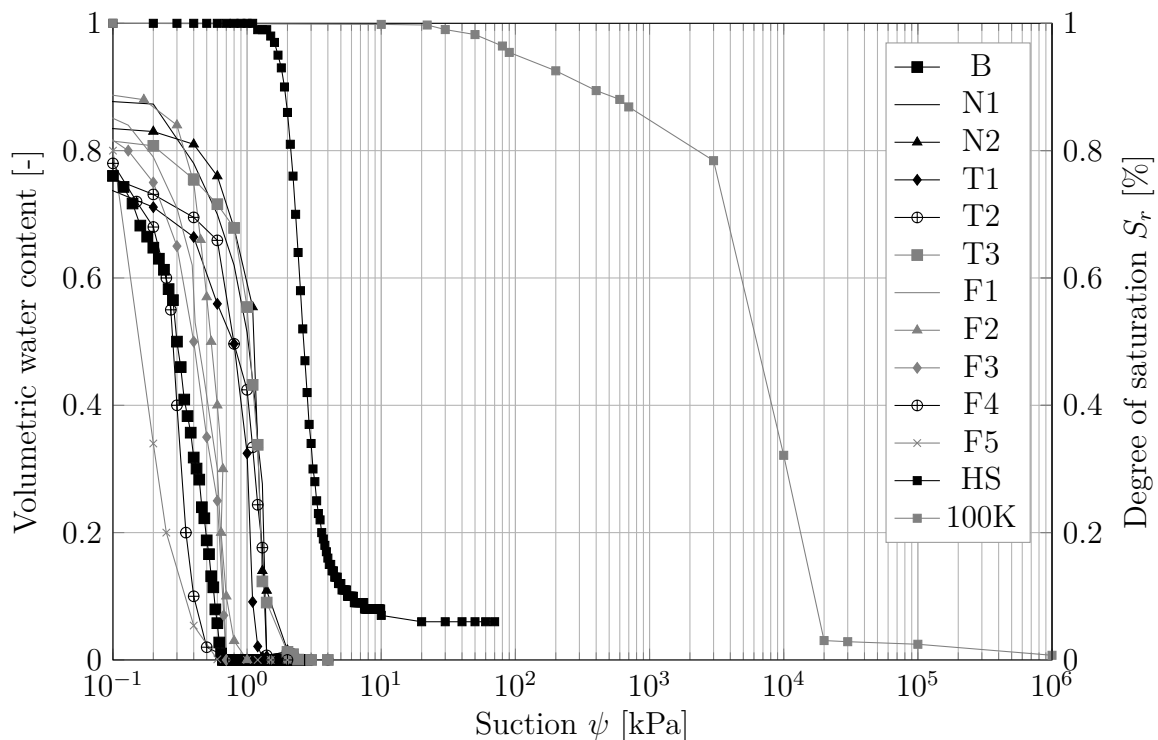


Figure 5.49.: GWCC of geotextiles and SWCC of Hostun sand and kaolin

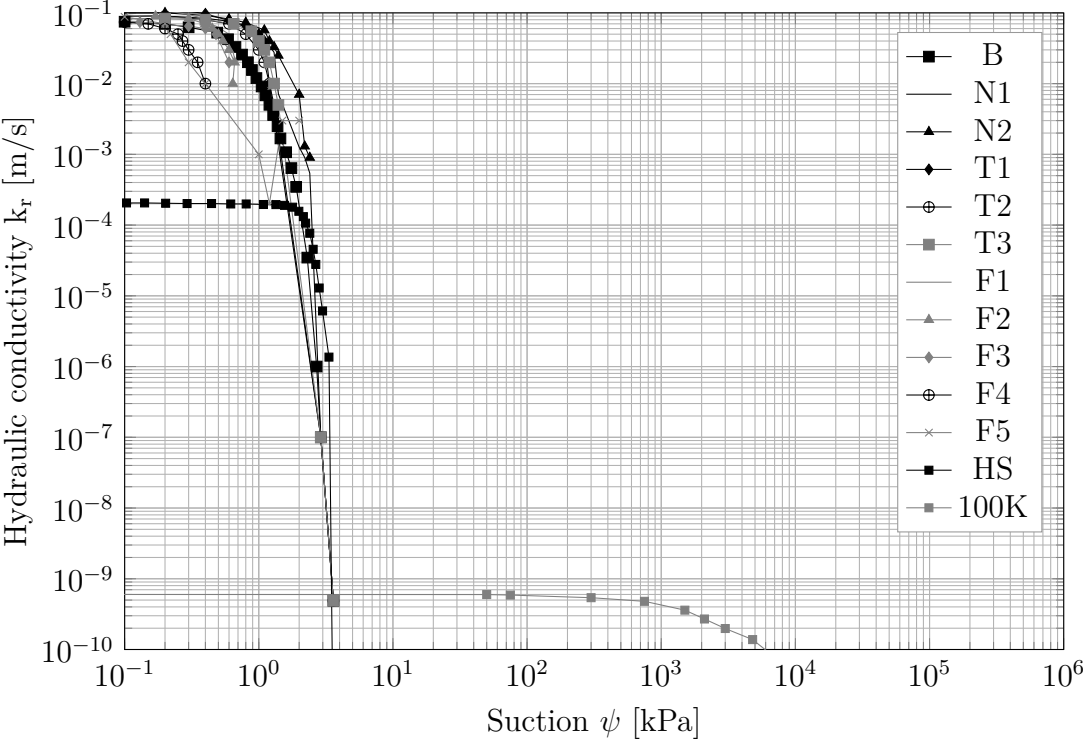


Figure 5.50.: Hydraulic conductivity function of geotextiles and soils

6. Soil/geotextile column interaction

6.1. Introduction

In this chapter, the column equipment is described which was used to perform the one-dimensional flow tests; water through a soil layer with a layer of nonwoven geotextile. A description of the cell and the equipments which are used measuring the volumetric water content and the positive and negative pore water pressure are also described. The tests results and the discussion of the results are also presented in this chapter.

The aim of these tests is to evaluate the performance of a selected nonwoven geotextile to drain and filtrate water through a layered system (soil-geotextile layer system) under partially saturated condition. The results obtained from this analysis will be evaluated from different perspectives:

1. Is the nonwoven geotextile layer however still capable to drain water under partially saturated condition (qualitative analysis)?
2. The effect of the value of the matric suction on the hydraulic conductivity function of both soil and geotextile (quantitative analysis).
3. Testing different types of soils which have different values of AEV to evaluate the usability of the SWCC parameters to the understanding of such a system.

After reviewing the tests results, a separate capital will discuss the above mentioned points and will try to reach common conclusions which will be helpful to understand such systems under partially saturated conditions.

Few tests were performed to analyze the flow of water through a column of soil geotextile interface. Most of the tests were performed using sand material, while others were performed using clay material. However, using pure sand material is not suitable to perform as a top soil layer above the drainage matrix because of the relatively high permeability values and the low cohesion between the sand grains ($c = 0$ kPa). On the

other hand the clay material is considered as a low permeable material which will lead to hold the water on the surface or in the vegetative supporting layer and thus will allow small amount of water to pass through the clay layer to be drained through the geocomposite drainage layer.

In the current study, 4 soil mixtures were used. The tests were analyzed using the SWCC and the hydraulic conductivity curves.

Valuable information will be collected by analyzing the hydraulic conductivity curves of both soil and geotextile. This will help to predict the behavior of the nonwoven geotextile in the field in association to the selected top soil layer. Therefore, this study is focusing on selecting four types of soil with different AEV and to evaluate the unsaturated parameters on the drainage performance of the filter geotextile.

The initial void ratio of the selected soils is defined in accordance to the element tests. The objective here is to use the results of the element tests to explain the behavior of the soils and geotextile in the column test.

After reviewing the state of art of the performed tests in this topic, it was observed that the tests were performed on initially dry soil material or initially defined volumetric water content. In the current study, the soil is initially saturated and then was drained from water from the bottom until reaching equilibrium water distribution at the different soil heights. Later, the water was added to the column from the top. The infiltration stage was stopped when the water filled the column. The final stage was the second drainage stage after the infiltration.

Two sets of sensors are connected to the column device. Time Domain Reflectometry Sensors (TDR) to monitor the change of the volumetric water content and tensiometers to record the change in pore-water pressure.

During the test the zero water level was set to two levels. During the saturation stage, the water level was set to a height of 3 cm above the soil level inside the column, also the water level was set to the level of the base of the column during the drainage stage, infiltration stage, and the 2nd drainage stage.

6.2. Test equipment and test procedure

The 1-D flow test has been performed using a clear hollow Plexiglas cylinder of 240 mm inner diameter and 630 mm in height as shown in Figures 6.1a and 6.1b. Three threaded screws hold the Plexiglas cylinder with the upper and lower caps. The upper cap has a valve used for air ventilating and two other valves connected by plastic tubes to an

electrical pump which allows adding water to the column from a reservoir. The pump has different flow rates to simulate the rainfall on the soil. The pumped water falls from the two valves over a hollowed disk which helps to distribute the water equally over the cross-section area of the column. The lower cap has two valves allowing to saturate or desaturate (drain) the water from the soil during different stages of the test and to flush the water at the lower cap from any trapped air by circulation. The column is connected to a stand pipe through plastic tube to define the zero water level. During the infiltration stage, two types of pumps, available at the laboratory, were used based on the hydraulic conductivity of the soil layer; a relatively high one and another slower one. For 15%K and 20%K tests, as the infiltration stage needs long time to fully saturate the top soil layer, a security system was used to stop the pump when the water starts to flow outside the column and therefore stops the test.

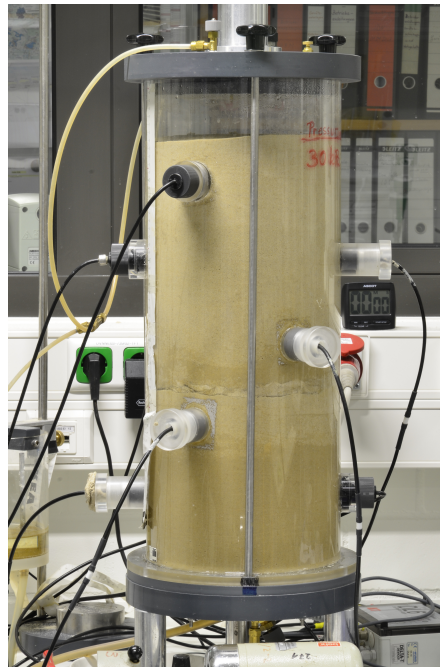
At five different heights (namely; 110, 210, 310, 410, 510 mm), a set of time-domain reflectometer (TDR) and pore water pressure sensors (Tensiometers) are installed in order to monitor the volumetric water content and also positive and negative pore water pressures, respectively. The tensiometer's tubes were filled with distilled water and submerged in a container of distilled water to make sure the ceramic tips are fully saturated.

All the measuring devices were checked and calibrated before starting the test and the pump device was tested to provide the correct flow rate needed in this study. Due to the fact that the TDR needs to be surrounded by soil, it was not possible to install the geotextile layer close to the TDR and Tensiometer.

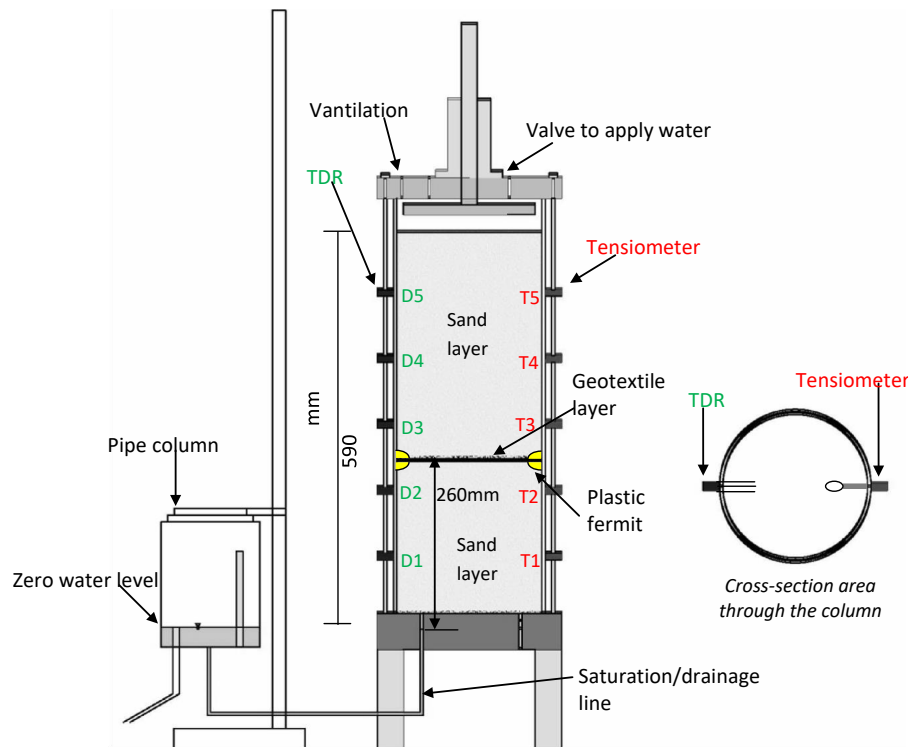
The soil was mixed by weight the target proportions of Hostun sand and kaolin after drying them inside the oven. Then water was added to the dry soil mixture reaching the optimum water content. After that the soil mixture was protected with plastic folie to prevent the evaporation.

During sample preparation, water was allowed to flow from the stand pipe through the bottom of the column to a certain height, and then a defined amount of sand was pluviated from the top of the column and compacted in layers of about 100 mm in thickness using a 700 g weight hammer to ensure homogeneity of the soil column model. Care is needed at this stage in order not to damage the electronic equipment connected to the cell which is installed at each level before adding the soil. Afterward, water level was increased again and another amount of soil was pluviated. The procedure was repeated until the reaching a height of 65 cm along the column. Two combined geotextile layers are placed in a height of 260 mm from the base of the column in the middle distance between sensors (2) and (3). The perimeter of the geotextile layers was sealed from above and below with plastic fermit to prevent the water from seeping around its perimeter. The sealing material was tested

using a small prototype column and it showed efficiency to prevent water from sinking.



(a) photograph



(b) schematic diagram

Figure 6.1.: Schematic sketch and a photograph of the column apparatus

The reason using two layers of geotextile rather than one is to prevent the water from flowing in the opening made by the rods used to combine the elements of the geocomposite drainage layer together (a geonet sandwiched between two nonwoven geotextiles). The vertical displacement was monitored for any possible settlement may occur during the test. After constructing the sand column, flashing has been made at the lower cap by circulating the water between the two valves connected to the lower cap, this procedure is useful to remove any air bubbles trapped below the filter paper. The water level during this stage was increased to 30 mm above the soil surface level by pumping it from the bottom. The TDR and Tensiometer sensors are set to monitor the volumetric water content and pore water pressures. The readings from the TDR sensors are checked with the water-retention curve of the soil and they were located on fully saturated zone. The tensiometers readings were compared with the hydrostatic pressure and the results were accepted. After 24 hours, the valve at the bottom of the cell was opened and water was allowed to drain. The water head was fixed at elevation ($z = 0$).

During the drainage stage, the column was monitored to check the suction value and the corresponding volumetric water content. The infiltration stage simulates a scenario in which a rainfall will take place. The flow rate of water through the pump was controlled to be less than the saturated hydraulic conductivity of each of the selected soils. This will assure an existing of partially saturated condition among the column profile. The analysis of the column tests results will be better explained using the SWCC to understand the behavior of such systems. At selected points over the height of the column, the TDRs are used to measure the volumetric water content and the tensiometers to measure the positive and negative pore water pressure at different stages of the test. The test was performed inside a controlled temperature room inside the laboratory. During the drainage stage, with the increase in the suction (negative pore water pressure), the measuring points will follow paths on drying curve of the SWCC and during the infiltration stage (positive pore water pressure), the points will follow paths on the wetting curve of the SWCC.

The final stage (2nd drainage stage) in which the water was allowed to drain from the column immediately after the infiltration stage may provide an understanding to the new moist content profile within the soil after a rainfall, which indicates initial conditions in case a possible rain season will occur soon after the previous one. According to the case studies presented earlier, the failure stability problem had occurred after rainy weather and therefore it will be helpful to understand the moist profile around the column and compare it with the drainage condition. The boundary conditions in this stage are similar to the first drainage stage.

The drainage stage was continued until complete equilibrium was reached. The rainfall

stage started by applying colored water from the top of the column using potassium permanganate (KMnO_4), which allows a better observation of the water flow through the column. This color can be washed out from the soil after the test easily. At the final stage, the column was left for one day to observe the redistribution of the moist over the soil profile after the infiltration stage.

6.3. Tensiometer Sensors

The tensiometer used in this study is a Miniature Pressure Transducer Tensiometer (UMS-Umweltanalytische Mess-Systeme, today METER Group Munich). As show in Figure 6.2, it consists of a body and a tensiometer cup including a ceramic cup and a water filled tube. The tensiomter has an overall length of 81 mm and the body is 20 mm wide. The body consists of the pressure transducer, the acrylic plastic body and the lead.

Based on the piezoresistive effect of the silicon semiconductor, the sensor measures the change of the specific electric resistance due to deformations. These deformations are caused on the sensitive silicon chip by changes in pore-water pressure. By using a Wheatstone Bridge the change of the specific electrical resistance is processed to a signal, which corresponds to certain pore-water pressure value. The ceramic cup has an active surface of 0.5 cm^2 and is 5 mm in diameter. Thus the soil disturbance of the tested soil is small. The response time of the sensor is fast. The tube is transparent and thus air bubbles are easily detectable.

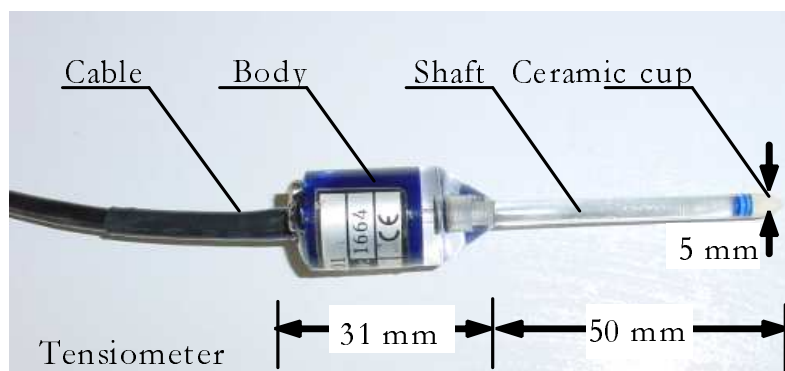


Figure 6.2.: Tensiometer Sensor, after Lins (2009)

6.4. Time Domain Reflectometry Sensors

The TDR sensor used in this study is a Mini Buriable Waveguide (Soil-moisture Equipment Corp.). It consists of 3 parallel rods and a cable as shown in Figure 6.3. It is designed to be installed permanently in the soil and allows the measurement of the dielectric constant of the tested soil. The rods of the mini TDR sensor are 80 mm long with a 25 mm spacing between the outer rods. The wire spacing is 12.5 mm. For computing, analyzing and saving the test results the TDR sensors (TDR SOILMOISTURE METERS (TRASE)) are connected to a multiplexer and then to a Trase System. The multiplexer allows measurements to be made automatically of several TDR sensors. A switching board with 16 channels for connecting up to 16 TDR sensors was used. Measurements, computations and analysis of the data are done by the trase system. A computer connected to the Trase system is used to display the results.

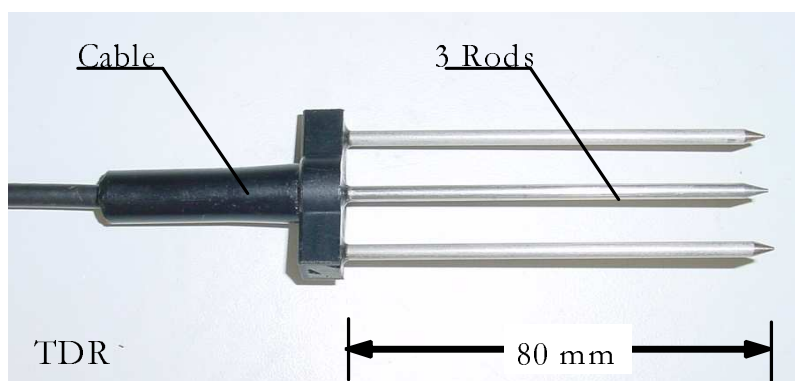


Figure 6.3.: Time Domain Reflectometry Sensor (TDR), after Lins (2009)

6.5. Testing program

Few tests were performed to analyze the flow of water through a column of soil geotextile interface. Most tests were performed using sand material or using clay material. However, for the testing program the materials should be selected satisfying the drainage and filtration design criteria.

In the current study, five column tests were performed. One test was performed using pure sand without geotextile. The aim of the test is to evaluate the quality of the test, the performance and accuracy of the sensors, and to analysis the results of a column test at different saturation and de-saturation stages.

Four tests were performed on Hostun sand and three soil mixtures (10K, 15K, and 20K) in which a geotextile layer was placed at elevation of 260 mm from the bottom base of the column device as shown in Figure 6.1.

6.6. Tests results

The tests results will be presented for each test separately and the observations of the tests will be explained. The main results and final conclusions will be described later.

6.6.1. Hostun sand (without geotextile layer)

In this test, the column has been filled with Hostun sand only. The objective of this test is to observe the infiltration process using the column device and to check the performance of the measuring equipments (Tensiometers and TDRs). The results will be taken as a reference and will be compared with the following test in which a horizontal layer of nonwoven geotextile is placed between two Hostun sand layers.

The target void ratio of the test was 0.66. The achieved void ratio was 0.64. The reason is because of installing the sensors which made the densifying of the sand not easy using a 2.5 kg hammer without damaging the equipments.

6.6.1.1. Saturation stage

In this stage, the top of the soil layer was located at elevation 550 mm and the water level was fixed at elevation 570 mm. The readings were observed for more than 24 hours to make sure that the column is fully saturated and stable and reliable readings were measured as shown in Figure 6.4. Figure 6.5a shows a comparison between the values of the pore water pressure during the saturation stage with the hydrostatic pressure values determined using the following equation:

$$p = h \cdot \rho \cdot g \quad (6.1)$$

where, p : water pressure [kN/m²], h : height of the point [cm], ρ : density of water [kN/m³], g : the gravitational constant [9.81 m/s²]. Figure 6.5b shows the location of the five points on the SWCC.

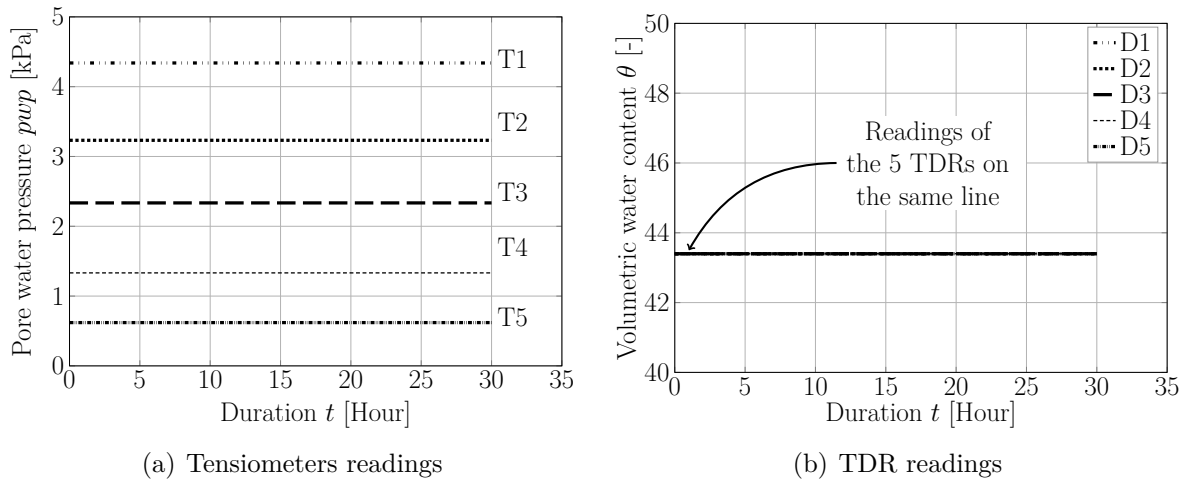


Figure 6.4.: Saturation stage: Change of the readings vs time [HS]

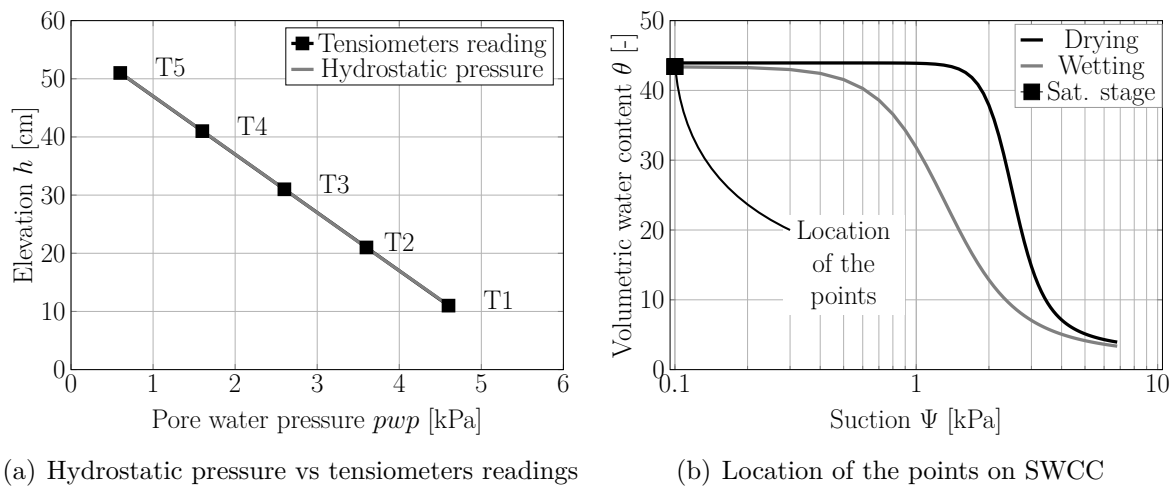


Figure 6.5.: Saturation stage: Tensiometer readings, location of the points on SWCC [HS]

6.6.1.2. Drainage stage

The drainage stage was started by allowing the water to drain from the bottom of the column. The zero level is already defined at the bottom of the column. The readings from the TDRs and tensiometers are observed (Figure 6.6) to be able to define the end of the stage when the readings show no change versus time. The curves show a relatively fast graduate reduction in the readings due to water drainage. A small change in the water content was observed by D1 and D2 while D3, D4, and D5 at the middle and the top of the column recorded a reduction in the water content. The drainage of the water is relatively fast due to the poor grading of irregular shape of the grains of Hostun sand. Figure 6.7 shows the path of the five reading points (pore-water pressure and volumetric

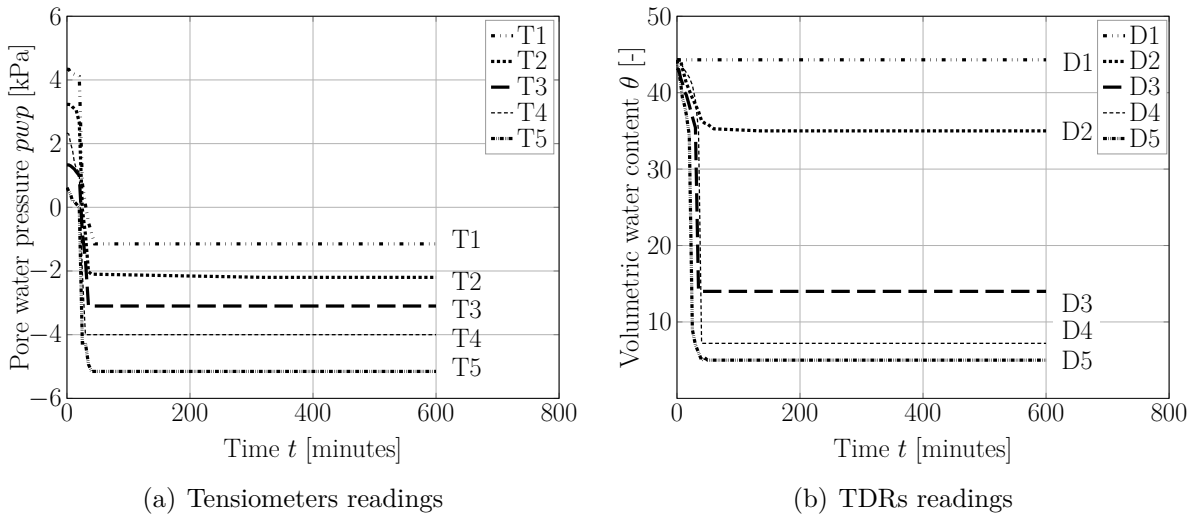


Figure 6.6.: Drainage stage: The readings of the tensiometers and TDRs [HS]

water content) on the drying path of the water retention curve of Hostun sand. It can be seen that P1 (related to point 1) was above the air-entry value of the sand while P2, P3, and P4 were past the AEV. P5 was located at the residual suction value.

Figure 6.8 project the location of the final position of the 5 points using the suction values

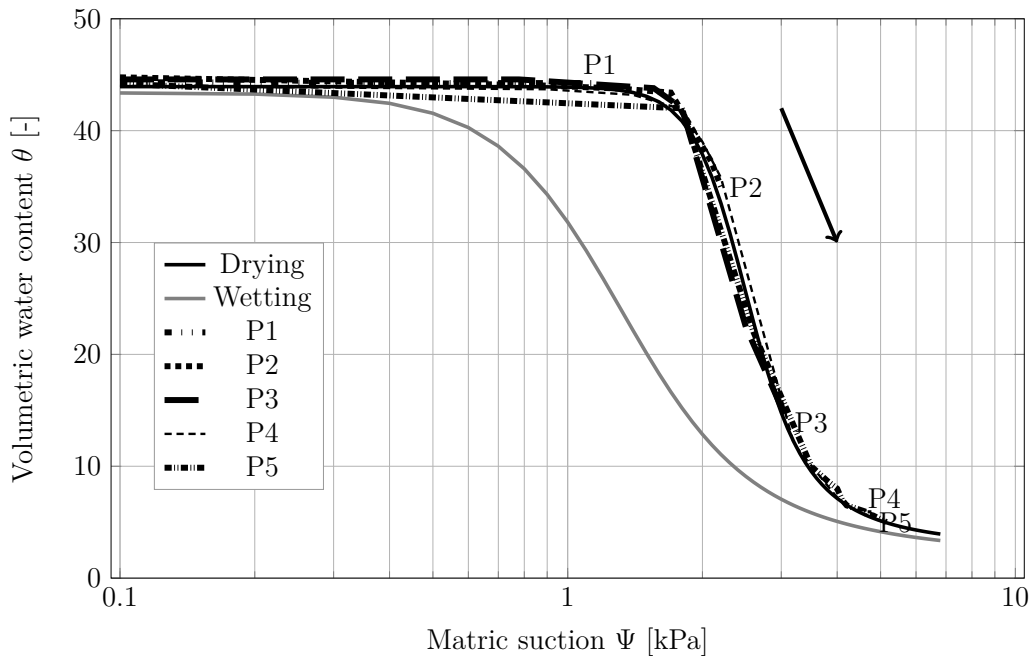


Figure 6.7.: Drainage stage: Location of the points on the SWCC for different elevation [HS]

on the hydraulic conductivity - suction curve of Hostun sand for drying path. Point P1 is

still within the saturated zone and the permeability is equal to the saturated permeability of the sand, while P2 and P3 are beyond the AEV suction. The points P4 and P5 are at low suction range in which the permeability values are very low.

Figure 6.19 shows the position of the five points on the height - vol. WC curve based on the location of each point inside the column device at the end of the drainage stage. The results look compatible with the data measured from the sensors during the test.

Lins (2009) performed series of imbibition and drainage tests on Hostun sand using a column device (240 mm inner diameter and 282 mm height). A similar sample preparation method was used to the current study. The distribution of void ratio along the height was homogeneous and the drainage curve, imbibition curve, scanning drainage and scanning imbibition curves were measured by using similar tensiometers and TDRs setup.

Figure 6.10 shows the the volumetric water content values versus suction for three different reading points for two different soil samples; loose state ($e_o \approx 0.89$) and dense state ($e_o \approx 0.66$). The two tests show good results and the results were comparable. The established SWCCs were in good agreement with the determined in the current study.

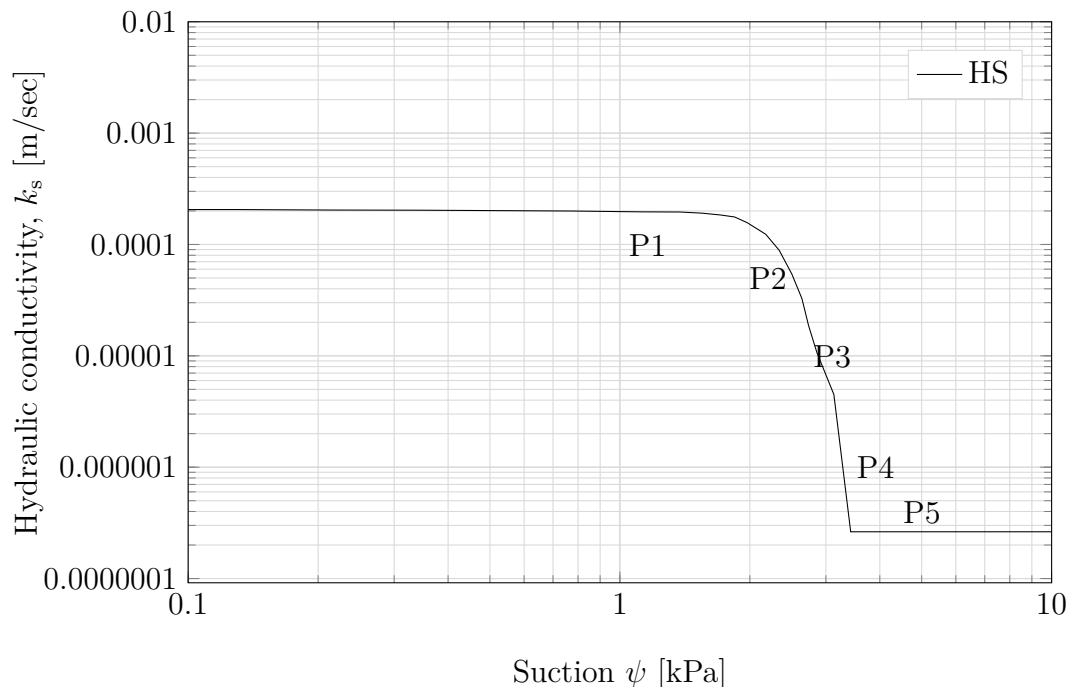


Figure 6.8.: Drainage stage: Location on the points on the HC-suction function [HS]

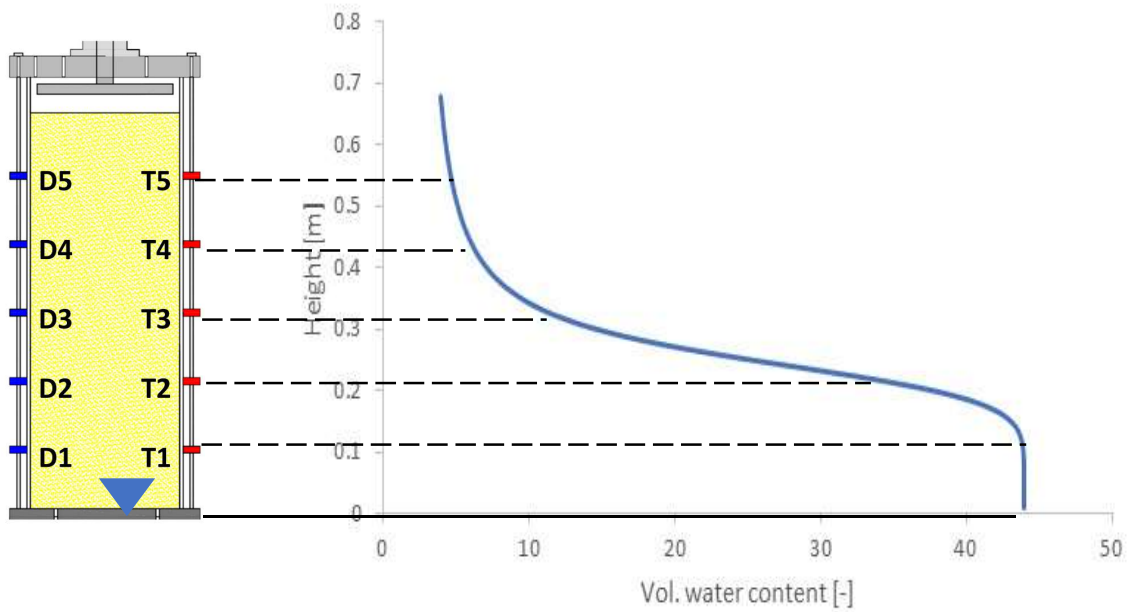


Figure 6.9.: Location of the points on the height - vol. WC relation

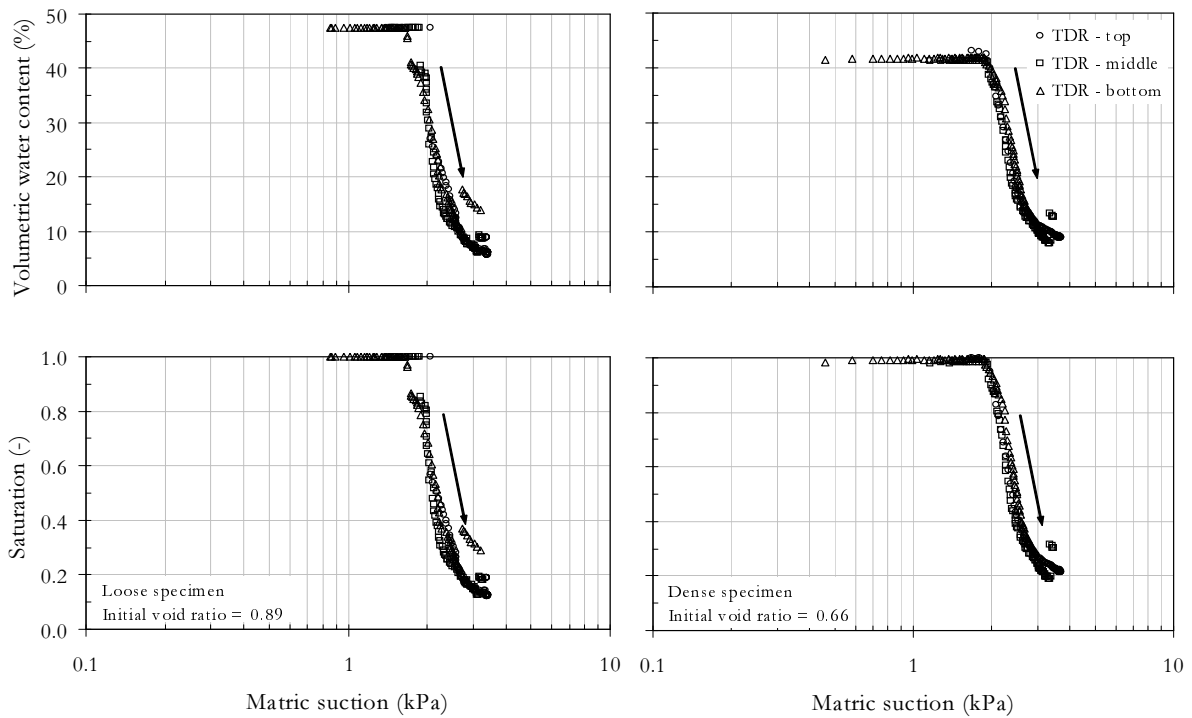


Figure 6.10.: Readings of tensiometers and TDR sensors for drainage and imbibition SWCCs for column test I (loose specimen-left, dense specimen-right) after Lins (2009)

6.6.1.3. Infiltration stage

After the drainage stage, the water was added to the column through the two openings in the top cap with a rate less than the saturated hydraulic conductivity of the sand. The calibration was made earlier during the preparation stage.

The readings were taken every 5 minutes. Figures 6.11(a) and 6.11(b) show the change in pore water pressure and volumetric water content versus time respectively. Figures 6.12 presents the location of the points on the SWCC of Hostun sand.

Figure 6.13 presents the location of the five points on the hydraulic conductivity - suction curve on the wetting path on the end of the infiltration stage.

Lehmann et al. (1998) investigated the water dynamic in a sand column with fluctuating capillary fringe for different flux and pressure boundary conditions. The observations indicate an influence of the hysteresis of the water retention curve on water dynamic. The same matric potential fluctuations lead to different water content variations.

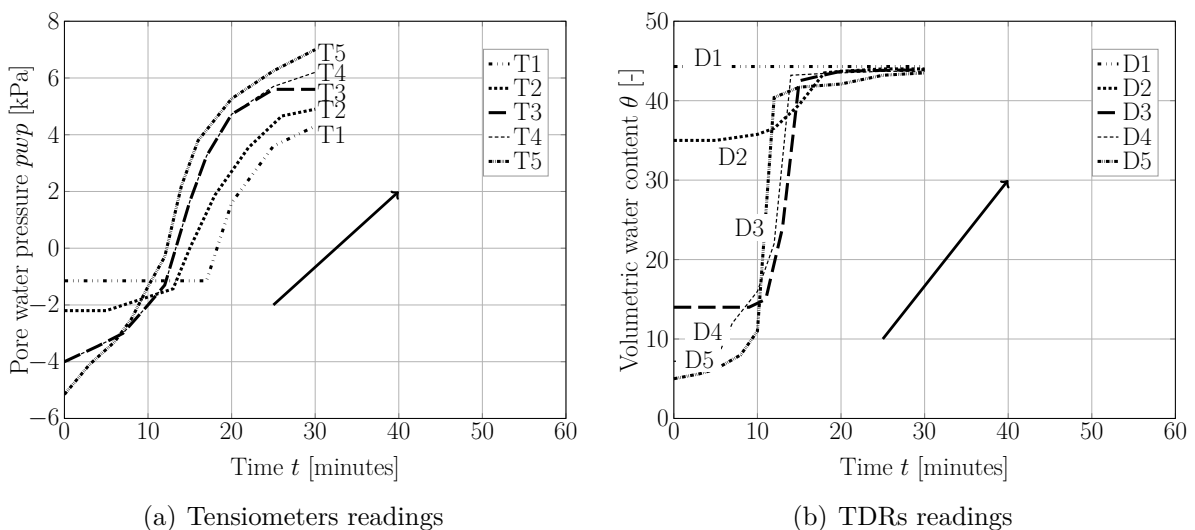


Figure 6.11.: Infiltration stage: Readings of the tensiometers and TDRs [HS]

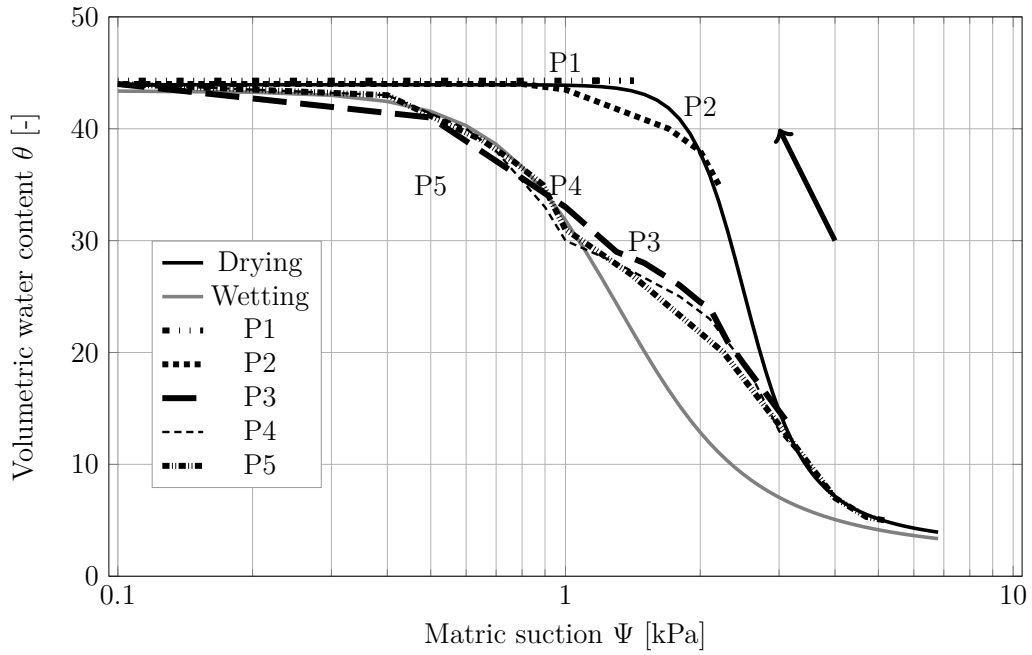


Figure 6.12.: Infiltration stage: Location of the points on the SWCC for different elevation [HS]

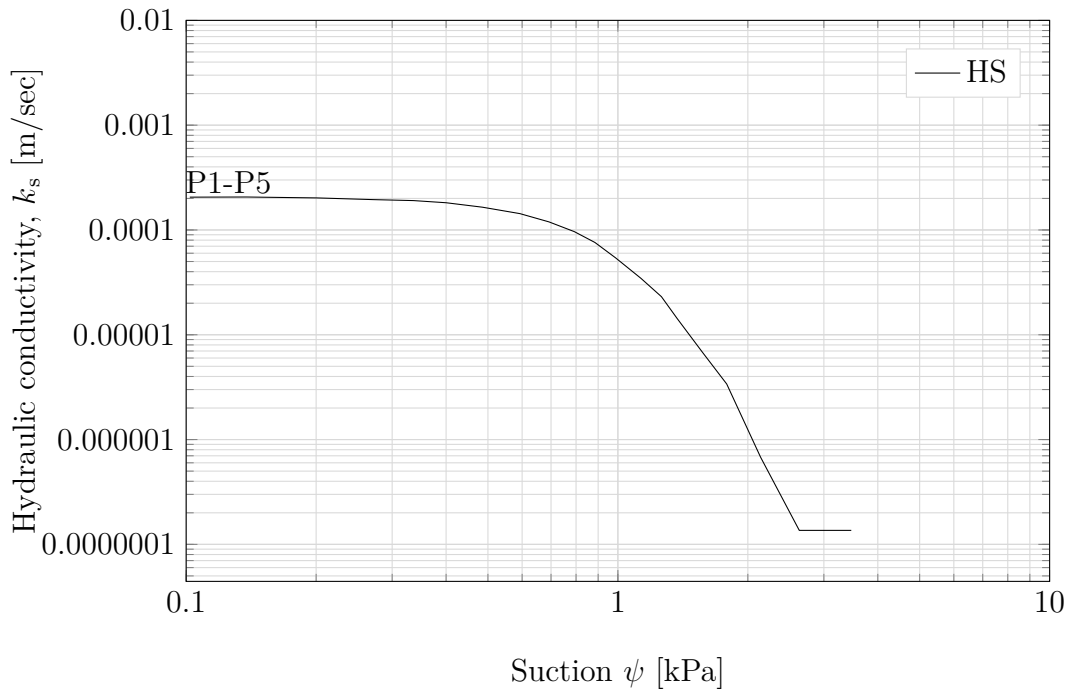


Figure 6.13.: Infiltration stage: Location on the points on the HC-suction function [HS]

6.6.1.4. 2nd drainage stage

During this stage, the column was left in order to reach an equilibrium in the readings of the sensors. Figure 6.14 shows that the reading is reducing with time until reaching values close to those recorded during the drainage stage.

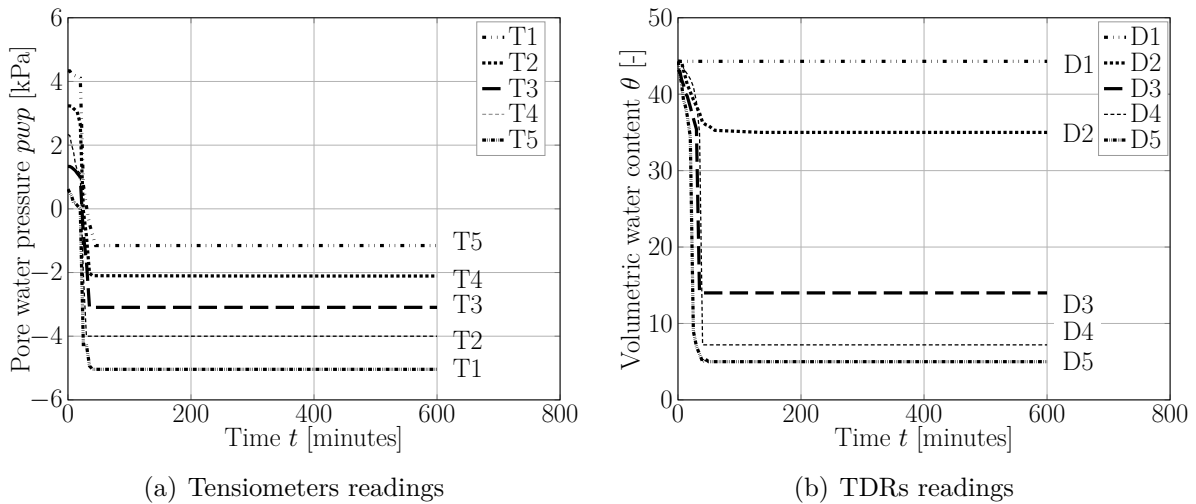


Figure 6.14.: 2nd drainage stage: The readings of the tensiometers and TDRs [HS]

6.6.1.5. Main points from the test (HS)

During this test, a column filled with clean Hostun sand was initially saturated and then drained from water until reaching an equilibrium. The column was infiltrated from the top to simulate a season of fall of water. Until the water level reached a height of 50 mm above the soil layer the column was again drained until reaching stable readings.

Figure 6.15 summaries the results of the test by presenting the readings of the pore-water pressure at the end of each stage of the test. The pore water pressure distribution is demonstrated by the hydraulic gradient. During the following tests, the pore-water pressure distribution will be changed due to the influence of the nonwoven geotextile layer. The air-entry value of the soil and geotextile is different which will lead to shift the hydraulic pressure.

Pore water pressure is decreased rapidly during the drainage stage and a rapid increase during the infiltration stage, this could be due to the granular and edgy shape of the particles of Hostun sand and also to the poor-graded grain size distribution curve which leads to a relatively high permeability.

From this test, it can be seen that during the drainage stage, the water level after reaching

an equilibrium, the water did not reach a level higher than 245 mm. This will help to plan the elevation of placing the geotextile layer at elevation around 245 mm. to avoid making the geotextile layer fully saturated due to its location inside the column.

During the infiltration test, Figure 6.12, P1 was saturated and thus when the point moved to the left until the suction reduced to zero. Similarly, point P2 below the AEV moved to the zero suction following the drying path. However, the points P3, P4, and P5 moved following an individual scanning path until reaching the main wetting path.

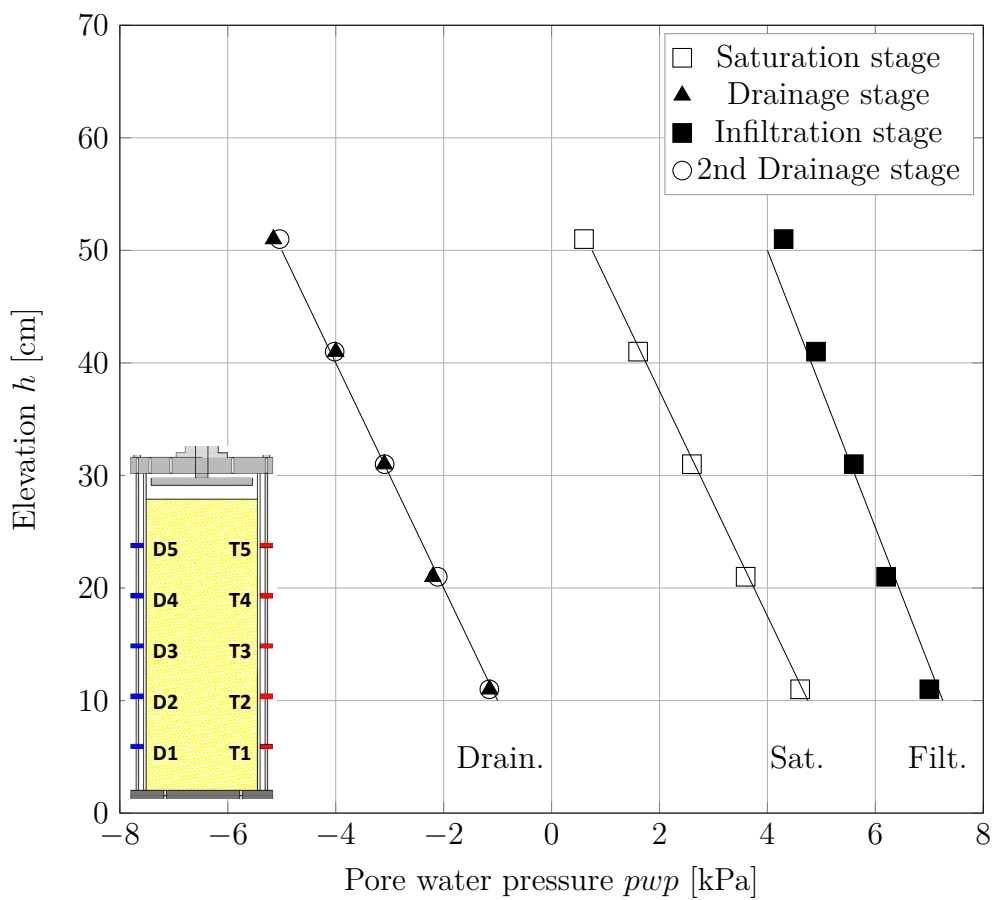


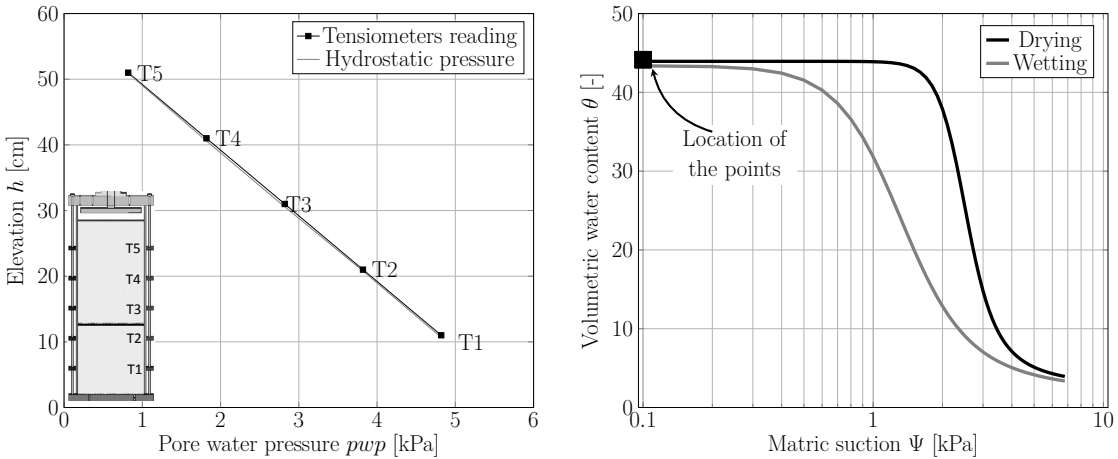
Figure 6.15.: Location of the points during the test stages for different elevation [HS]

6.6.2. Hostun sand with geotextile

In this test, a horizontal layer of nonwoven geotextile has been placed at elevation 260 mm from the base bottom of the column ($z=0.26$ m). The void ratio of the sand layer is approximately 0.627.

6.6.2.1. Saturation stage

After the construction of the column, the test was left for 24 hours in order to assure fully saturated condition. Figure 6.16a shows the values of the pore water pressure versus depth at the saturation stage measured from the tensiometers devices. The readings are compared with the hydrostatic pressure values as the water level was fixed at height 560 mm ($z=0.56$ m). Figure 6.16b shows the location of the points on the soil-water retention curve for sand. It show that each soil layer was fully saturated during the saturation stage as it can be observed from the stable readings of the sensors and the location of all the points through the profile on the SWCC. That shows, the method used to prepare the soil initially with its optimum water content and then adding it to the column in small portions with increasing the water height every time was suitable and helped to achieve a fully saturated column setup.



(a) Hydrostatic pressure versus the tensiometers readings (b) Location of the points on the SWCC

Figure 6.16.: Saturation stage: Tensiometer readings, location of the points on SWCC [HS+G]

6.6.2.2. Drainage stage

Figure 6.17a shows the change of pore water pressure at different depths with time during the drainage stage. Figure 6.17b presents the reduction in volumetric water content during the drainage stage. Figure 6.18 presents the same results for the first 100 minutes to have a close view to the change in the readings during the drainage stage.

In Figure 6.19, the effect of suction on the five points is illustrated.

The pore water pressure started to reduce with time. The drop in pore-water pressure did not develop gradually over the sensors at different depth. The reductions started from sensor T5 and T4 at the top of the column followed by sensor T3 and later sensor T2.

About 25 minutes after starting the drainage stage, the reduction of water content above the geotextile layer was in different slope from that below the geotextile. The geotextile layer started to suffer from an increase in matric suction which led to reduction in the flow rate through it as the air started to replace the water inside the pores of the geotextile.

As shown in Figure 6.17b, the increase in the suction is associated with the increase of the overall suction inside the column and since the air-entry value of the nonwoven geotextile is smaller than the one for sand, the geotextile started to have an effective reduction in the water permeability.

The reduction in the drainage performance of the geotextile due to the increase in the suction is not related to the drop of the water content in the soil layer below the geotextile. The reduction in the water flow through the geotextile occurred earlier before the moist content measured by T2 reached a suction value higher than the air-entry value of the sand also without considering the effect of the capillary rise of water above sensor T2. Figure 6.18 represents the readings of the tensiometers and TDRs for the first 100 minutes of the drainage stage.

As a result, the water started to be stored above the geotextile layer. It can be noticed at tensiometer T3, located 40 mm above the geotextile layer, the pore-water pressure stopped to reduce at suction value ≈ 2.2 kPa and then started to have an opposite behavior with an increase in the pore water pressure to 1.8 kPa followed by a reduction again. This phenomenon can be explained using the hydraulic conductivity curves of the soil and the geotextile which are determined using a fitting model based on the water-retention curves from the element tests in the previous chapter.

The unsaturated hydraulic conductivity curves for soil and geotextile are shown in Figure 6.20. The geotextile reached the point in which the hydraulic conductivity drops below the conductivity of the soil (point A) and therefore the water started to be stored above the geotextile which leads to an increase in the moist and pore water pressure due to the

water coming from the overlying layers of the column. This stored water led to a reduction in the matric suction which caused the water to flow through the geotextile with slow rate. The figure shows also the location of each point at the end of the drainage stage. The flow of the water at point 3 is lower than the saturated permeability of the sand and it shows how it is difficult to allow the water to flow to the geotextile layer.

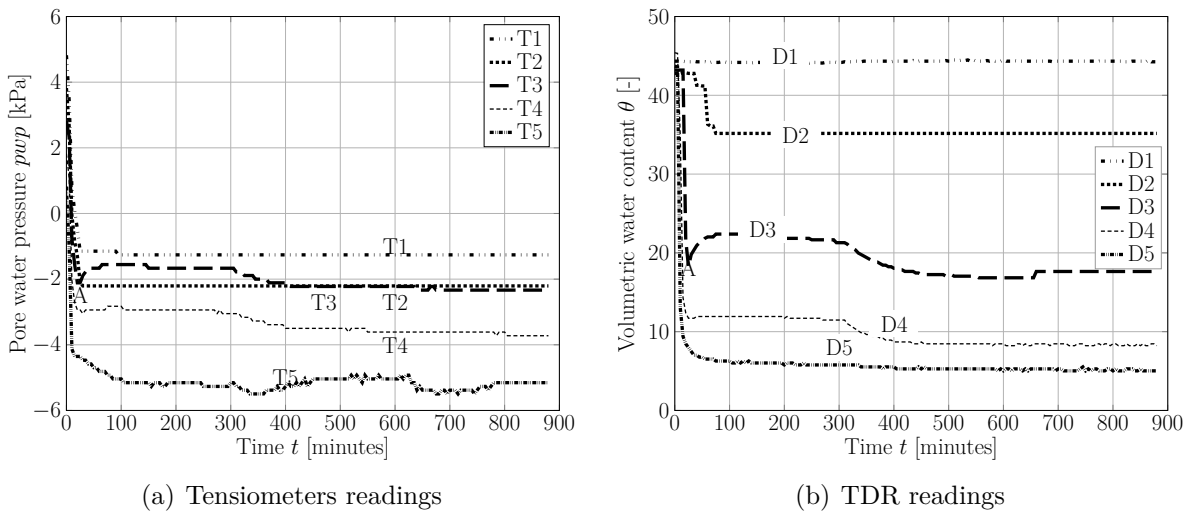


Figure 6.17.: Drainage stage: Sensors readings [HS+G]

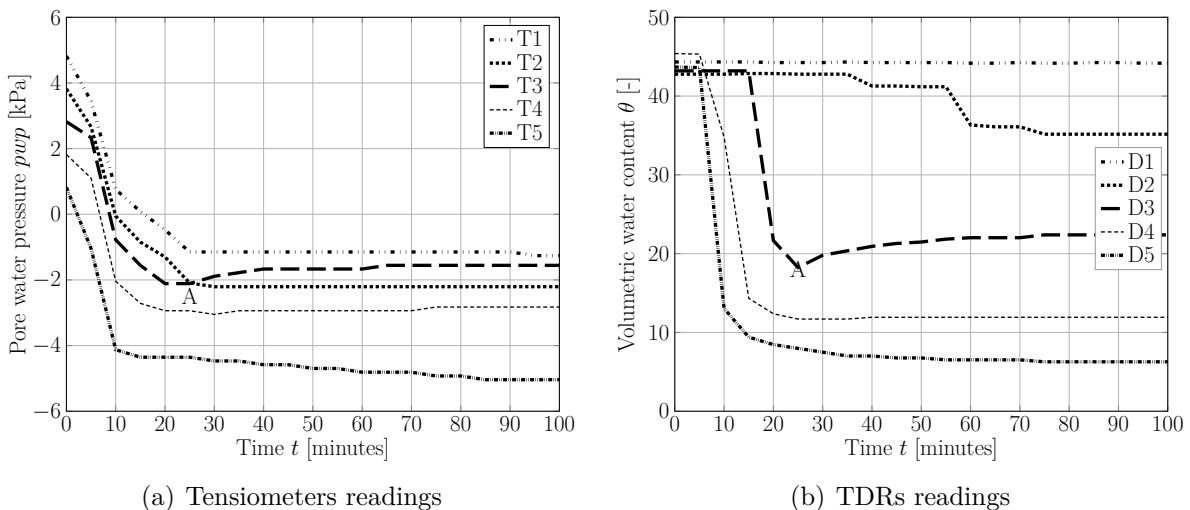


Figure 6.18.: Drainage stage: Sensors readings [HS+G]

Figure 6.19 shows the location of the TDR and Tensiometers sensors on the water-retention curve of the sand. It can be seen that P1 at elevation 110 mm from the bottom of the

column stayed above the air-entry value AEV of the sand, while point P2 located at 210 mm started dropped down below the AEV. For the Points P4 and P5, the reduction on the water-retention curve continued to drop at the transition zone and residual zone, respectively. For point P3, it can be seen that it dropped to a certain point in which it started to follow a hysteresis path from the drying curve towards the wetting curve. During this stage, it can be seen clearly dark areas of moist developing above the geotextile layer and above the bottom of the column due to capillary forces as shown in Figure 6.21. The moisture development above the geotextile is a sign of reduction in the hydraulic conductivity of the geotextile due to increase of suction and thus the water started to be blocked above the geotextile layer.

Iryo & Rowe (2003) and Krisdani et al. (2008b) reported an increase in the water moist above the geotextile after the drainage stage which is an evidence of a capillary break at the geotextile layer as shown in Figure 6.22.

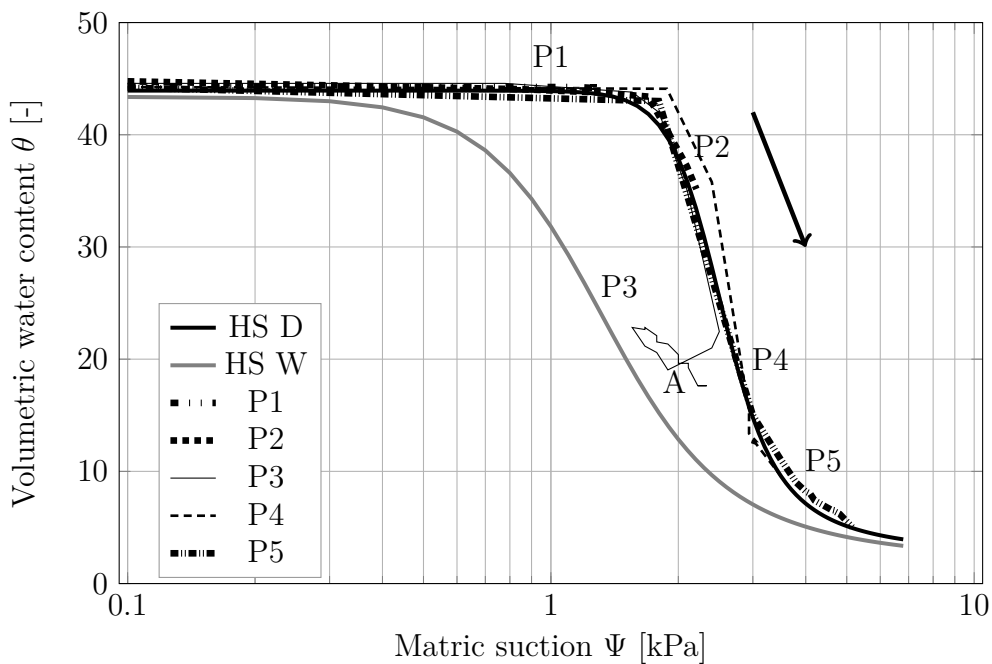


Figure 6.19.: Drainage stage: Location of the points on the SWCC [HS+G]

6.6.2.3. Infiltration stage

In this stage, the water was pumped into the the column from the top of the column apparatus. The rate of the water flow was $1.8E-4$ m/s which was selected to be less than

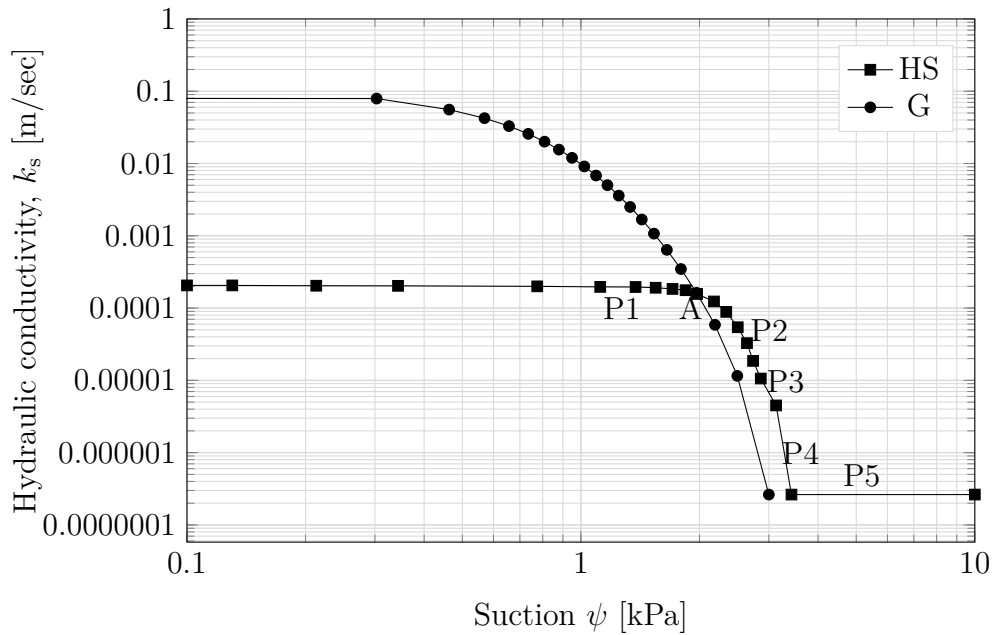


Figure 6.20.: Hydraulic conductivity function of Hostun sand and geotextile and location of the points P1 and P5 at the end of the drainage stage on the function of Hostun sand [HS+G]

the saturated hydraulic conductivity of Hostun sand. Figure 6.23(a) shows the readings of the tensiometers with time. The change of the volumetric water content is presented in Figure 6.23(b).

The water pressure starts to increase in tensiometer T5 at the top of the column followed by tensiometer T4 and T3 consequently. After 43 minutes from starting the infiltration stage, the water started to infiltrate through the geotextile layer and tensiometer T2 started to show an increase in the pore water pressure. The increase in pore water pressure continued as the water level inside the column was increasing until the water filled the column and the test has been stopped. In figure 6.24 the volumetric water content suction path determined from the tensiometers TDRs readings during the infiltration stage are compared to the main drying and wetting SWCC of the Hostun sand.

It can be noticed from the figure, that the points T3, T4, and T5 started to follow hysteresis path in order to reach the wetting path of the water retention curve of the soil. After the infiltration stage, it can be noticed that the moist re-blocked above the geotextile layer which gives the evidence that the unsaturated condition will affect again the performance of the geotextile layer to transfer the water.

Figure 6.25 shows the location of the points the hydraulic conductivity function of Huston sand at the end of the infiltration stage.

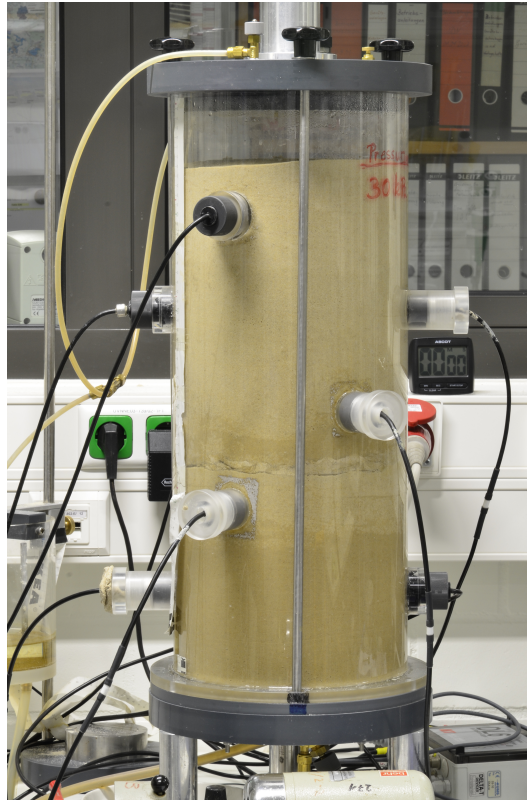


Figure 6.21.: The state of the column at the end of the drainage stage

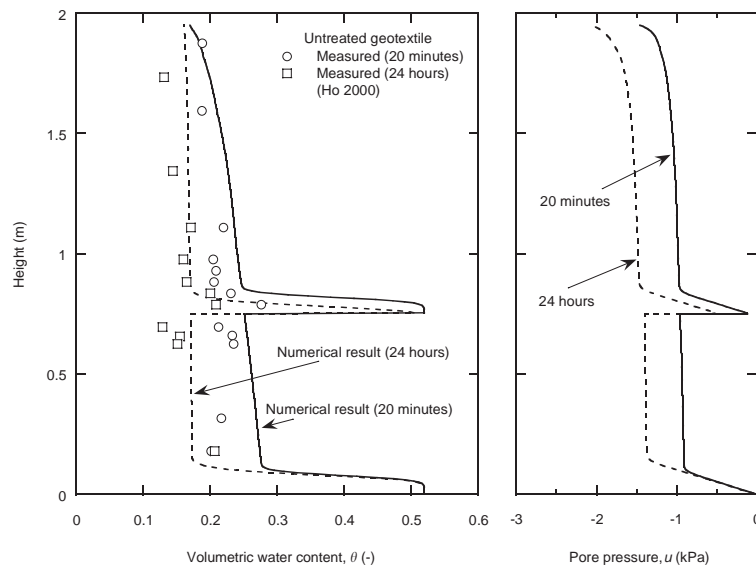


Figure 6.22.: WC & pwp profiles from experiment & numerical simulation after Iryo & Rowe (2003)

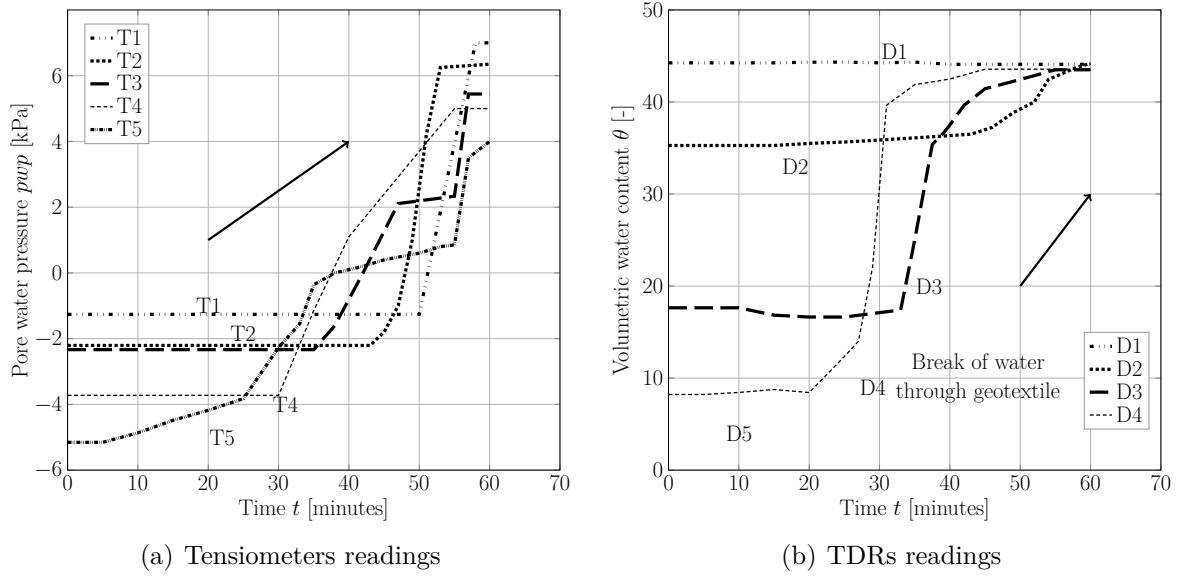


Figure 6.23.: Infiltration stage: The tensiometers and TDRs readings [HS+G]

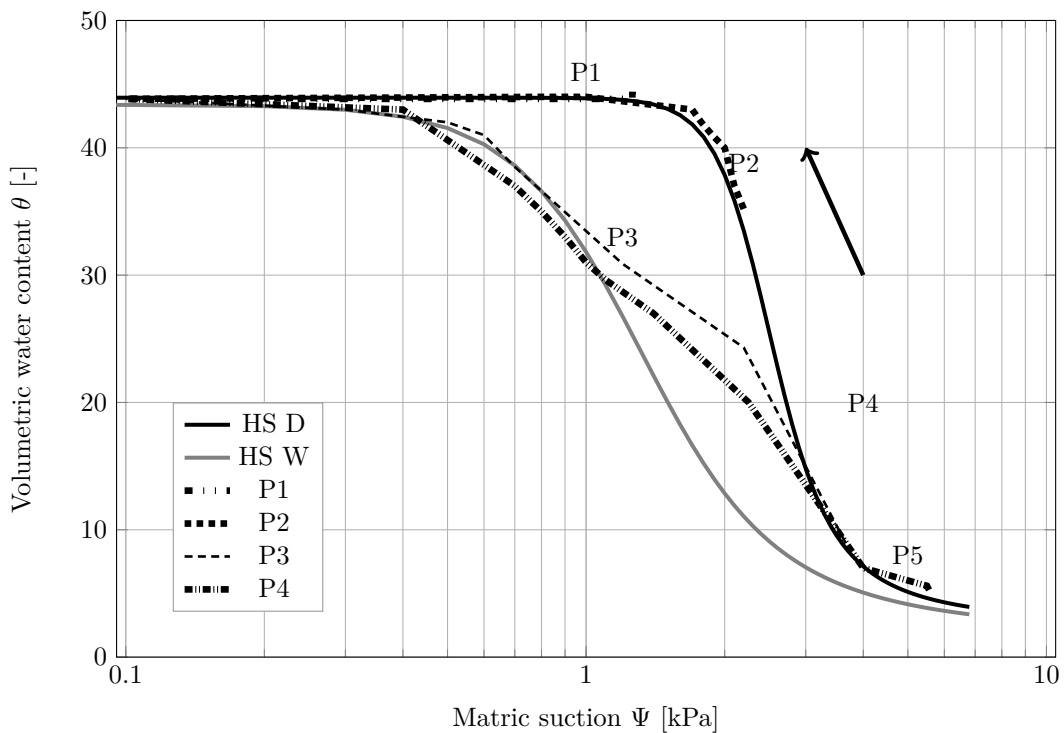


Figure 6.24.: Infiltration stage: Location of the points on the SWCC for different elevation [HS+G]

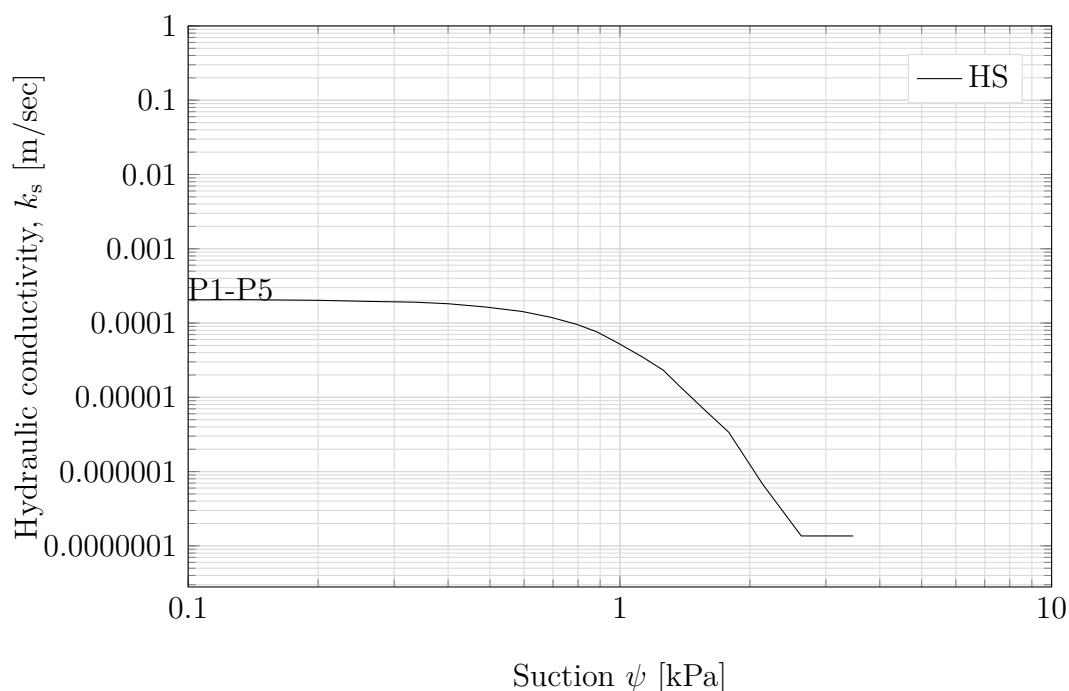


Figure 6.25.: Infiltration stage: Hydraulic conductivity function of Hostun sand [HS+G]

6.6.2.4. 2nd drainage stage

This stage starts after the infiltration stage. The sensors recorded the reduction in the pore-water pressure and volumetric water content with time until reaching stable reading. Figure 6.26 shows the recorded readings of the sensors. The curves show that the top soil layer (above the geotextile) will be in unsaturated condition again after a rainfall condition. The geotextile layer will become impermeable again and the potential to develop water moist above the geotextile layer may occur again.

6.6.2.5. Main points from the test (HS+G)

During this test, a geotextile layer was placed at elevation 260 mm from the bottom of the column. The elevation was selected carefully that the sand layer below the geotextile layer will not be fully or nearly saturated during the drainage or the infiltration stages. This step is important to avoid any chance of re-saturating the geotextile layer from bottom. During the drainage stage, it can be seen from Figure 6.19 that the geotextile created a capillary break and diverted the flow of water above it due to the low air-entry value of the geotextile layer compare to the above sand layer.

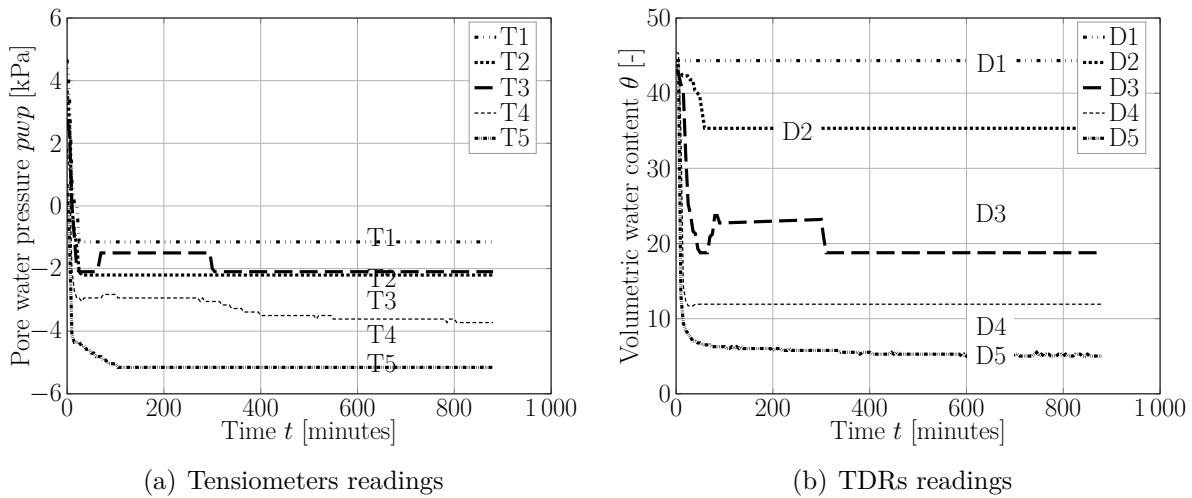


Figure 6.26.: 2nd drainage stage: The readings of the tensiometers and TDRs [HS+G]

The hydraulic conductivity curves show that the sand layer above the geotextile was desaturated and the flow of the water through the sand is limited. This phenomenon will exist due to the effect of suction and thus the risk of having a partially saturated conditions is very likely which is opposite to the current design methods which assume that the soil and the geotextile are saturated during the workability time of the drainage system.

During infiltrating the column, the water started to flow through the upper part of the column. As the wetting front reaches the location of each of the TDR waveguides the water content is observed to increase, up to a value of approximately 18%. Once the wetting front reached the geotextile layer, water did not immediately flow through the geotextile. Instead, because of the capillary break, water accumulated within the soil immediately above the geotextile until the matric suction was reduced to a value at which capillary breakthrough could occur. Specifically, outflow was collected from the base of the column only once the soil reached a water content of approximately 36% (degree of saturation of 80%). The breakthrough suction is consistent with the suction value expected based on the WRCs for these materials (see discussion in Section 4.2). Once outflow was collected after breakthrough, steady downward flow of water was established through the soil-geotextile system.

Figure 6.27 summarizes the location of the pore-water pressures of the points at different heights.

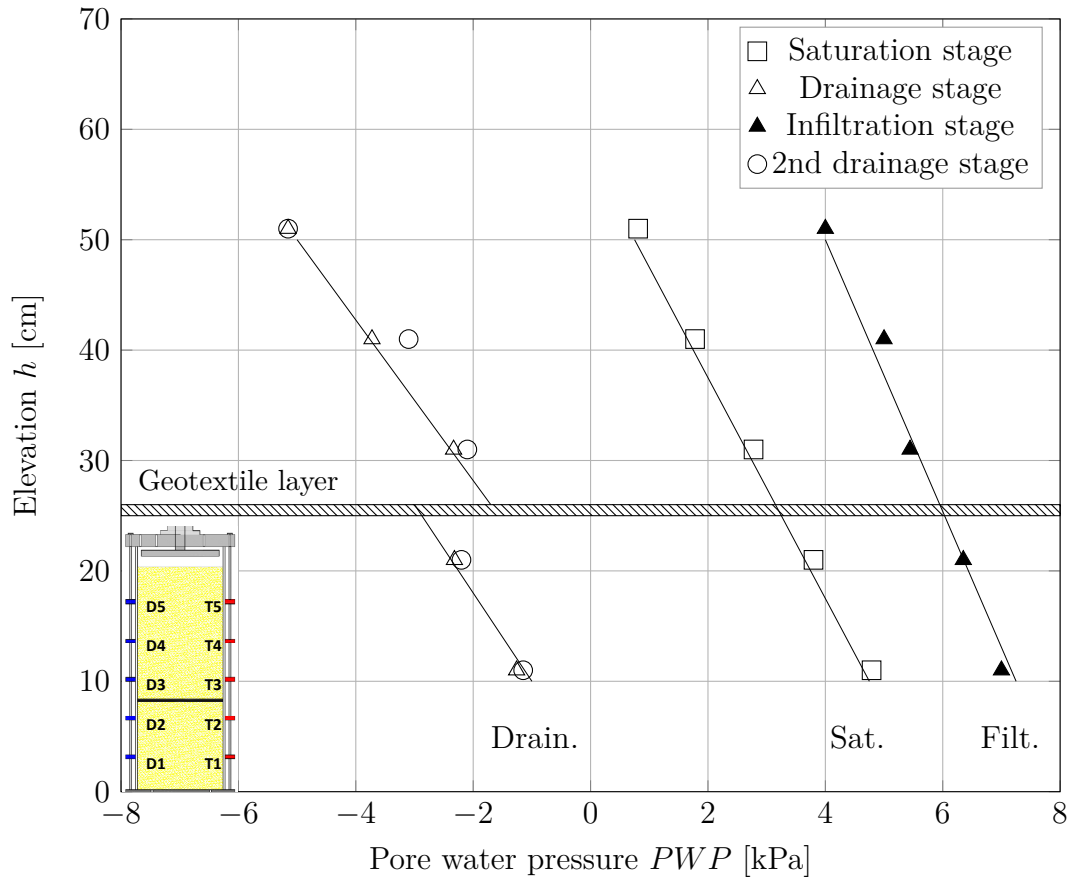


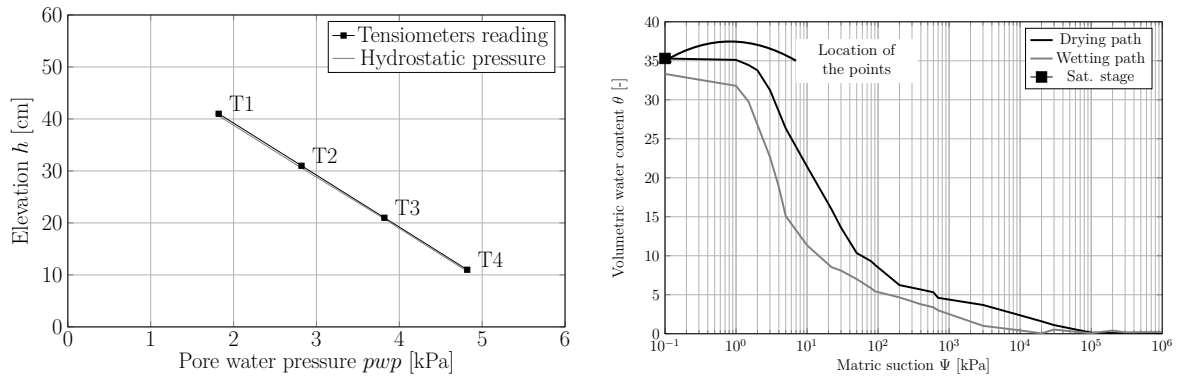
Figure 6.27.: Location of the points during the test stages for different elevation [HS+G]

6.6.3. Mixture 10K

In this test, a mixture of 90% Hostun sand and 10% kaolin clay is used as a top soil layer. Beneath the geotextile layer, a layer of Silver sand was used. The soil-water retention curve of Silver sand has been determined based on the grain size distribution curve using the proposed model by Fredlund (1997a).

6.6.3.1. Saturation stage

Figure 6.28(a) presents the pore pressures measured during saturation stage versus depth. The readings are compared with the hydrostatic pressure values as the water level was fixed a height of 559 mm. Figure 6.28(b) shows the location of all the four points on the soil-water retention curve SWCC for mixture 10K which are located as one point at zero suction.

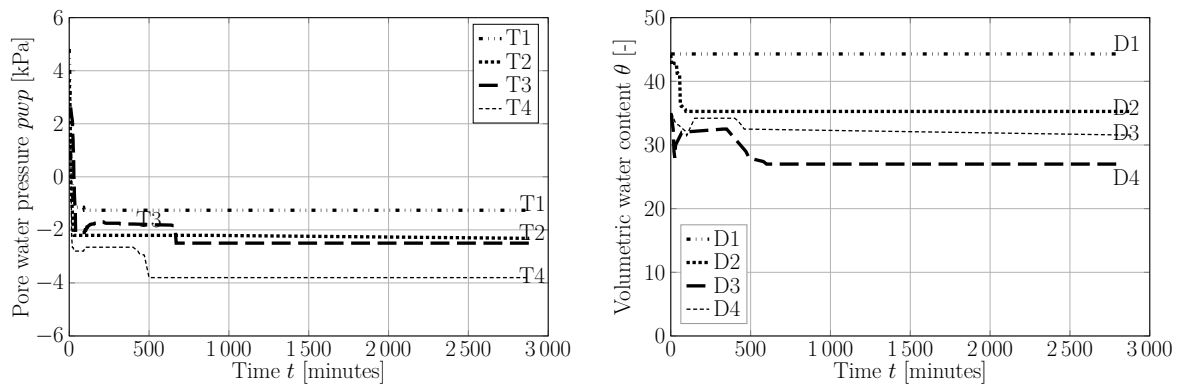


(a) Hydrostatic stress vs tensiometers readings (b) Location of the points on the SWCC (D3 & D4)

Figure 6.28.: Saturation stage: Readings of the tensiometers and the location of the points on the SWCC of 10K

6.6.3.2. Drainage stage

During this stage, the water was drained from the bottom of the column until reaching an equilibrium state along the column profile similar to the previous tests. Figures 6.29(a) and 6.29(b) show the change of the volumetric water content and the pore-water pressure with time, respectively. Figure 6.30 shows the location of the points on the SWCC. The time needed to reach stable readings is longer in comparison to the previous tests (pure Hostun sand). This is due to the lower hydraulic conductivity of mixture 10K under saturated and partially saturated conditions. The degree of saturation of the mixture 10K reaches about 75% at the end of this stage. Figure 6.30 indicates that adding the kaolin made the soil layer at points 3 and 4 to be near the AEV compared to the test with only sand in which the points were settled above the residual suction value. Figure



(a) Change of pwp with time (b) Change of Vol. WC with time

Figure 6.29.: Change of the reading during the drainage stage [10K]

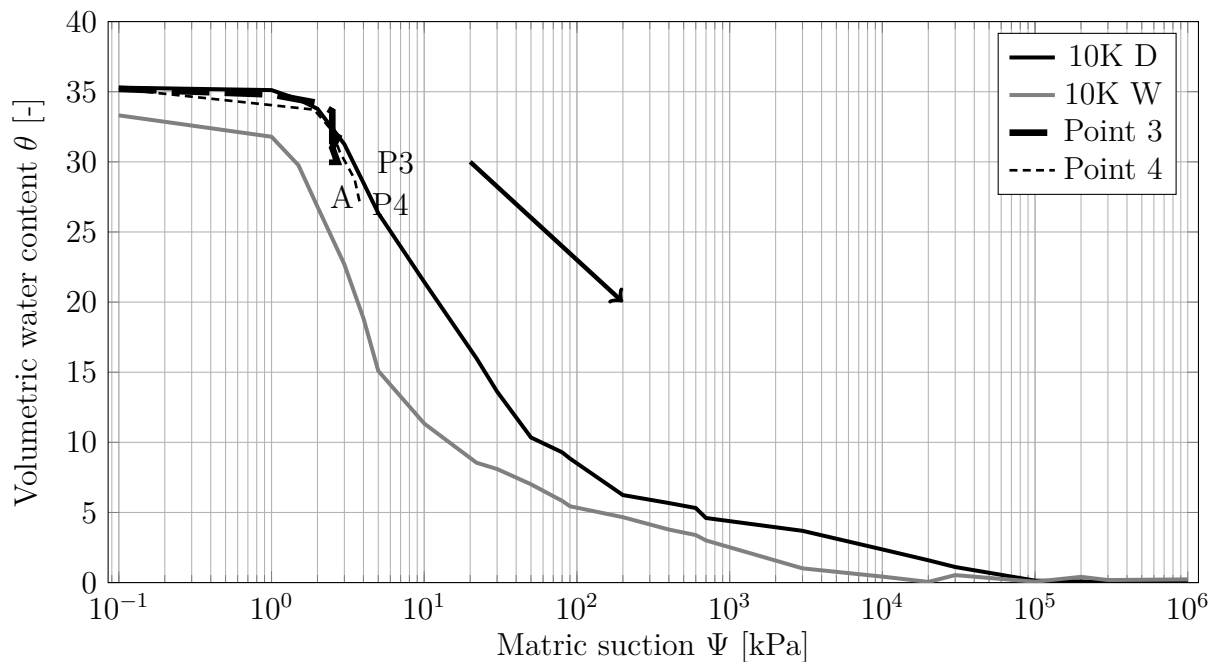


Figure 6.30.: Drainage stage: Location of the points on the SWCC for different elevation [10K]

6.31 shows a suction value of ≈ 2.2 kPa in which the capillary break will occur between the soil mixture 10K and the nonwoven geotextile (Point A). This value is similar to that recorded in the previous test HS+G but the hydraulic conductivity of the 10K is relatively smaller and the potential to transfer the water through the geotextile layer is lower at this suction.

6.6.3.3. Infiltration stage

After the drainage stage, the water was pumped top of the column to simulate a rain. The flow rate was $4.E-07$ m/sec which is smaller than the saturated hydraulic conductivity of mixture 10K. Figures 6.32a and b present the change in the tensiometers readings and the volumetric water content respectively. Figure 6.33 shows the location of the points on the SWCC.

The tests results showed an existence of capillary break during the drainage stage at suction value (3.6 kPa). The hydraulic conductivity function versus suction curves show that the curve of soil 10K and the geotextile intersects at this suction value.

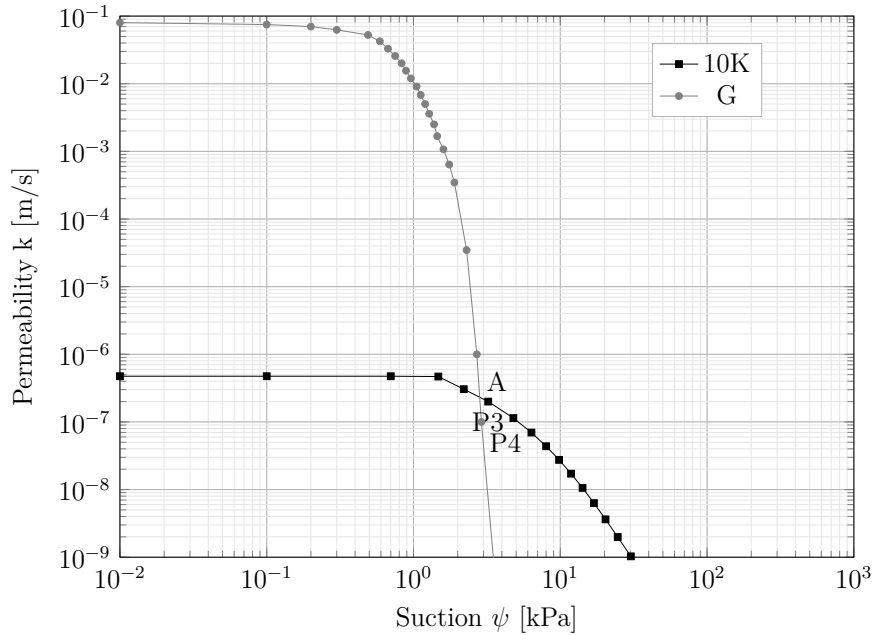


Figure 6.31.: Hydraulic conductivity function of 10K and geotextile

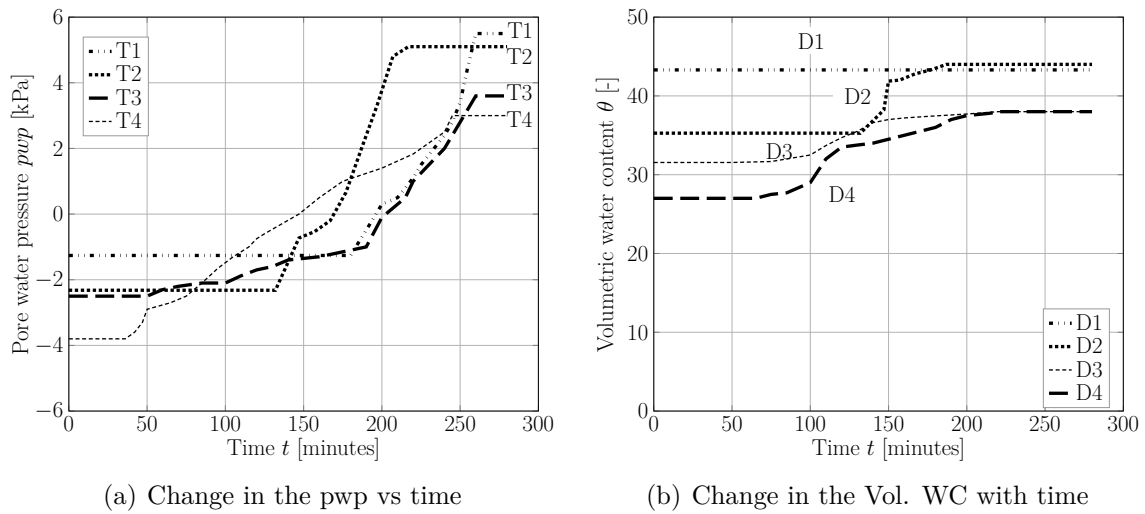


Figure 6.32.: Infiltration stage [10K]

6.6.3.4. 2nd drainage stage

Similar to the previous tests, the water was allowed to drain from the column during this stage, water started to drain until it reached an equilibrium phase. Figures 6.34a and 6.34b show the reading of the pore-water pressure and volumetric water content versus time, respectively.

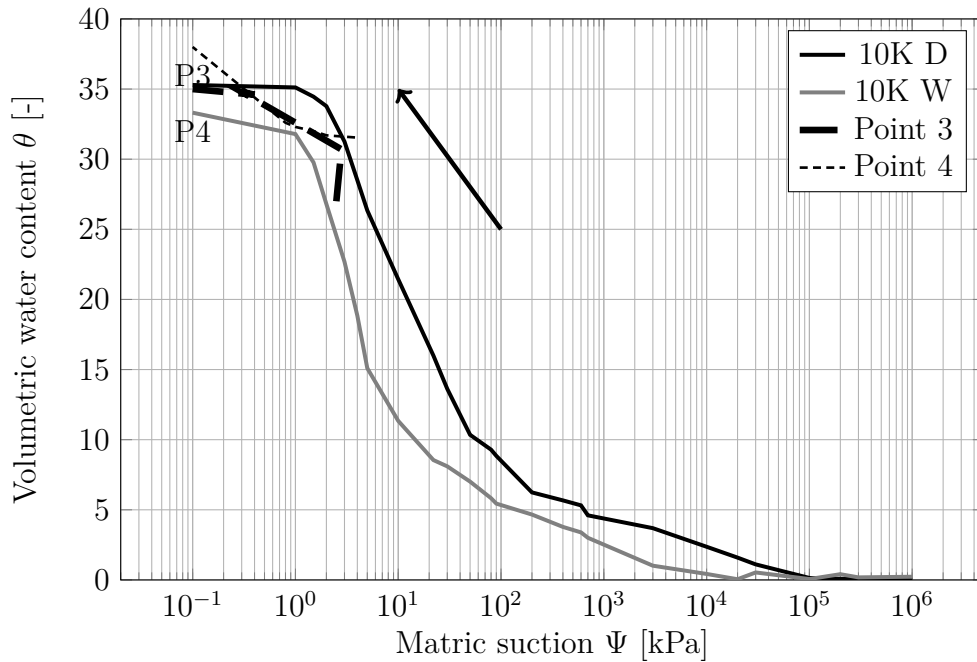


Figure 6.33.: Infiltration stage: Location of the points on the SWCC for different elevation [10K]

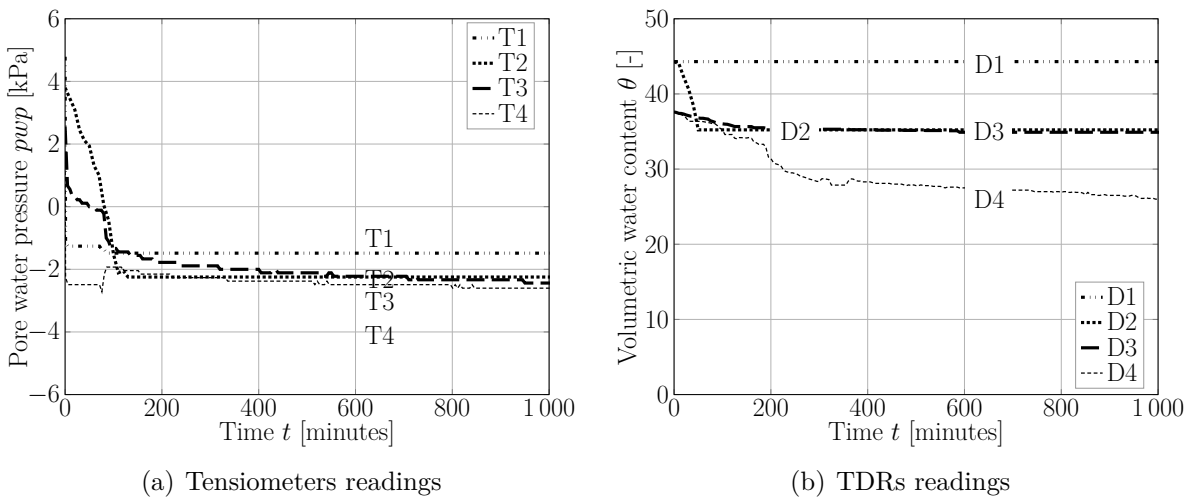


Figure 6.34.: 2nd drainage stage: The readings of the tensiometers and TDRs [10K]

6.6.3.5. Main points from the test (10K)

In this test, a kaolin sand mixture was used above the geotextile. The main observations from the test is that during the drainage stage, the soil layer above the geotextile reached the almost same suction value as in the (HS+G) test but the equivalent value of the degree of the saturation was relatively higher. In other words, the soil layer reached similar value

of suction when using the same geotextile but the soil layer has higher degree of saturation which may allow the soil layer to be more saturated.

During the infiltration stage, the paths of points P3 and P4 followed hysteresis paths to reach a fully saturated volumetric water content.

Figure 6.35 review the value of the pore-water pressure at the end of each stage of the test. The existing of the geotextile layer which has a different characteristics of the water-retention curve compare to the soil mixture will affect the location of the points above and below the geotextile layer.

The time needed to reach stable readings after the drainage stage was longer in comparison to pure sand due to the low permeability of the mixture.

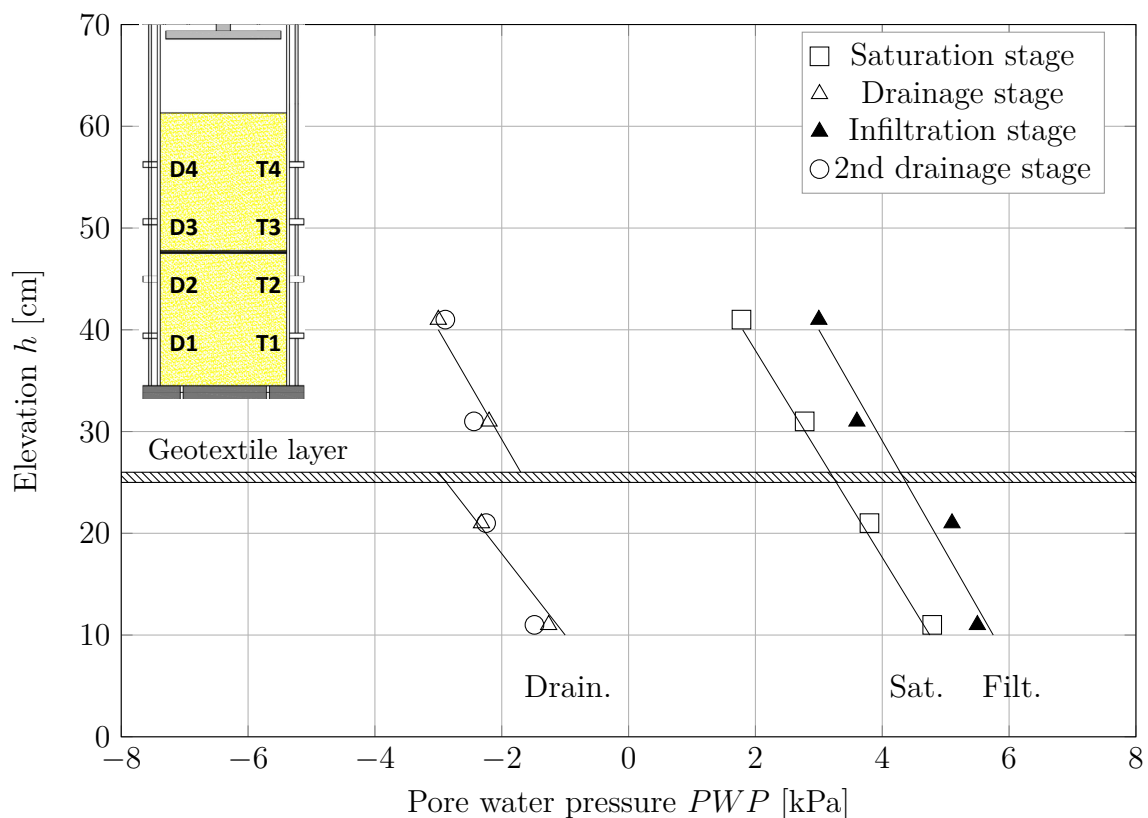


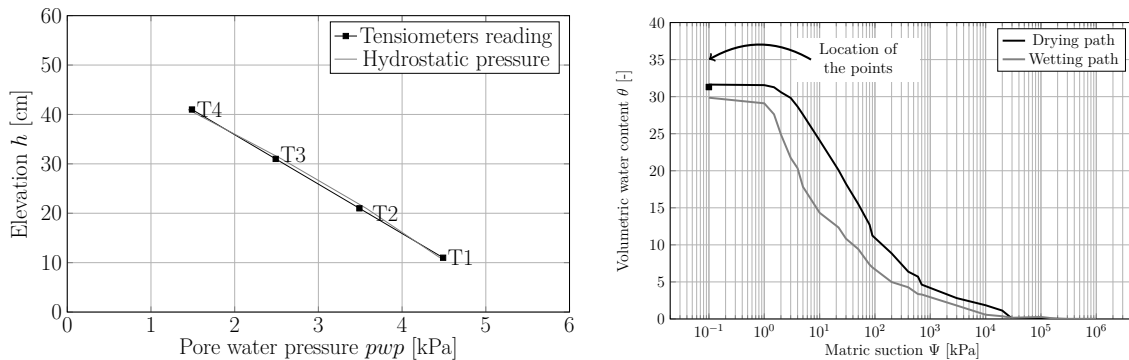
Figure 6.35.: Location of the points during the test stages for different elevation [10K]

6.6.4. Mixture 15K

In this test, the soil material used was a mixture of a 85% Hostun sand with 15% kaolin clay. This increase in the kaolin content still keeps the soil mixture (15K) within the recommendations of the stable design filter from mechanical and hydraulic perspectives.

6.6.4.1. Saturation stage

Figure 6.36(a) shows the values of the pore water pressure versus depth at the saturation stage measured from the tensiometers devices. The readings are compared to the hydrostatic pressure values as the water level was fixed at height 559 mm. Figure 6.36(b) shows the location of the points on the soil-water retention curve for mixture 15K.



(a) Comparison between the readings and the hydrostatic pressure

(b) Location of the points on the SWCC

Figure 6.36.: Saturation stage readings [15K]

6.6.4.2. Drainage stage

During this stage, the water was drained from the column by opening the valve at the bottom. Figure 6.37a presents the pore-water pressure readings vs time. Figure 6.37b shows the volumetric water content readings vs time. In this test the time needed to reach equilibrium of the moist distribution around the profile of the column (stable readings) was 750 minutes. The tensiometer readings indicate that the geotextile layer is required longer time in comparison to the previous tests (HS and 10K) to become desaturated. Figure 6.38 shows the location of the points P3 and P4 on the SWCC of 15K mixture. Due to the higher air-entry value of the mixture, the points were located beneath the AEV which shows that the soil was capable to hold more moist compare to the HS and 10K mixtures at the same suction range. Figure 6.39 presents the hydraulic conductivity functions of the 15K and the geotextile. However point A which represents the threshold between having a permeable soil-geotextile system and having a capillary break, it can be seen that, the permeability of the geotextile layer has to reach approximately 5×10^{-8} m/sec which is below than the saturated permeability of the geotextile which is expected during the design stages of the drainage system.

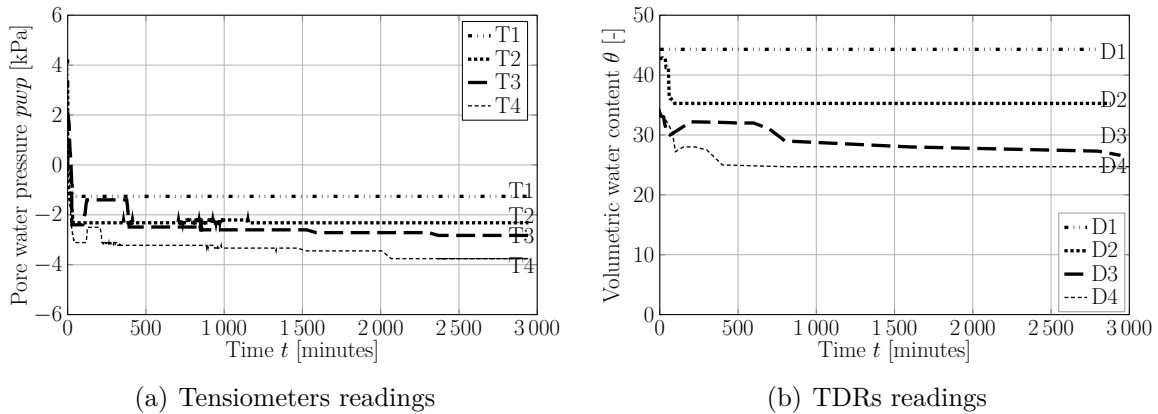


Figure 6.37.: Reading during the drainage stage [15K]

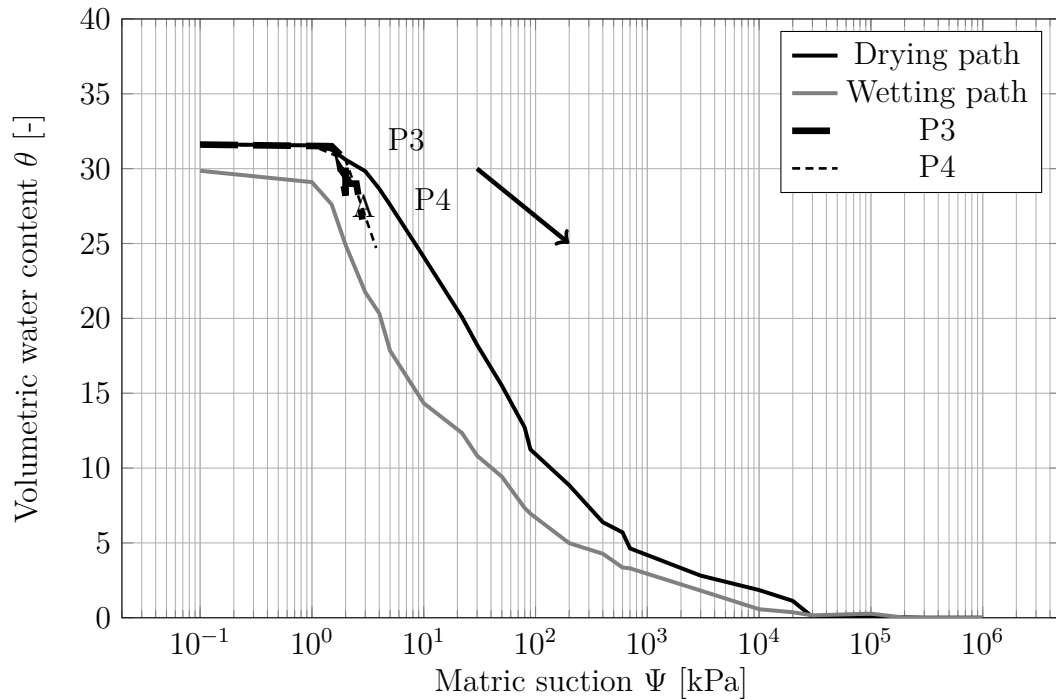


Figure 6.38.: Drainage stage: Location of the points on the SWCC for different elevation [15K]

6.6.4.3. Infiltration stage

Figure 6.40a presents the pore-water pressure readings vs time. Figure 6.40b shows the volumetric water content reading vs time. Figure 6.41 shows the location of the points on the SWCC. Figure 6.42 shows the location of P3 and P4 at the end of the infiltration

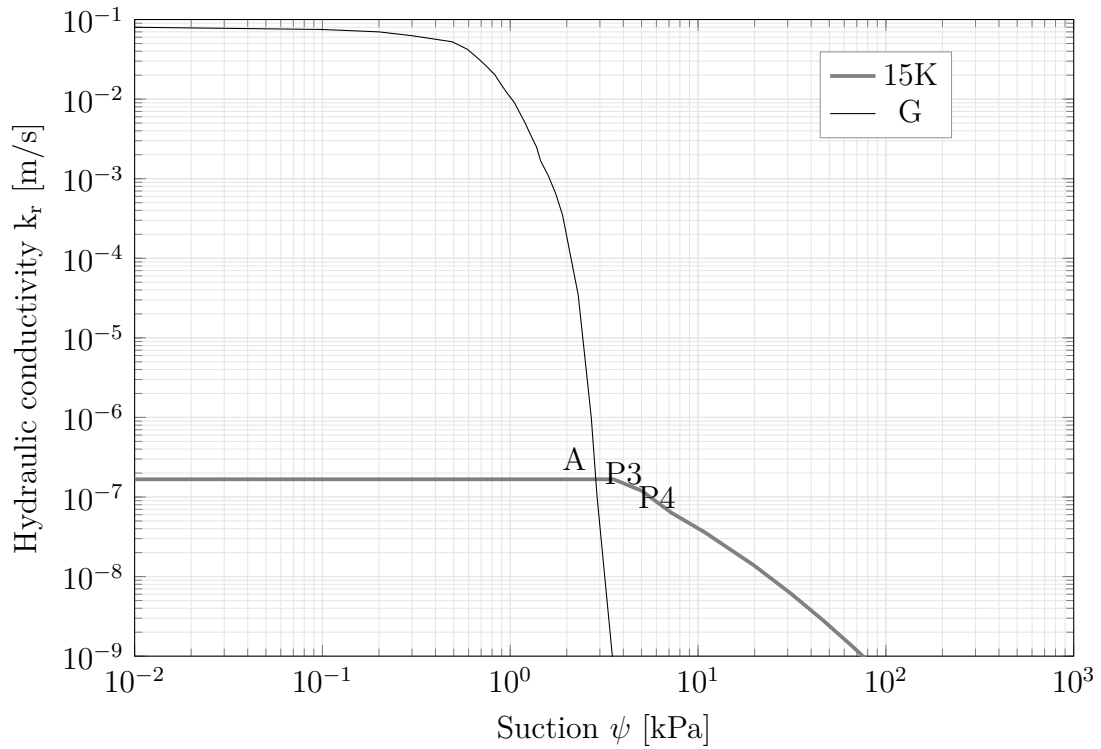


Figure 6.39.: Hydraulic conductivity function of 15K and geotextile [15K]

stage.

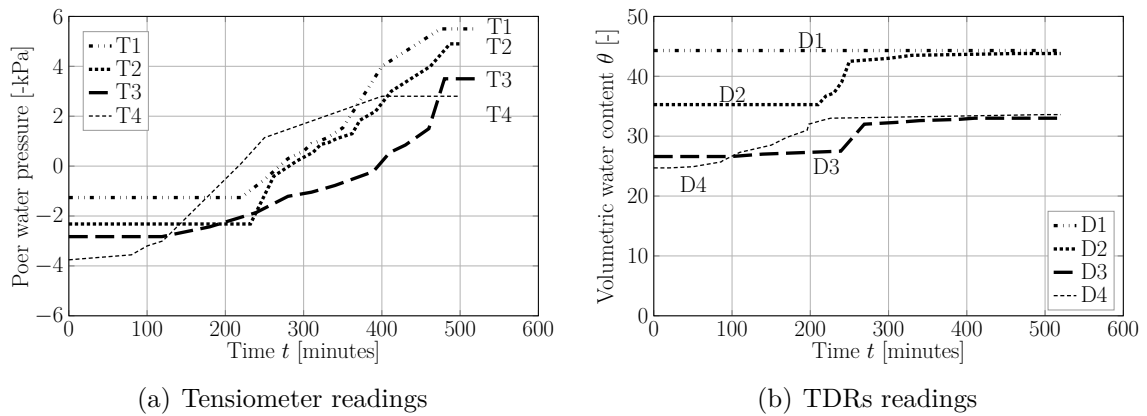


Figure 6.40.: The readings of the Tensiometers and TDRs during the infiltration stage [15K]

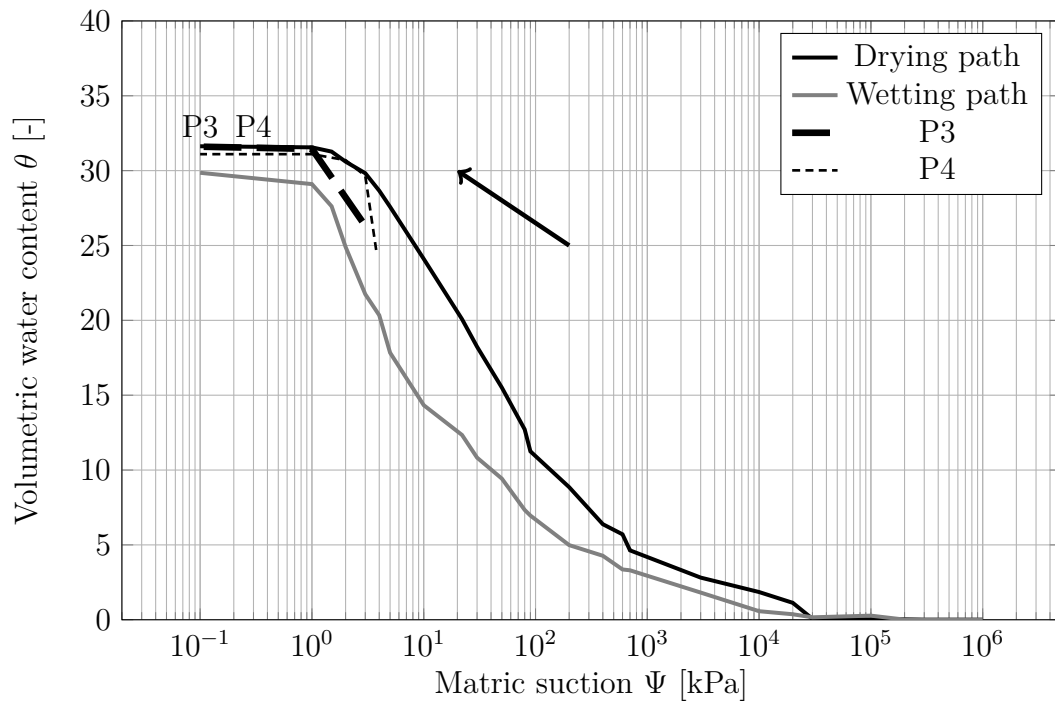


Figure 6.41.: Location of the points on the SWCC for different elevation during the infiltration stage [15K]

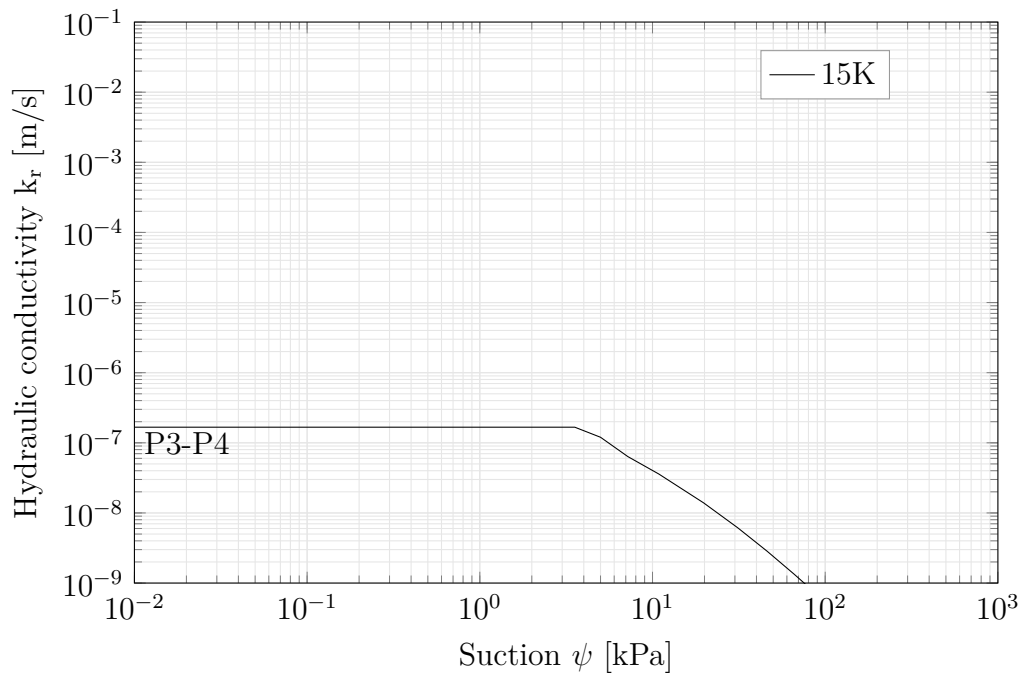


Figure 6.42.: Location of P3 and P4 on the hydraulic conductivity function of 15K at the end of the infiltration stage

6.6.4.4. 2nd drainage stage

Figure (6.43a) presents the pore-water pressure readings vs time while Figure (6.43b) shows the volumetric water content reading vs time.

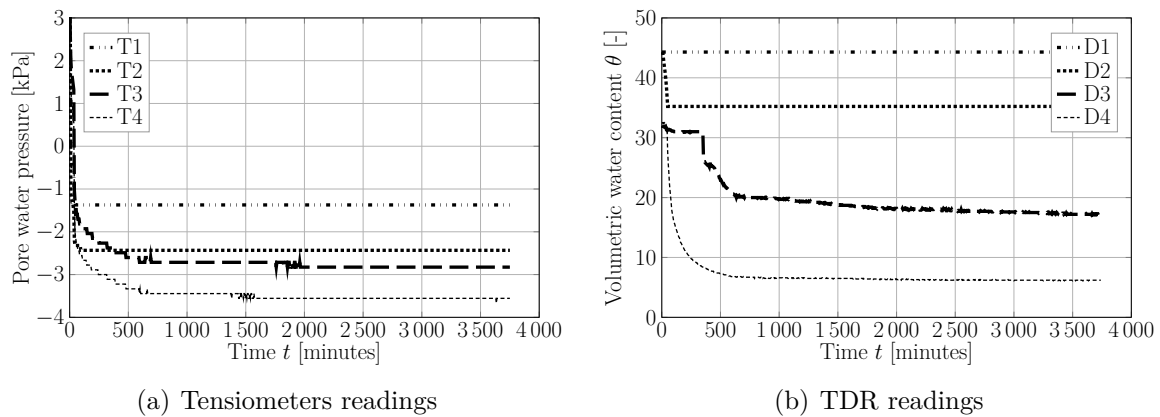


Figure 6.43.: The readings for after the infiltration stage [15K]

6.6.4.5. Main points from the test (15K)

In this test, the soil mixture 15K was tested.

Figure 6.44 presents the values of the pore-water pressures during the test for different heights. During the drainage stage, the measured suction readings after reaching stable readings were in similar ranges to the previous tests however, the recorded volumetric water content values were higher in comparison to HSG and 10K tests.

During the infiltration stage, the soil at P3 and P4 has more moist in comparison to the previous tests, so it is predicted that a breakthrough in the geotextile sample occurs earlier however, due to the lower permeability of the 15K mixture, the time needed is longer.

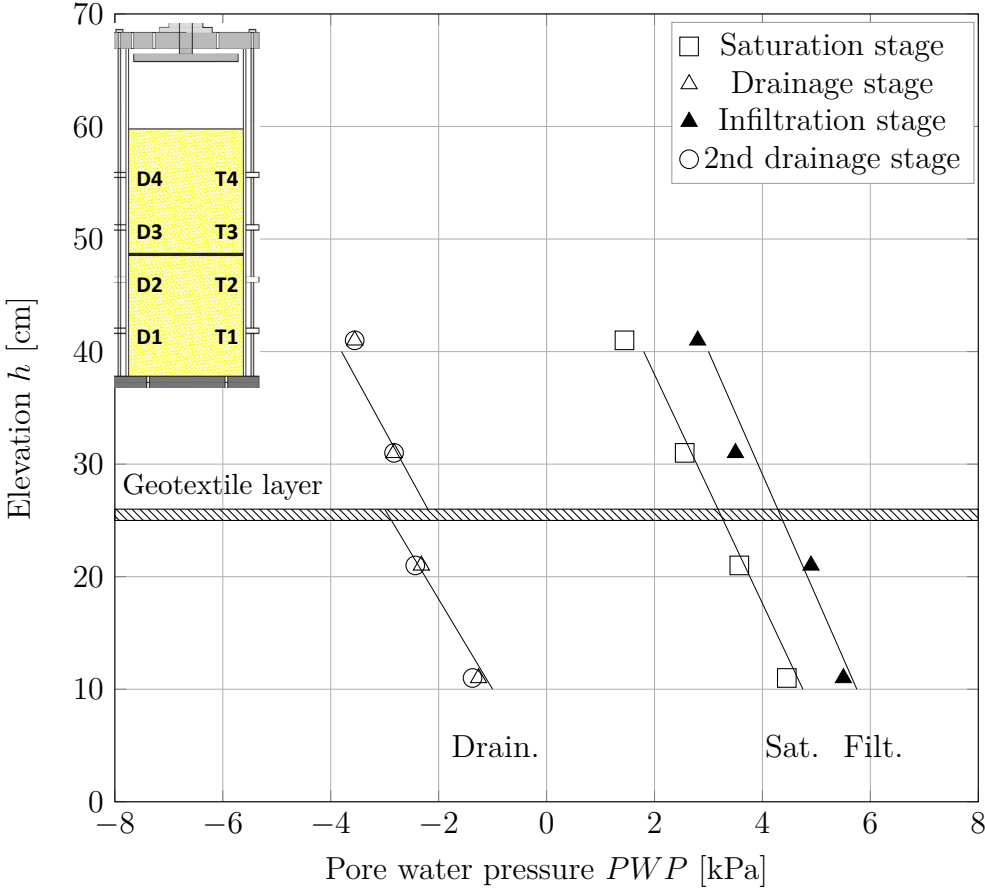


Figure 6.44.: Location of the points during the test stages for different elevation [15K]

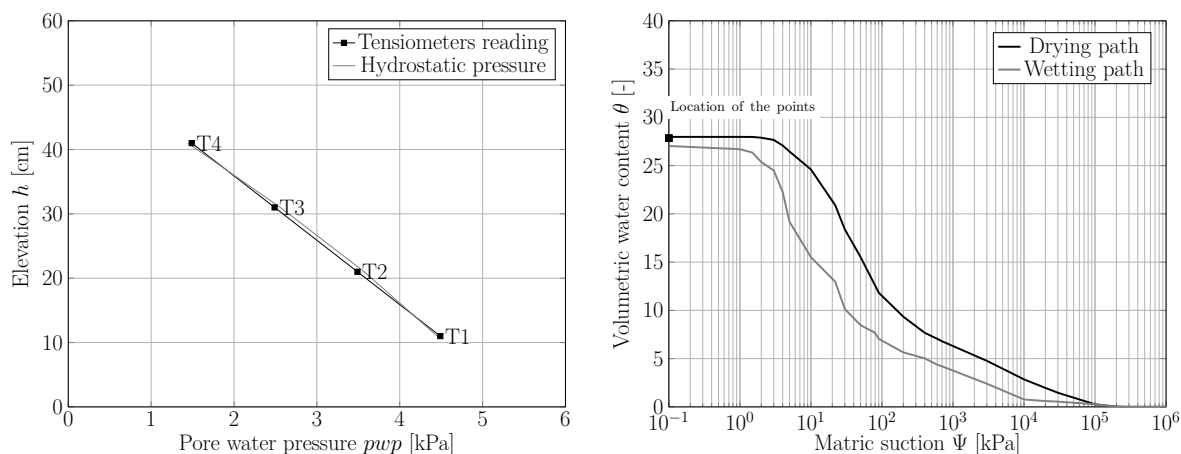
6.6.5. Mixture 20K

In this test, the amount of the fines content (kaolin) has been increased to 20% by weight while the percentage of Hostun sand was reduced to 80%. The same procedure from the previous tests were used during the current test.

6.6.5.1. Saturation stage

Figure 6.45(a) shows the values of the pore water pressure versus depth at the saturation stage measured from the tensiometers equipments. To assure saturated conditions at the beginning of the test, the readings were compared with the hydrostatic pressure values as the water level was fixed at height 559 mm. Figure 6.45(b) shows the location of the

measured points on the soil-water retention curve for the soil mixture 20K.



(a) Comparison between the hydrostatic pressure and the tensiometers readings (b) Location of the points on the SWCC for different elevation

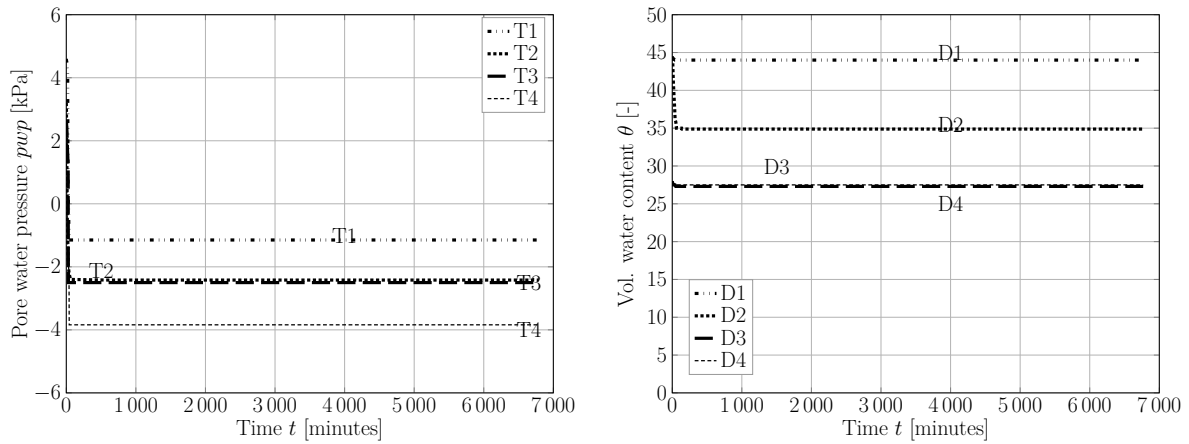
Figure 6.45.: Saturation stage: The pwp level and the location of the points on the SWCC [20K]

6.6.5.2. Drainage stage

Similar to the previous tests, the water valve in the bottom of the column was opened and water was allowed to drain, the readings were monitored until equilibrium readings was observed. Figure 6.46(a) shows the change in the pore-water pressure pwp with time during this stage. Figure 6.46(b) presents the change in TDR reading with time. Figure 6.47a shows the location of the points P3 and P4 on the SWCC of 20K and Figure 6.47b the location of Point P1 and P2 on the SWCC of Silver sand SS.

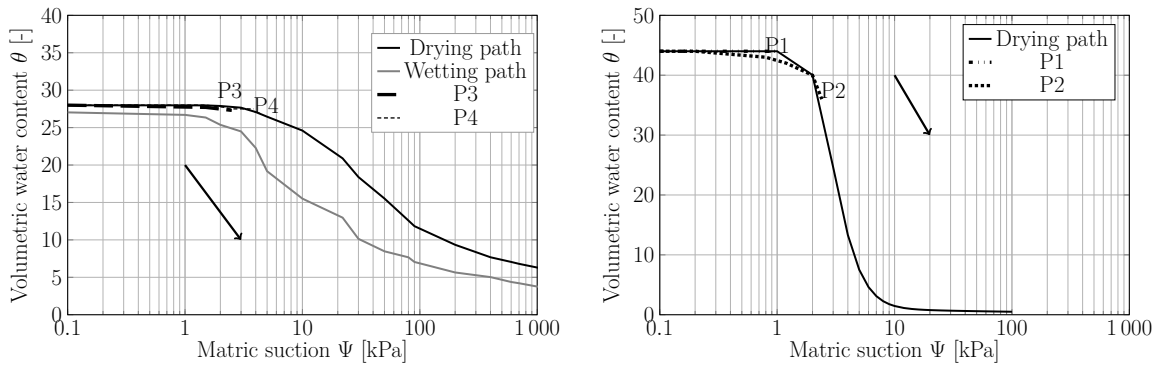
The time duration needed to achieve stable readings was 1000 minutes. However the amount of the kaolin was increased in this test, there was no volume change recorded due to the drainage of the column.

Figure 6.48 shows the location of point A on the hydraulic conductivity function curves of the soil mixture 20K and the geotextile.



(a) Change in pwp with time during drainage stage (b) Change in Vol. WC with time during drainage stage

Figure 6.46.: Drainage stage: Location of the points at different elevations [20K]



(a) Location of the points on SWCC of 20K (b) Location of the points on the SWCC of sand

Figure 6.47.: Drainage stage: Location of the points on the SWCC for different elevation [20K]

6.6.5.3. Infiltration stage

The infiltration stage continued for 1600 minutes. Because the test suppose to run without break, a special device was installed at the top of the column to break the infiltration of water if the column was filled with water during the night. The readings of the tensiometers and TDRs are presented in Figure 6.49 and the locations of the points P3 and P4 are placed on the SWCC of 20K are shown in Figure 6.50.

The Tensiometer T4 started to record increase in the pore-water pressure about 200

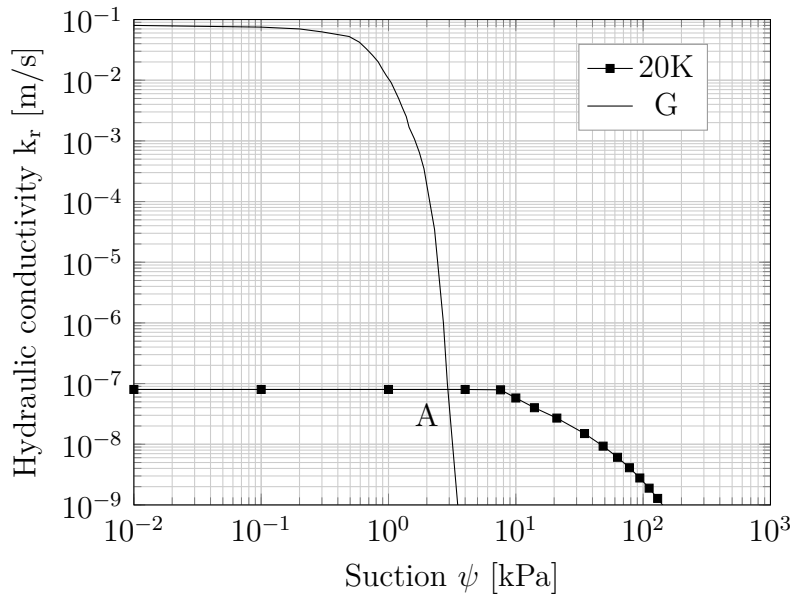


Figure 6.48.: Hydraulic conductivity function of 20K and geotextile

minutes from starting the infiltration stage. The tensiometer T3 followed T4 by 5 minutes.

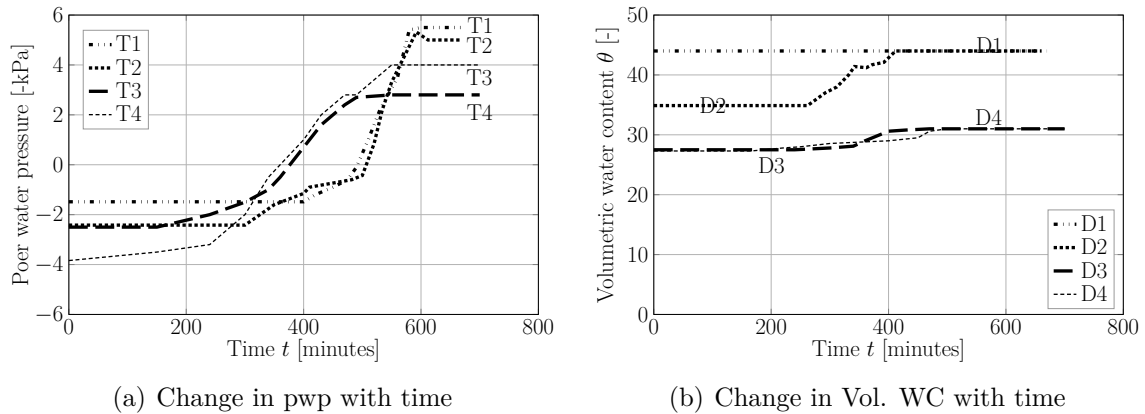
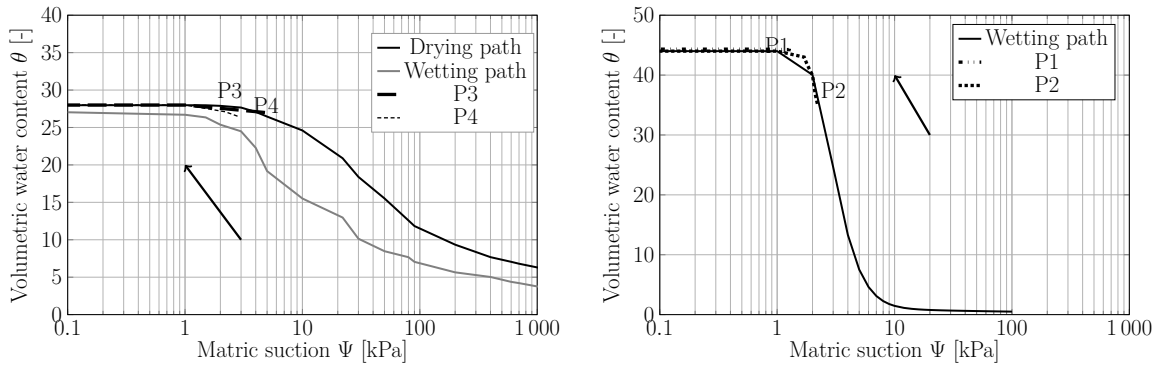


Figure 6.49.: Infiltration stage: The readings of the Tensiometers and TDRs [20K]

6.6.5.4. Main points from the test (20K)

During the drainage stage of this test, the water content of the soil material at P3 and P4 (above the geotextile layer) was above the air-entry value. In this case, the soil layer 20K is still saturated. During the infiltration stage, the permeability of 20K will be close to the saturated permeability and therefore the layer of the geotextile will be re-saturated



(a) Location of the points on SWCC of 20K (b) Location of the points on the SWCC of sand

Figure 6.50.: Infiltration stage: Location of the points on SWCCs [20K]

and then starts to drain the water. Figure 6.51 shows the final point of the pore-water pressure readings at different heights during the stages of the test.

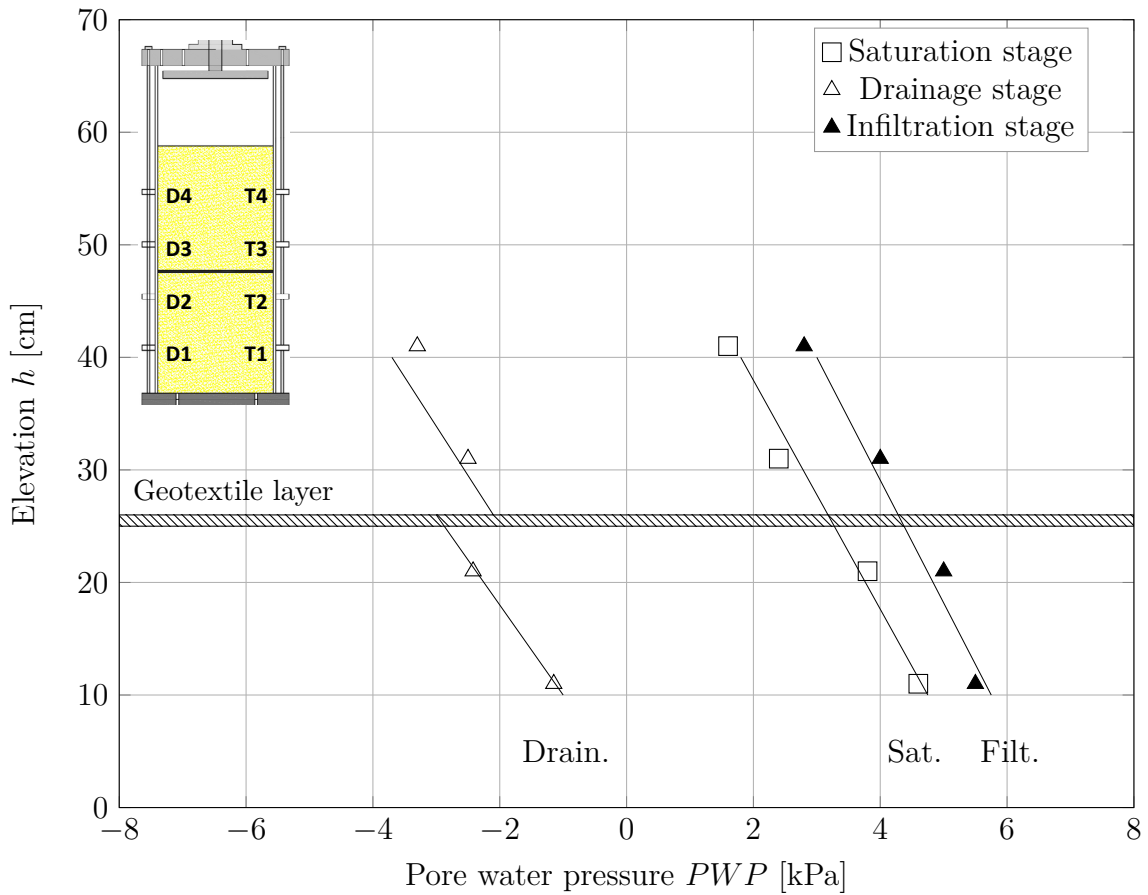


Figure 6.51.: Location of the points during the test stages for different elevation (20K)

6.7. Discussion of the column tests

The column tests studies have been conducted to reproduce the hydraulic interaction between soil and geotextile drainage system under controlled laboratory conditions. In all the soil / geotextile tests, the same subsequent stages were followed in order to evaluate the performance of the nonwoven geotextile during different saturation / de-saturation conditions. All the tests were started from fully saturated condition. In this way the results can be explained on the mean drying and mean wetting paths of the SWCC. If the tests were conducted from an initial water content followed by a drainage or infiltration stage, the tests results could follow a scanning curve. The flow rate of water during the infiltration stage of each test was less than the saturated hydraulic conductivity of the selected top soil layer. The objective was to ensure an unsaturated condition in each test during the infiltration stage.

The comparison between these tests will be based on the time duration needed to re-saturate the top soil layer, and the time of breakthrough of the water through the geotextile layer. The results are discussed together with the soil and geotextile water retention curves (SWCC and GWCC) and the hydraulic conductivity curves determined in chapter 5. The infiltration properties of each soil layer on the over all performance of the soil/geotextile drainage system will be analyzed since there is a graduate increase in the air entry value for each soil type and a decrease in the hydraulic conductivity.

In the first two tests, HS and HSG, Hostun sand was used. In the three other tests, 10K, 15K, and 20K Silver sand SS was used to replace Hostun sand in the soil layer below the geotextile due to limitation in the amount of Hostun sand at the time during preparing the tests. Figure 6.52 shows the SWCC curve for both materials. The curve for Hostun sand was performed in the laboratory while the curve of the Silver sand was determined using the proposed model by Fredlund (2002). The results show that the SWCC of Silver sand is not significantly different from that of Hostun sand. The use of Silver sand as a soil layer beneath the geotextile layer will not have a major influence on the tests results of the column tests.

Figures 6.5, 6.16, 6.28, 6.36, and 6.45 show that each soil layer was fully saturated during the saturation stage as it can be seen from the projection of the measured suction and volumetric water content to the SWCCs. That shows, that the method used to prepare the soil initially with its optimum water content and then adding it to the column in small portions with increasing the water height every time was suitable to achieve a fully saturated column even with increasing the fines content. Nahlawi et al. (2007b) performed

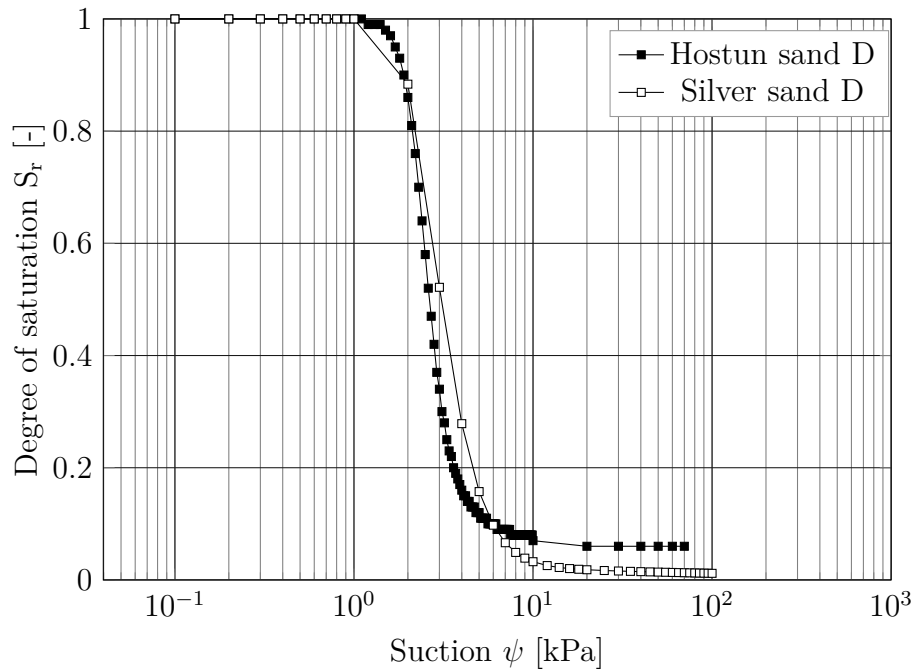


Figure 6.52.: SWCCs of Hostun sand (test) and Silver sand (Model)

two types of tests, an initially dry sand and an initially saturated sand tests, for the second test, the column was filled with water and then the sand was pluviated through the water which is similar technique to Ho (2000). McCartney et al. (2008a) started the test from relatively low initial water content.

The "plastic fermit" used to seal the contact line between the column and the geotextile layer at the perimeter found to be suitable in all the tests without problems even when un-assembling the column and cleaning the Plexiglas cylinder. Ho (2000); Nahlawi et al. (2007b) suggested using silicon, McCartney et al. (2008a) preferred to use grease to minimize side-wall leakage.

In Figure 6.53 the pore water pressures or suction measured at the end of the drainage stage are plotted versus the height of the sample for all the four tests with geotextile. Below the geotextile layer hydrostatic pore water pressure develops in all the tests with zero pressure at water level at the bottom of the sample. Closely above the geotextile layer the suction does not exceed values between 2.2 and 2.8 kPa. Figure 6.54 shows the hydraulic conductivity curves derived for the geotextile as well as the soils. Points A for each soil material are marked at which hydraulic conductivity of the geotextile drops below the hydraulic conductivity of the soil materials by increasing suction. The corresponding critical suctions are between 2 and 3 kPa which is in the range of the suction measured closely above the geotextile in the column tests. This means that the drainage process is

interrupted in case critical suction values are reached close to the geotextile.

This explains the suction - water content development in the HS+G test displayed in Figure 6.19. Up to approximately the critical suction the path follows the main drying curve. From there tendency is changing and at least the water content is increasing and the path followed a kind of scanning curve. Suction is increasing up to a value in the order of the WEV of the geotextile, which can be estimated from the measured GWCCs in chapter 5.6 to 1 kPa. Reaching this value the direction of the path is changing again and drainage process starts again. Of course it has to be taken into account that the suction value measured at point P3 may differ slightly from the suction at the soil-geotextile interface. Transferred to Figure 6.53 this means that reaching the critical suction at the level of the geotextile the drainage process is stopped and water is ponding above the geotextile. Reaching suctions close to WEV of the geotextile drainage starts again. So suction is varying between critical suction and WEV and flow of water is reduced.

The suction at the beginning of the drainage process above the geotextile is increasing. When reaching approximately the critical suction the increase stopped and after a short time suction is decreasing until reaching a value close to WEV of the geotextile (ca. 1 kPa). After that, suctions stay constant for a while before decreasing again. The water content shows corresponding changes, first decrease, followed by an increase and a second decrease. It may be concluded that water is accumulating above the geotextile. The mixtures with higher fine content stay saturated during this process due to higher air entry value. The low permeability of the 20K mixture may cause that no additional drainage occurs after reaching the critical suction.

Figures 6.55, 6.56 , 6.57, and 6.58 summarize the readings of the tensiometers and TDRs during the drainage stage for the four tests with geotextile.

Figures 6.55 and 6.56 showing the suction values and the volumetric water content below the geotextile. It can be concluded that the results are similar to each other during the four tests when using Hostun sand and Silver sand. The soil behavior of the soil layer below the geotextile is not influenced by the properties of the soil layer above the geotextile. The drainage in this part of the column occurred relatively fast and after reaching hydrostatic pressure profile (compare Figure 6.53) pore water pressures and volumetric water content are remain constant.

From Figure 6.57(a) it is obvious that suction above the geotextile did not exceed the critical suction values mentioned above and that drainage restrained when reaching this suction values. From Figure 6.58(a) it can be seen that the soil-geotextile interaction explained above effects also the water content and suction distribution in the upper soil part.

In Figure 6.59(a) the degree of saturation is plotted versus suction for the soil layer above the geotextile starting from the level of the sensors 3. It is assumed that suction at this level is for all tests 2.2 kPa (see Figure 6.53) and that suction decreases with height following the hydrostatic pressure distribution. It is obvious, that with increasing fine content the water content over the height measured at the end of the drainage state in the column tests is increasing. On the other side, Figure 6.59(b) shows the unsaturated permeability versus suction. From this figure it becomes clear, that unsaturated permeability of the sand is still high over the complete upper soil layer in comparison to the permeability of the mixtures. For 20K soil mixture, the degree of saturation remains close to one for the whole drainage period which explains why no increase in water content with time is measured after reaching the critical suction (Figure 6.57(a)).

The suction profiles which are observed for HSG, 10K, and 15K after the end of the second drainage stage (Figures 6.26, 6.34, and 6.43) are similar to the once discussed before after the first drainage stage (Figures 6.17, 6.29, 6.37, and 6.46). This indicates that the process is repeatable.

Figures 6.60, 6.61 , 6.62, and 6.63 summarize the readings of the tensiometers and

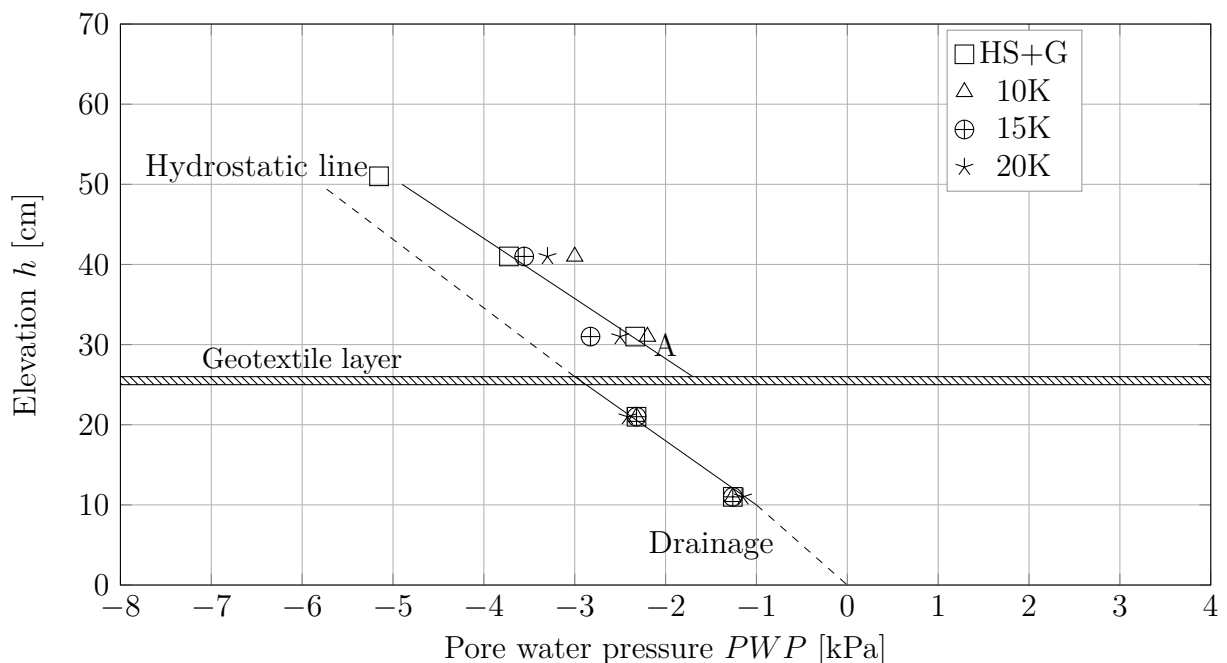


Figure 6.53.: The PWP points during the test stages for different elevation (All tests)

TDRs during the infiltration stage. With increasing the fines content, the flow of the water through the soil mixture is becoming slower and the potential to store the water in the soil mixture is increasing.

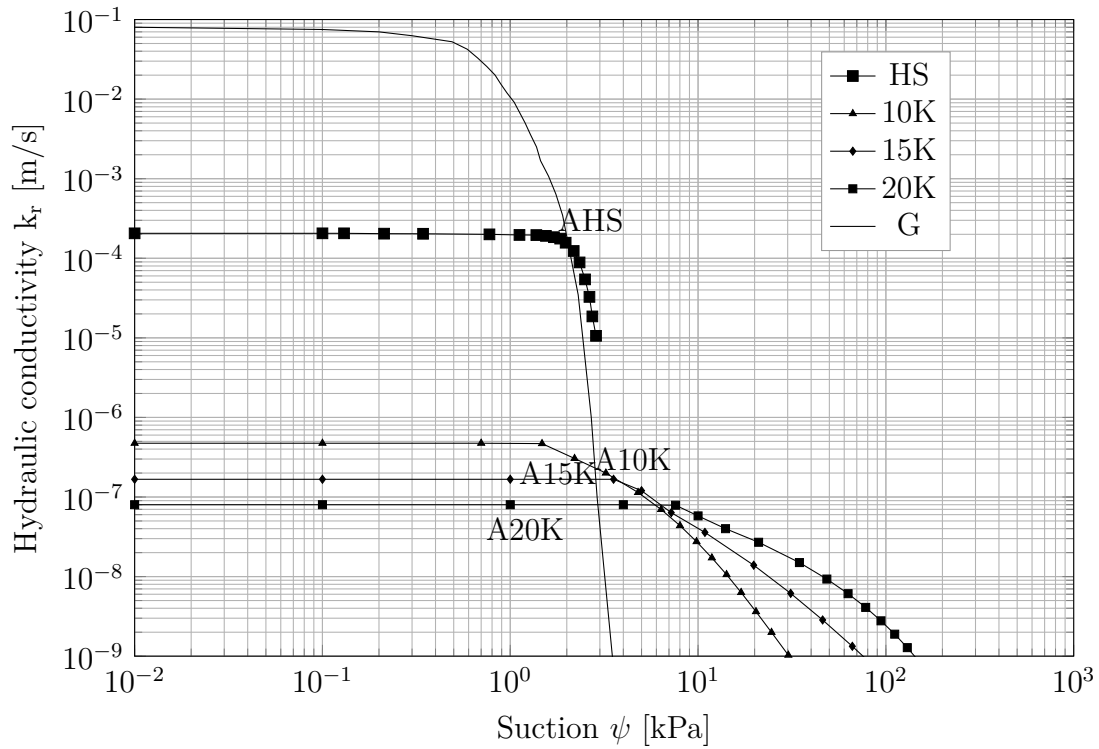


Figure 6.54.: Permeability function vs suction for the soil mixtures (Drying curves)

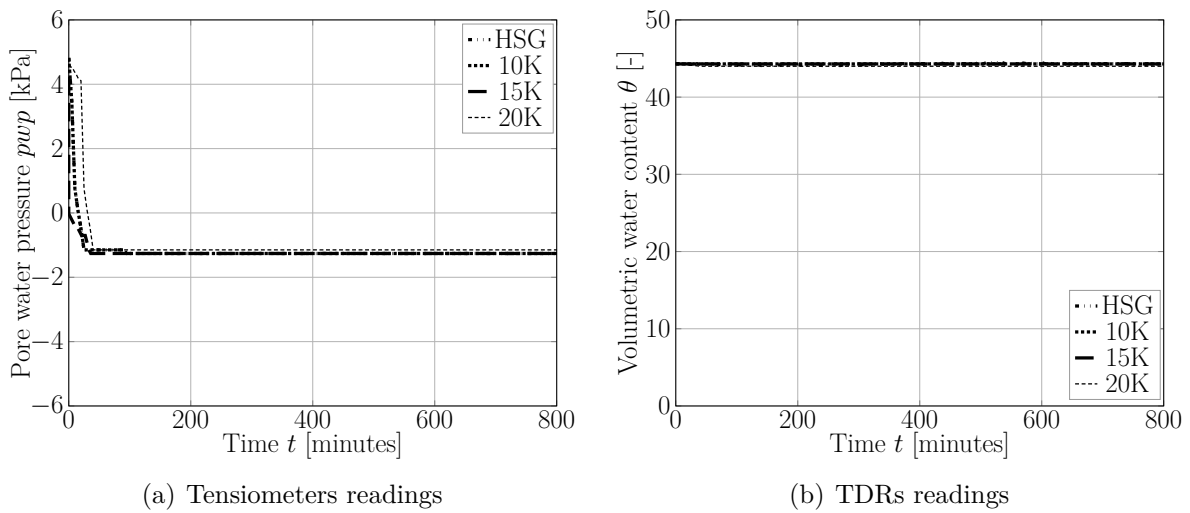


Figure 6.55.: Drainage stage: The readings of the tensiometers and TDRs (Sensors at level 1)

During the infiltration stage water starts to flow through the column apparatus. The higher point P4 will start to gain moist first than followed by P3 until reaching the geotextile layer. As the water starts to accumulate above the geotextile layer and as the suction value reduces to become less than critical suction (point A), water starts to flow through

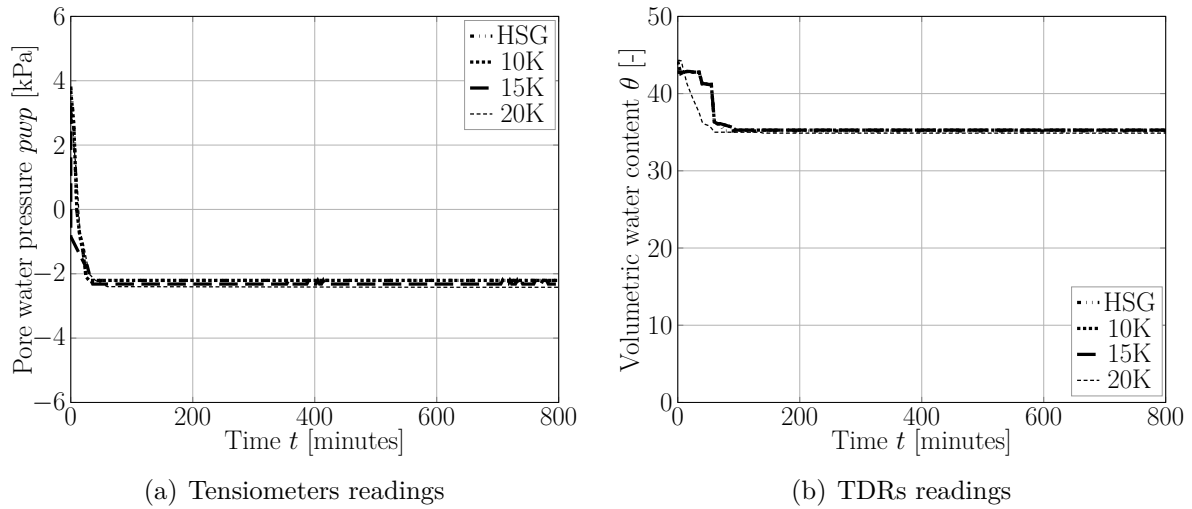


Figure 6.56.: Drainage stage: The readings of the tensiometers and TDRs (Sensors at level 2)

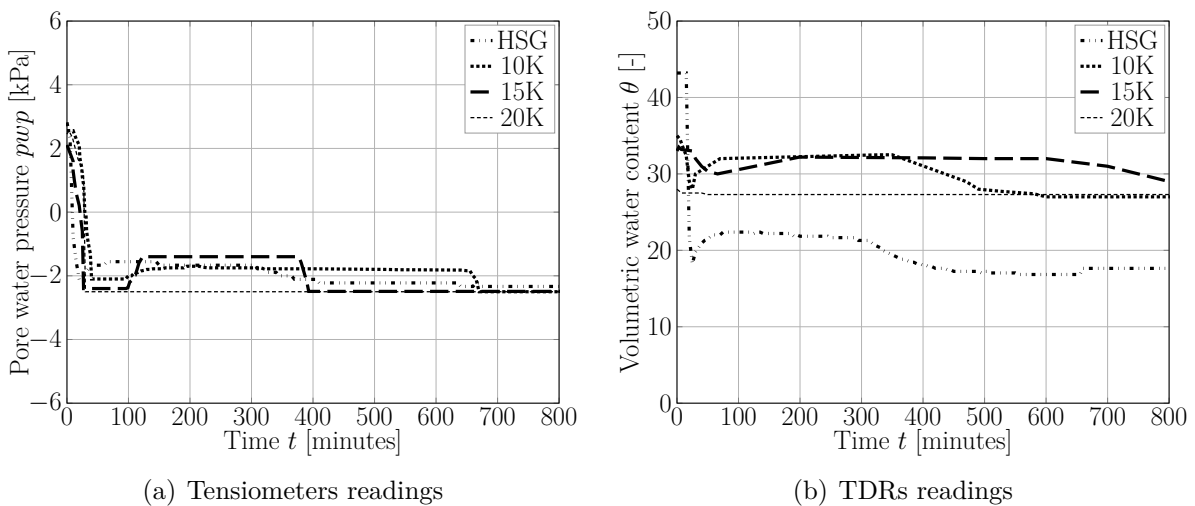


Figure 6.57.: Drainage stage: The readings of the tensiometers and TDRs (Sensors at level 3)

the geotextile layer. The increase in the readings of point 2 (40 mm below the geotextile) is a clear indication of the break of the water through the geotextile layer. For HS the increase in the moist in P2 was about 42 minutes after the start of the infiltration stage. For the soil mixture 10K, the increase in the moist was at a time of 140 minutes. For the mixture 15K was 260 minutes. For the last soil mixture 20K the time duration was about 350 minutes.

The test results show that the increase in the water content during the infiltration stage is relatively more pronounced in HS compared to the soil mixtures. The increase of

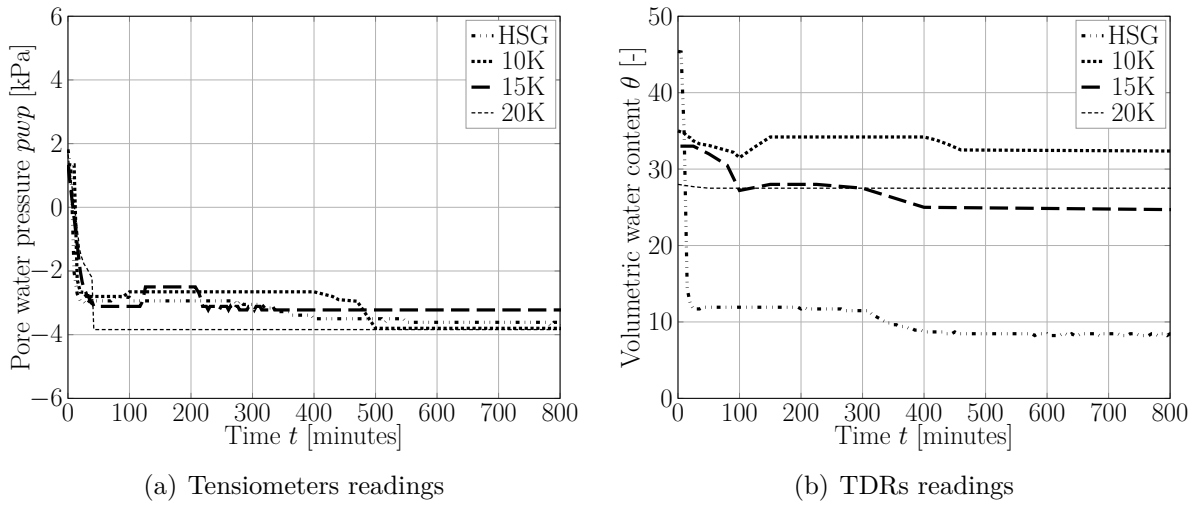


Figure 6.58.: Drainage stage: The readings of the tensiometers and TDRs (Sensors at level 4)

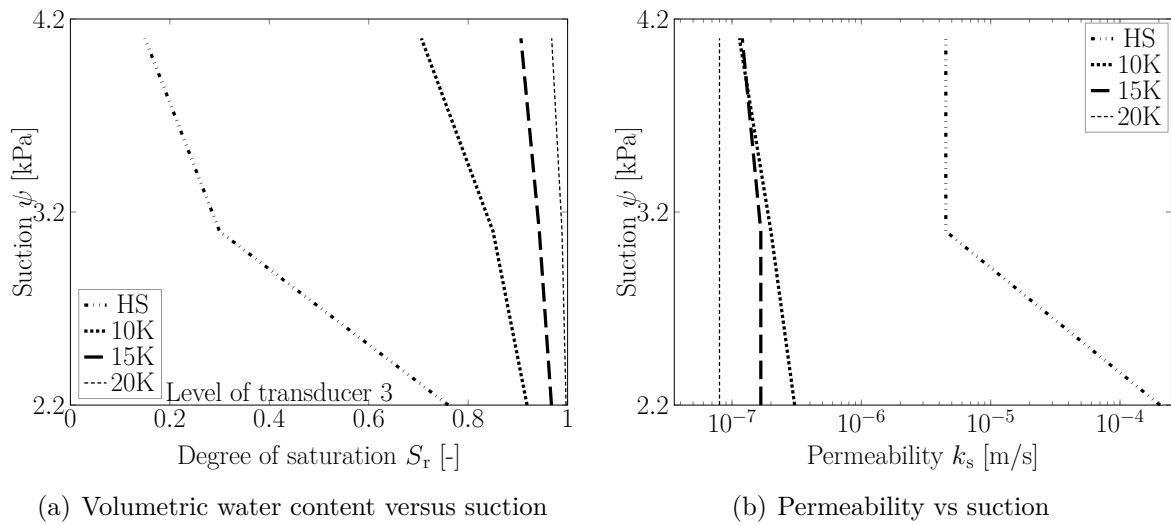


Figure 6.59.: Drainage stage: Degree of saturation and permeability versus suction, which is related to height.

permeability of the sand is significant with small decrease in the suction value while for the soil mixtures, the increase of the permeability with decrease of suction is less important for the flow process due to the lower saturated permeability of these mixtures. For the soil mixture 20K, the flow of the water through the geotextile was slower however the sensors P3 and P4 are considered saturated but the low saturated permeability of the mixture affected the infiltration velocity through the whole soil layer.

Bouazza & Nahlawi (2006) performed a 1-D column test using clay as top soil layer above the geotextile. The clay has 12% volumetric water content as initial condition before the

infiltration of the water with a flow rate less than the saturated permeability of the clay. Test results showed that it required around 4500 minutes to achieve a breakthrough in the geotextile layer and about 8180 minutes to saturate the clay layer.

It can be concluded from the test that the initial water content of the soil layer will control the time needed to get a breakthrough and to saturate the soil layer. In the current study, the time needed to have a breakthrough in the geotextile layer was about 200 minutes which is mainly due to the volumetric water content of the mixture before the infiltration stage which was 28%.

Comparing the soil-geotextile interaction for different soil materials it becomes clear that in all cases the drainage process is restrained in a similar manner. This is related to the critical suction values of the soil mixtures in combination with the used geotextile which are also in the same range (Figure 6.54). This critical suction is mainly defined by the significant drop of the hydraulic conductivity with decreasing suction at suctions about 2 to 3 kPa. However, for the sand, the influence of the restrained drainage process on the water content profile above the geotextile is limited to relative narrow zone (Figure 6.59(a)). Therefore, with increasing fines content this zone is expanding which may affect the mechanical behavior of the layered system.

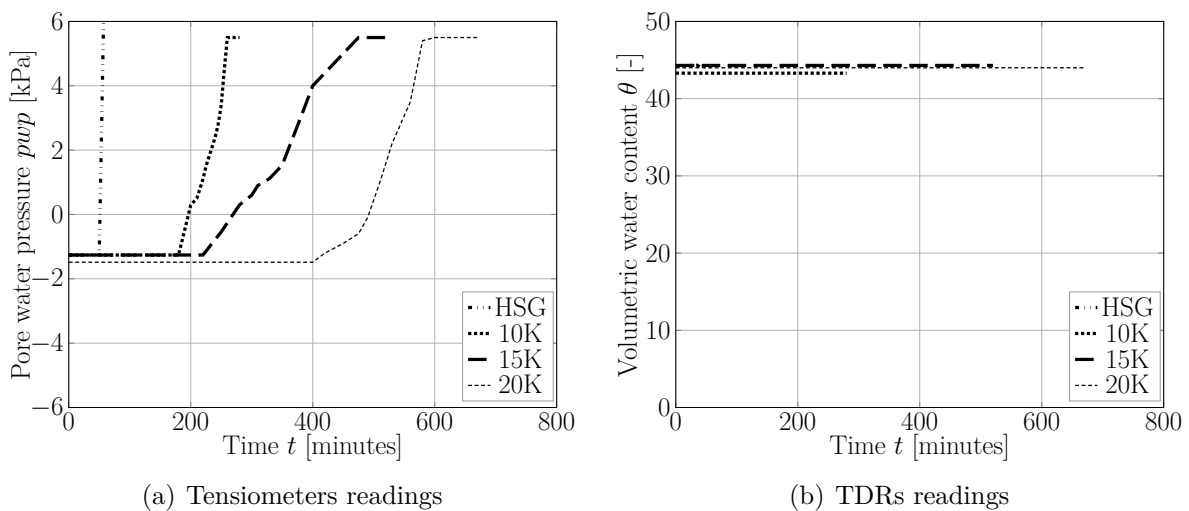


Figure 6.60.: infiltration stage: The readings of the tensiometers and TDRs (Sensors at level 1)

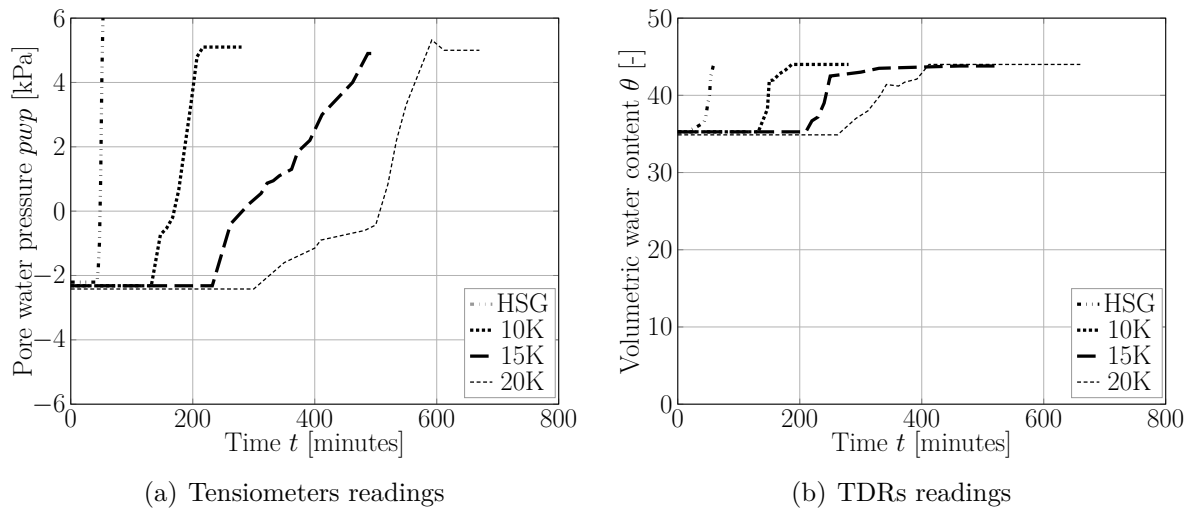


Figure 6.61.: Infiltration stage: The readings of the tensiometers and TDRs (Sensors at level 2)

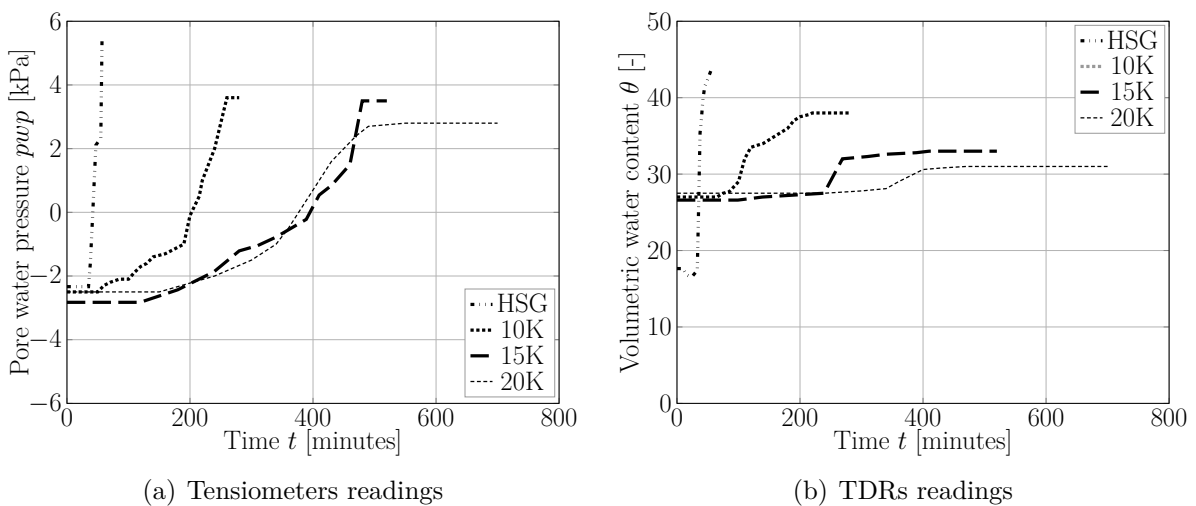


Figure 6.62.: Infiltration stage: The readings of the tensiometers and TDRs (Sensors at level 3)

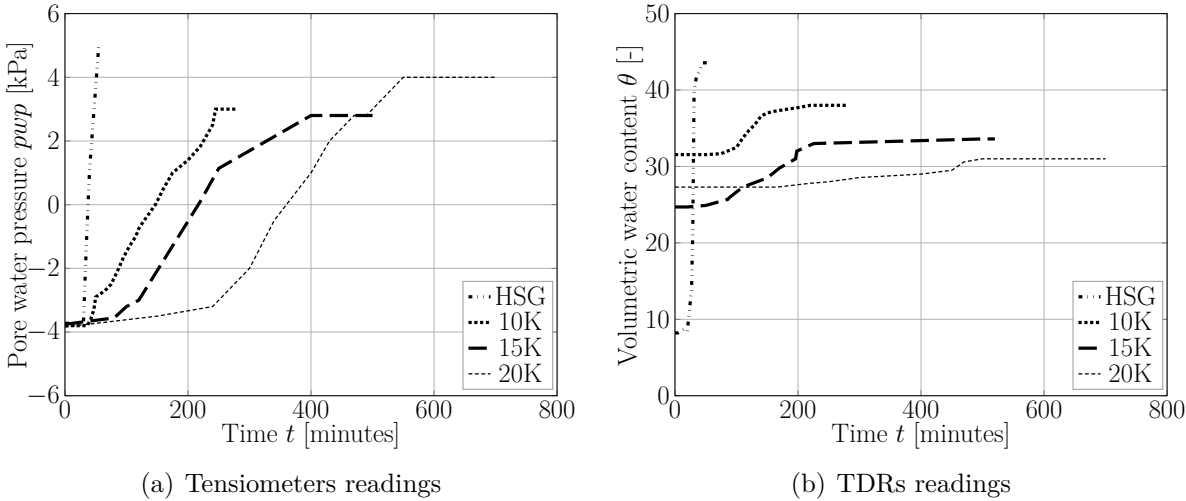


Figure 6.63.: Infiltration stage: The readings of the tensiometers and TDRs (Sensors at level 4)

7. Shear strength

7.1. Introduction

In this chapter, the direct shear device used to perform the saturated and partially saturated shear tests is presented, the shear results are presented and discussed. The results are analyzed using the Soil-water retention curves for the different soil mixtures, namely; HS, 10K, and 15K. The shear strength at the post-failure and also the dilatancy angle with suction are studied.

Table 7.1.

Initial conditions of specimens for SWCC tests										
Nr.	Mixture	Net normal stress [kPa]			Matric suction [kPa]					
1	100H:0K	80	120	250	0	2	3	4	10	100
2	90H:10K	80	120	250	0	2	3	4	10	100
3	85H:15K	80	120	250	0	2	3	4	10	100

7.2. Direct shear device

The device was designed and constructed by the manufacturer Wille Geotechnik. It consists of an air pressure chamber which includes a room for a square shear box with dimensions 100×100×20 mm. A circular 3-bar high air entry ceramic disk was glued on the base of the lower half of the shear box. The axis translation technique is used to apply the matric suction. The shear box is restrained from the inclined and vertical movements, it is only allowed to move in the horizontal direction. The device has the ability to apply vertical load in the axial direction and restricted from any tilting or movement in any other direction. The device can reach maximum 15 mm horizontal displacement.

Features of the direct shear device:

7.2.1. General description

An automated device that uses feedback from vertical and horizontal load cells and displacement transducers to provide real-time control of vertical and horizontal loading. The vertical and horizontal loadings are applied using stepper motors. The basic device consists of a shear box to retain the sample, two loading mechanisms for horizontal and vertical motions, two load cells, two displacement transducers, and two microprocessors for control of vertical and horizontal motions and data acquisition, and a personal computer with Windows-XP compatible software (Geosys 8.7.8.2) to setup the test conditions and reduce the test results.

7.2.2. Air pressure chamber

The air pressure chamber made from Plexiglas (internal dimensions) is 220 mm diameter, and 150 mm high with wall thickness of 13 mm as depicted in Figure (7.1). The cell can carry air pressure up to 10 MPa. The top of the air pressure chamber has two air/water ports, and another port for venting.

7.2.3. Shear box

The shear box, constructed of stainless steel, has a square cross section with the dimensions of 100×100×20 mm and consists of two halves that are held together with two screws. The bottom half has a high air entry porous disk with two drainage connections, one for sending water and the other for flushing water and air. The shear box is placed over the shear box holder. The shear box holder, which is rigidly fitted to the lower half of the shear box, it slides over the rollers while the upper half of the box is fixed to the horizontal load cell shaft. The ceramic plate can be removed and replaced with another one which can have higher or smaller air-entry value or also replaced with a plate for testing soils using vapor equilibrium technique.

7.2.4. Controlling suction

The axis-translation technique ATT was used to control the suction in the soil specimen. A 30 mm diameter 3-bar HAEPD was fixed to the base of the shear box. It has very fine pores that allow water to pass through, but not air, provided that the air pressure is

less than the air entry value of the HAEPD. The shear box has the ability to replace the HAEPD with different different air-entry value.

For smaller suction values (less than 10 kPa), an air-water interface device was used to control the suction. The air pressure applied with the same quantity to two lines, the air-pressure chamber and to the air-water device, the air pressure will blow a balloon inside the cylindrical cell which will apply water pressure to the water line connected to the ceramic desk. Adjusting the height of the cell to create a difference between the water pressure and the applied air pressure which will cause suction to occur. The system was checked using sensitive pressure measuring device.

7.2.5. Software and results monitoring

The software used during the testing program is Geosys 8.7.8.2 which allows to apply the vertical stress, to set the shear rate, and to shear the soil sample. The software allows to monitor the results during the test and to save the data in order to be presented using any suitable software (e.g. Microsoft Excel) for the whole test or for certain stage of the test (e.g. consolidation during applying the vertical stress or the shear-displacement curve during shearing).

7.3. Direct shear tests

In the following section, the results of the direct shear tests are presented. The tests can be divided into two categories; (1) validation tests, in these tests the results are compared with other tests performed using the classical direct shear device to check the accuracy of the new shear cell, these tests were performed on Hostun sand and on Silver sand/ Kaolin mixtures, (2) partially saturated tests, these tests were performed on mixtures of Hostun sand/ Kaolin mixtures (HS, 10K, and 15K) which are part of the current doctoral study.

7.3.1. Validation tests

The tests are performed on dry Hostun sand (dense state, $e_i=0.66$ & loose state, $e_i=0.89$), the vertical stress applied on the samples was in the range between (10-300) kPa. Similar tests were performed using the classical device on the lab. Tests were also performed on dense, medium dense and loose Silver sand and on Silver sand/Kaolin clay mixtures. The

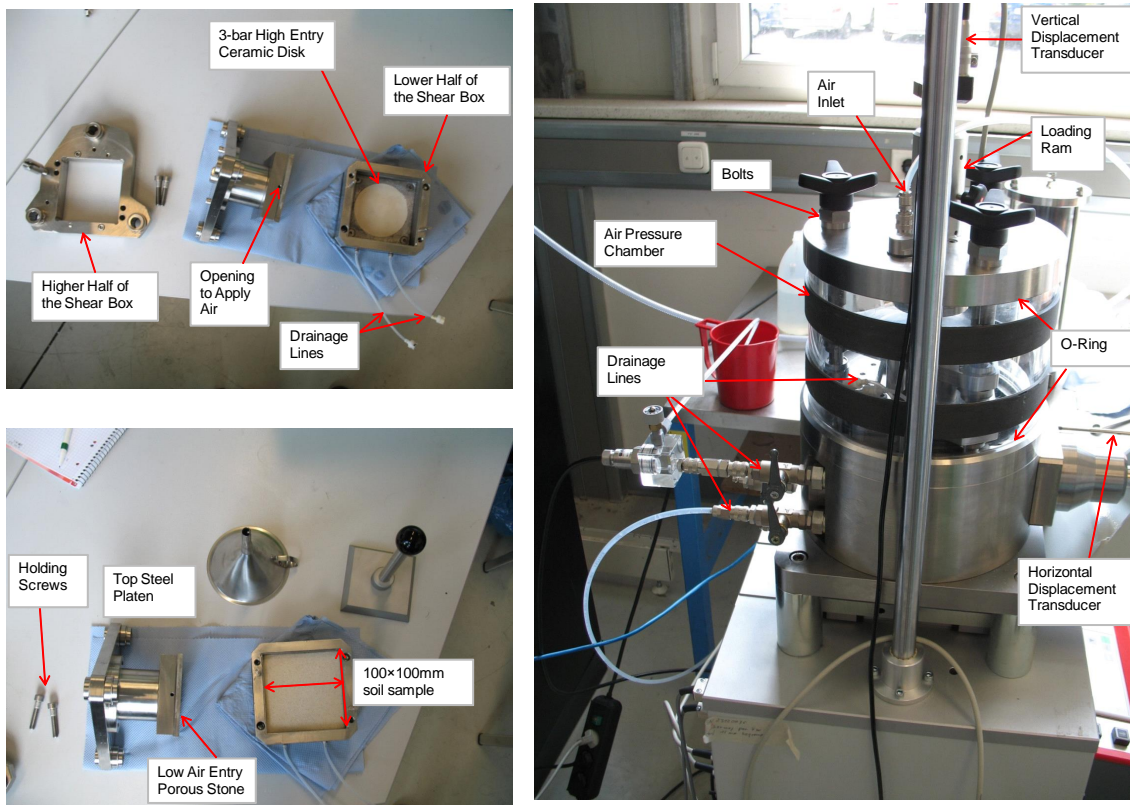


Figure 7.1.: The new direct shear device

tests results were compared with the tests performed also on a classical device by Röchter (2011).

7.3.1.1. Hostun sand

Two sets of tests were performed on Hostun sand; dry condition and saturated condition. The tests were performed using the new device with similar boundary conditions: initial density, vertical stress, and shearing rate which were used by the conventional direct shear device. The test results established for Hostun sand will be used to investigate the shear stress parameter under fully saturated, partially saturated, and fully dry condition.

In the dry tests, series of test in a range between 10 kPa and 300 kPa vertical stress had been performed, the idea from these tests was to evaluate the performance of the new direct shear device. The results shown in Figure (7.2) were compared with similar tests performed on the classical device in the laboratory. It can be seen from the tests results that the shear tests are in good agreement and the device is able to measure the shear

strength parameters properly. The tests results of the validation tests are presented in Figure 7.3.

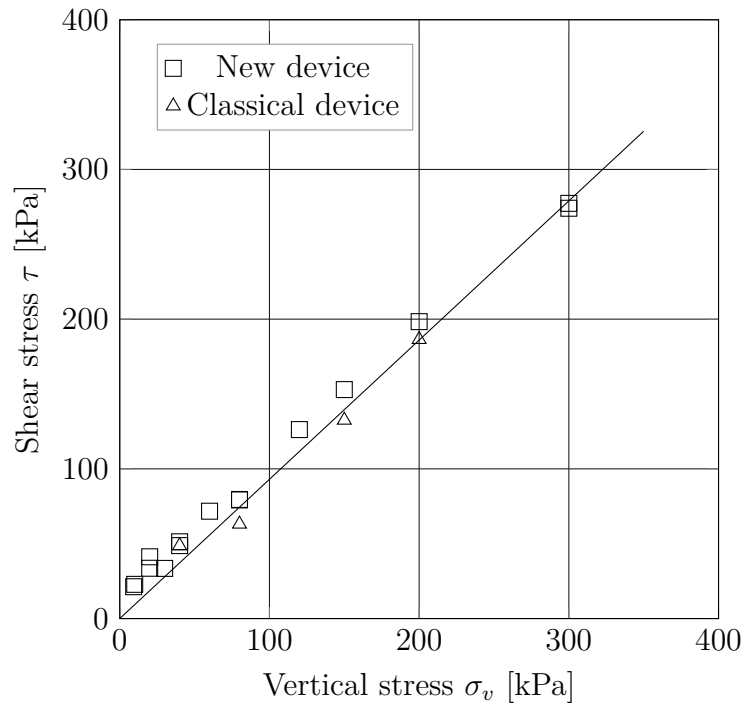


Figure 7.2.: Dense Hostun sand (Dry) $e = 0.66$

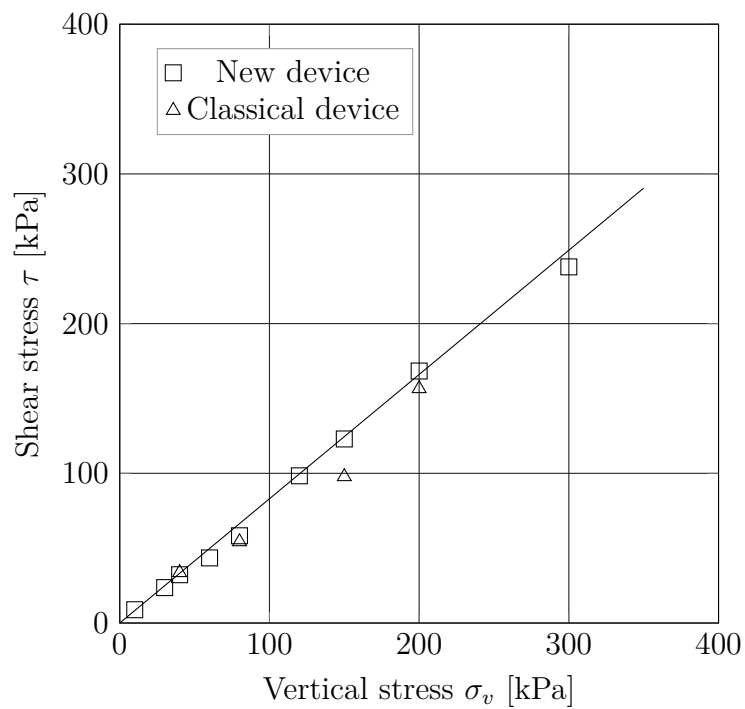


Figure 7.3.: Loose Hostun sand (Dry) $e=0.89$

7.3.1.2. Validation tests: Silver sand and kaolin

Series of tests on silver sand and mixtures of silver sand and Kaolin clay were performed in order to validate the performance of the new direct shear test device. The results were compared with the results performed by Röchter (2011). The vertical stress for these tests was 15, 30, 55, and 105 kPa. The shearing rate used during these tests was 0.04 mm/min

7.3.1.3. Silver sand

These tests were performed on Silver sand in loose state ($\rho = 1.5 \text{ g/cm}^3$), middle-dense density ($\rho = 1.55 \text{ g/cm}^3$), and dense state of the sand ($\rho = 1.60 \text{ g/cm}^3$).

The results were compared with the shear tests results presented by Röchter (2011). Figures (7.4),(7.5), and (7.6) shows a comparison between the results performed by Röchter (2011) and the new direct shear device. The results show a good agreement between the two devices which leads to the conclusion that the new direct shear device is suitable to perform direct shear tests.

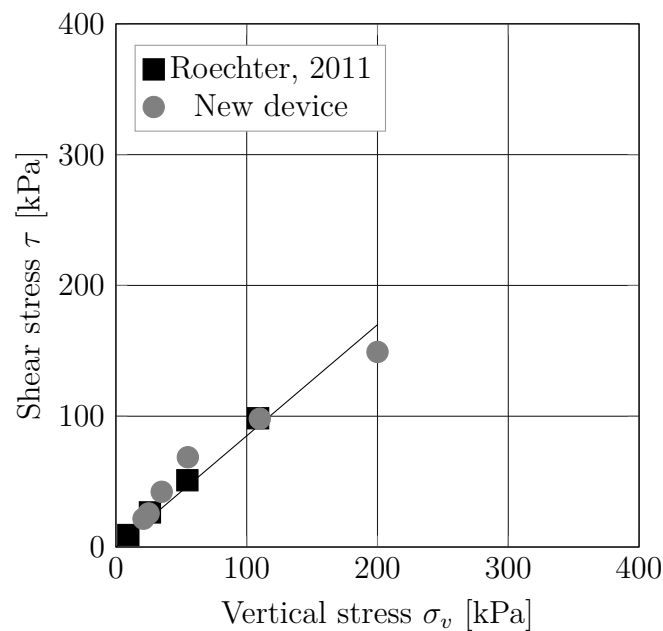


Figure 7.4.: Dense Silver sand

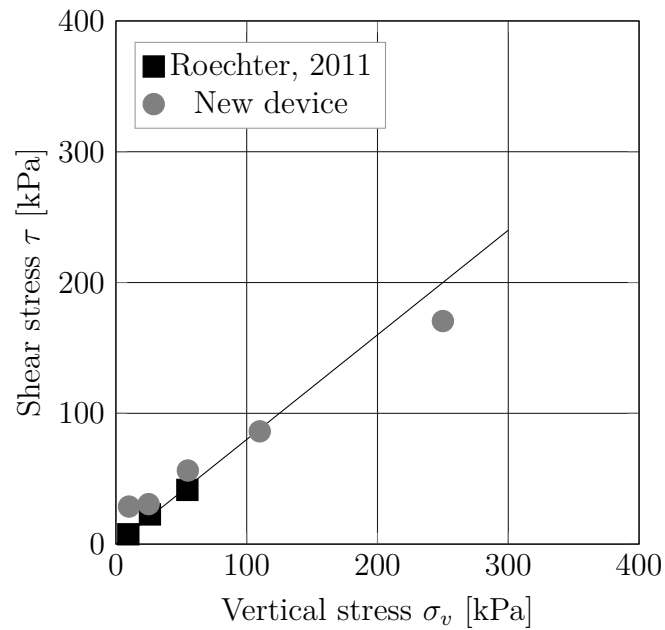


Figure 7.5.: Medium dense Silver sand

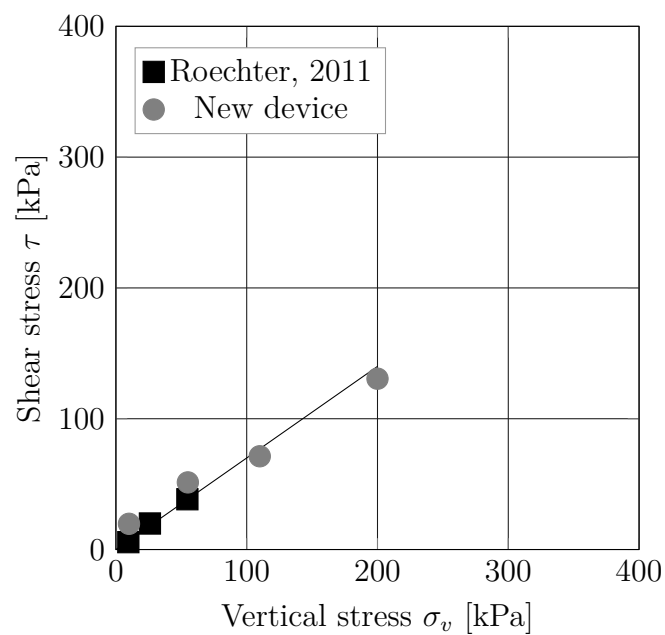


Figure 7.6.: Loose Silver sand

7.3.1.4. Silver sand-kaolin mixtures

The silver sand-Kaolin mixtures were performed under dry state in four groups; M1 = Silver sand 5% - Kaolin clay 95%, M2 Silver sand 7% - Kaolin clay 93%, M3 Silver sand

10% - Kaolin clay 90%, and M4 Silver sand 20% - Kaolin clay 80%. The initial densities were 1.75, 1.67, 1.67, and 1.67 g/cm³, respectively.

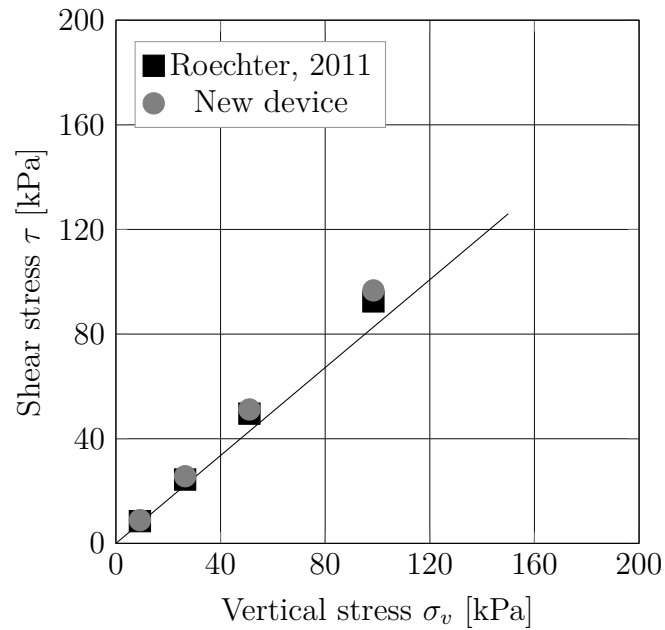


Figure 7.7.: Mixture 1

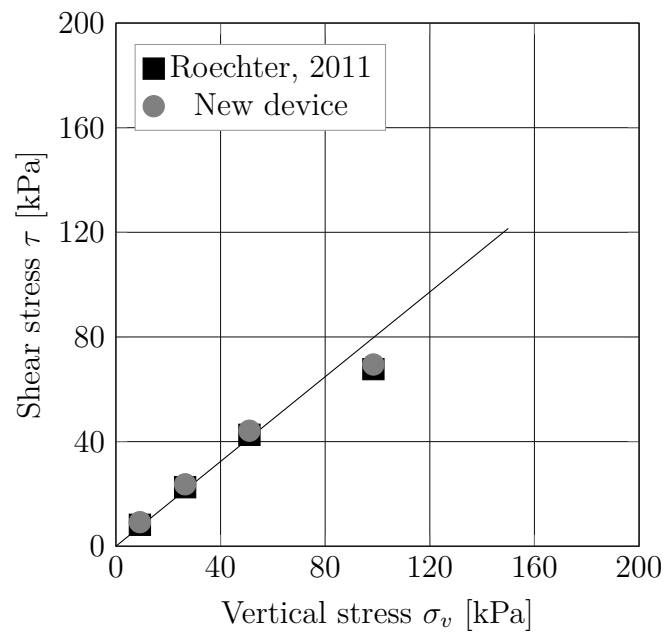


Figure 7.8.: Mixture 2

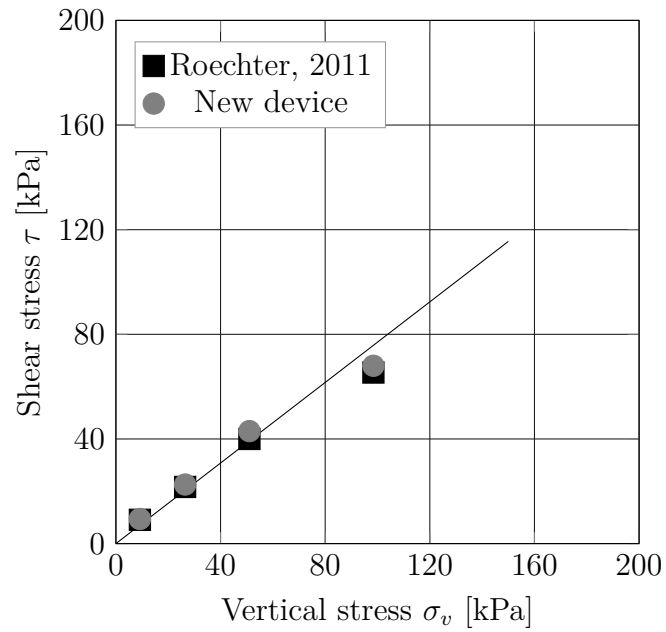


Figure 7.9.: Mixture 3

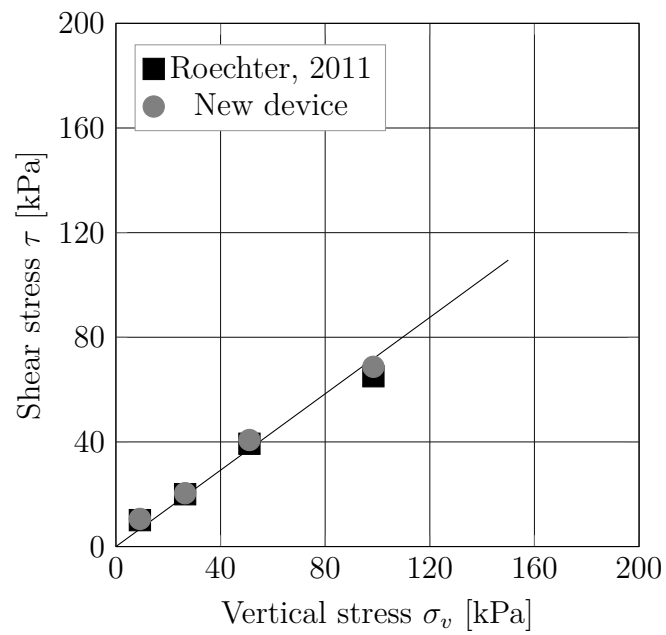


Figure 7.10.: Mixture 4

7.3.2. Partially saturated tests

The tests were performed on three different soil mixtures; dense state clean Hostun sand HS ($e_i=0.66$), mixture 10K, and mixture 15K. The objective of these tests was to cover a wide range of suction in order to have a sufficient understanding to the behavior of each soil mixture under partially saturated condition with focusing on the critical suction range before and after the AEV and at relatively higher suction.

The tests results will be analyzed and fitted using the proposed models by Vanapalli 1996*b* (Model 1) and Khalili & Khabbaz 1998 (Model 2) and after validating the model with the best fit parameters, the shear strength of soil mixture 20K will be calculated based on the previous model.

The tests were performed by preparing the soil sample with its initial water content inside the shear box, adding the seating load (about 1 kPa) by lowering the axial stress ram until it touches the plate above the soil sample. This process is important because the device starts to record the magnitude of the vertical stress, vertical displacement, and horizontal displacement versus the time after initiating this contact. The saturation of the soil sample is achieved by adding water to the air chamber. The water enters the soil sample from the gap between the two shear boxes and from the top of the sample. After this stage, the suction is applied to the soil sample by controlling the water pressure and air pressure simultaneously. The excess added water drains from a special valve located at the bottom of the air chamber. To reach suction equilibrium, the readings of the water inside the burette and the change in the height of sample is constant. The target vertical stress is applied with small rate (5 kPa/min) and the soil sample is checked until reaching stable reading for the settlement versus time. In this study, the secondary consolidation was not important and thus the consolidation stage did not exceed two days for soil sample 15K under 200 kPa vertical stress. The shearing stage was done with small shearing rate to avoid any change in water pressure during shearing process.

7.3.2.1. Hostun sand

The development of the shear force with horizontal displacement as well as the development of the vertical displacement with horizontal displacement of Hostun sand under controlled suction are presented in appendix B for different vertical stresses.

Figure (7.11) presents the change in the peak shear strength results for Hostun sand for different suction values (0, 2, 3, 4, 8, 14) kPa. The vertical stress applied on the samples is (60, 80, 120, and 250) kPa. Similar tests were performed by Alabdullah 2010 on Hostun

sand with similar density using controlled suction plane-strain device as shown in Figure (7.12)

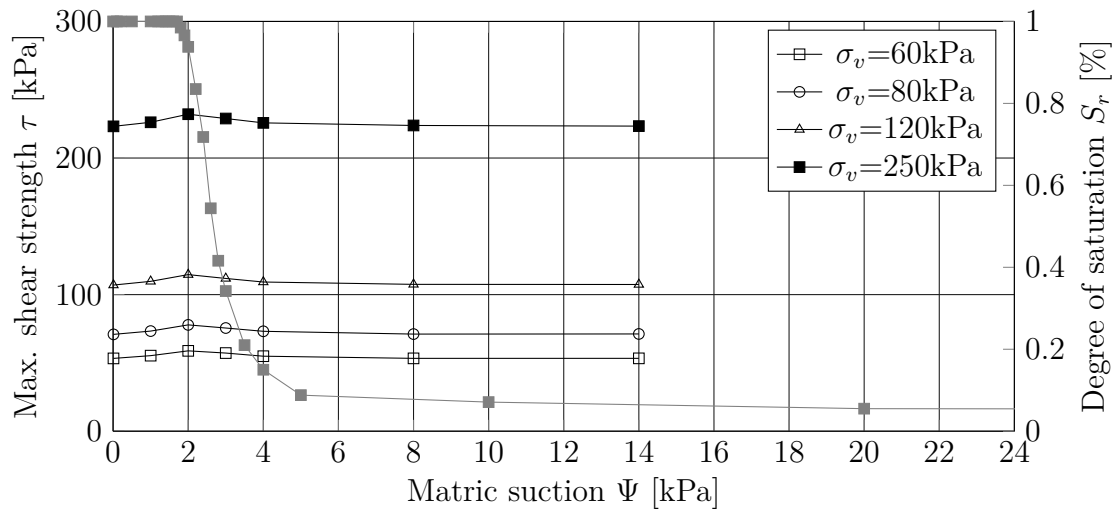


Figure 7.11.: Effect of suction on shear strength for Hostun sand

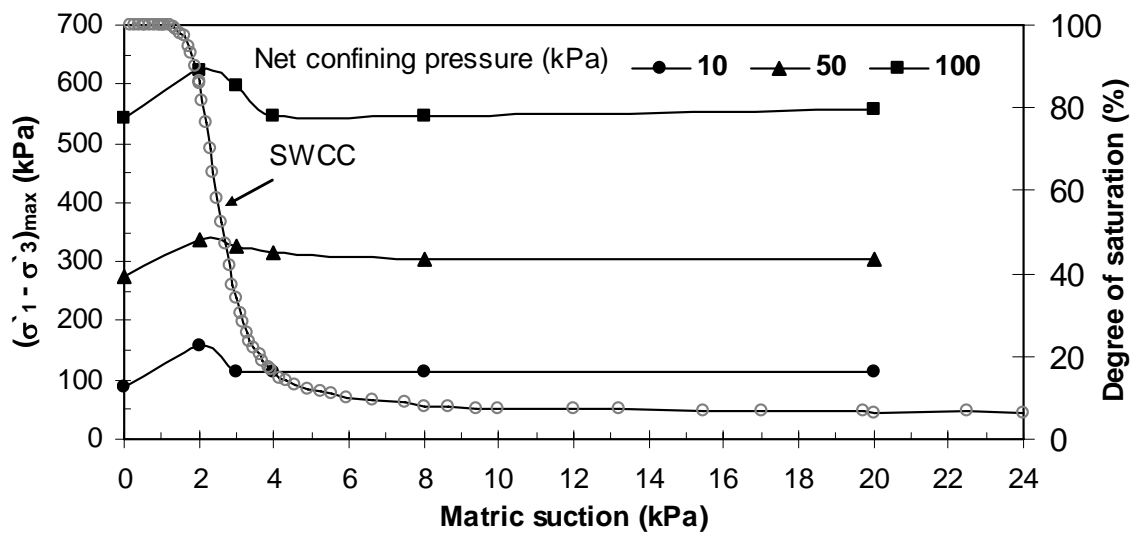


Figure 7.12.: Effect of the matric suction on the maximum deviator stress after Alabdullah (2010)

7.3.2.2. 10K

Appendix C presents the the detailed of the tests results for different vertical stresses. Figure (7.13) presents the change in the peak shear strength results for soil mixture 10K

for different suction values (0, 2, 3, 4, 50, and 100) kPa. The vertical stress applied on the samples is (60, 80, 120, and 250) kPa.

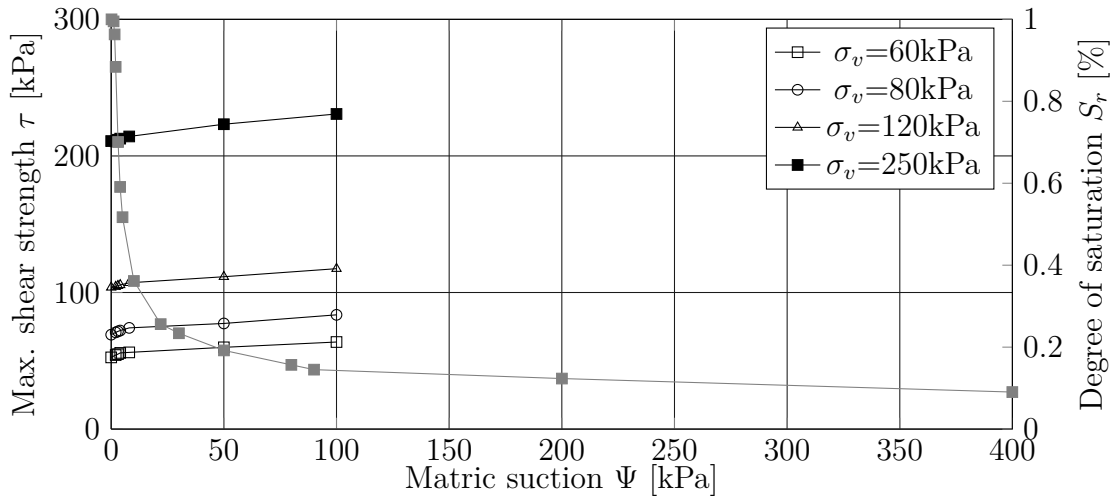


Figure 7.13.: Effect of suction on shear strength for 10K

7.3.2.3. 15K

Appendix C presents the the detailed of the tests results for different vertical stresses. Figure (7.14) presents the change in the peak shear strength results for the soil mixture 15K for different suction values (0, 2, 3, 4, 50, and 100) kPa. The vertical stress applied on the samples is (60, 80, 120, and 250) kPa.

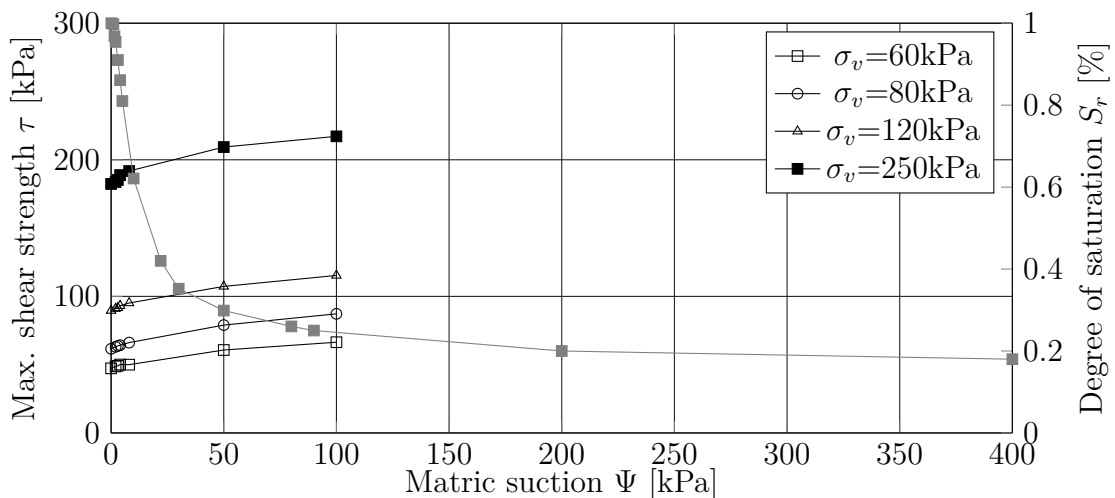


Figure 7.14.: Effect of suction on shear strength for 15K

7.3.2.4. Fitting the results

As presented in chapter 3, several models exist to predict and fit the shear results based on the SWCC and shear strength parameters. Since the shear tests under partially saturated conditions are difficult to perform and could be time consuming, these models could be used the shear parameters (fully saturated) and the SWCC to predict the shear strength for wide range suction. However, the fitting parameters which are proposed by the literature could not give suitable results for all soil types.

In the current result of Hostun sand HS and the soil mixtures 10K and 15K are fitted using the empirical model proposed by Vanapalli 1996*b* (Model 1) and Khalili & Khabbaz 1998 (Model 2) as shown in appendix D for the maximum shear strength, angle of friction due to suction, and the apparent cohesion developed due to the suction for different suction range.

The fitting parameters κ and r for the selected models proposed by Vanapalli (1996*b*) and Khalili & Khabbaz (1998) must be selected based on the best fit of the results.

The values chosen for κ and r , which had the best fit with the experimental results, are presented in Table 7.2.

For Hostun sand, the fitting using model 1 was used only since the model proposed by Khalili & Khabbaz (1998) did not show good results for pure sand.

Both models were able to produce good results when fitting the shear results for both mixtures 10K and 15K.

Table 7.2.: Fitting parameters of model 1 and Model 2

Soil	κ	r
HS	1	-
10K	1	0.4
15K	1	0.33

7.4. Discussion of shear tests results

The analysis to the effect of the suction on the shear strength of the soil using the direct shear device with controlled suction will be presented in this section. The results can be analyzed using the SWCC of each soil mixture. Following the literature of the shear strength under partially saturated condition, the shear behavior of sand may be different from clayey or sand/clay soils.

7.4.1. Hostun sand

Figure 7.11 shows that the peak shear strength is almost constant with small increase in the suction values up to the suction lower than the air-entry value AEV in which the sand is still considered saturated, also known as the boundary effect zone (Vanapalli 1996*b*). With further increase in the suction, the desaturation process starts to occur (reducing the degree of saturation of the soil sample), the shear strength starts to increase, beyond this value, the shear strength drops down but still relatively higher than the saturated shear strength of the sand. Also, the increase of the suction did not affect the general shape of the stress-strain relationship. Similar observations were presented by other studies like Donald (1956); Farouk et al. (2004); and also Alabdullah (2010) who performed series of tests on dense Hostun sand under plane-strain condition.

This phenomenon may be explained as follows; at low suction value (lower than the air-entry value), the pores between the coarse-grained soils (such as sand grains) are filled with free pore water and since the sand has a very low ability to sustain water menisci between the grains (no water adsorbed on particle surfaces) therefore, a small amount of suction beyond the air-entry suction will allow the air to start to enter the large pores, a contractile skin begins to form around the points of contacts between sand grains (act as a glue) which will increase the capillary action thus the normal forces at the inter-particle contacts will increase. These additional normal forces may enhance the friction and the cohesion (*Capillary cohesion*) at the inter-particle contacts. Consequently, the partially saturated sand exhibits higher strength than the saturated sand.

With further increase in suction, the shear strength starts to decrease. It can be explained that at lower suction range (still beyond the AEV), air replaces some of the water in the large pores which forces the water to flow through smaller pores and forms water menisci at contact points. At higher suction value, the sand starts to dry and the water menisci start to accumulate only between fewer sand grain Farouk et al. (2004). Sand has a very low ability to sustain water menisci between the particles. At higher suction values, a further decrease in water that occupies the pore volume will take place during the consolidation stage, which may result to a further decrease in the number of connections between the water and sand particles. The total contact area of the momentary contact surfaces arising from the water menisci may be radically decreased also as a great amount of continuous air phase is formed throughout the soil. Thus, the total number of water menisci, which act as a glue at the grain contact points, will be fewer than the number at lower matric suction. As a result, the amount of increase in the strength of the studied sand begins to drop.

Fisher (1926) proposed a model to explain the the effect of water-air meniscus on the stress state of two solid spheres. Figure (7.15a) shows two spherical grains of radius R in contact. The water meniscus between them is bound by the two grains and by an imaginary torus. The small radius of this doughnut-shaped torus is r_1 and the distance from the center to the inside wall of the torus is r_2 . Therefore, the local contact force (ΔN) which is the only force that the meniscus imposes on the particles, contributing by the pressure of the fluid acting on the cross-sectional area of the meniscus and the surface tension (T_s) acting along the perimeter of the meniscus, can be expressed as Fisher (1926); (Gili 1988); and Cho & Santamarina (2001):

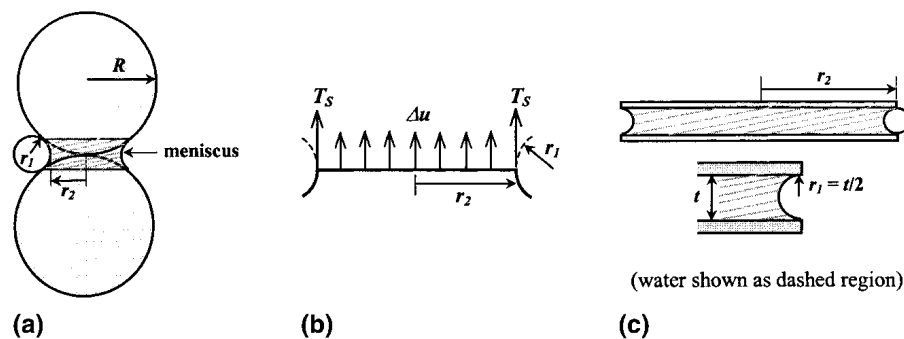


Figure 7.15.: Microscale Models-Schematic Representation: (a) Spherical Particles; (b) Forces Involved; (c) Disk Particles, after Cho & Santamarina (2001)

$$\Delta N = (u_a - u_w)(\pi \cdot r_2^2) + T_s(2\pi \cdot r_2) \quad (7.1)$$

This force increases by increasing the suction. Therefore as a result of increasing the suction, a normal force holds the two soil grains together and limiting slippage strength (Sawangsuriya (2006)). Consequently, the stiffness and the strength of unsaturated soils increase with increasing matric suction. This effect does not increase infinitely since the contact force (ΔN) tends toward a limiting value due to progressive reduction in the meniscus radius as suction increases (Mancuso et al. 2002). Figure (7.16) shows the increase of the stiffness of Hostun sand with increasing suction proposed by Lins (2009).

As a fact of both the geometrical packing of grains (fabric) and the contact forces between them are strongly controlling the mechanical behavior of particulate systems, such as sand. When a sand body is sheared, an increase in volume (dilation) ensues due to the geometrical constraints imposed by the fabric against applied stresses. This important phenomenon, coined as stress dilatancy, hinges on particle kinematics (slip and spin) as the grains override each other against confinement Wan & Guo (2004). The physical manifestation

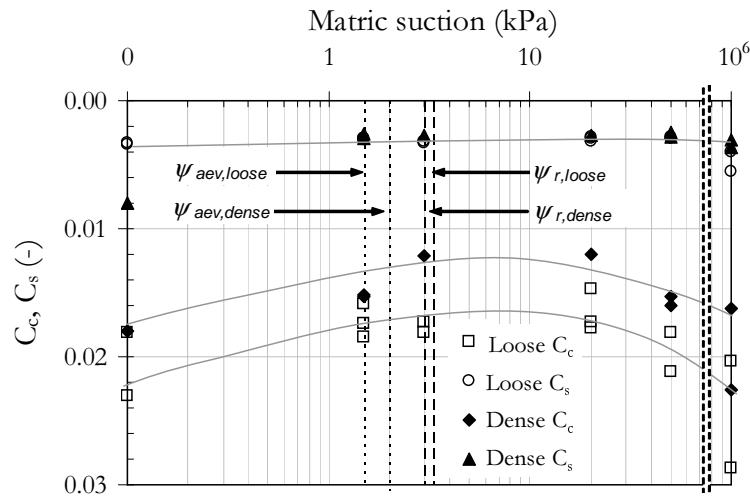


Figure 7.16.: Compression and swelling index versus suction for Hostun sand after Lins (2009)

of dilatancy was first identified by Reynolds (1885) and Rowe (1962) introduced a stress-dilatancy theory.

The characteristics of the volume change of sand during shearing depends on the confining pressure (or vertical stress) and the initial void ratio e_i Lee & Seed (1967). While applying the vertical stress during the consolidation stage, the void ratio reduces and thus the tendency of the sample to dilation will increase. However, the increase in the vertical stress will tend to suppress the dilatancy. Applying a vertical stress higher than the preconsolidation stress will reduce the dilation of the sand sample. From another side, the denser the specimen, the higher the dilation compared to a looser specimen under the same confining stress. For specimens with the same initial void ratio e_i , the confining pressure suppresses the degree of dilation.

Bilinear lines are intentionally drawn for each relationship under the different normal stress Shimada (1998). Figure 7.17 shows that the dilation of the samples increases after the AEV and then it starts to relatively decrease with further increase in the suction. The increase in suction causes an increase in shear resistance between soil particles due to an increase in normal stress which leads to an increase in rigidity for soil structure. As a result, the dilatation of the soil increases during shearing Gan & Fredlund (1994); de Campos & Carillo (1995); Shimada (1998); Cattoni et al. (2005). For fully saturated soil specimen, the magnitude of the change of the pore water pressure equals to that of the change of the effective stress. However, under unsaturated condition, the effective stress

can be expressed as Bishop et al. (1960):

$$\sigma' = (\sigma - u_a) + \chi(u_a - u_w) \quad (7.2)$$

The increase in suction may increase the effective stress but its effect is not strong enough compare to the applied vertical stress and therefore, the effect of the suction on volume change is different from that for saturated samples. The influence of the application of the suction on the volume change behavior is not so strong compare to that of the application of the consolidation pressure itself. Then, the volume change behavior of unsaturated specimens during shear can be different from that of saturated specimens.

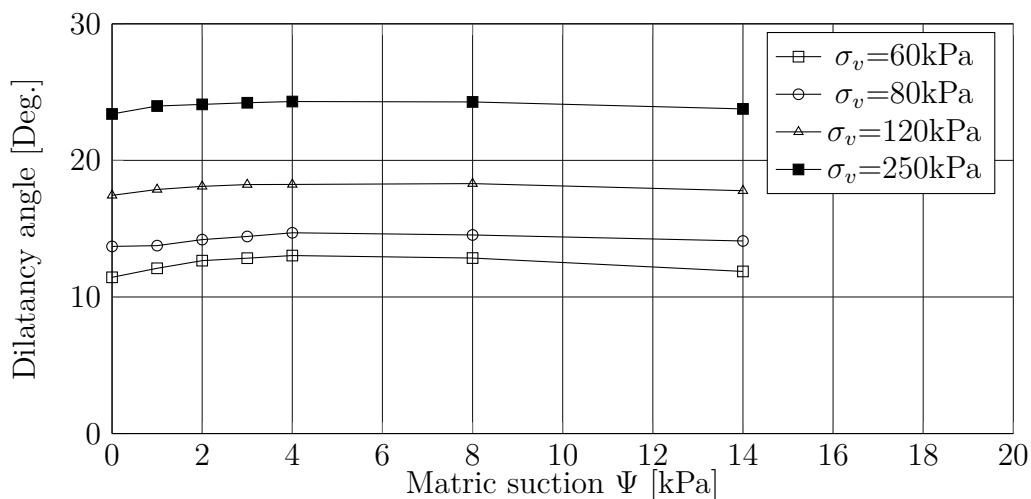


Figure 7.17.: Effect of vertical stress on the maximum angle of dilatancy (HS)

7.4.2. Sand-kaolin mixtures

As the suction increased (with an associate decrease in the degree of saturation), the shear strength increases and the drop in post peak strength (critical state shear strength) becomes more visible.

With increasing the suction value up to the AEV, the angle of friction is similar to the saturated one, while with further increase in the suction, the angle of friction starts to reduce as shown in Appendix D (Figures D.13, D.14, D.15, and D.16).

White et al. (1970) identified different desaturation stages of the soil, Vanapalli (1996b) presented these stages as shown in Figure (7.18):

- The boundary stage, the soil is essentially saturated. The water menisci in contact with the soil particles are continuous. Degree of saturation in the soil does not change with increasing matric suction. In this stage the variation of shear strength is assumed to be linear.
- The transition stage, (i.e. primary and secondary transition stages), in which suction $>$ AEV. In this stage S_r reduces with increasing matric suction. Specifically, the air starts to enter into the soil and the shear strength varies non-linearly with suction.
- The residual stage, the change in the water content is very small. Beyond this stage shear strength with respect to the matric suction decreases or remains relatively constant for sandy and silty soils. However, a slight increment in the shear strength can be observed for clayey soils. The general nature of SWCC gives an indication of the shear strength behavior over a wide range of suction.

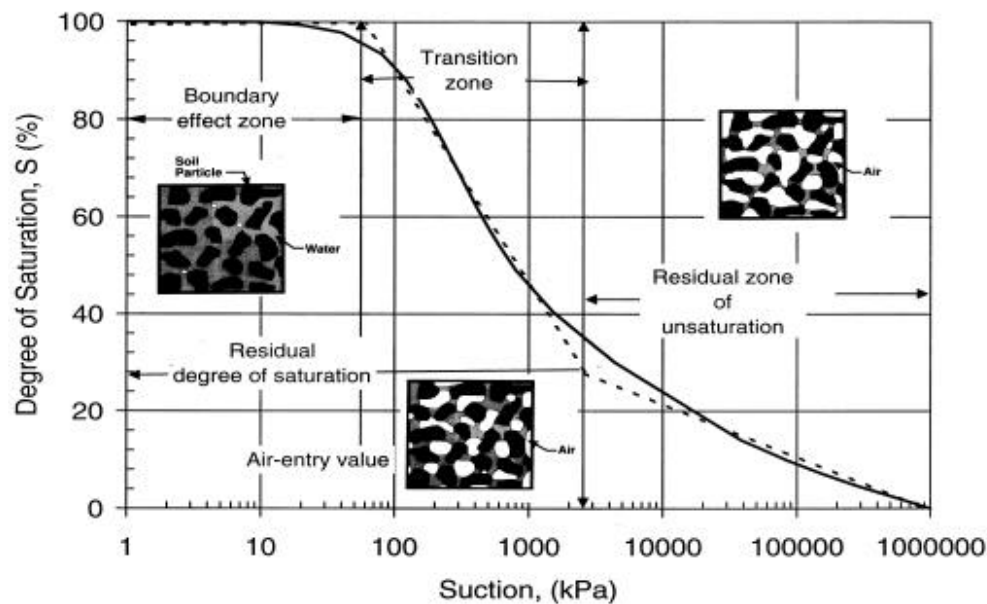


Figure 7.18.: Typical soil- water characteristic curve showing zones of desaturation Vanapalli & Fredlund (2000)

The angle of dilatancy may be considered independent of testing conditions. Schanz & Vermeer (1996) reported a dilatancy angle of $13.3-14.0^\circ$ for dense Hostun sand specimen tested in triaxial test under confining pressure of 300 kPa. In the present study, dense Hostun sand specimen tested under the same confining pressure shows a dilatancy angle of $13.3-13.8^\circ$. This is also supported by the data presented by Bolton (1986).

Increasing the suction leads to an increase in shear resistance between soil particles due

to the increase in normal stresses. This increase in normal stresses will contribute to an increase in the rigidity for the soil structure. The rigid soil structure has the tendency to increase the dilatancy of the soil during shearing. The increase in the dilation is reflected as an increase in the shear resistance of the soil Gan & Fredlund (1994).

With increasing the suction, the water, air, soil three-phase coexistence system of unsaturated soil, the air bubbles will be larger and joint the surface of particle, crescent water film between the particle began to emerge and independent of each other. At this point, the suction which was formed by the pressure differential between hydrostatic pressure in crescent water film and the outside atmospheric pressure gradually increased, and because the role of suction, shear strength of unsaturated silty sand gradually increase. When the moisture content continues to reduce to a certain extent, crescent water film content to reach the highest levels, forming the largest area of the suction effect and improve the shear strength of unsaturated silty sand to the peak value. After a while with a further reduction in moisture content, suction will increase, but at the same time crescent water film shrinkage and collapse will occur, resulting in reduced suction effect area. The decreasing of suction effect area and the increasing of suction formation of two growth and decline factors affect the shear strength of unsaturated silty sand. And when moisture content is reduced to a certain extent, the rate of suction increases will slow. The rate of suction effect area reduce will increase with the contraction and disintegration of crescent water film leading to the shear strength decreased with the moisture content showed lower and the suction increased. It should be noticed that: First, when the silt content of soil in a significant increase, the internal force chain and transmission of interaction gradually controlled by the silt, and the sand surrounded by silt become suspended in the particles, so the no contact or little contact with each other, the impact on soil properties is very small. Therefore, the peak phenomenon of unsaturated silty sand only occurs in the certain components. Secondly, the water-holding capacity of unsaturated silty sand increased with the increases in fine-grained. Therefore, the amount of fine fraction was effected the shear strength of silty sand Dong et al. (2012).

The shear strength depends on cohesion and angle of friction, when both increases, the shear strength increases however, it can be seen that the angle of friction due to suction reduces when increasing the suction. This is due to the increase in the cohesion.

For sandy and silty soils, the shear strength is independent of suction; by contrast for clayey soils, it increases slightly with suction increase Unlike sand, fine-grained soils can absorb the water on particle surface. the water adsorbed on particle surfaces becomes dominant.

The value of the internal angle of friction is not constant for a given soil, even for a

constant void ratio, it was found that it changes greatly depending on: the confining pressure, principle stress direction with respect to the bedding plane (anisotropy), and the intermediate principle stress Oda & Iwashita (1999). It is important to obtain the values of c and ϕ from test data in the pressure range which will be felt in the soil Kutter et al. (1988).

7.5. Suction stress

The suction stress can be related to the degree of saturation (or matric suction). This relation is called suction stress characteristic curve SSCC (Song 2014).

Lu et al. (2010) proposed the following closed-form equation to determine the suction stress using the fitting parameters n and α from van Genuchten 1980 fitting model:

For $(u_a - u_w) \leq \psi_{AEV}$

$$\sigma^s = -(u_a - u_w) \quad (7.3)$$

For $(u_a - u_w) > \psi_{AEV}$

$$\sigma^s = -\frac{(u_a - u_w)}{(1 + [\alpha(u_a - u_w)]^n)^{\frac{n-1}{n}}} \quad (7.4)$$

The parameter α is the inverse of the air-entry value AEV of the soil, and the parameter n is related to the pore size distribution and describes the slope of the SWCC. If the target suction is less than the AEV, equation (7.3) is valid and the suction stress equals to the value of the AEV. For higher suction range, equation (7.4) can be used for predicting the suction stress.

To determine the suction stress from the direct shear tests results under partially-saturated condition, Figure () describes the Mohr-Coulomb failure envelope of the shear strength. Suction stress at a given matric suction is then reduced from (Lu & Likos (2004)):

$$\sigma^s = -\frac{\tau_f - c' - (\sigma - u_a) \tan \phi'}{\tan \phi'} \quad (7.5)$$

7.5.1. Suction stress for Hostun sand

Figure 7.19 presents the calculation of the suction stress for Hostun sand using the SWCC under unconfined stress condition.

In the current study, the proposed model by van Genuchten (1980) has been used to determine the fitting parameters for predicting the suction stress using equations (7.3) and (7.4). Figure (7.19a) presents the suction stress characteristic curve (SSCC) for Hostun sand. Figure (7.19b) shows the relationship between suction stress and degree of saturation. The results show an increase in the suction stress with increasing the suction until reaching the air-entry value of the sand followed by a decrease until vanishing at a suction value of about 10 kPa. This behavior has been observed and reported by other researchers (Kim 2001).

By calculating the suction stress based on the direct shear tests results as shown in Figure (7.19a), an obvious increase in the suction stress with increasing the applied vertical stress is observed. Similar observations are shown on the suction stress and degree of saturation curves in Figure (7.19b).

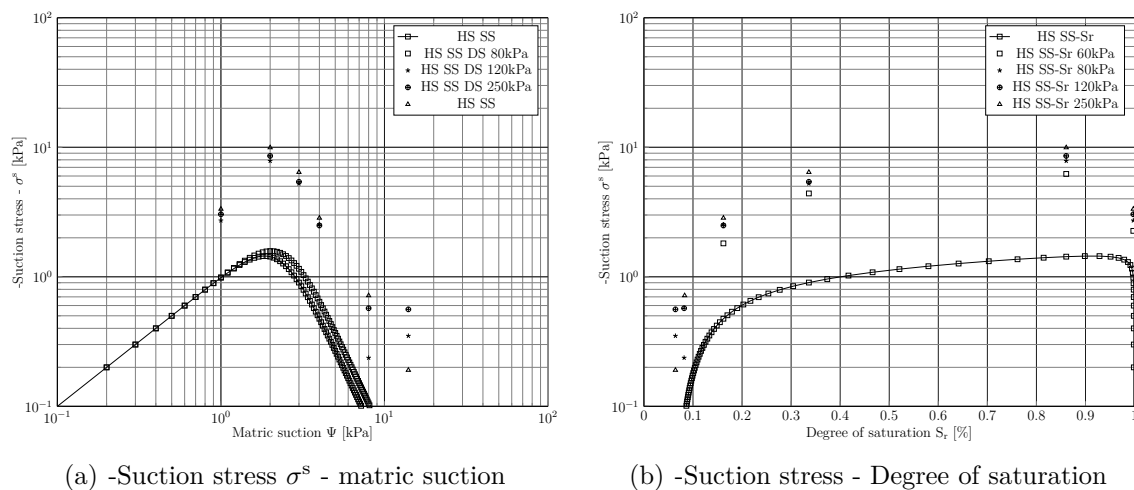


Figure 7.19.: SSCC for Hostun sand

7.5.2. 10K

Figures (7.20)a and (7.20)b show the suction stress curves SSCCs and suction stress - degree of saturation curves for the soil mixture 10K based on the SWCC and on the direct shear tests results. As the suction is increased, the suction stress increases gradually.

7.5.3. 15K

Figures (7.21)a and (7.21)b show the values of the suction stress and suction stress - degree of saturation when increasing the the amount of the fines content to 15%. The results are

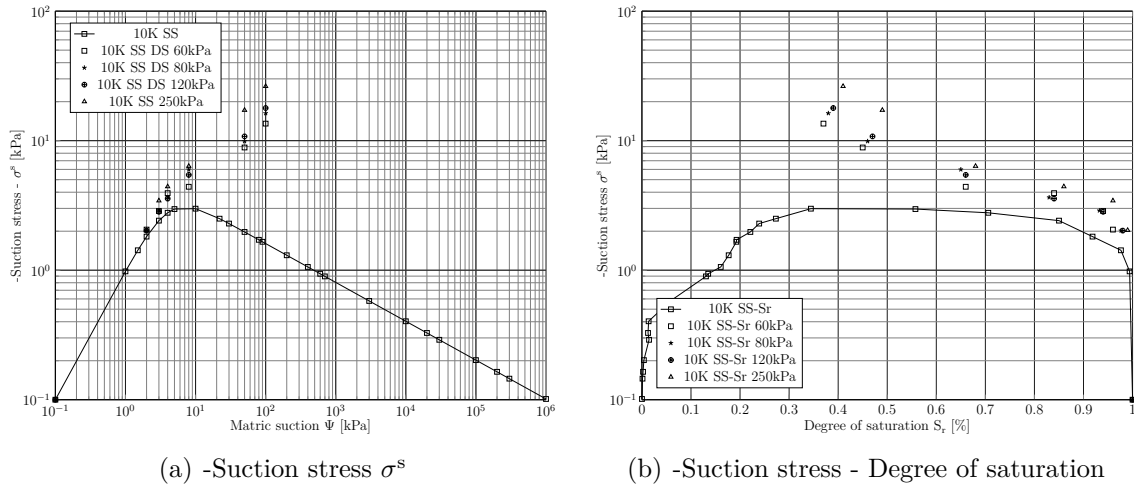


Figure 7.20.: SSCC for 10K

also based on the SWCC and on the direct shear test results. Similar observations have been seen with 15K mixture as in 10K. There is an increase in the suction stress with the increase in the suction value. The suction stress was calculated from the SWCC curves

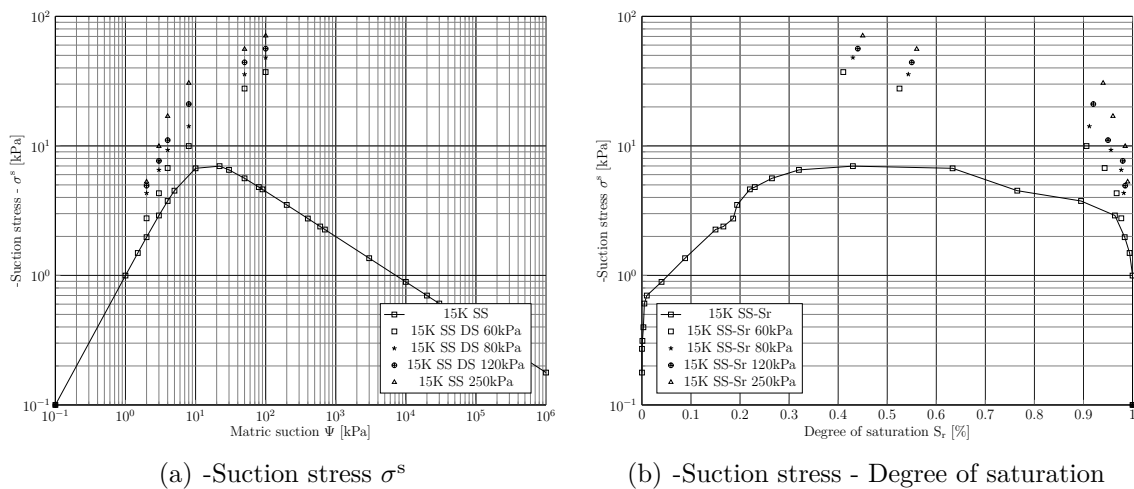


Figure 7.21.: SSCC for 15K

based on the fitting parameters α and n . The parameter α represents the suction value when the air starts to replace the water inside the voids (the curve is shifting to larger values of suction and the air-entry value is increasing), in which the parameter n reflects the pore size distribution of the soil.

The results of the suction stress calculated from the SWCC show that with the increase in the fines content, the magnitude of the suction stress increases. The increase is relatively small which could be due to the small percentage of the fines were added to the pure sand.

Dry sand has minimal suction stress close to zero. With further increase in the moist content, the suction stress increases to a peak value (around the suction value at the AEV) and then reduces to nearly zero at fully saturated condition.

For the soil mixtures 10K and 15K, the suction stress increases with reducing the degree of saturation and tends to remain constant with further increase in the suction. The tensile strength is increasing with the increase in the fines content. Similar observations were reported by other researchers (Tamrakar et al. 2007; Barzegar et al. 1995; Song 2014).

The results of the suction stress calculations from the direct shear tests for Hostun sand and thwe soil mixtures 10K and 15K show a small shift upwards with the increase in the vertical stress.

7.5.4. Discussion of the results

The suction stress values are increased until the soil was nearly fully saturated and then decreased rapidly to zero. When the suction is lower than the AEV or WEV of the soil, the suction stress remains at the stress of the saturated condition. When the matric suction is higher than the AEV or WEV, the suction stress decreases. Therefore, the effective stress of partially saturated sand differs from that of saturated sand due to the suction stress. The suction stress of different soil mixtures was investigated using the soil-water characteristics curve SWCC under unconfined stress and also using the tests results of direct shear under partially saturated conditions.

The selected soil materials are pure Hostun sand HS, and also sand-kaolin mixtures 10K, 15K, and pure kaolin.

In case of sand, it is obvious that the capillary stress is the major reason for the suction stress. The general increase and decrease in the suction stress is due to the reduction of the degree of the saturation with increasing the suction.

For the soil mixtures, 10K and 15K, the behavior is somehow similar. The results show an increase in the suction stress with increasing the suction value and also with increasing the applied vertical stress. The increase in the vertical stress will lead to increase the effective stress and to shift the air-entry value (increase in the AEV) which as a result will increase the suction stress value.

The suction stress developed from the direct shear results is higher than that calculated from the SWCC. There are several factors control the increase in the suction stress; the applied vertical stress which increases the effective stress, the increase in the cohesion between the soil grains due to the shearing process and increase in the capillary forces, and the effect of soil dilation on the volume change of the soil sample during shearing.

Similar observations were reported when analyzing the results of the plane-strain of Hostun sand of Alabdullah 2010.

7.6. Summary

This chapter can be divided into two main parts; validation shear tests, and partially saturated shear tests. In the first part, three sets of soils, which were available in the laboratory were tested in similar conditions to the once documented in the literature. The objective of these tests is to validate the new direct shear device. The results were found in good agreement to the once produced using the conventional direct shear device.

In the second set of tests, the shear strength of three soil materials was determined under partially saturated conditions. The objective of these tests is to understand the shear parameters under partially saturated condition and also to understand the risks when introducing suction to the soil.

8. Summary and Outlook

8.1. Summary

The aim of this work is to get an insight into the complex hydraulic interaction between soil and geotextiles within drainage and infiltration processes in a system of a soil layer above a nonwoven geotextile. For this soils with characteristics, which may be typical for cover soils of landfills above a drainage system, from a pure sand to sand kaolin mixtures with increasing fine content have been selected. Furthermore, 11 samples of nonwoven geotextiles showing a bandwidth of apparent opening size has been chosen. First, the relevant properties of the materials have been determined experimentally, like grain size distribution and soil water characteristic curve (SWCC) for the soils and apparent opening size distribution (AOS) and geotextile water retention curve (GWCC) for the nonwoven geotextiles. Within this part of the work a method has been developed to derive the GWCC from the AOS and this method has been validated by the experimental results. Using existing models, the hydraulic conductivity curves for the soils and the geotextiles have been determined from the SWCC and GWCC, respectively.

Secondly, one dimensional column tests have been performed using one typical nonwoven geotextile and four different soils with increasing fine content and due to that different SWCCs and hydraulic conductivity curves. The test results show that the hydraulic interaction and the drainage behavior are influenced by the soil type. In all cases the flow of water through entering the geotextile is disabled when degree of saturation of the soil above the geotextile is decreasing and the suction exceeds a certain value. The test results are analyzed and explained by the properties of the materials, which have been determined in the first part.

In addition, a separated part of the work is related to the unsaturated shear strength of the studied soils. Experimental data are compared to different theoretical approaches to describe unsaturated shear strength based on e.g. saturated shear strength and degree of saturation.

The main results of the investigations are summarized in the following

Geotextile material

1. The GWCC test results showed that the geotextile material has a water-retention curve similar in shape to the SWCC for soils.
2. The air-entry value of the nonwoven geotextile materials is relatively small (0.2-2 kPa) and in the range of granular materials.
3. The hydraulic conductivity of the geotextile will drop down with small increase in the suction value.
4. The geotextile material showed a hysteresis between the drying and the wetting curves which is similar to the observations on the SWCC.
5. Several geotextile materials have been tested in the current study and it has been observed that the GWCC and the permeability-suction relationship are similar for the tested materials.
6. Oedometer tests show, that the influence of suction on the compressibility of the geotextile in the measured stress range is small. On the other hand, the influence of the stress level and the compression of the geotextile due to the stress level have a significant influence on the GWCC. AEV is increasing with increasing stress.
7. Experimental determination of the GWCC is difficult and time consuming. A method has been developed to derive the GWCC from AOS. Comparison of measured and derived GWCCs for different geotextiles shows, that the developed method is applicable and allows a simplified determination of GWCC.

Soil materials

1. The effect of the fines content has been studied on the SWCC and its parameters and also on the permeability relations.
2. The SWCC curves of the tested soil showed an increase in the AEV with the increase in the fines content.
3. The tested soils have higher AEV compared to the geotextile materials.

4. SWCCs and hydraulic conductivity - suctions relationship of the tested materials show a much wider range compared to the narrow band of the related functions of the geotextiles. Due to this, soils with different fine content have been used in the column tests.

1-Dimensional flow of water through sand/geotextile column

1. Five column tests were performed to study the effect of partially saturated conditions on the soil and soil/geotextiles following four consequence stages: saturation stage, drainage stage, infiltration stage, and drainage after the infiltration stage.
2. The sand column test (without geotextile) showed that the used setup was sufficient to study the effect of the suction on the column apparatus.
3. The soil/geotextile tests showed that the geotextile suffers from the effect of the suction on its drainage performance since the AEV of the geotextile is very small.
4. It is observed in the column tests, that the drainage process is restrained at suction values of 2-3 kPa close to the geotextile. These suctions are corresponding to the critical suction for which unsaturated hydraulic permeability of the geotextiles drops below the one of the soil materials.
5. At the end of the drainage stage, a moist layer will develop inside the column layer above the geotextile layer. The thickness of this layer depends on the AEV of the soil layer. The higher the fines content, the thicker the existing moist to develop above the geotextile layer.
6. As the fines content was increased in the soil mixtures 10K, 15K, and 20K, the saturated permeability of the soil is reduced. However, as the AEV is higher, the drop in the values of the permeability relationship with increasing the suction will be less.
7. A soil mixture with lower fines content tends to transfer the water to the geotextile layer faster but a small suction value has higher influence on its drainage potential.
8. The breakthrough will occurs through the geotextile layer at a suction range relatively close to its own WEV. At this value, the geotextile layer will become permeable and capable to transfer the water.

Shear results under unsaturated conditions

1. The new direct shear device showed good and reliable results to study the influence of the suction on the shear strength.
2. The shear strength of the sand increases with the increase of the suction at suction range higher than the AEV due to the capillary forces between the soil grains however with further increase in the suction (beneath the residual suction) the shear strength reduces and will be similar to the shear strength at the saturated condition
3. The shear strength of the soil mixtures increases with increasing the suction value due to the effect of the capillary forces between the soil grains.
4. the soil materials tested in the current study have low range of the AEV and it is possible that the effect of the suction is limited on the shear strength parameters in comparison to clayey soils.

During the current study some work packages were initiated, which are not included due to the quality of the results and the challenges which appeared with the tests.

1. It was planned to study and determine the shear parameter between the soil and the geotextile under partially-saturated conditions in modified direct shear device. However, it has been observed that the shear results were not regular and the stress-strain curves did not flow the ideal shear results. It could be due to the influence of the surface of the geotextile material which created un-smooth surface during the shearing stage.
2. As part of the current study, a numerical analysis of some case studies using different soil properties was planned.
Due to the limitations of the used software, it was difficult to adopt the drying and the wetting curves of the SWCC and the GWCC curves during the change from the drainage and the infiltration stages.
The representation of the permeability of the soil material was not systematic. It has been observed that the numerical results could match the experimental results when using a lower permeability values in the numerical model rather than the determined once in the laboratory and also the infiltration rate during the infiltration stage which is a function of the saturated permeability.

This observation put a challenge to validate the results accurately however, it was reported by other authors in the literature.

3. An attempt was started to measure the hydraulic conductivity relationship of the nonwoven geotextile at different suction range. A special cell called multi-task cell was used for this purpose. The test was performed initially using a ceramic disk however when controlling the suction to the target value using the hanging column method, the measured permeability was for the ceramic disk rather than the geotextile layer due to higher saturated permeability of the nonwoven geotextile.

8.2. Outlook

Based on the findings of the experimental work and the proposed model in this thesis the following further works are suggested:

1. Performing laboratory tests using one-dimensional flow of water through a column of soil and a layer of geotextile using woven geotextile material.
2. Performing laboratory tests using large scale equipment to study the distribution of the water during the infiltration stage in 2-dimensional set-up that drainage systems are inclined, so that in addition to vertical percolation lateral flow arises. This leads to a two dimensional flow problem, which has to be studied in 2-dimensional test set up.
3. Performing further tests using different soil mixtures to study the use of higher plastic soil mixture and the influence of wetting/drainage cycles on the swelling/shrinkage behavior of the soil.
4. Include a numerical analysis using a suitable software or a code capable to simulate unsaturated flow. The code must handle the numerical difficulties arising from the steep SWCC / GWCC and hydraulic conductivity - suction relationship within the range, where water content and hydraulic conductivity is significantly changing with small variation of suction, and can detect the influence of the hysteresis of the drying and wetting paths of the SWCC/GWCC on the column test.
5. The influence of change of water content on the shear strength at the soil geotextile interface is of interest. For this the development of an adequate test set up is necessary.

A. Appendix A Measured and fitted SWCC

In the current appendix, the fitting curves of the soil-water characteristic curves and the hydraulic conductivity curves of the tested soils are presented.

In this appendix, the results of the soil-water characteristic curves for Hostun sand, 10K, and 15K, 20K, 25K, and Kaolin clay consequently including the fitting curve using Fredlund & Xing (1994).

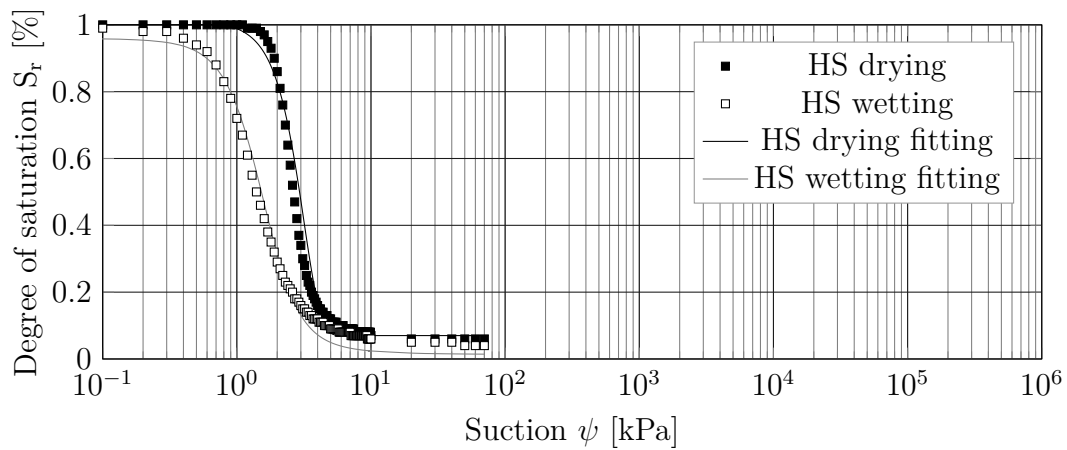


Figure A.1.: SWCC of Hostun sand

- The water-retention curve of Silver sand was determined based on the grain size distribution curve following the model proposed by Fredlund (1997b).

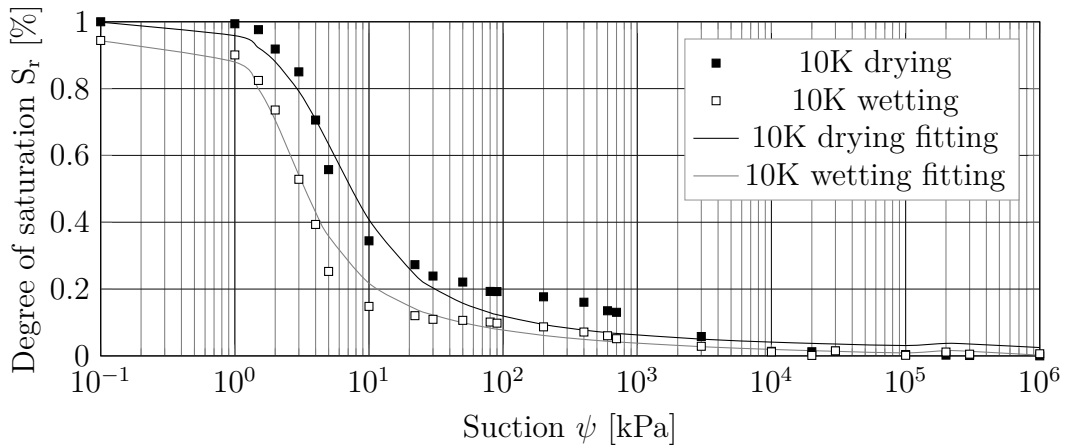


Figure A.2.: SWCC of 10K

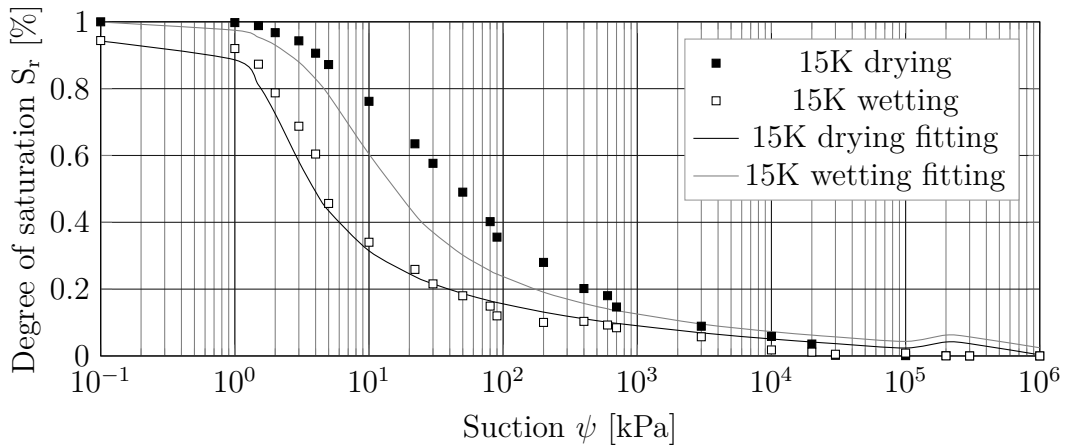


Figure A.3.: SWCC of 15K

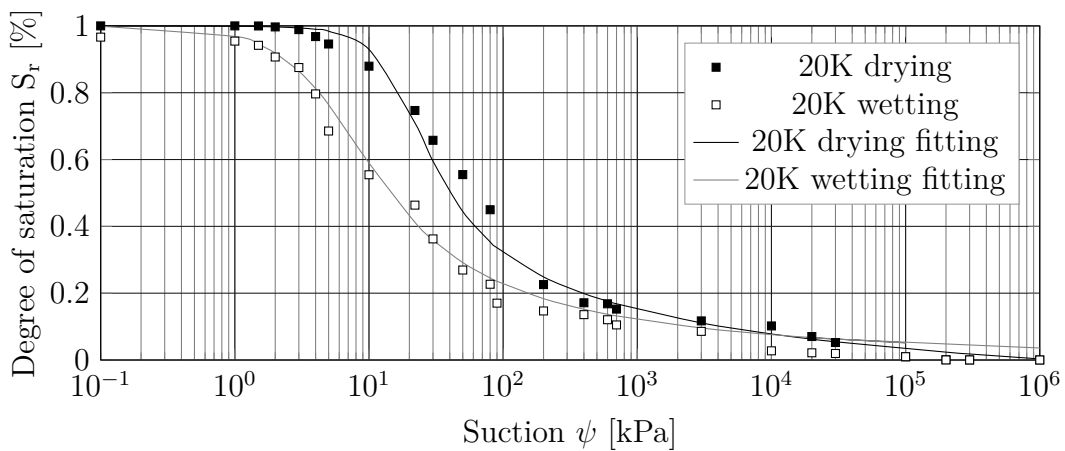


Figure A.4.: SWCC of 20K

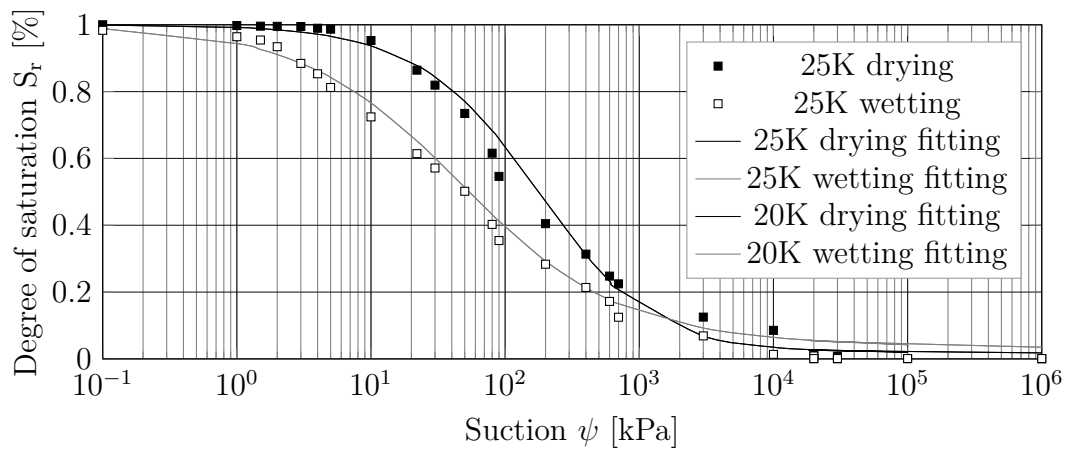


Figure A.5.: SWCC of 25K

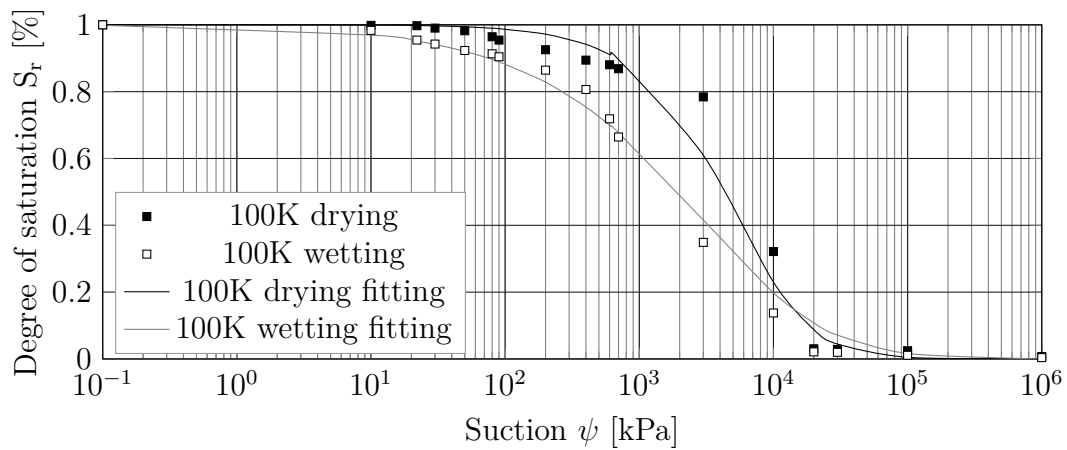


Figure A.6.: SWCC of 100K

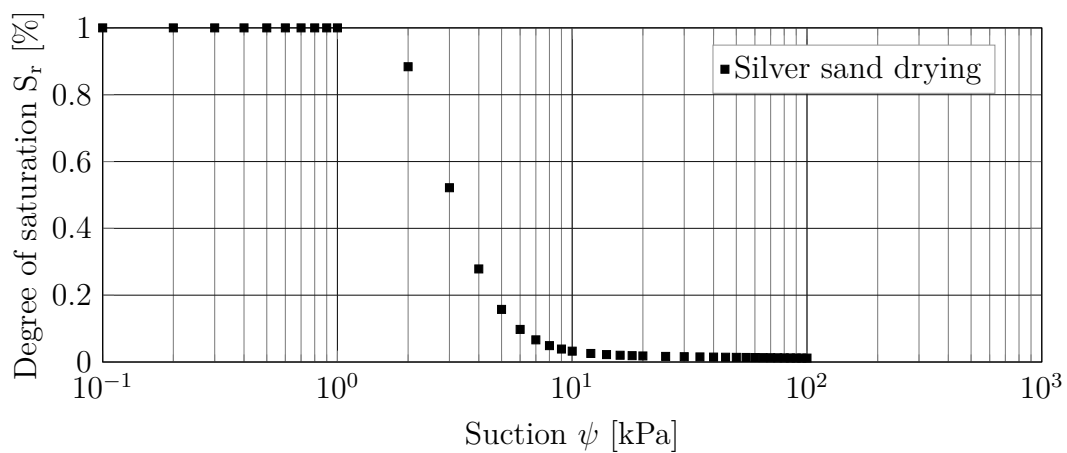


Figure A.7.: SWCC of Silver sand based on fitting model by Fredlund (1997b)

- The hydraulic conductivity function versus suction derived based on the suggested model by Fredlund & Xing (1994).

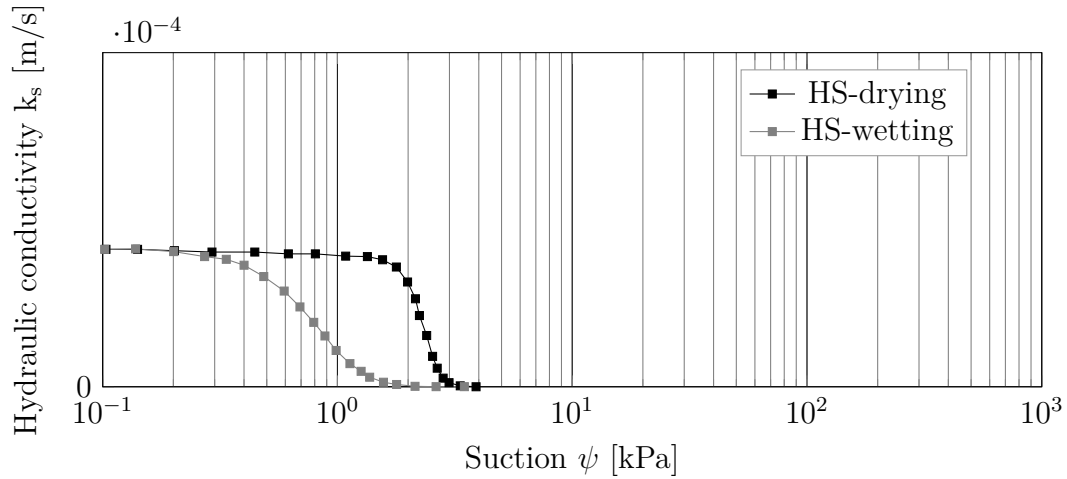


Figure A.8.: Hydraulic conductivity function vs suction for Hostun sand

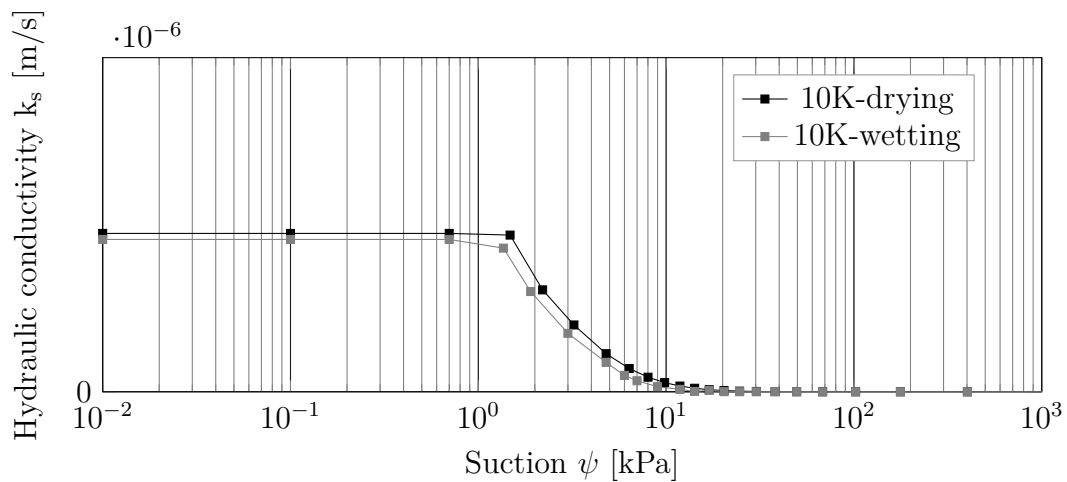


Figure A.9.: Hydraulic conductivity function vs suction for 10K

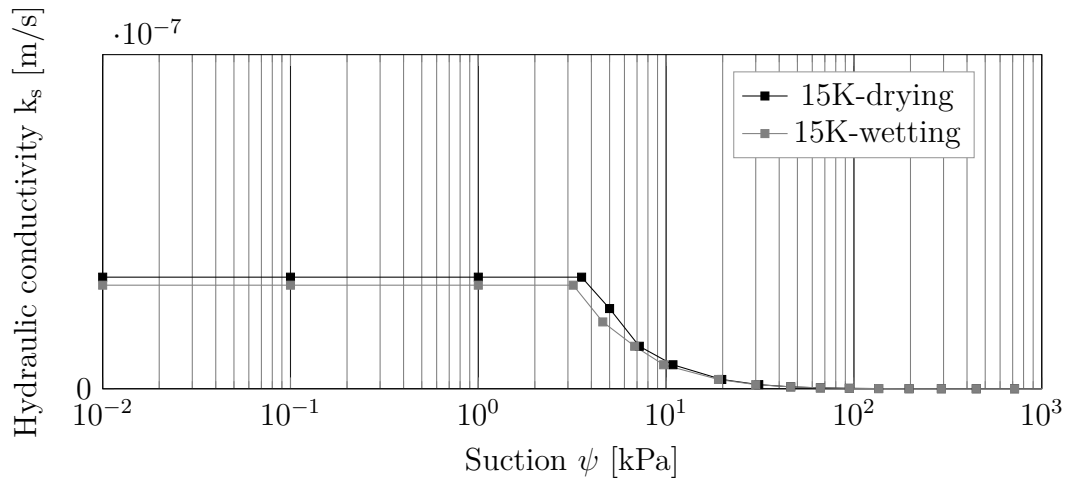


Figure A.10.: Hydraulic conductivity function vs suction for 15K

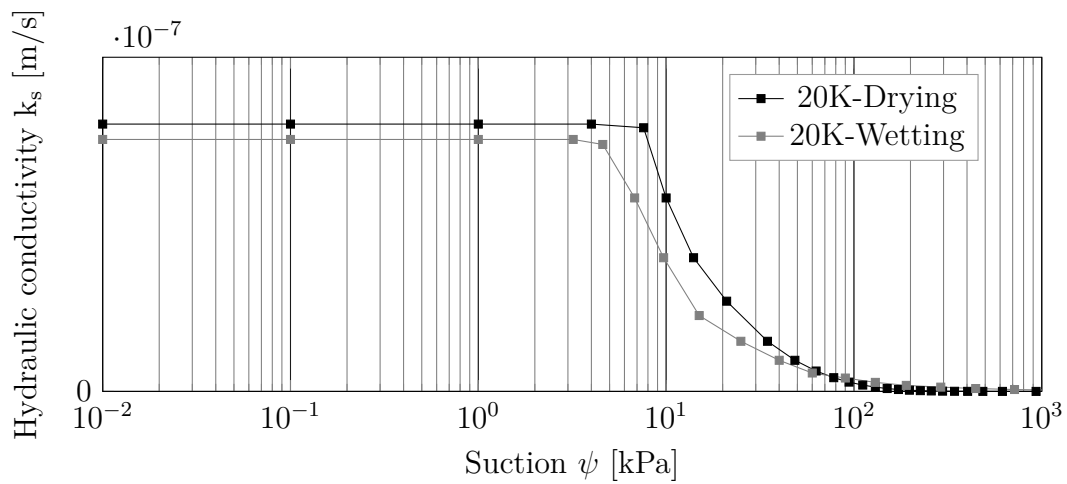


Figure A.11.: Hydraulic conductivity function vs suction for 20K

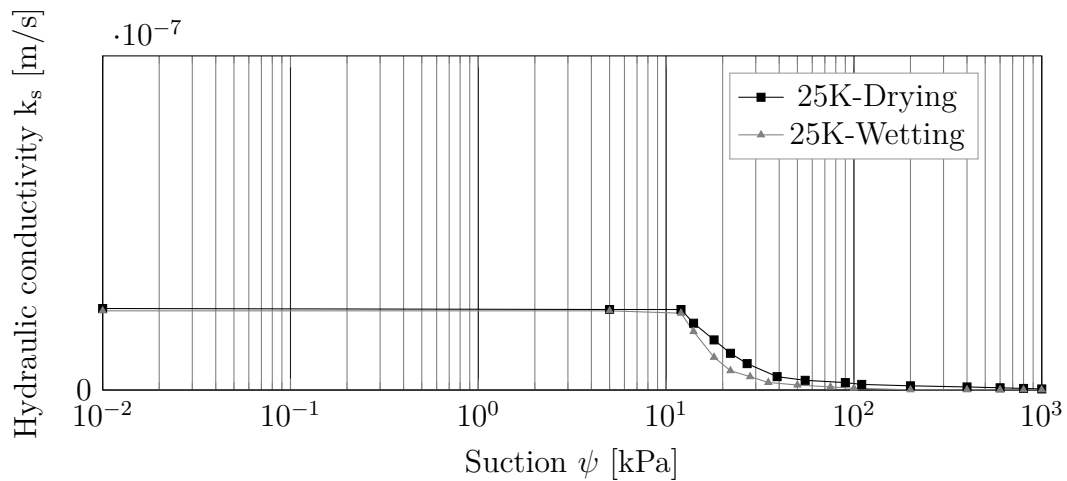


Figure A.12.: Hydraulic conductivity function vs suction for 25K

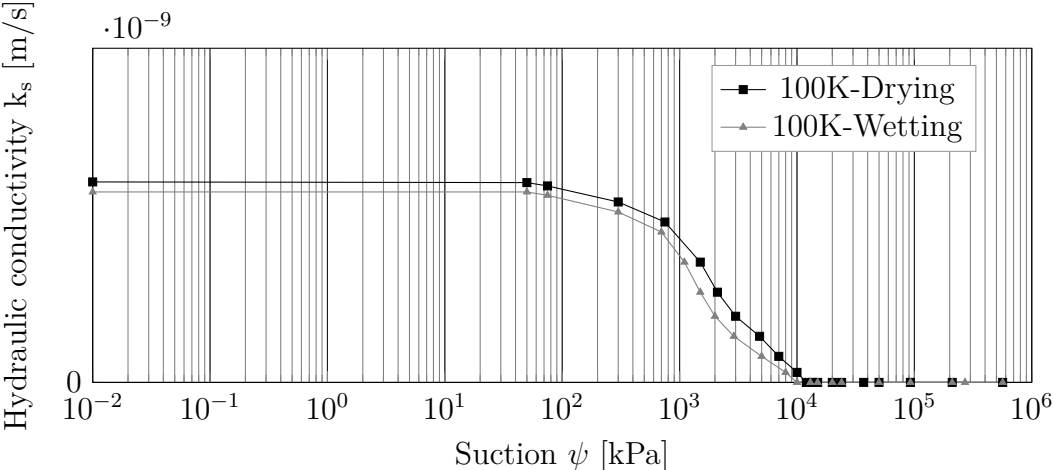


Figure A.13.: Hydraulic conductivity function vs suction for 100K

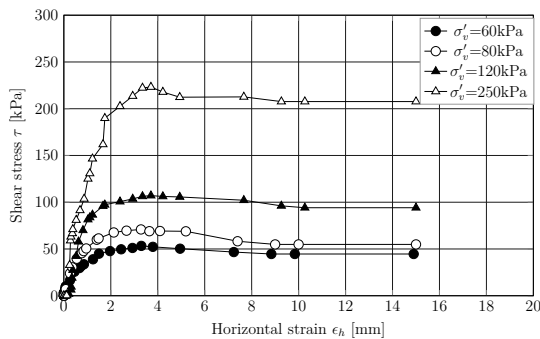
B. Appendix B (Direct shear tests under dry and saturated conditions)

In this appendix, the results of the direct shear tests under fully dry and fully saturated conditions are presented for Hostun sand, Silver sand, and Silver sand-kaolin mixtures, consequently.

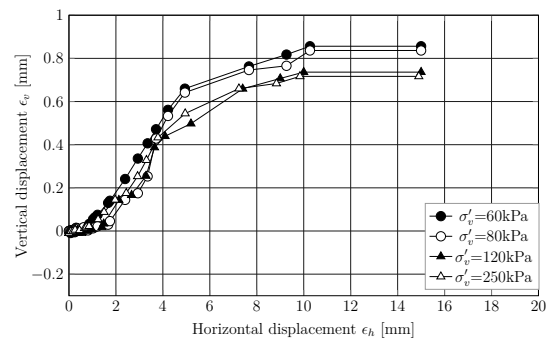
B.1. Hostun sand

B.1.1. Dense Hostun sand

Figure B.1 presents the tests results for dry dense Hostun sand using the new direct shear device. Figure B.2 shows the results using the traditional device. The vertical stresses applied on the samples are (60, 80, 120, 250) kPa.



(a) Shear stress vs Horizontal disp.



(b) Vertical disp. vs Horizontal disp.

Figure B.1.: Hostun sand: dry samples (new device)

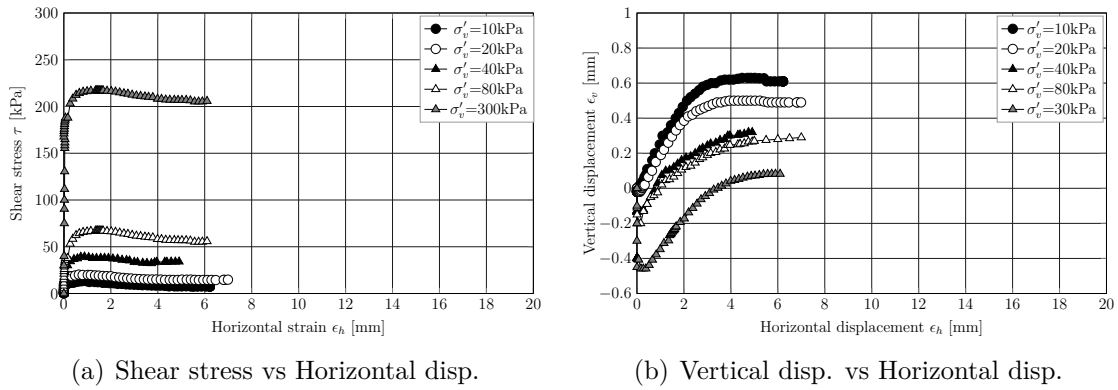


Figure B.2.: Hostun sand: dry dense samples (traditional device)

B.2. Silver sand

B.2.1. Dense Silver sand

Figures B.3 and B.4 show the tests results for dry dense Silver sand using the new direct shear device and the traditional device, respectively under the vertical stresses 10, 25, 35, 55, and 110 kPa.

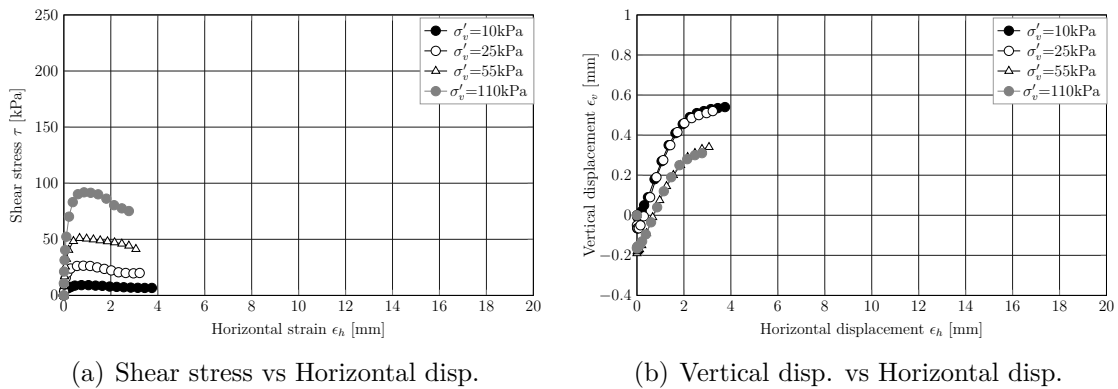


Figure B.3.: Silver sand: dry dense samples (traditional device)

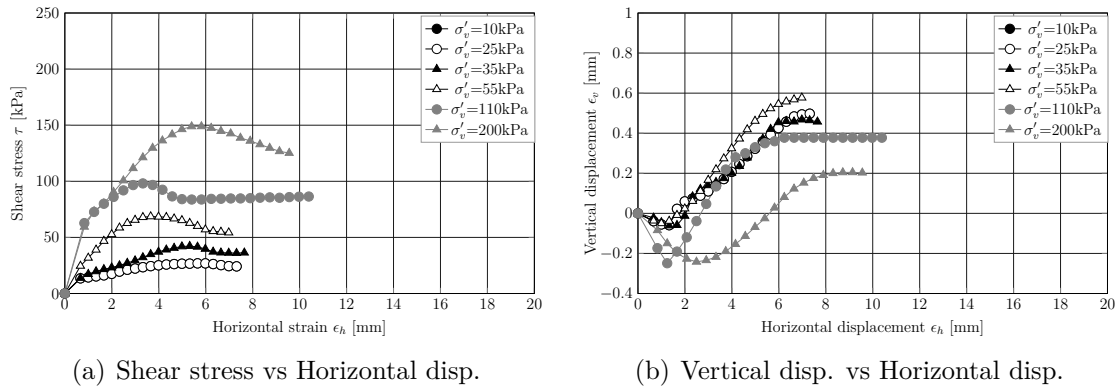


Figure B.4.: Silver sand: dry dense samples (new device)

B.2.2. Medium dense Silver sand

Figure B.5 presents the tests results for dry medium dense Silver sand using the new direct shear device under the vertical stresses 10, 25, 55, and 110 kPa.

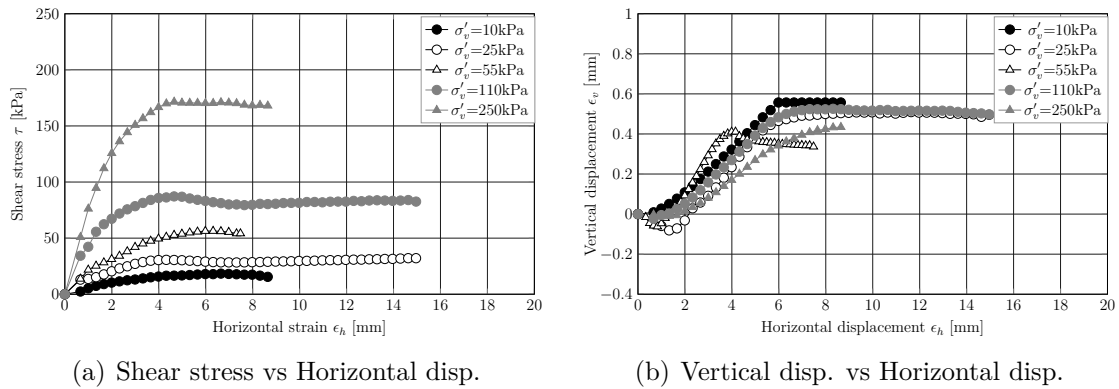
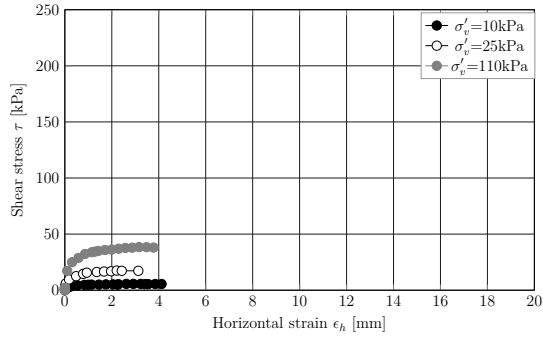


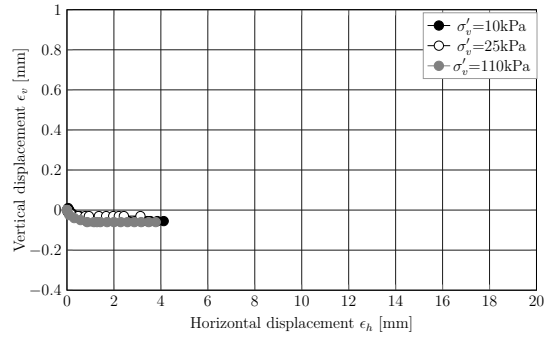
Figure B.5.: Silver sand: dry medium dense samples (new device)

B.2.3. Loose Silver sand

Figures B.6 and B.7 illustrate the tests results for dry loose Silver sand using the new direct shear device and the traditional device, respectively under the vertical stresses 10, 25, 35, 55, and 110 kPa.

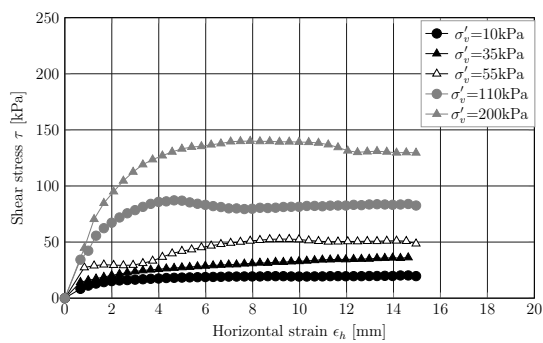


(a) Shear stress vs Horizontal disp.

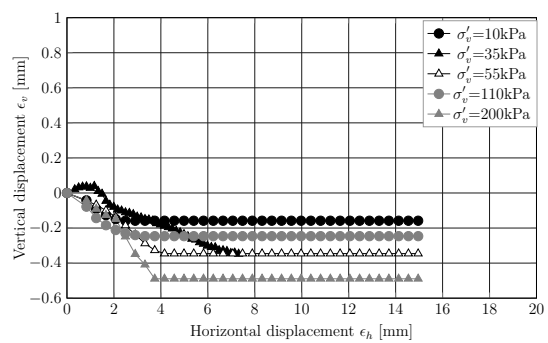


(b) Vertical disp. vs Horizontal disp.

Figure B.6.: Silver sand: dry loose samples (traditional device)



(a) Shear stress vs Horizontal disp.



(b) Vertical disp. vs Horizontal disp.

Figure B.7.: Silver sand: dry loose samples (new device)

B.3. 95% Silver sand + 5% kaolin clay

Figures B.8 and B.9 illustrate the tests results of dry 95% Silver sand + 5% kaolin clay using the new direct shear device and the traditional device, respectively under the vertical stresses 10, 25, 35, 55, and 110 kPa.

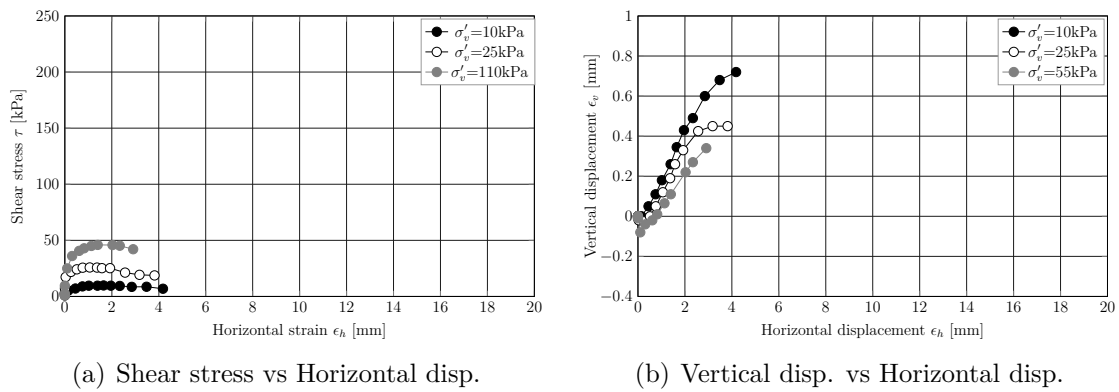


Figure B.8.: 95% Silver sand + 5% kaolin clay (traditional device)

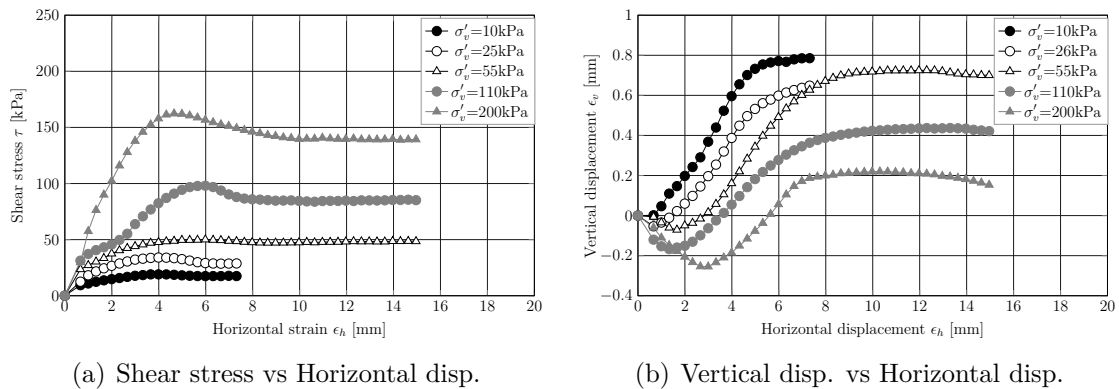
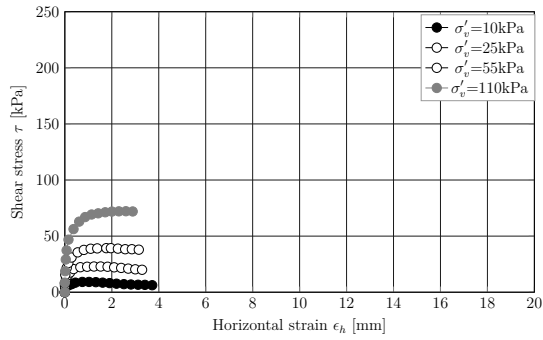


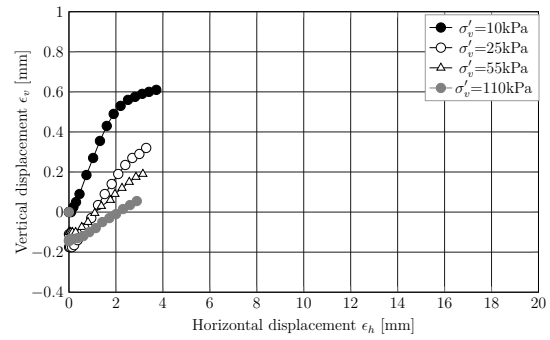
Figure B.9.: 95% Silver sand + 5% kaolin clay (new device)

B.4. 93% Silver sand + 7% kaolin clay

Figures B.10 and B.11 illustrate the tests results of dry 93% Silver sand + 7% kaolin clay using the new direct shear device and the traditional device, respectively under the vertical stresses 10, 25, 35, 55, and 110 kPa.

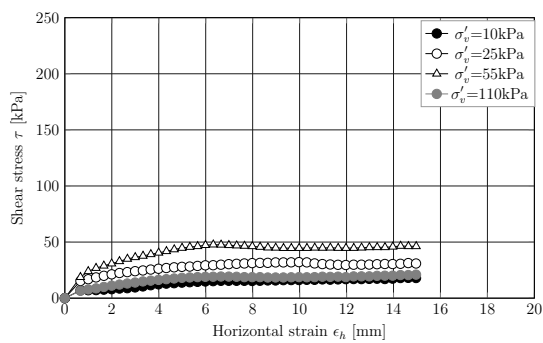


(a) Shear stress vs Horizontal disp.

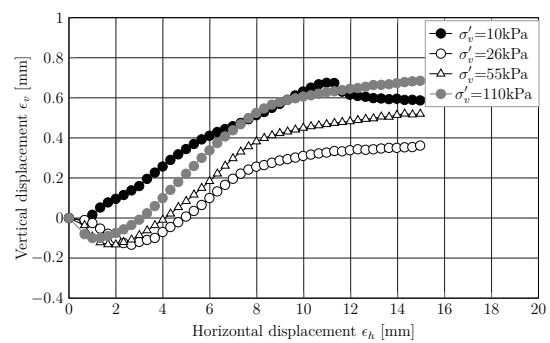


(b) Vertical disp. vs Horizontal disp.

Figure B.10.: 93% Silver sand + 7% kaolin clay (traditional device)



(a) Shear stress vs Horizontal disp.



(b) Vertical disp. vs Horizontal disp.

Figure B.11.: S93% Silver sand + 7% kaolin clay (new device)

B.5. 90% Silver sand + 10% kaolin clay

Figures B.12 and B.13 illustrate the tests results of dry 90% Silver sand + 10% kaolin clay using the new direct shear device and the traditional device, respectively under the vertical stresses 10, 25, 35, 55, and 110 kPa.

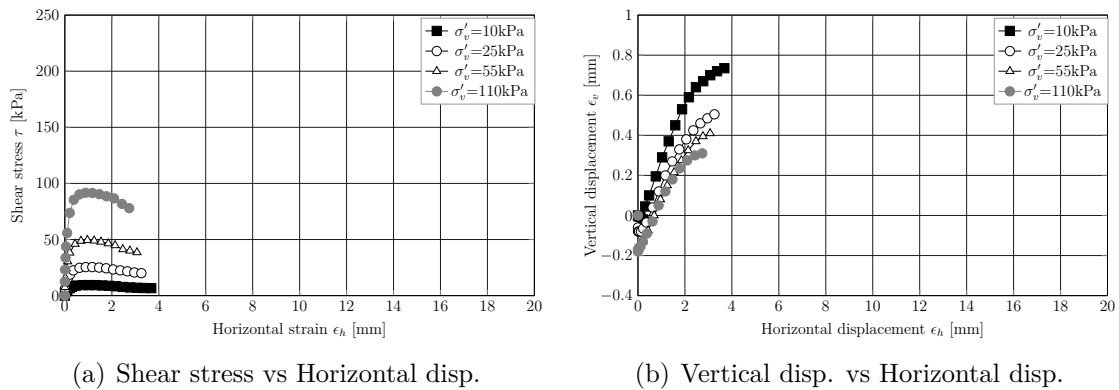


Figure B.12.: 90% Silver sand + 10% kaolin clay (traditional device)

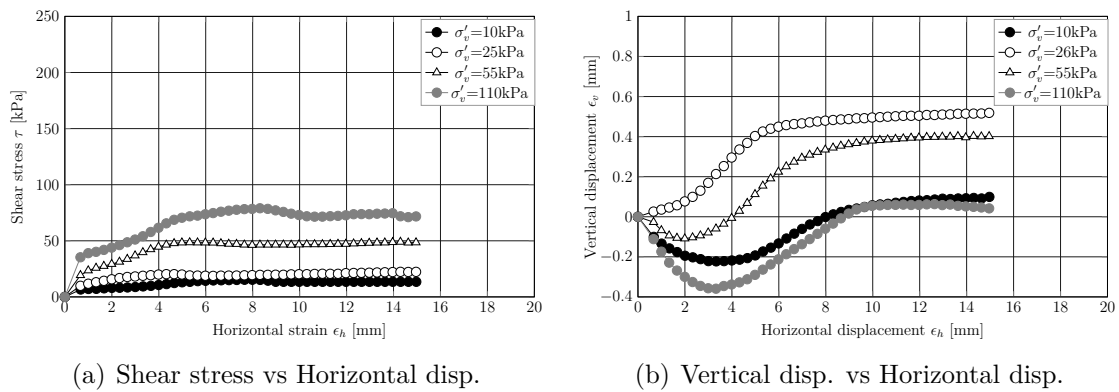
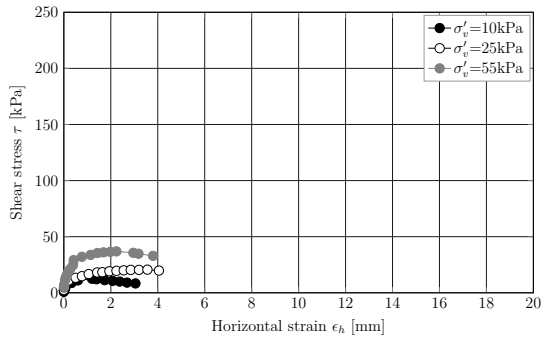


Figure B.13.: 90% Silver sand + 10% kaolin clay (new device)

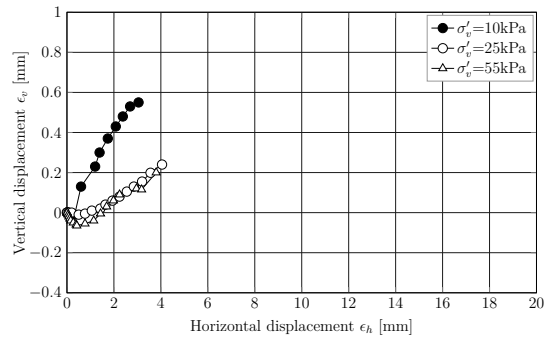
B.6. 80% Silver sand + 20% kaolin clay

Figures B.14 and B.15 illustrate the tests results of dry 80% Silver sand + 20% kaolin clay using the new direct shear device and the traditional device, respectively under the

vertical stresses 10, 25, 35, 55, and 110 kPa.

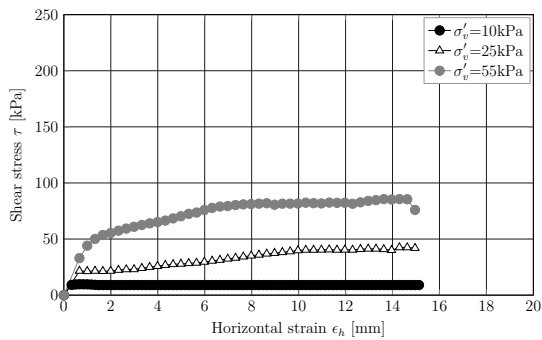


(a) Shear stress vs Horizontal disp.

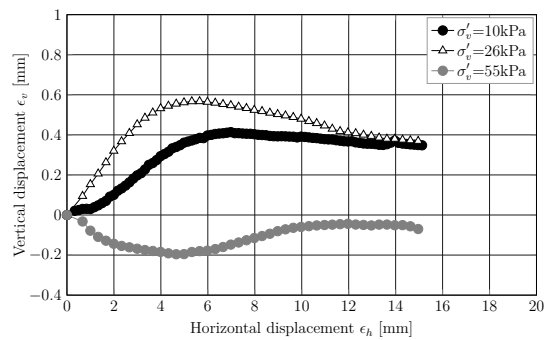


(b) Vertical disp. vs Horizontal disp.

Figure B.14.: 80% Silver sand + 20% kaolin clay (traditional device)



(a) Shear stress vs Horizontal disp.



(b) Vertical disp. vs Horizontal disp.

Figure B.15.: 80% Silver sand + 20% kaolin clay (new device)

C. Appendix C (Direct shear tests under unsaturated saturated conditions)

In this appendix, the results of the direct shear tests under partially saturated conditions are presented for HS, 10K, and 15K, consequently.

C.1. Hostun sand

Figures C.1 to C.6 present the tests results for HS for different suction values 0, 1, 2, 3, 4, 8, and 14 kPa. The vertical stress applied on the samples is 60, 80, 120, and 250 kPa. A summary of the results for the same vertical stress under different suction range are presented in Figure C.7 to C.10.

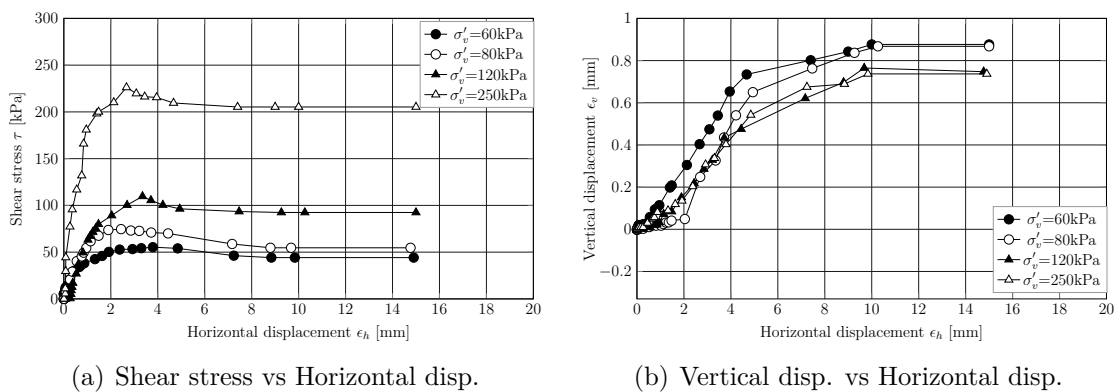
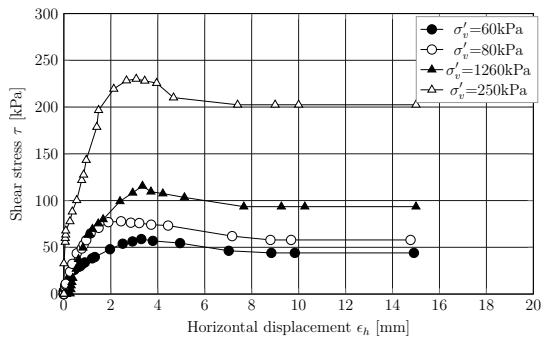
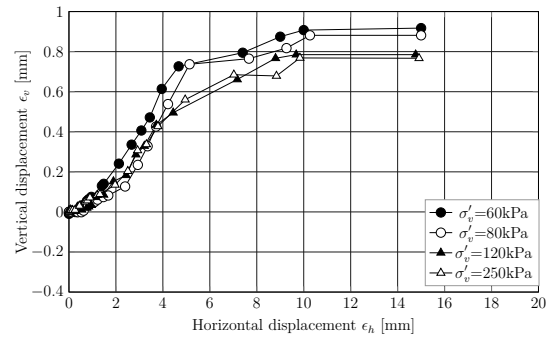


Figure C.1.: Hostun sand: Suction = 1 kPa

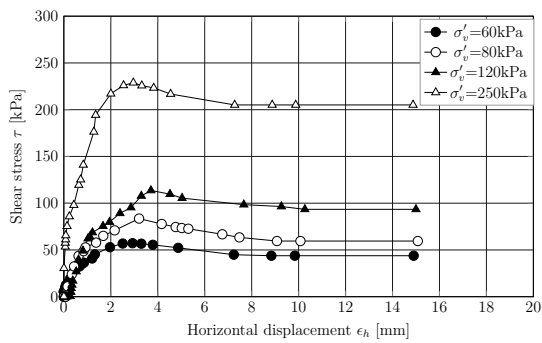


(a) Shear stress vs Horizontal disp.

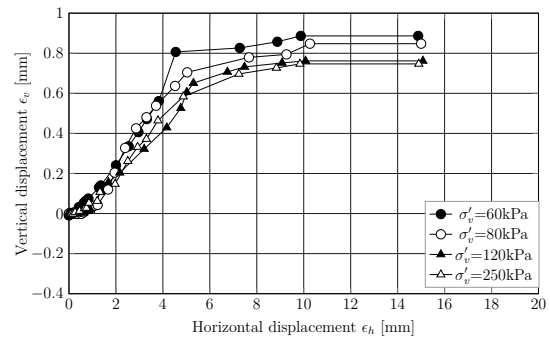


(b) Vertical disp. vs Horizontal disp.

Figure C.2.: Hostun sand: Suction = 2 kPa

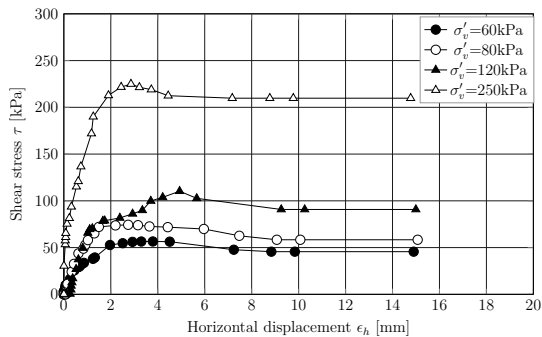


(a) Shear stress vs Horizontal disp.

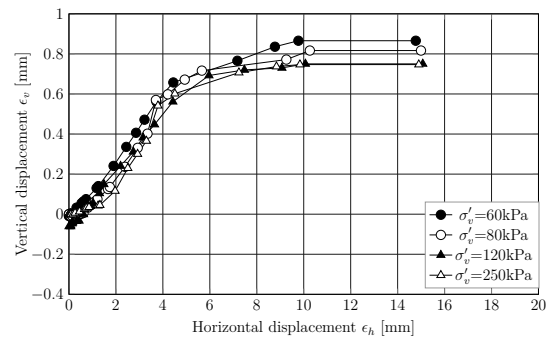


(b) Vertical disp. vs Horizontal disp.

Figure C.3.: Hostun sand: Suction = 3 kPa

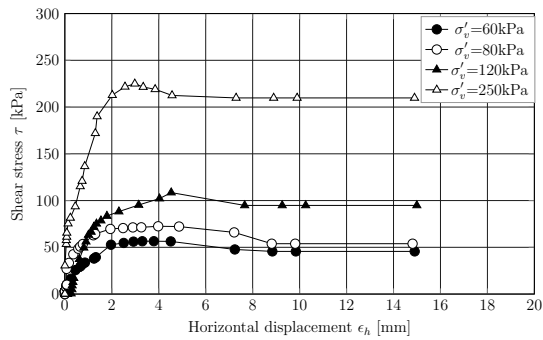


(a) Shear stress vs Horizontal disp.

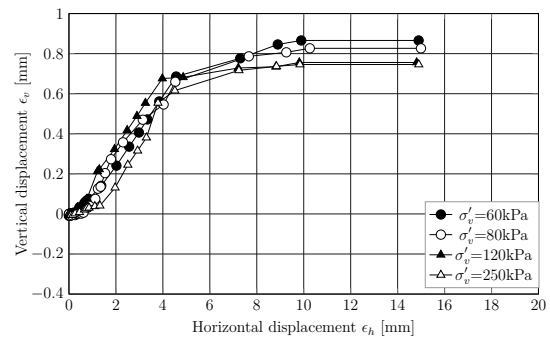


(b) Vertical disp. vs Horizontal disp.

Figure C.4.: Hostun sand: Suction = 4 kPa

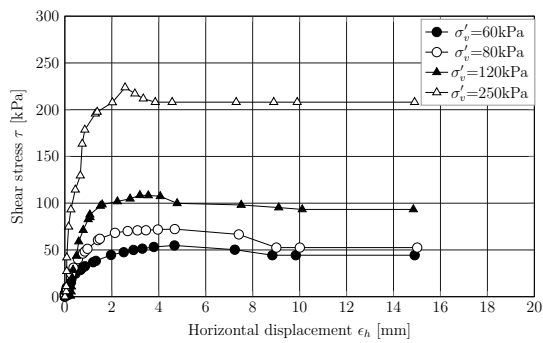


(a) Shear stress vs Horizontal disp.

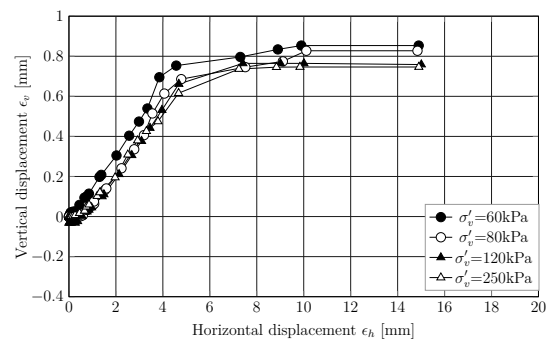


(b) Vertical disp. vs Horizontal disp.

Figure C.5.: Hostun sand: Suction = 8 kPa

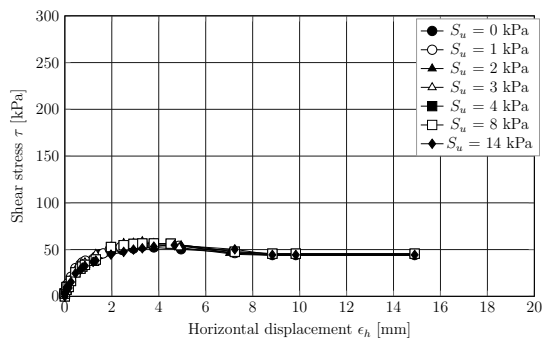


(a) Shear stress vs Horizontal disp.

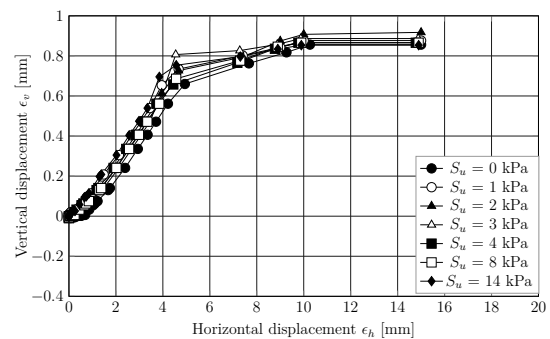


(b) Vertical disp. vs Horizontal disp.

Figure C.6.: Hostun sand: Suction = 14 kPa

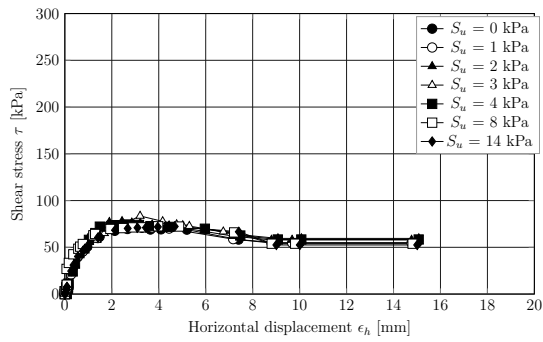


(a) Shear stress vs Horizontal disp.

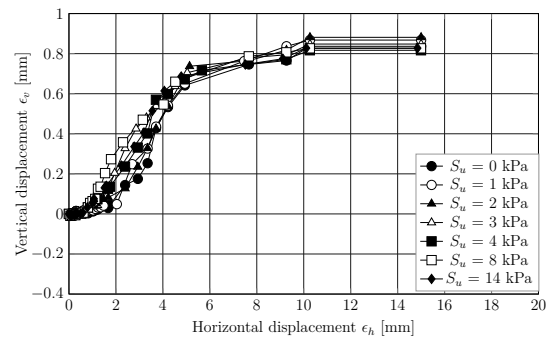


(b) Vertical disp. vs Horizontal disp.

Figure C.7.: Hostun sand: Vertical stress $\sigma'_v=60\text{kPa}$

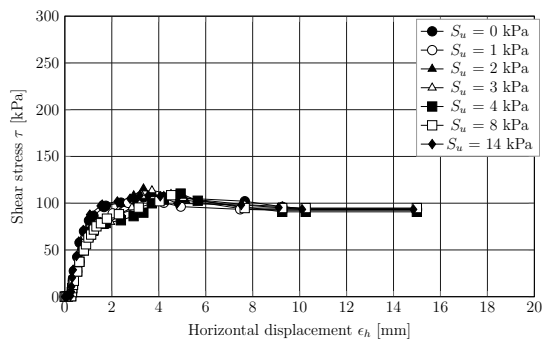


(a) Shear stress vs Horizontal disp.

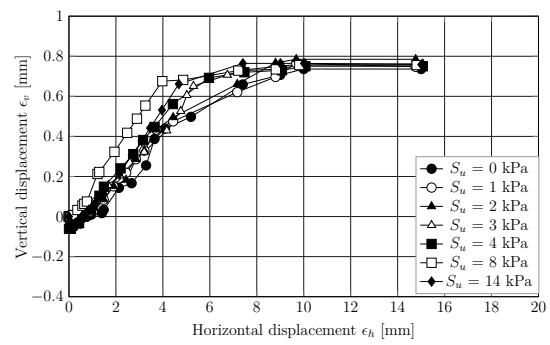


(b) Vertical disp. vs Horizontal disp.

Figure C.8.: Hostun sand: Vertical stress $\sigma'_v=80\text{kPa}$

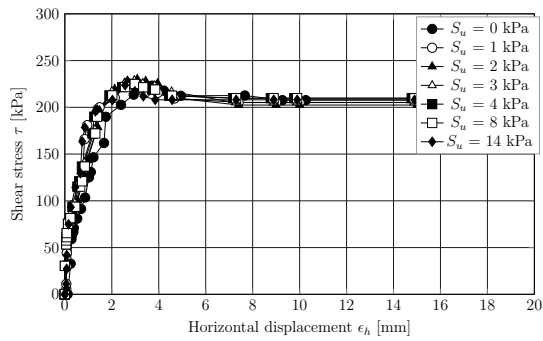


(a) Shear stress vs Horizontal disp.

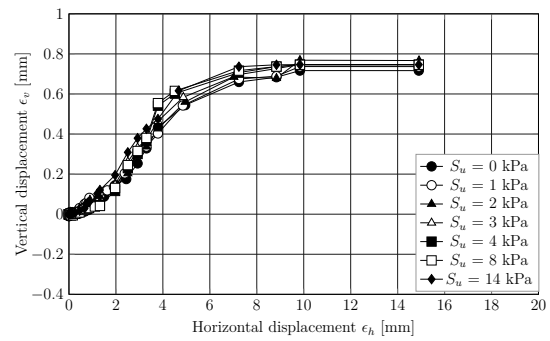


(b) Vertical disp. vs Horizontal disp.

Figure C.9.: Hostun sand: Vertical stress $\sigma'_v=120\text{kPa}$



(a) Shear stress vs Horizontal disp.



(b) Vertical disp. vs Horizontal disp.

Figure C.10.: Hostun sand: vertical stress $\sigma'_v=250\text{kPa}$

C.2. 10K

Figures C.11 to C.17 present the tests results for 10K for different suction values 0, 2, 3, 4, 8, 50, and 100 kPa. The vertical stress applied on the samples is 60, 80, 120, and 250 kPa. A summary of the results for the same vertical stress under different suction range are presented in Figure C.18 to C.21.

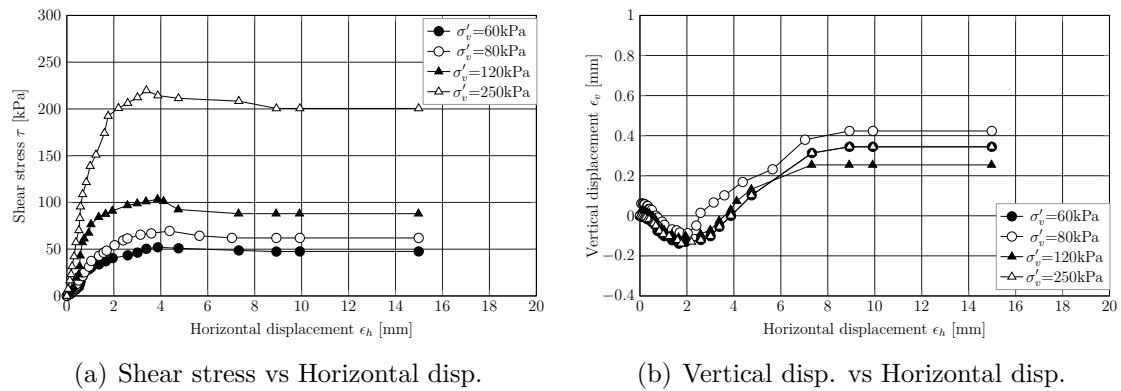


Figure C.11.: 10K: Saturated samples

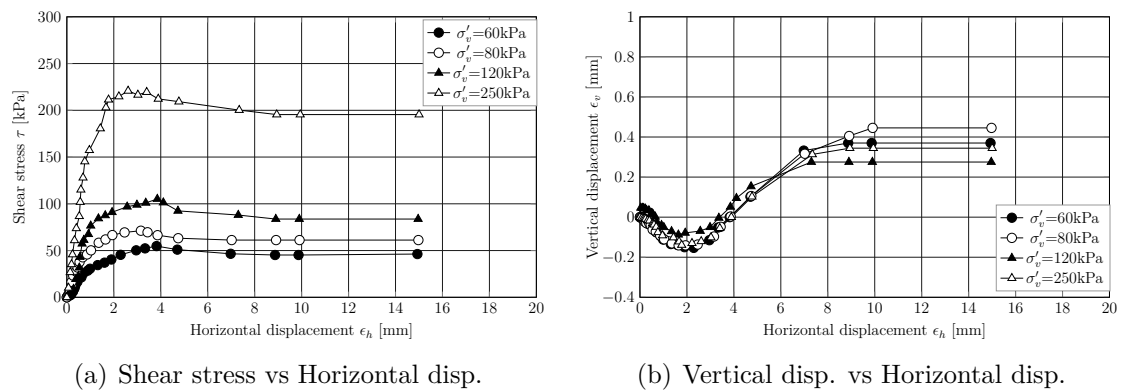
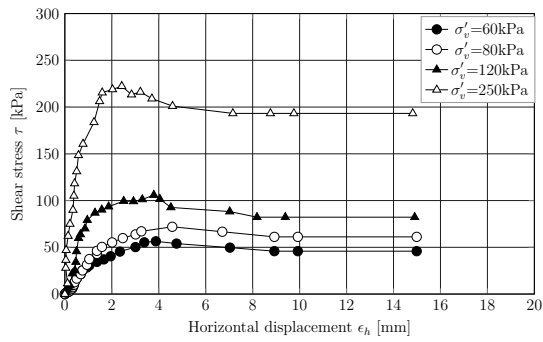
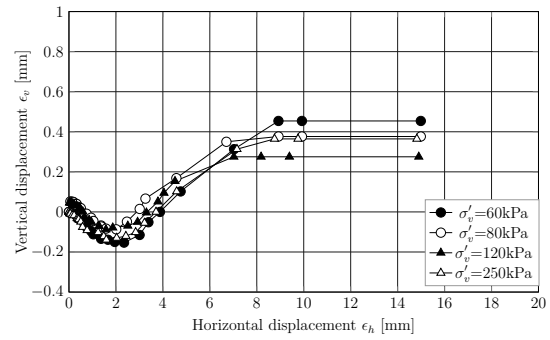


Figure C.12.: 10K: Suction = 2 kPa

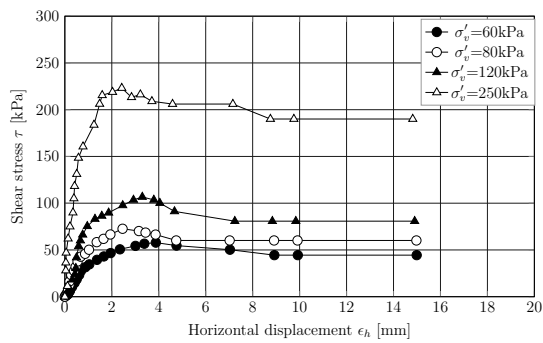


(a) Shear stress vs Horizontal disp.

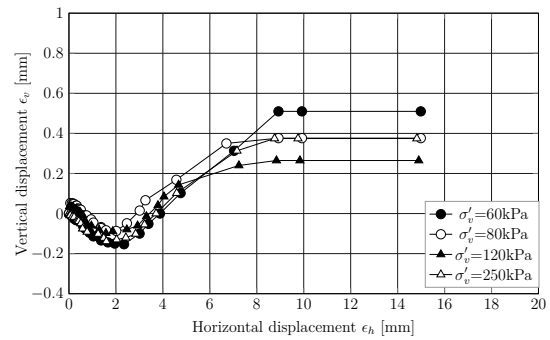


(b) Vertical disp. vs Horizontal disp.

Figure C.13.: 10K: Suction = 3 kPa

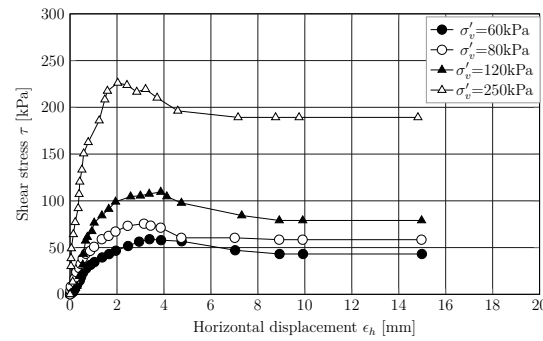


(a) Shear stress vs Horizontal disp.

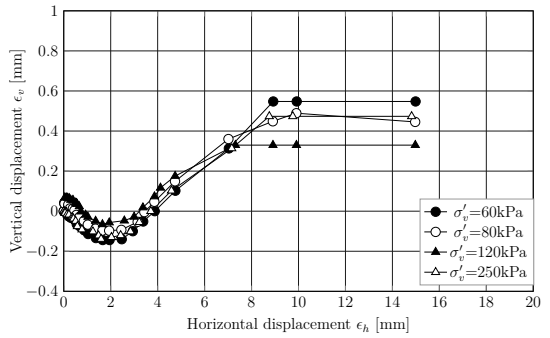


(b) Vertical disp. vs Horizontal disp.

Figure C.14.: 10K: Suction = 4 kPa

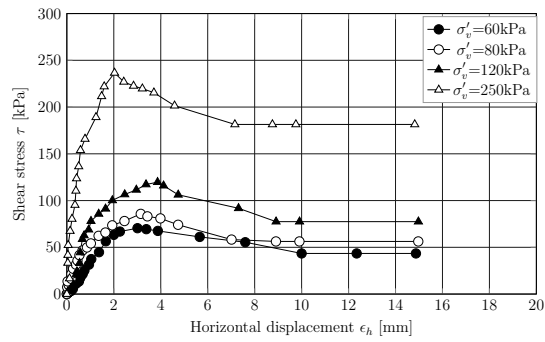


(a) Shear stress vs Horizontal disp.

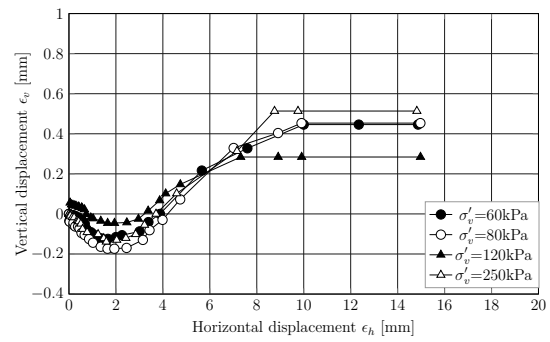


(b) Vertical disp. vs Horizontal disp.

Figure C.15.: 10K: Suction = 8 kPa

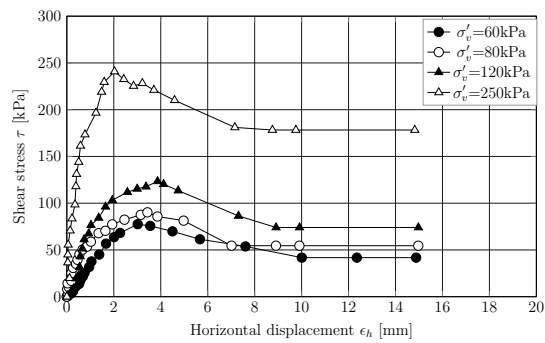


(a) Shear stress vs Horizontal disp.

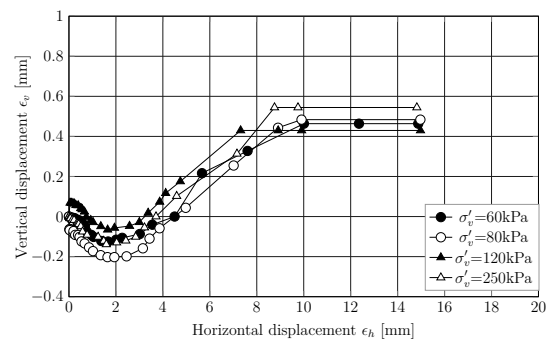


(b) Vertical disp. vs Horizontal disp.

Figure C.16.: 10K: Suction = 50 kPa

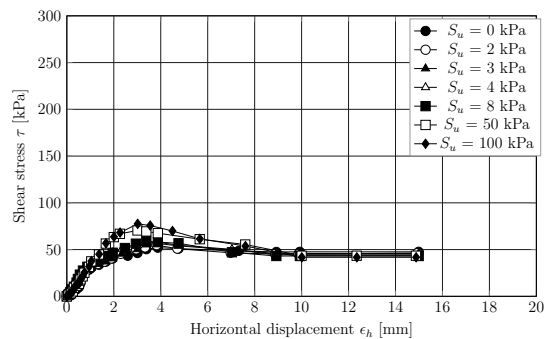


(a) Shear stress vs Horizontal disp.

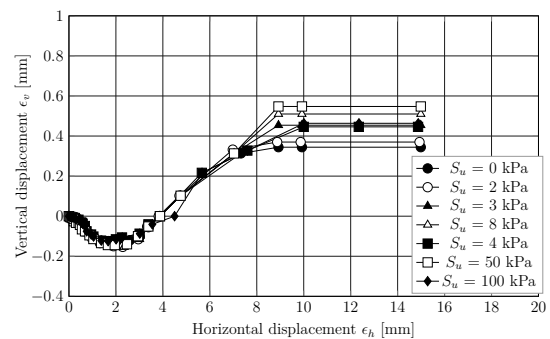


(b) Vertical disp. vs Horizontal disp.

Figure C.17.: 10K: Suction = 100 kPa

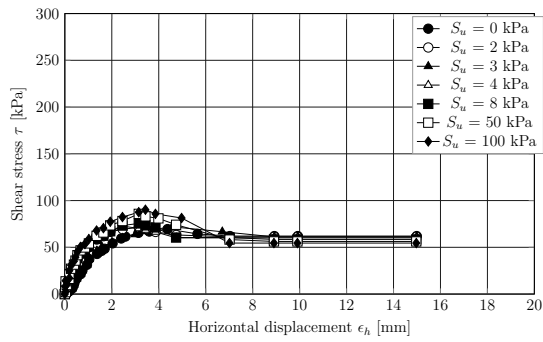


(a) Shear stress vs Horizontal disp.

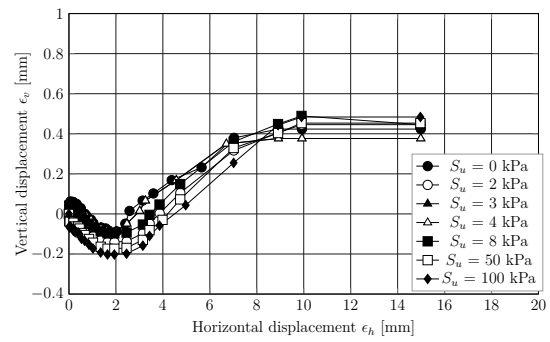


(b) Vertical disp. vs Horizontal disp.

Figure C.18.: 10K: Vertical stress $\sigma'_v=60\text{kPa}$

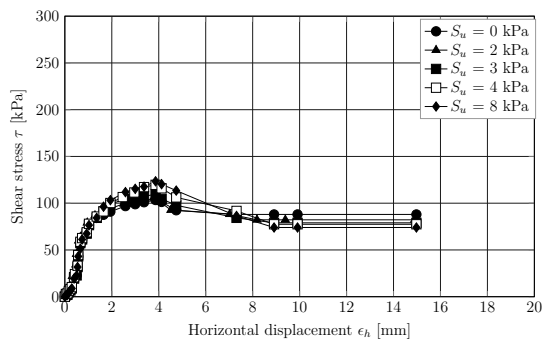


(a) Shear stress vs Horizontal disp.

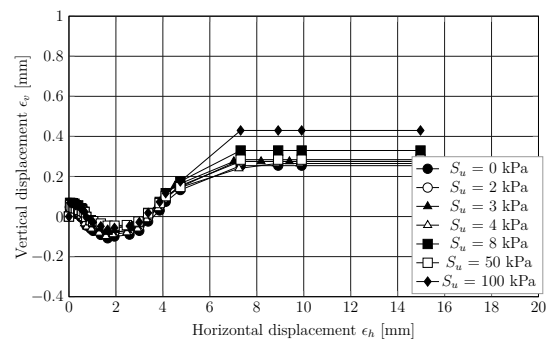


(b) Vertical disp. vs Horizontal disp.

Figure C.19.: 10K: Vertical stress $\sigma'_v=80\text{kPa}$

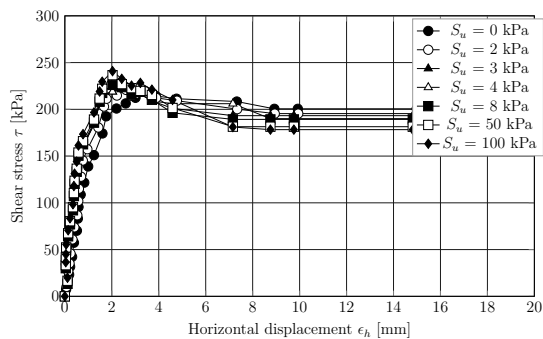


(a) Shear stress vs Horizontal disp.

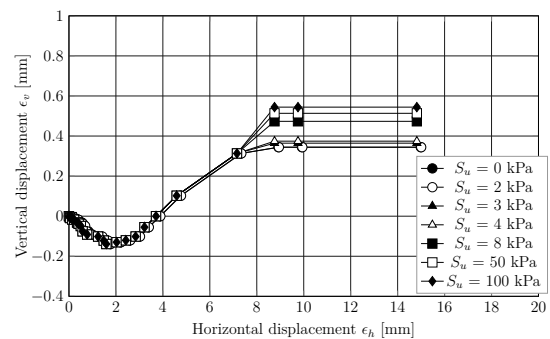


(b) Vertical disp. vs Horizontal disp.

Figure C.20.: $\sigma'_v=120\text{kPa}$



(a) Shear stress vs Horizontal disp.



(b) Vertical disp. vs Horizontal disp.

Figure C.21.: 10K: Vertical stress $\sigma'_v=250\text{kPa}$

C.3. 15K

Figures C.22 to C.29(b) present the tests results for 15K for different suction values 0, 2, 3, 4, 8, 50, and 100 kPa. The vertical stress applied on the samples is 60, 80, 120, and 250 kPa. A summary of the results for the same vertical stress under different suction range are presented in Figure C.29 to C.32.

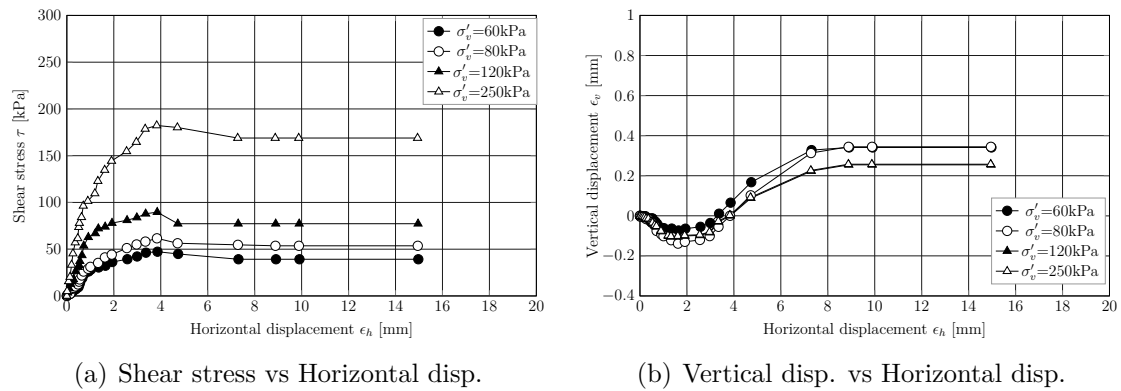


Figure C.22.: 15K: Saturated samples

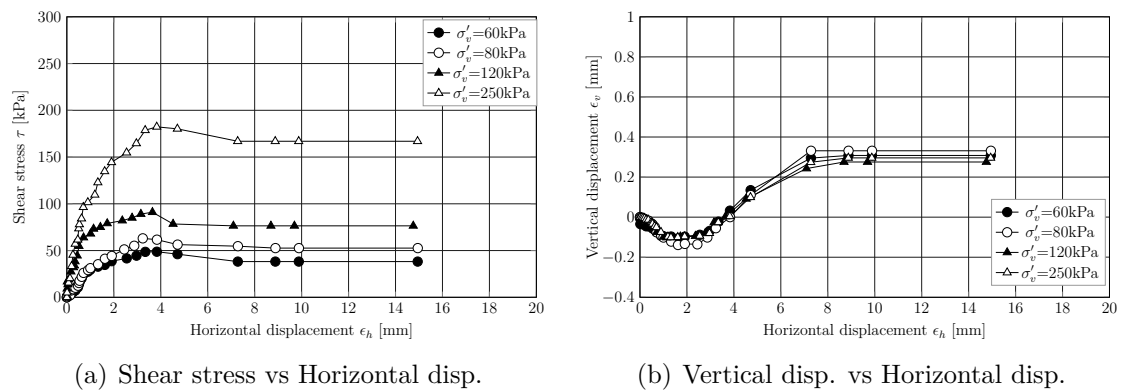
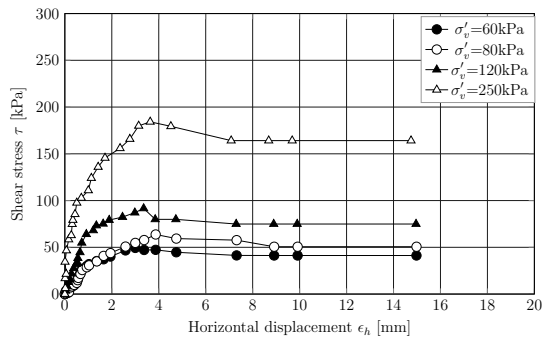
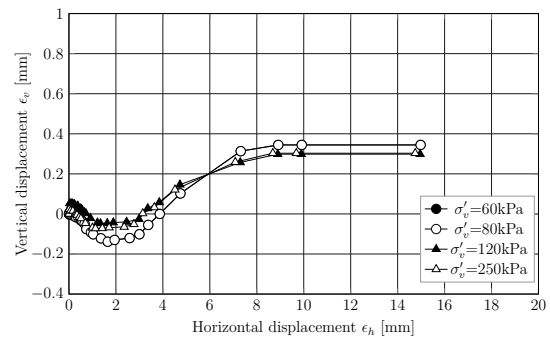


Figure C.23.: 15K: Suction = 2 kPa

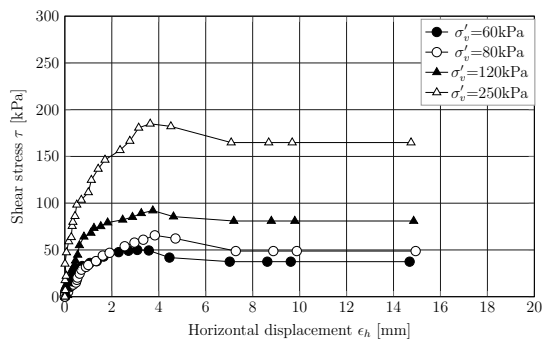


(a) Shear stress vs Horizontal disp.

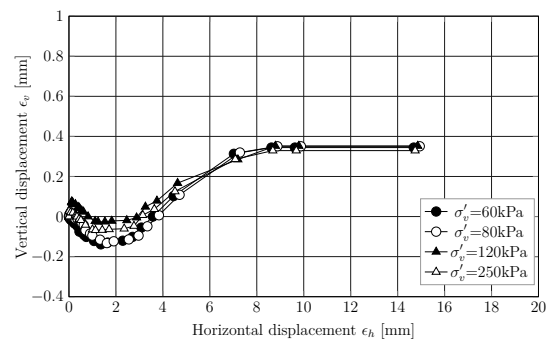


(b) Vertical disp. vs Horizontal disp.

Figure C.24.: 15K: Suction = 3 kPa

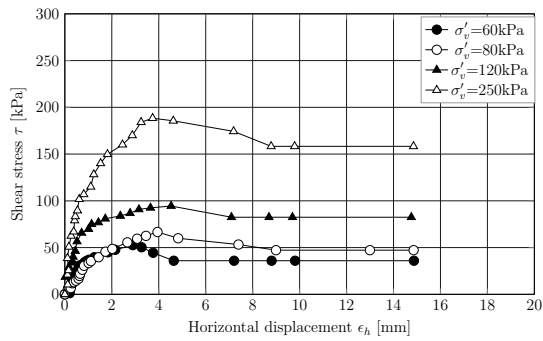


(a) Shear stress vs Horizontal disp.

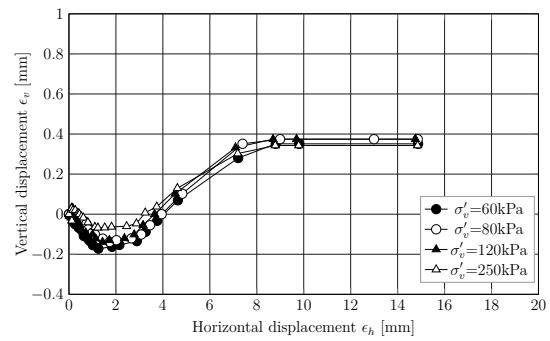


(b) Vertical disp. vs Horizontal disp.

Figure C.25.: 15K: Suction = 4 kPa

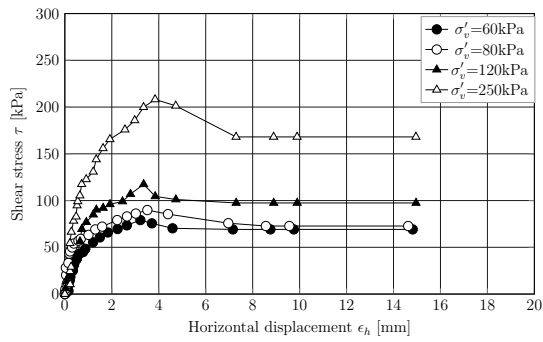


(a) Shear stress vs Horizontal disp.

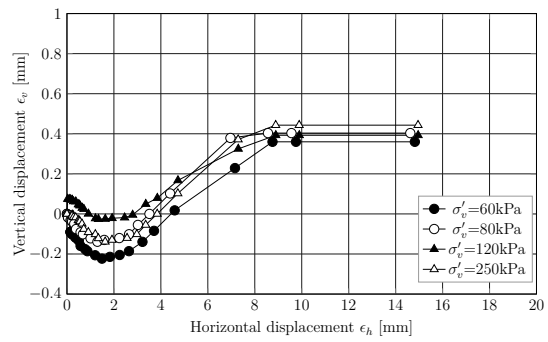


(b) Vertical disp. vs Horizontal disp.

Figure C.26.: 15K: Suction = 8 kPa

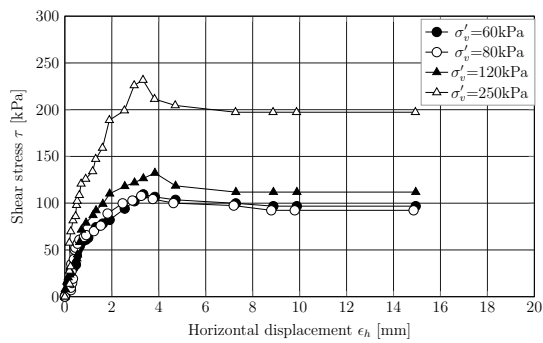


(a) Shear stress vs Horizontal disp.

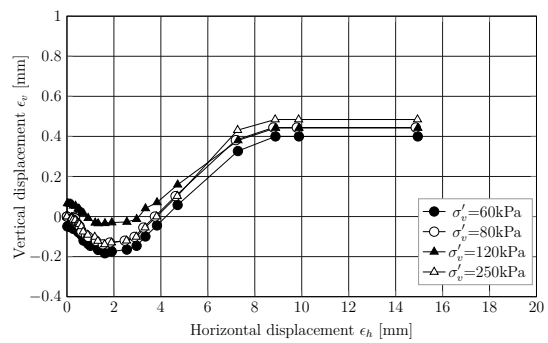


(b) Vertical disp. vs Horizontal disp.

Figure C.27.: 15K: Suction = 50 kPa

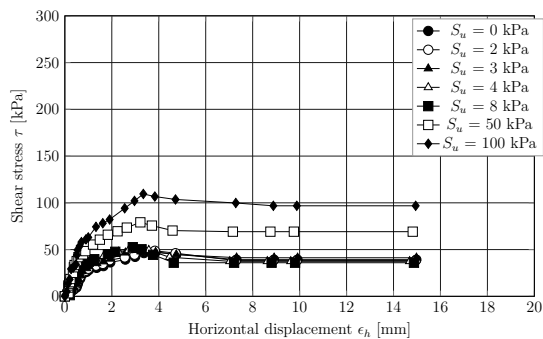


(a) Shear stress vs Horizontal disp.

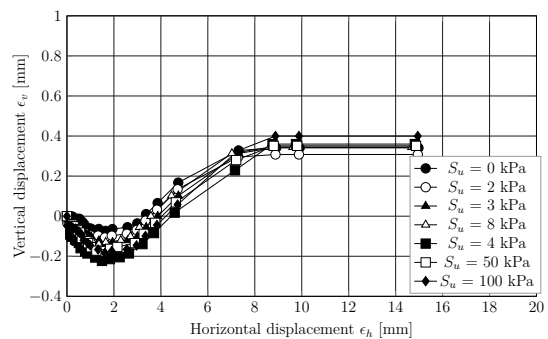


(b) Vertical disp. vs Horizontal disp.

Figure C.28.: 15K: Suction = 100 kPa

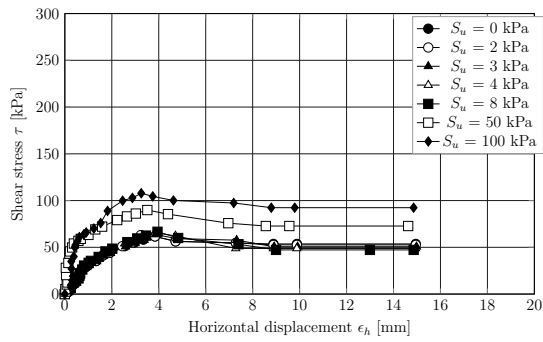


(a) Shear stress vs Horizontal disp.

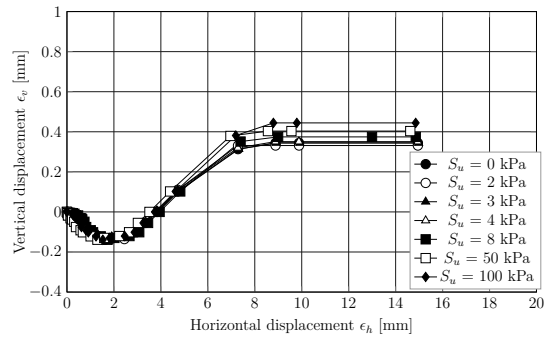


(b) Vertical disp. vs Horizontal disp.

Figure C.29.: 15K: Vertical stress $\sigma'_v=60$ kPa

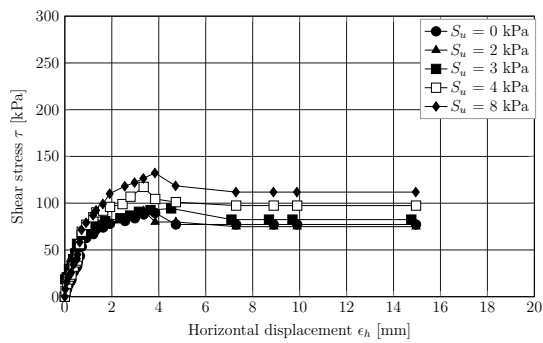


(a) Shear stress vs Horizontal disp.

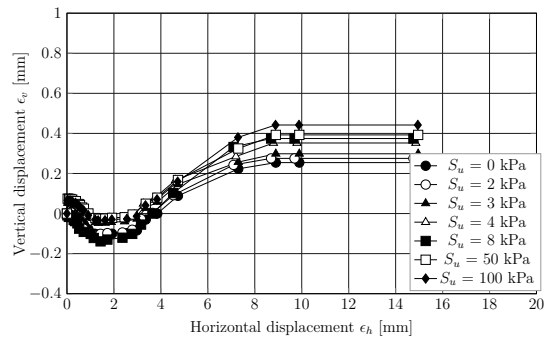


(b) Vertical disp. vs Horizontal disp.

Figure C.30.: 15K: Vertical stress $\sigma'_v=80\text{kPa}$

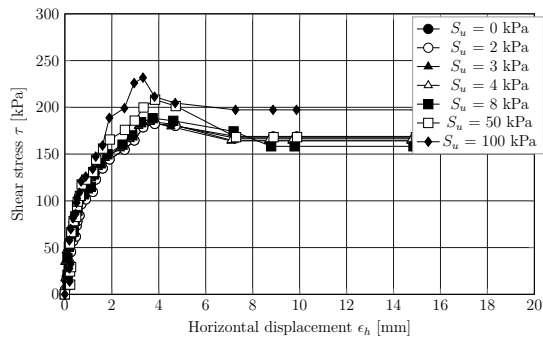


(a) Shear stress vs Horizontal disp.

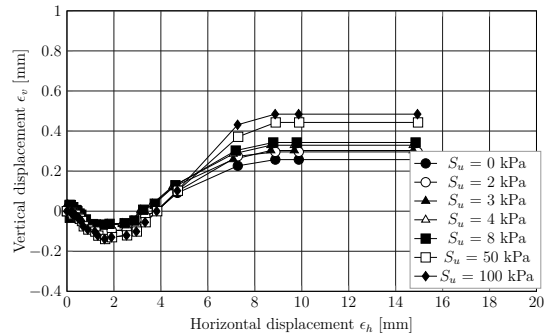


(b) Vertical disp. vs Horizontal disp.

Figure C.31.: 15K: Vertical stress $\sigma'_v=120\text{kPa}$



(a) Shear stress vs Horizontal disp.



(b) Vertical disp. vs Horizontal disp.

Figure C.32.: 15K: Vertical stress $\sigma'_v=250\text{kPa}$

D. Appendix D (Fitting of direct shear tests results)

In this appendix, the fitting curves of the direct shear results under partially saturated condition using the model proposed by Vanapalli (1996b) (Model 1) and Khalili & Khabbaz (1998) (Model 2).

D.1. HS

The tests results of Hostun sand for the direct shear device under partially saturated conditions are fitted using the model proposed by Vanapalli (1996b) as shown in Figures D.1 to D.4.

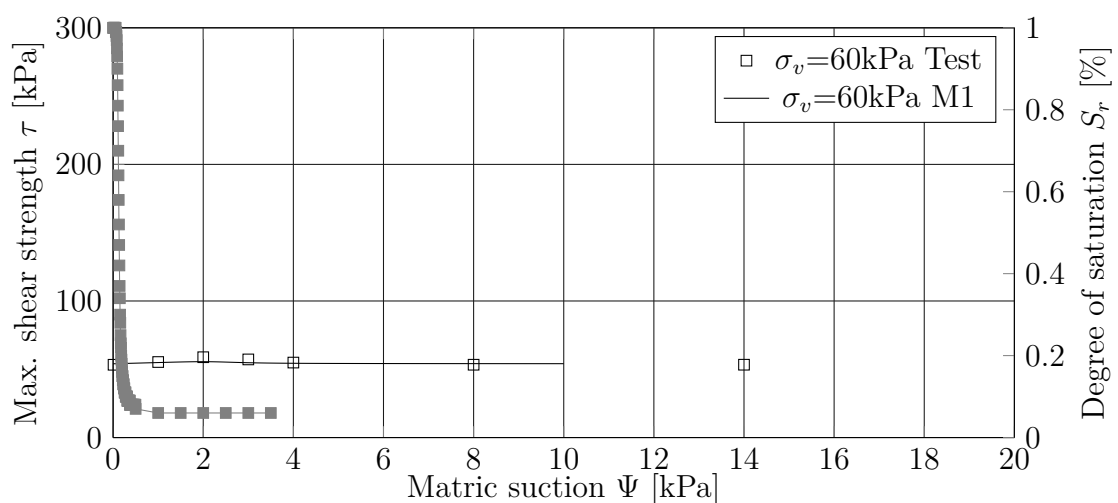


Figure D.1.: Fitting the results of max. shear strength under $\sigma_v=60\text{kPa}$ for HS

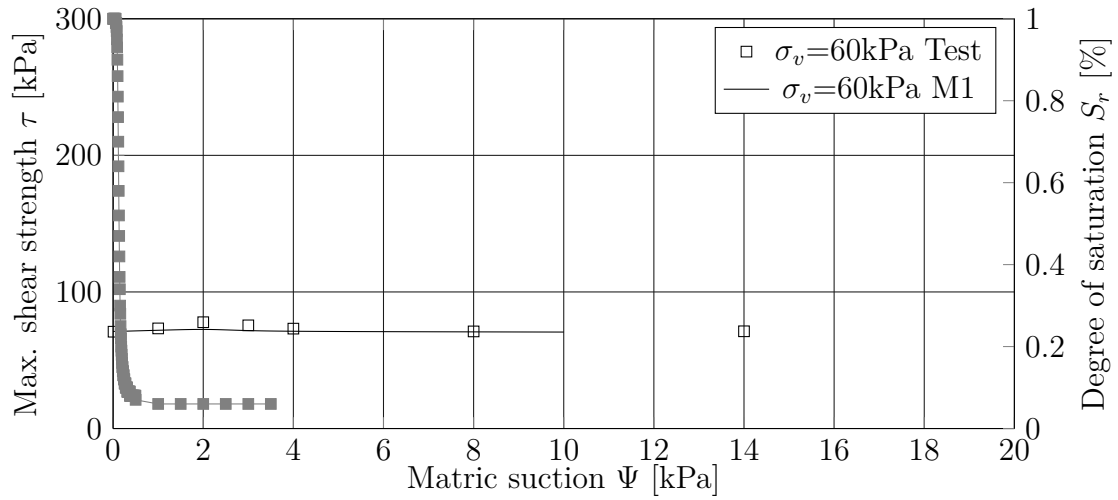


Figure D.2.: Fitting the results of max. shear strength under $\sigma_v=80\text{kPa}$ for HS

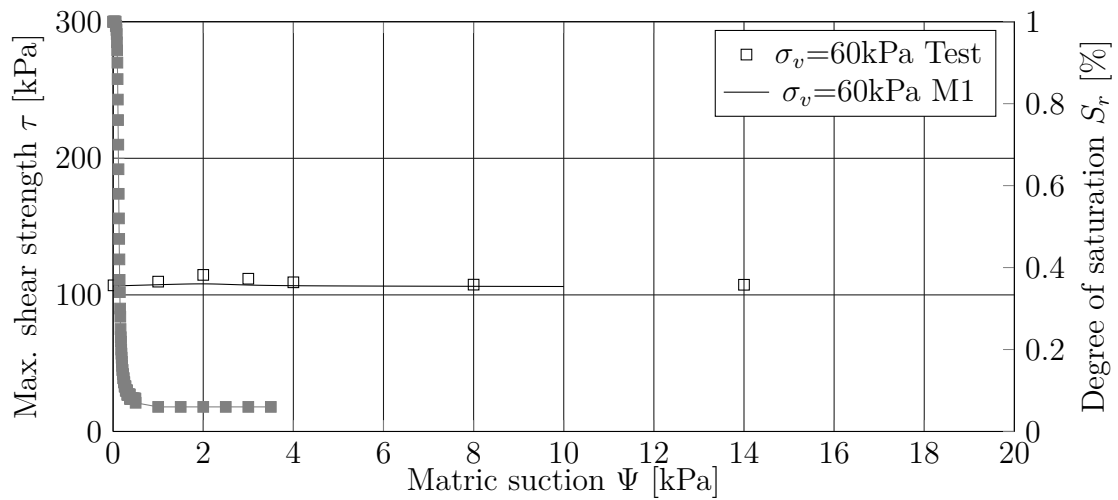


Figure D.3.: Fitting the results of max. shear strength under $\sigma_v=120\text{kPa}$ for HS

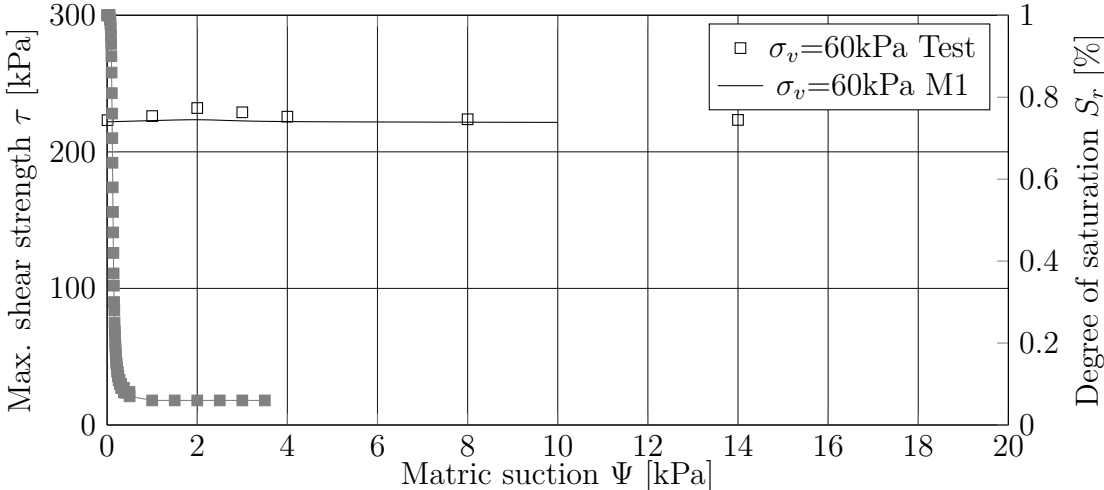


Figure D.4.: Fitting the results of max. shear strength under $\sigma_v=250\text{kPa}$ for HS

D.2. 10K

In this section, a review to the fitting results of the shear results for the soil mixture 10K. Figures D.5 to D.12 present the fitting curves for maximum shear strength vs suction for the drying and wetting paths.

Figures D.13 to D.16 present the fitting curves for the angle of friction due to suction vs suction for the drying and wetting paths.

Figures D.17 to D.20 show the attempt to fit curves for the cohesion due to suction vs suction for the drying and wetting paths.

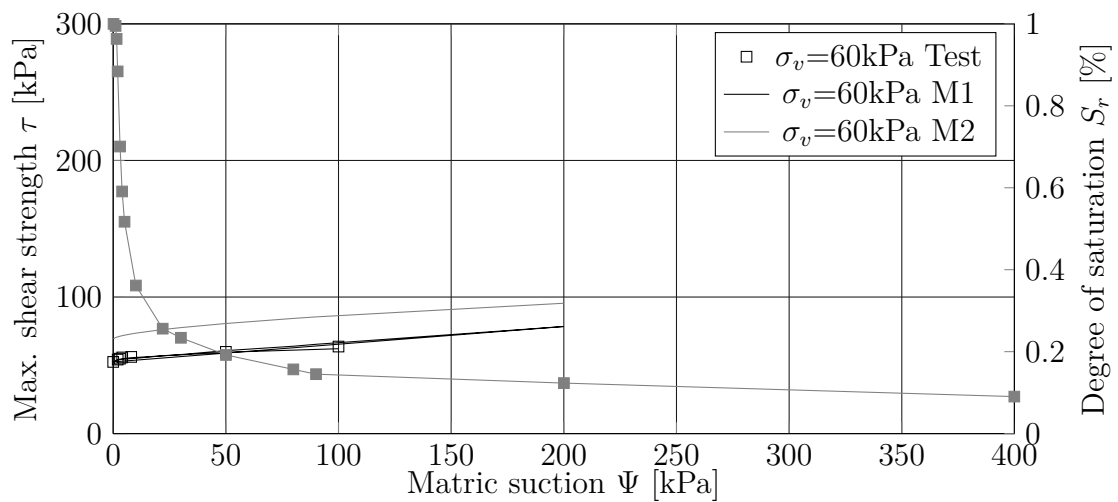


Figure D.5.: Fitting the results of max. shear strength under $\sigma_v=60\text{kPa}$ for drying path (10K)

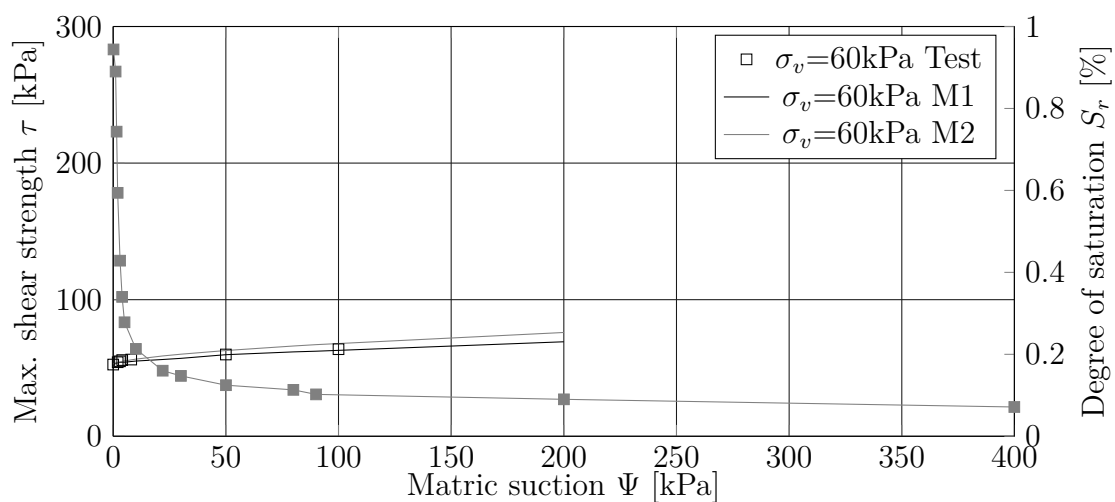


Figure D.6.: Fitting the results of max. shear strength under $\sigma_v=60\text{kPa}$ for wetting path (10K)

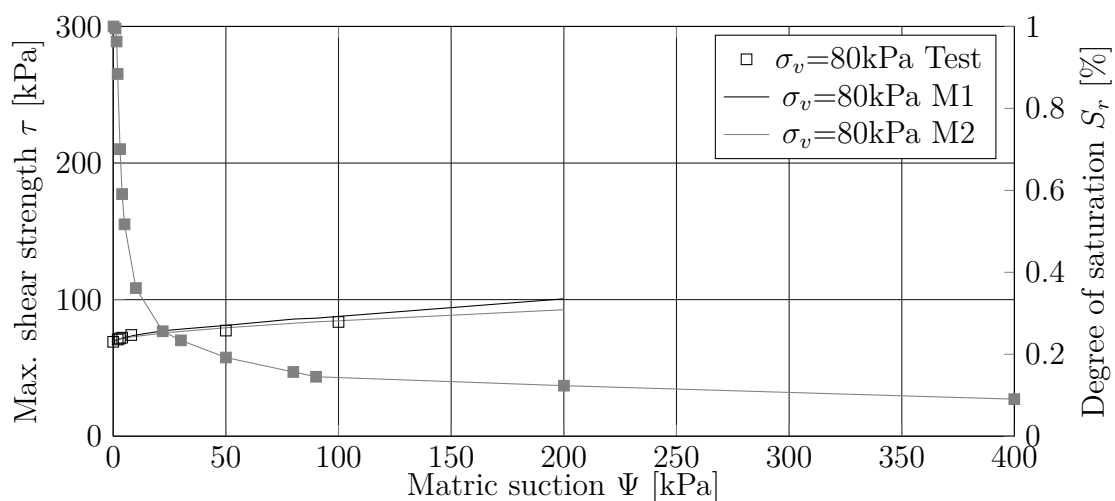


Figure D.7.: Fitting the results of max. shear strength under $\sigma_v=80\text{kPa}$ for drying path (10K)

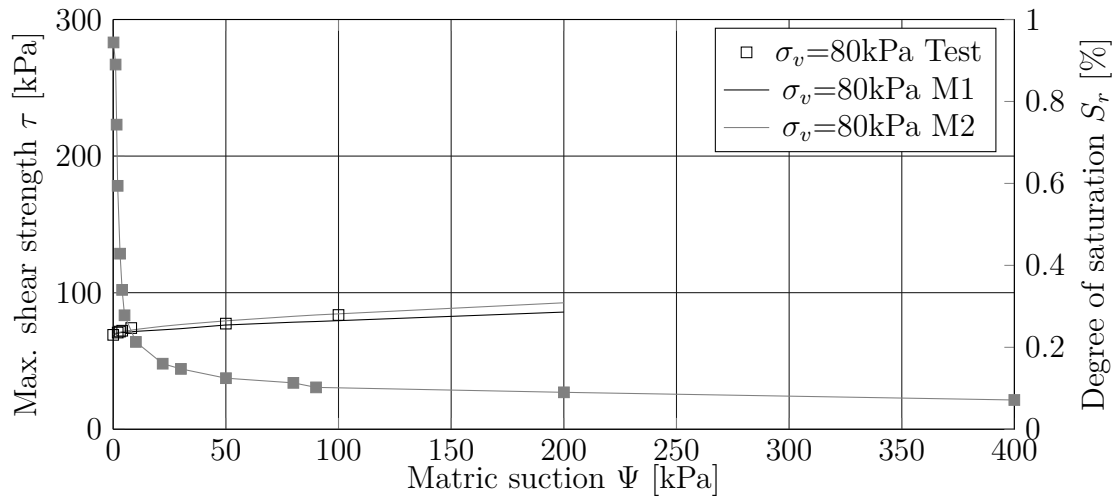


Figure D.8.: Fitting the results of max. shear strength under $\sigma_v=80\text{kPa}$ for wetting path (10K)

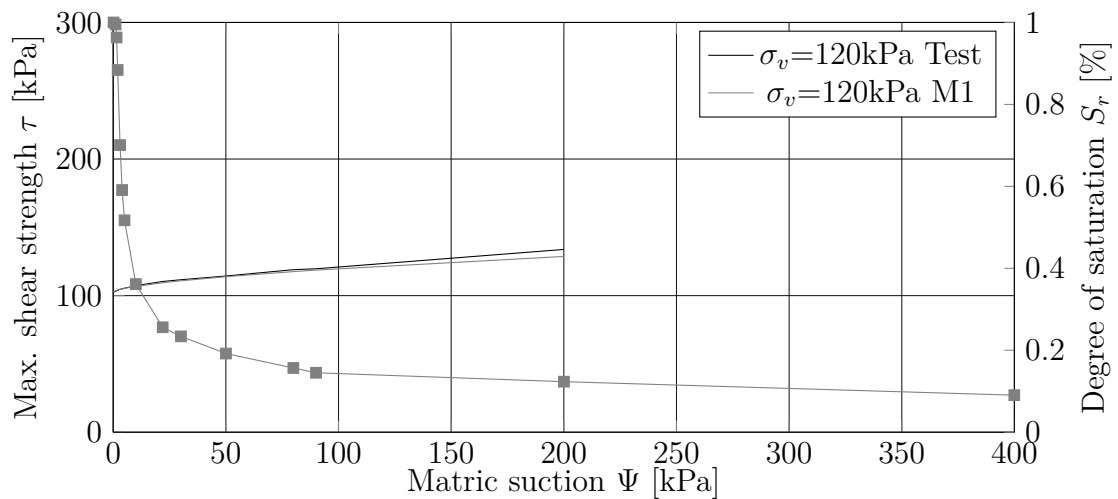


Figure D.9.: Fitting the results of max. shear strength under $\sigma_v=120\text{kPa}$ for drying path (10K)

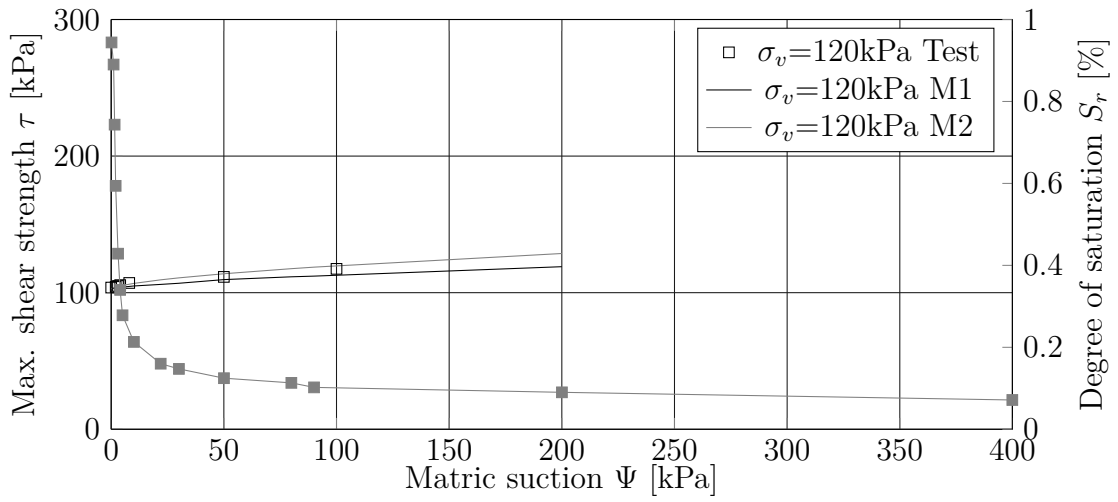


Figure D.10.: Fitting the results of max. shear strength under $\sigma_v = 120 \text{ kPa}$ for wetting path (10K)

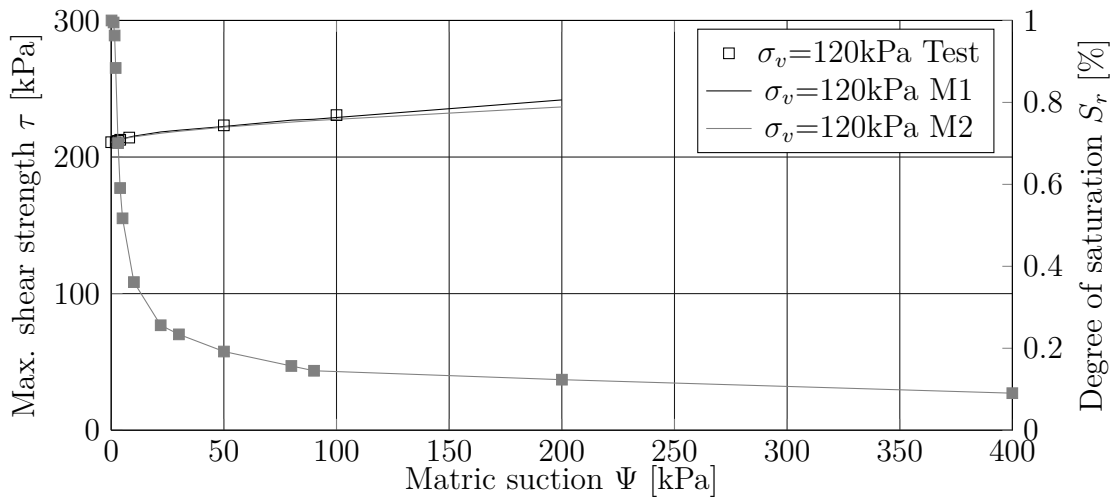


Figure D.11.: Fitting the results of max. shear strength under $\sigma_v = 250 \text{ kPa}$ for drying path (10K)

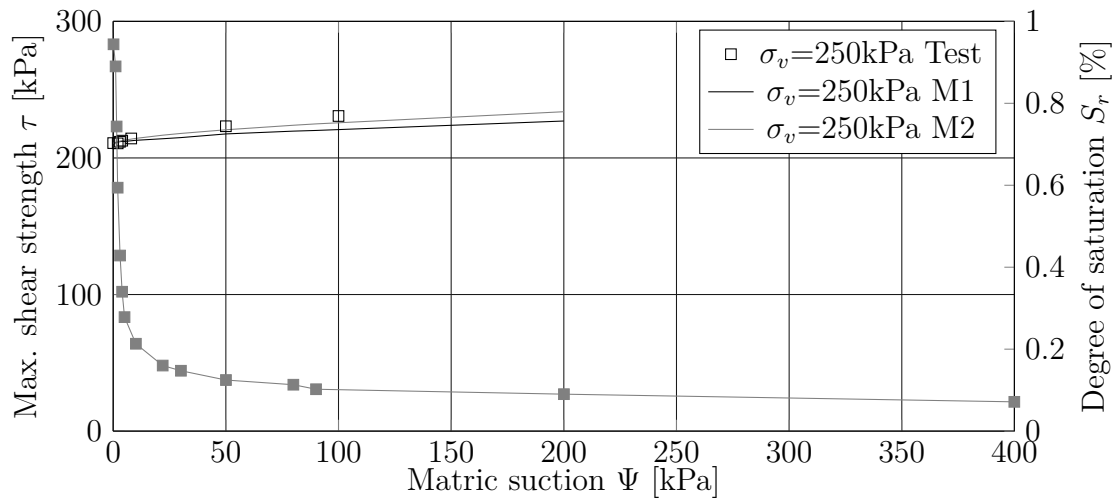


Figure D.12.: Fitting the results of max. shear strength under $\sigma_v=250\text{kPa}$ for wetting path (10K)

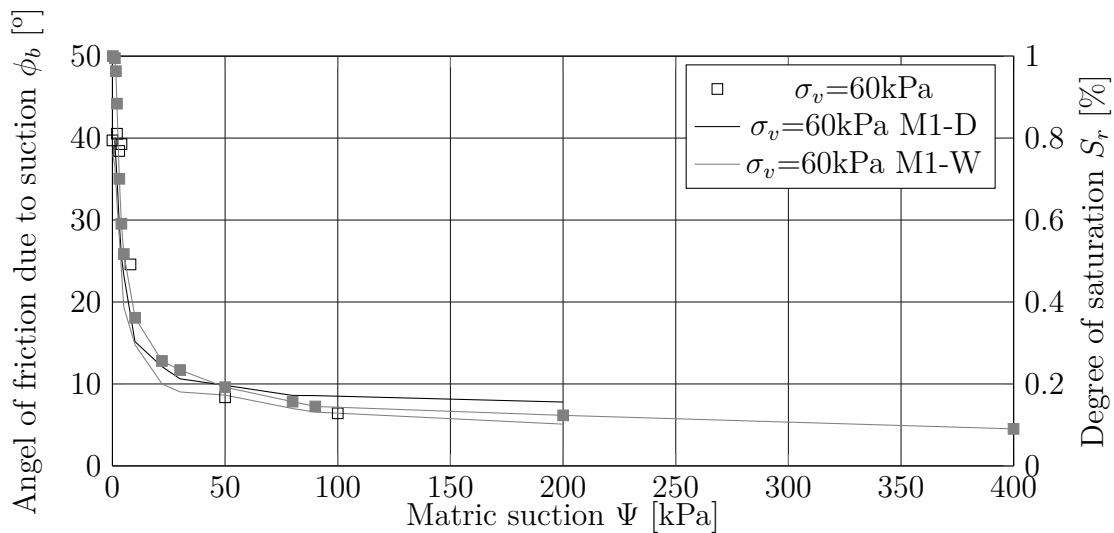
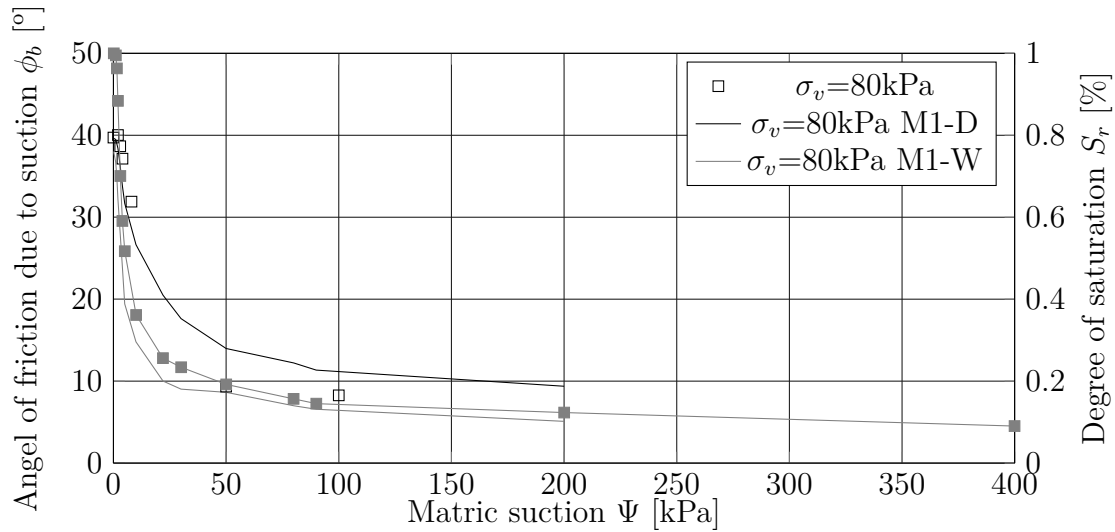
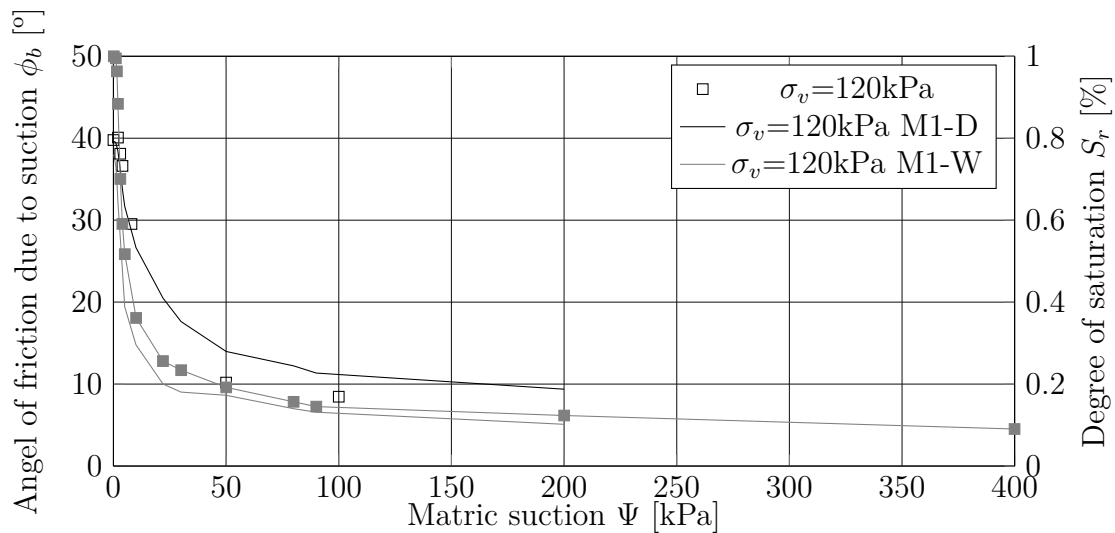


Figure D.13.: Fitting the results of ϕ^b under $\sigma_v=60\text{kPa}$ for (10K)

Figure D.14.: Fitting the results of ϕ^b under $\sigma_v=80\text{kPa}$ for (10K)Figure D.15.: Fitting the results of ϕ^b under $\sigma_v=120\text{kPa}$ for (10K)

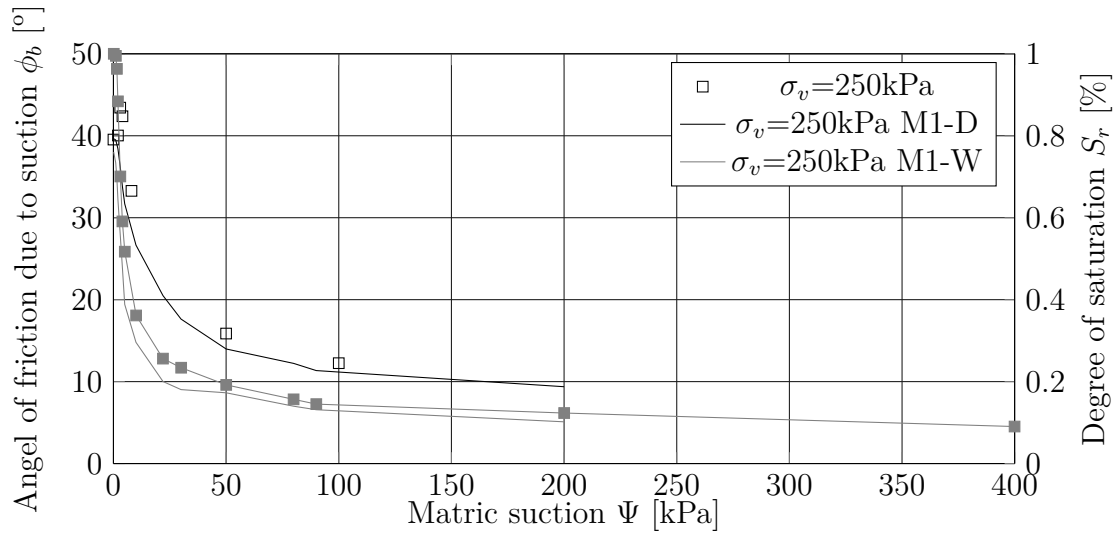


Figure D.16.: Fitting the results of ϕ^b under $\sigma_v=250\text{kPa}$ for drying path (10K)

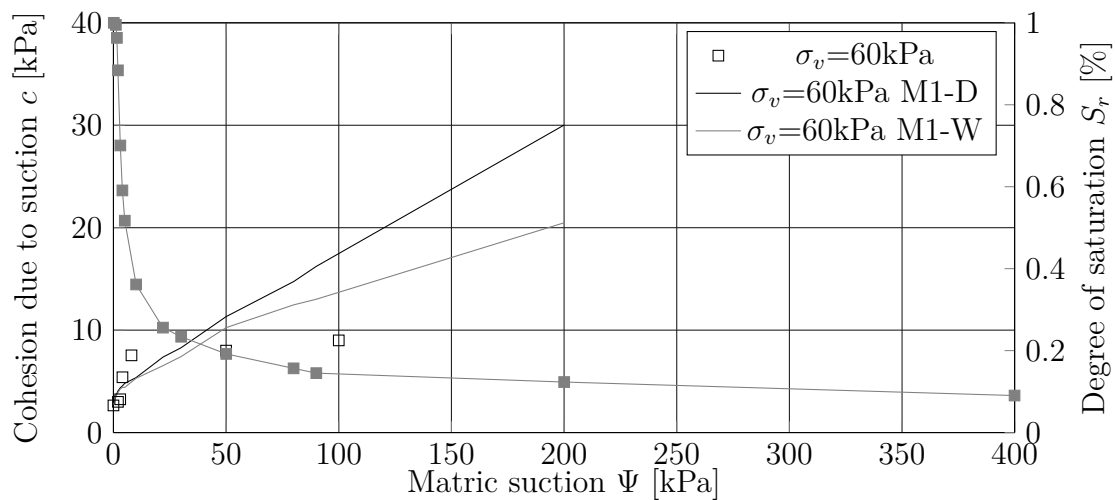
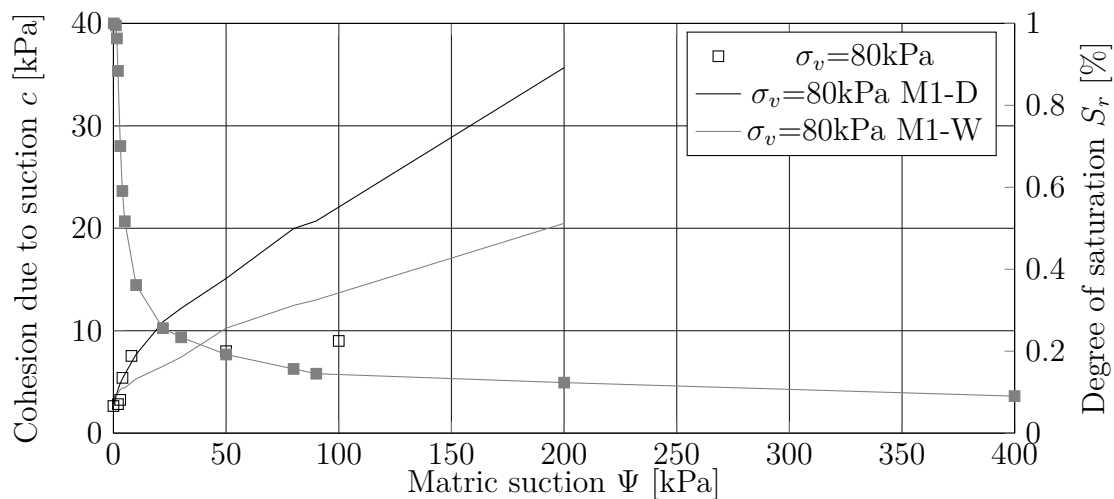
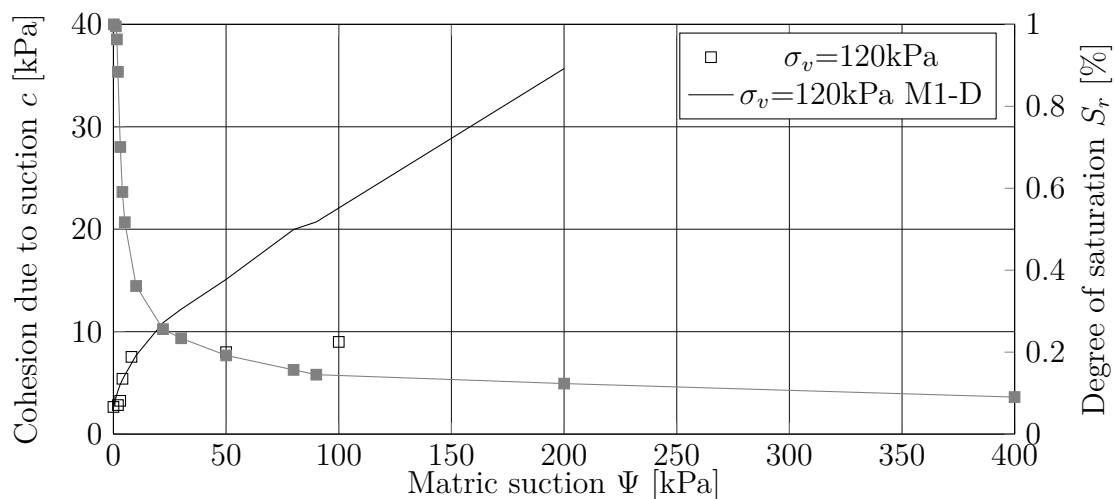


Figure D.17.: Fitting the results of app. cohesion strength under $\sigma_v=60\text{kPa}$ for (10K)

Figure D.18.: Fitting the results of app. cohesion under $\sigma_v = 80 \text{ kPa}$ for (10K)Figure D.19.: Fitting the results of app. cohesion under $\sigma_v = 120 \text{ kPa}$ for (10K)

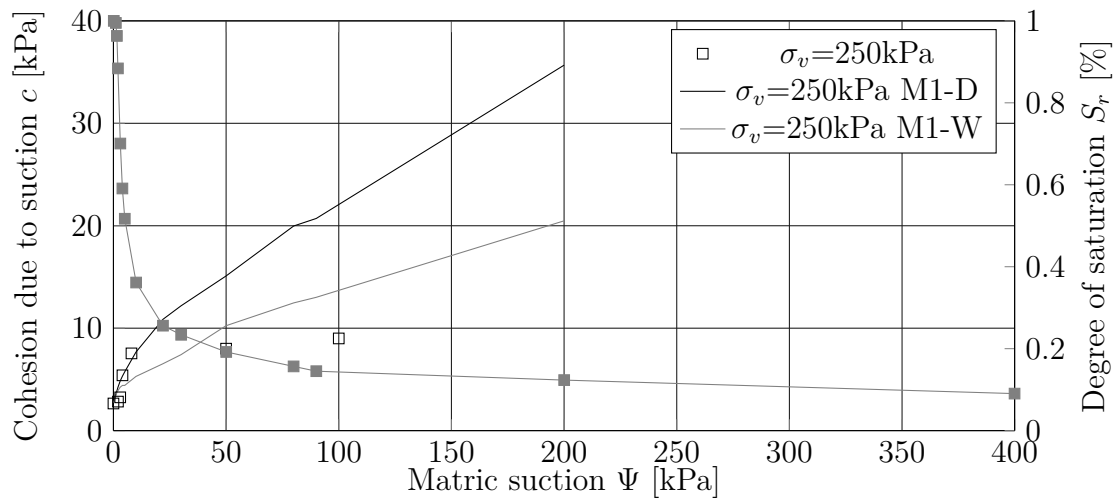


Figure D.20.: Fitting the results of app. cohesion under $\sigma_v=250\text{kPa}$ for (10K)

D.3. 15K

In this section, a review to the fitting results of the shear results for the soil mixture 10K. Figures D.21 to D.28 present the fitting curves for maximum shear strength vs suction for the drying and wetting paths.

Figures D.29 to D.32 present the fitting curves for the angle of friction due to suction vs suction for the drying and wetting paths.

Figures D.33 to D.36 show the attempt to fit curves for the cohesion due to suction vs suction for the drying and wetting paths.

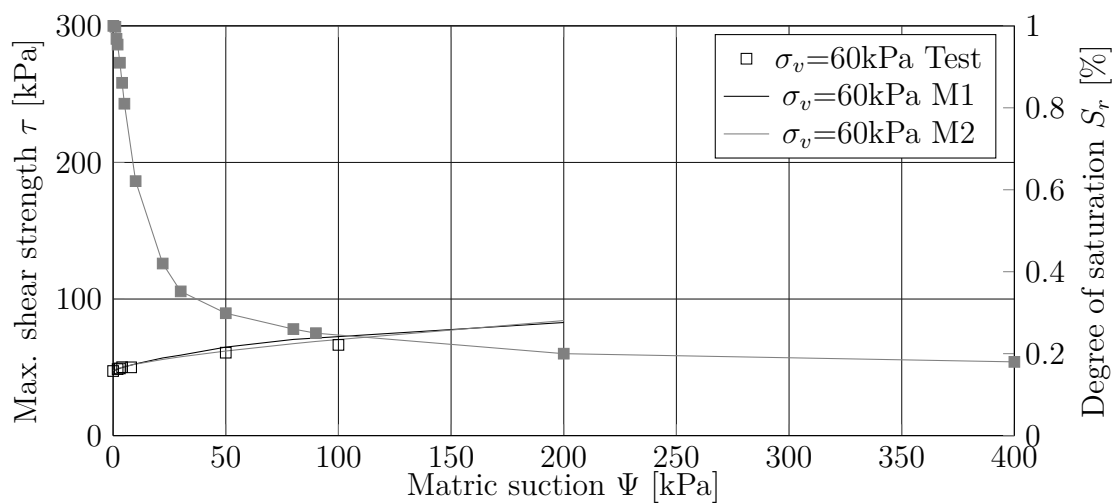


Figure D.21.: Fitting the results of max. shear strength under $\sigma_v=60\text{kPa}$ for drying path (15K)

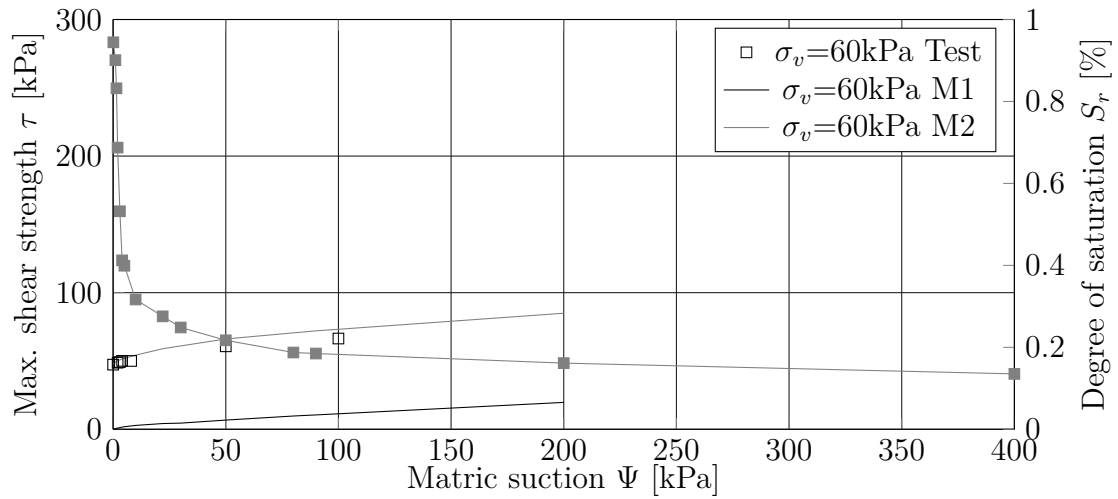


Figure D.22.: Fitting the results of max. shear strength under $\sigma_v=60\text{kPa}$ for wetting path (15K)

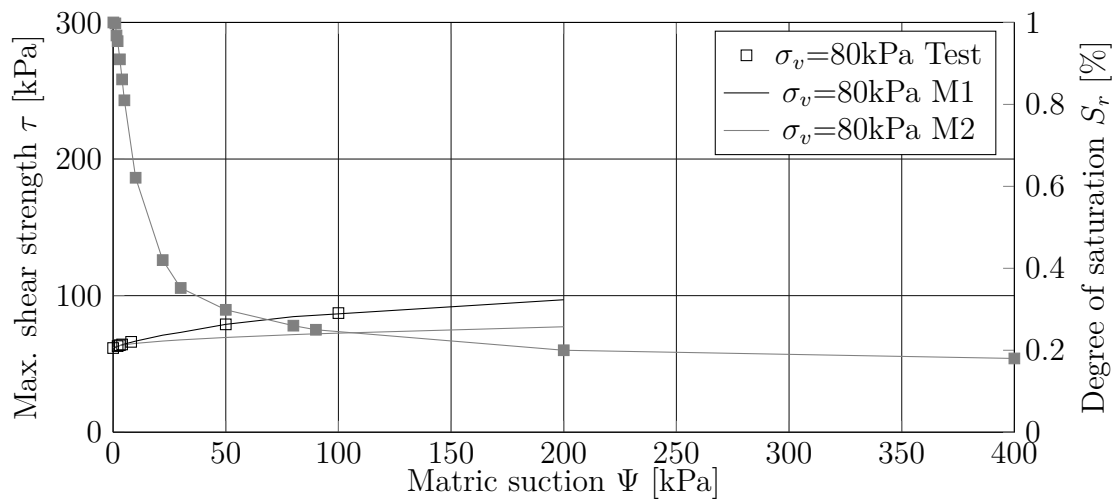


Figure D.23.: Fitting the results of max. shear strength under $\sigma_v=80\text{kPa}$ for drying path (15K)

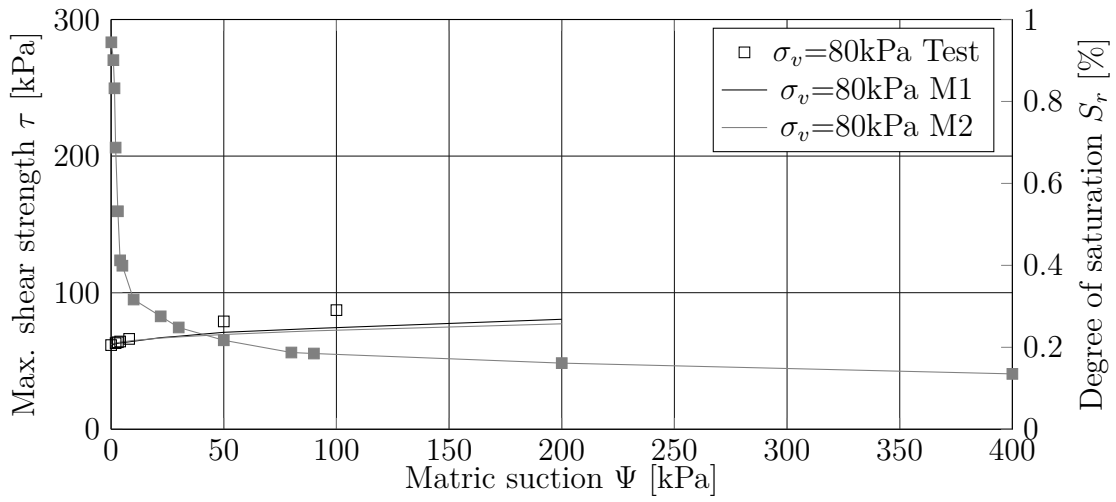


Figure D.24.: Fitting the results of max. shear strength under $\sigma_v=80\text{kPa}$ for wetting path (15K)

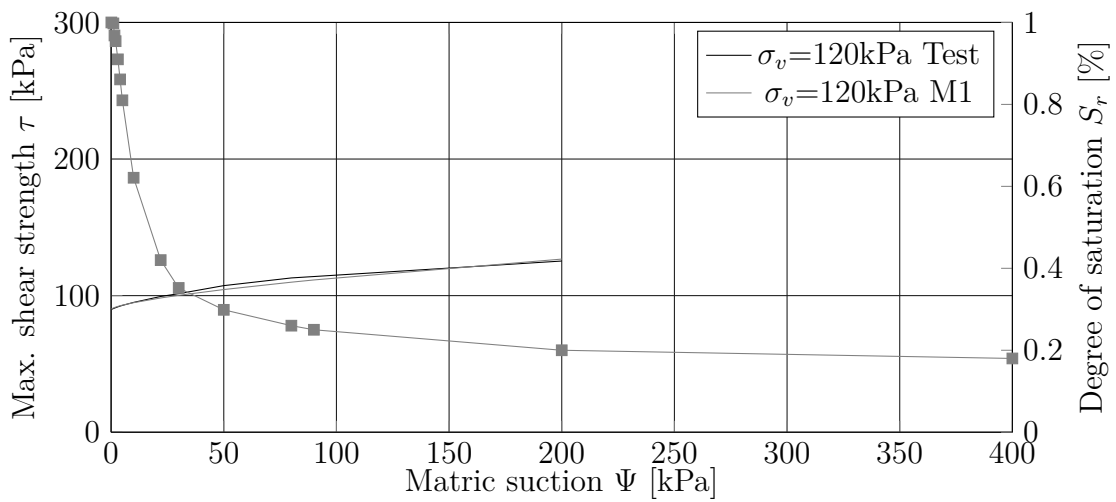


Figure D.25.: Fitting the results of max. shear strength under $\sigma_v=120\text{kPa}$ for drying path (15K)

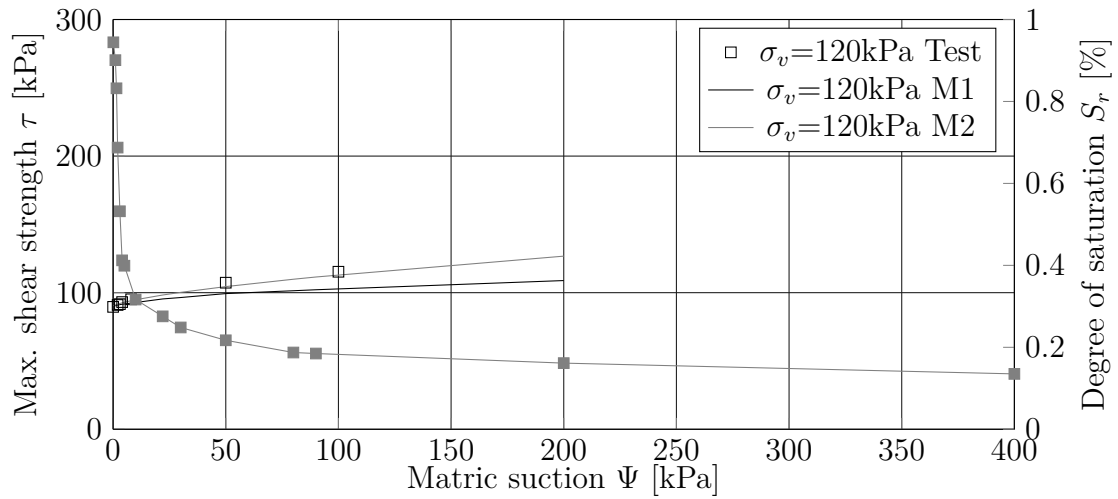


Figure D.26.: Fitting the results of max. shear strength under $\sigma_v=120\text{kPa}$ for wetting path (15K)

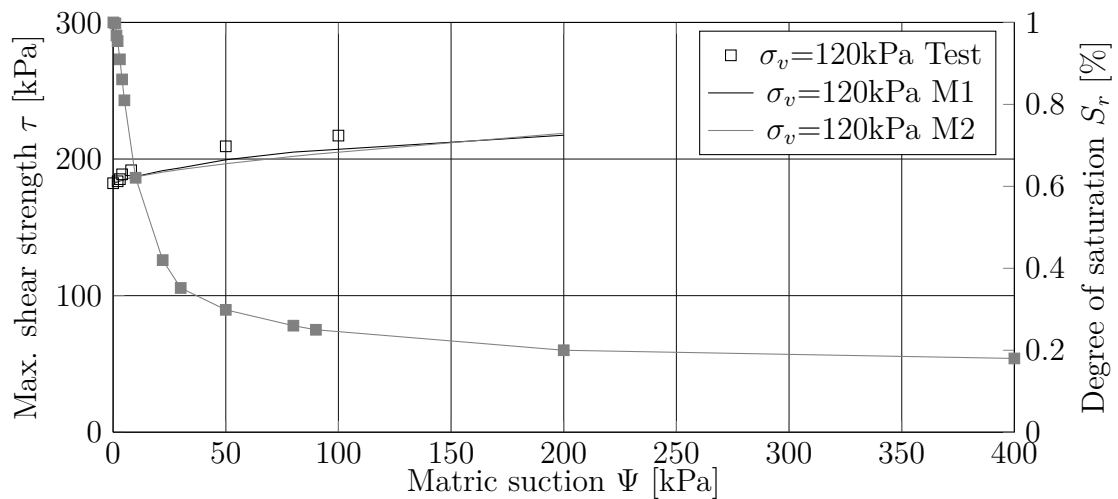


Figure D.27.: Fitting the results of max. shear strength under $\sigma_v=250\text{kPa}$ for drying path (15K)

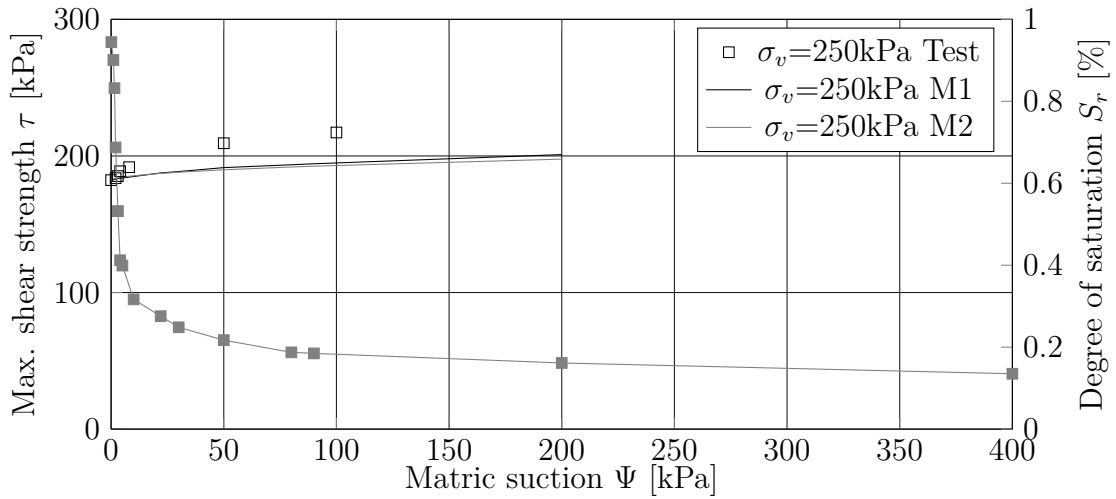


Figure D.28.: Fitting the results of max. shear strength under $\sigma_v=250\text{kPa}$ for wetting path (15K)

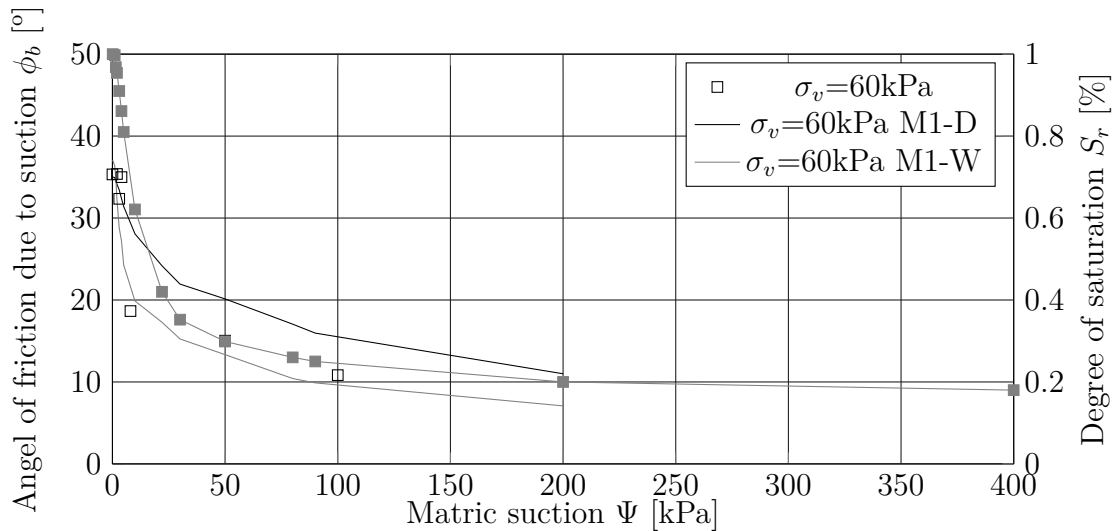


Figure D.29.: Fitting the results of ϕ^b under $\sigma_v=60\text{kPa}$ for (15K)

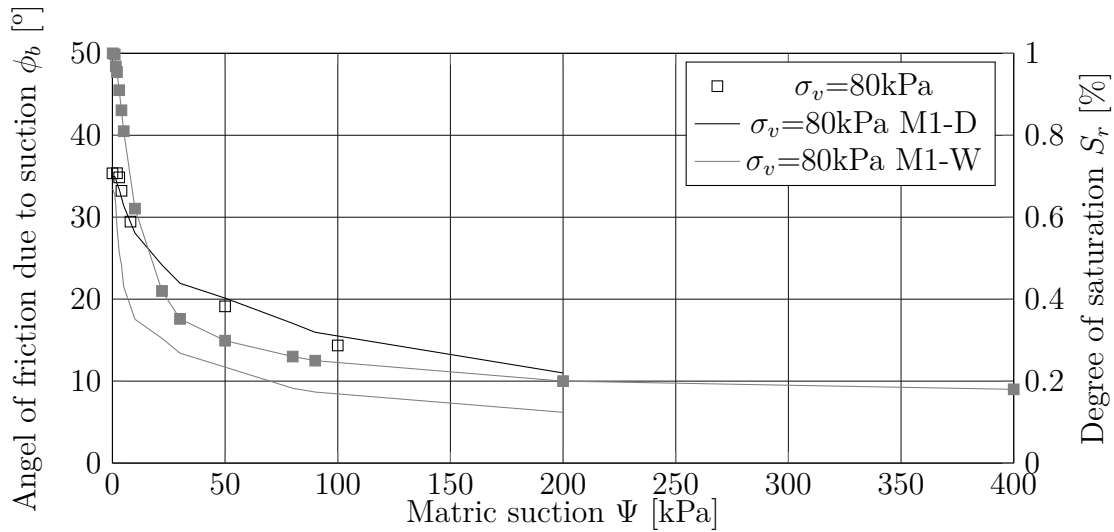


Figure D.30.: Fitting the results of ϕ^b under $\sigma_v=80\text{kPa}$ for (15K)

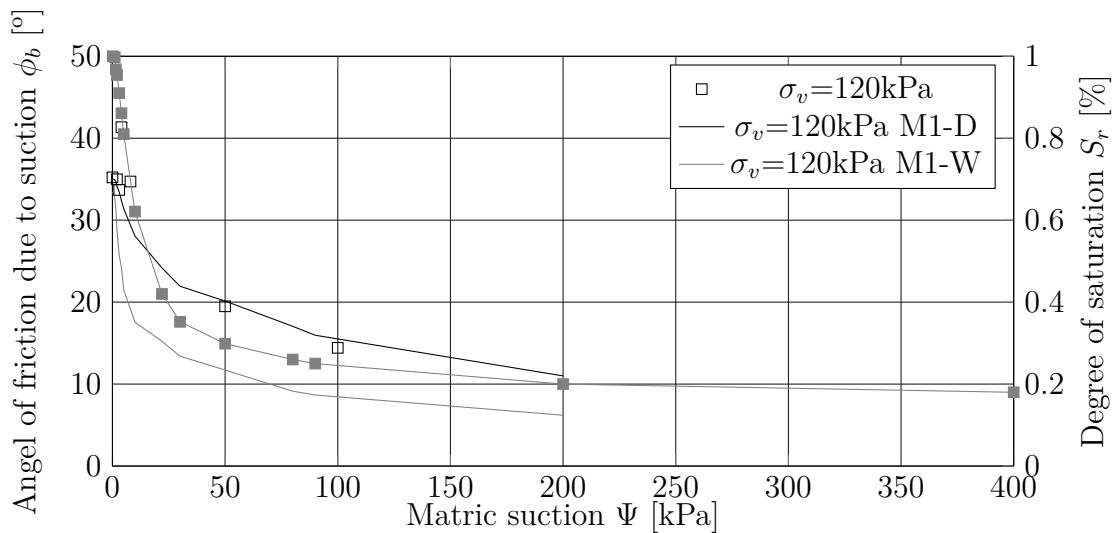


Figure D.31.: Fitting the results of ϕ^b under $\sigma_v=120\text{kPa}$ for (15K)

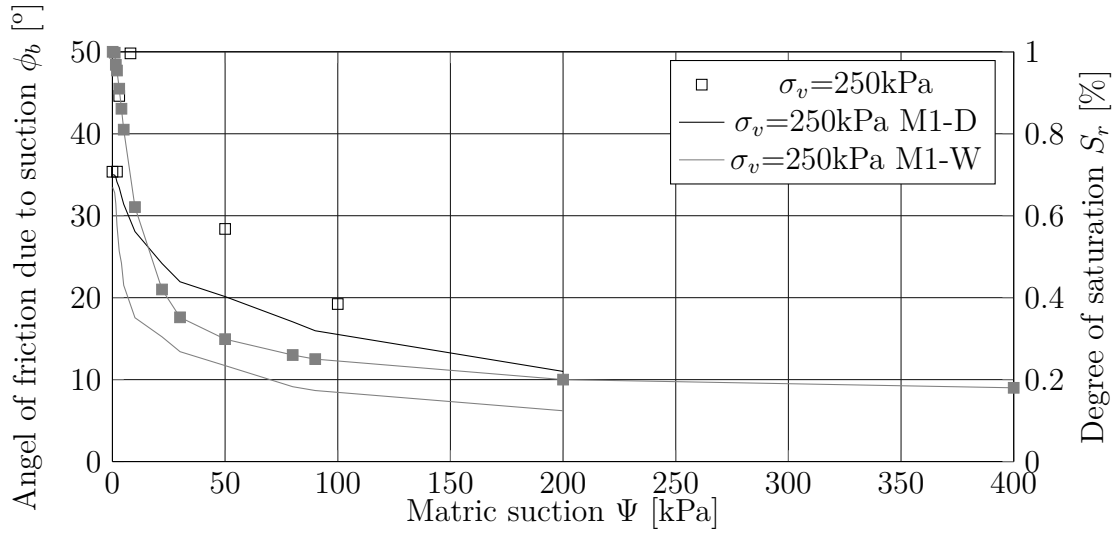


Figure D.32.: Fitting the results of ϕ^b under $\sigma_v=250\text{kPa}$ for (15K)

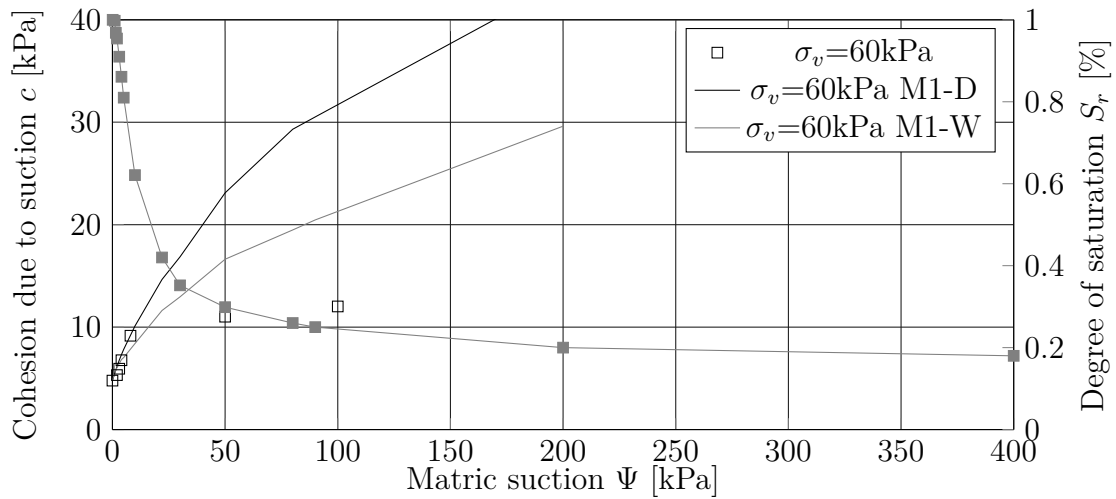


Figure D.33.: Fitting the results of app. cohesion under $\sigma_v=60\text{kPa}$ for (15K)

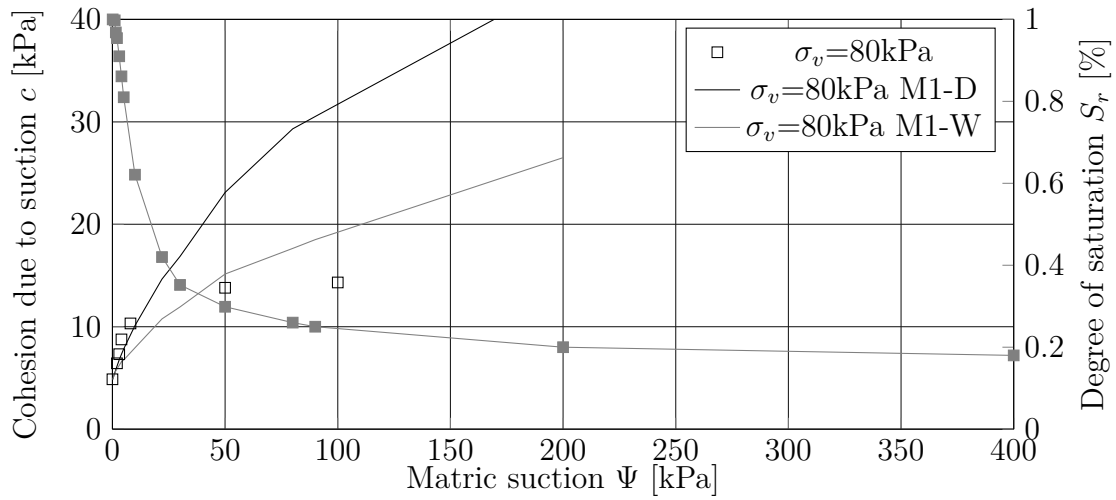


Figure D.34.: Fitting the results of app. cohesion under $\sigma_v=80$ kPa for (15K)

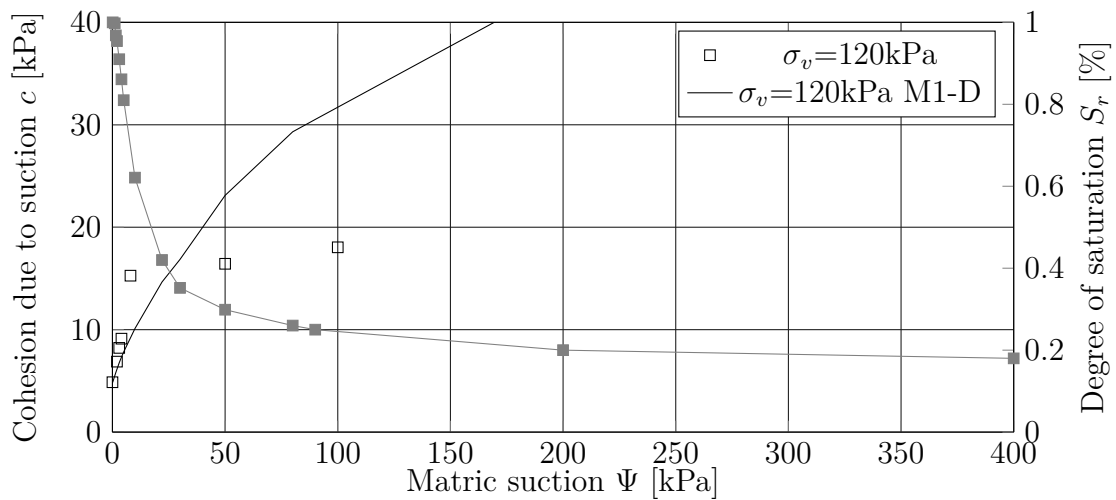


Figure D.35.: Fitting the results of app. cohesion under $\sigma_v=120$ kPa for (15K)

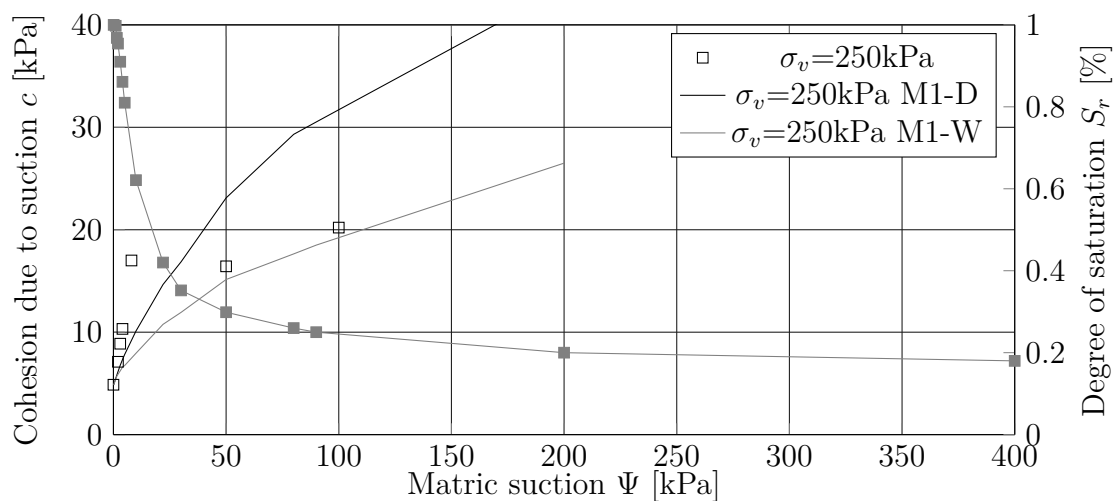


Figure D.36.: Fitting the results of app. cohesion under $\sigma_v=250\text{kPa}$ for (15K)

Bibliography

- Abramento, M. & Carvalho, C. S. (1989), Geotechnical pparameter for the study of natural slopes instabilization at "serra do mar" brazil, *in* 'Proc., 12th Int. Conf. on Soil Mechanics and Foundations Engineering, Rio de Janeiro', Vol. 3, pp. 1599–1602.
- Agus, S. S. (2005), An experimental study on hydro-mechanical characteristics of compacted bentonites and mixtures, PhD thesis, PhD Dissertation. Faculty of Civil Eng., Bauhaus-Universität Weimar, Germany.
- Agus, S. S., Leong, E. C. & Rahardjo, H. (2001), 'Soil-water characteristic curve of singapore residual soils', *Geotechnical and Geological Engineering* **19**, 285–309.
- Agus, S. S., Leong, E. C. & Schanz, T. (2003), 'Assessment of statistical models for indirect determination of permeability functions from soil-water characteristic curves', *Geotechnique* **53**(279–282).
- Agus, S. S. & Schanz, T. (2005*a*), 'Comparison of four methods for measuring total suction', *Vadose Zone J.* **4**, 1087–1095.
- Agus, S. S. & Schanz, T. (2005*b*), Swelling pressure and total suction of compacted bentonitesand mixtures., *in* 'Proceeding of International Conference on Problematic Soils (Eds. Bilsel, H and Nalbantoglu, Z), North Cyprus', Vol. 1, pp. 61–70.
- Agus, S. S. & Schanz, T. (2007), Error in total suction measurement., *in* 'Proc. 2nd International Conference Mechanics of Unsaturated Soils (Ed. Tom Schanz), Weimar, Germany. Springer proceedings in physics.', Vol. 1, pp. 59–70.
- Aitchison, G. D. (1960), Relationships of moisture stress and effective stress functions in unsaturated soils, *in* 'Proc. Conf. pore pressure. Butterworths. London'.
- Aitchison, G. D. (1965), Engineering concepts of moisture equilibria and moisture changes in soils, *in* 'Statement of the Review Panel, In Moisture Equilibria and Moisture Changes in Soils Beneath Covered Areas, A Symposium in Print, Butterworths, Sydney', pp. 7–22.

- Aitchison, G. D. & Donald, I. B. (1956), Effective stresses in unsaturated soils, *in* 'Proc. 2nd Aust. N.Z. Conf. Soil Mech.', pp. 192–199.
- Ajdari, M., Habibagahi, G., Nowamooz, H., Masrouri, F. & Ghahramani, . A. (2010), 'Shear strength behavior and soil water retention curve of a dual porosity silt-bentonite mixture', *Scientia Iranica* **17**(6), 430–440.
- Al-Badran, Y. (2011), Volumetric yielding behavior of unsaturated fine-grained soils., PhD thesis, Chair of foundation engineering, soil and rock mechanics, Ruhr-Universität Bochum, 46.
- Alabdullah, J. (2010), Testing Unsaturated Soil for Plane Strain Conditions: A New Double-Wall Biaxial Device, PhD thesis, PhD thesis at the Faculty of Civil Engineering Bauhaus-University Weimar, 44.
- Albrecht, B. A., Benson, C. H. & Beuermann, S. (2003), 'Polymer capacitance sensors for measuring gas humidity in drier soils.', *Geotechnical Testing Journal* **26**(1), 3–11.
- Amat, A. (2007), Elastic stiffness moduli of hostun sand, Master's thesis, Master Thesis, Department of Civil Engineering, University of Bristol.
- Ampadu, S. I. K. (2007), An investigation into the effect of water content on the direct shear strength characteristics of remoulded soil, *in* '14th ARC SMGE, Yaounde', pp. 23–30.
- Andrade, J. E. & Ellison, K. C. (2008), 'Evaluation of a predictive constitutive model for sands', *Journal of Geotechnical and Geoenvironmental Engineering* **134**(12), 1825–1828.
- Anthony, J., Bideaux, R., Bladh, K. & Nichols, M.C., E. (2001), *Handbook of Mineralogy*, Mineralogical Society of America, Chantilly, VA 20151-1110, USA.
- Arifin, Y. F. (2008), Thermo-Hydro-Mechanical behavior of compacted bentonite-sand mixtures: An experimental study, PhD thesis, Faculty of Civil Eng., Bauhaus-Universität Weimar, Germany.
- Arifin, Y. & Schanz, T. (2009), 'Osmotic suction of highly plastic clays', *Acta Geotechnica* **4**, 177–191.
- Asadzadeh, M. & Soroush, A. (2009), 'Direct shear testing on a rockfill material', *The Arabian Journal for Science and Engineering* **34**(2B), 376–396.

- ASTM (2002), 'Standard test methods for determination of the soil water characteristic curve for desorption using a hanging column, pressure extractor, chilled mirror hygrometer, and/or centrifuge', *ASTM International, West Conshohocken, PA D 6836-02*.
- ASTM (2006), 'Standard test method for particle-size analysis of soils', *ASTM International, West Conshohocken, PA*.
- ASTM (2015), 'Standard test method for moisture retention curves of porous building materials using pressure plates', *ASTM International, West Conshohocken, PA*.
- Aubeny, C. & Lytton, R. (2004), 'Shallow slides in compacted high plasticity clay slopes', *Journal of Geotechnical and Geoenvironmental Engineering* **130**(7), 717–727.
- Aubertin, M., a. J. F. & Chapuis, R. P. (1998), 'A predictive model for the water retention curve: application to tailings from hard-rock mines.', *Canadian Geotechnical Journal* **35**, 55–69.
- Aubertin, M., Mbonimpa, M., Bussiere, B. & Chapuis, R. P. (2003), 'A physically-based model to predict the water retention curve from basic geotechnical properties', *Canadian Geotechnical Journal* **40**, 1104–1122.
- Avci, O. & Ehlers, W. (2006), Parameteridentification of hostun-sand and shear-band simulation of landsliding, *in* 'Proceedings in Applied Mathematics and Mechanics (PAMM)', Vol. 6, pp. 351–352.
- Baille, W. (2014), Hydro-Mechanical Behaviour of Clays-Significance of Mineralogy Bochum, PhD thesis, Chair of foundation engineering, soil and rock mechanics, Ruhr-Universität Bochum, 53.
- Bao, C. G., Gong, B. & Zan, L. (1998), Properties of unsaturated soils and slope stability of expansive soils, *in* 'Key Note Lecture, UNSAT 98, 2nd International Conference on Unsaturated Soils, Beijing'.
- Barbour, S. L. (1998), 'Nineteenth canadian geotechnical colloquium: the soilwater characteristic curve: a historical perspective.', *Can Geotech J* **35**, 873–894.
- Barrett, R. J. (1966), Use of plastic filters in coastal structures, *in* 'Proceedings from the 16th International Conference Coastal Engineers, Tokyo', pp. 1048–1067.
- Barzegar, A. R., Oades, J. M., Rengasamy, P. & Murray', R. S. (1995), 'Tensile strength of dry, remoulded soils as affected by properties of the clay fraction', *Geoderma* **65**(1-2), 93–108.

- Bathurst, R. J., Ho, A. F. & Siemens, G. (2007), 'A column apparatus for investigation of 1-d unsaturated-saturated response of sand-geotextile systems', *Geotechnical Testing Journal* **30**(6), 433–441.
- Bathurst, R. J., Siemens, G. & Ho, A. F. (2009), 'Experimental investigation of infiltration ponding in one-dimensional sandgeotextile columns', *Geosynthetics International* **16**(3), 158–172.
- Bear, J. (1972), *Dynamics of fluids in porous media*, American Elsevier Publishing Company, Inc., New York.
- Öberg, A.-L. & Sällfors, G. . (1995), A rational approach to the determination of the shear strength parameters of unsaturated soils, *in* 'Proc. 1st Int. Conf on Unsaturated Soils UNSAT95', Vol. 1, pp. 151–158.
- Berg, J. C. (1989), The use of single fiber-wetting measurements in the assessment of absorption, *in* A. E. Turbak & V. Mrone, L., eds, 'Nonwovens: an advanced totutorials', TAPPI PRESS.
- Biarez, J., Fleureau, J. M., Indarto, S. T. & Zerhouni, M. I. (1989), Influence of water negative pore pressure on the flow of granular materials in silos, *in* 'In Powders and Grains, Rotterdam (1989), p. 385.', Rotterdam, The Netherlands, pp. 385–392.
- Biot, M. A. (1941), 'General theory of three-dimensional consolidation', *Journal App. Phys.* **42**, 155–164.
- Bishop, A. W. (1959), 'The principle of effective stress', *Tecnisk Ukebla* **106**(39), 859–863.
- Bishop, A. W., A. W., Alpan, I., Blight, G. E. & Donald, I. B. (1960), Factors controlling the shear strength of partly saturated cohesive soils., *in* 'ASCE Research Conference on Shear Strength of Cohesive Soils, University of Colorado, Boulder, CO.', pp. 503–532.
- Bishop, A. W. & Blight, G. E. (1963), 'Some aspects of effective stress in saturated and partially saturated soils', *Géotechnique* **13**(3), 177–197.
- Bishop, A. W. & Donald, I. B. (1961), The experimental study of partly saturated soil in the triaxial apparatus, *in* 'Proc. 5th International Conf. of Soil Mech.', number 1, pp. 13–21.
- Blatz, J. A. & Graham, J. (2003), 'Elastic-plastic modeling of unsaturated soil using results from a new triaxial test with controlled suction', *Géotechnique* **53**(1), 113–122.

- Bolt, G. H. & Miller, R. D. (1958), 'Calculation of total and component potentials of water in soil', *American Geophysical Union Transportation* **39**, 917–928.
- Bonaparte, R., Daniel, D. & Koerner, R. (2002), 'Assessment and recommendations for improving the performance of waste containment systems.'
- Borana, L., Yin, J.-H., Singh, D. N. & Shukla, S. K. (2015), 'A modified suction-controlled direct shear device for testing unsaturated soil and steel plate interface', *Marine Georesources & Geotechnology* **33**, 289–298.
- Bouazza, A., Freund, M. & Nahlawi, H. (2006), 'Water retention of nonwoven polyester geotextiles', *Polymer Testing* **25**(8), 1038–1043.
- Bouazza, A., Nahlawi, H. K. J. & Delage, P. (2006), Water retention curves of a non woven polyester geotextile, *in* 'Unsaturated Soils, Geotechnical Special Publication', Vol. 2, pp. 1651–1658.
- Bouazza, A., Zornberg, J. G., McCartney, J. S. & Nahlawi, H. (2006), 'Significance of unsaturated behaviour of geotextiles in earthen structures', *Australian Geomechanics Journal* **41**(3), 133–142.
- Bouferra, R., Benseddiq, N. & Shahrour, I. (2007), 'Saturation and preloading effects on the cyclic behavior of sand', *International journal of geomechanics, ASCE* **7**(5), 396–401.
- Bowles, J. E. (1984), *Physical and Geotechnical Properties of Soils*.
- Brooks, R. H. & Corey, A. T. (1964), Hydraulic properties of porous media, Technical report, Hydrol. Pap. 3, Colo. State Univ., Fort Collins, 1.
- Buckingham, E. (1907), *Studies of the movement of soil moisture*, Vol. 38, Milton Whitney, Chief.
- Burland, J. B. (1965), Some aspects of the mechanical behaviour of partly saturated soils., *in* 'Moisture Equilibria and Moisture Changes in the Soils Beneath Covered Areas, G. D. Aitchison, ed., Butterworth, Sydney, Australia', pp. 270–278.
- Caruso, M. & Tarantino, A. (2004), 'A shearbox for testing unsaturated soils at medium to high degrees of saturation', *Géotechnique* **5**(4), 281–284.
- Casini, F., Minder, P. & Springman, S. (2011), Shear strength of an unsaturated silty sand, *in* A. Gens, ed., 'Unsaturated Soils', CRC Press, pp. 211–216.

- Cattoni, E., Cecconi, M. & Jommi, C. (2005), Soil dilatancy and suction: some remarks on their mutual effects on the shear strength of granular soils, *in* '11th.; INTERNATIONAL CONFERENCE, Computer methods and advances in geomechanics, Bologna (Italy)', Vol. 2, pp. 19–26.
- Chapuis, R. P. & Legare, P. P. (1992), A simple method for determining the surface area of fine aggregates and fillers in bituminous mixtures, *in* 'Effects of Aggregates and Mineral Filters 15 on Asphalt Mixture Performance, edited by: Meininger, R. C., ASTM, Philadelphia, ASTM', Vol. STP 1147, pp. 177–186.
- Chen, G., Lv, Y., Huang, Z. & Chang, Y. (2013), 'Study on shear strength experiments base on the modified direct shear apparatus for unsaturated soils', *Applied Mechanics and Materials* **438-439**, 1176–1180.
- Chin, D. A. . (2000), *Water-Resources Engineering*, Prentice Hill, Upper Saddle River, N. J.
- Cho, G. C. & Santamarina, J. C. (2001), 'Unsaturated particulate materialsparticle-level studies', *Journal of Geotechnical and Geoenvironmental Engineering* **127**(1), 84–96.
- Conciani, W., Herrmann, P. P., Machado, S. L. & Soares, M. M. (1996), 'O uso da técnica de reflectometria no domínio do tempo (tdr) para determinacao da umidade do solo in situ.', *Revista Solos e Rochas, Sao Paulo*, **19**, 189–199.
- Coulomb, C. A. (1776), 'Essai sur une application des regles des maximis et minimis a quelques problemes de statique relatifs a l'architecture', *Memoires de l'Academie Royale pres Divers Savants, Vol. 77*, 65–78.
- Coussy, O. (1995), *Mechanics of Porous Continua*, John Wiley and Sons, New York.
- Croney, D. & Coleman, J. (1961), Pore pressure and suction in soil, *in* 'In Proceedings of Conference on Pore Pressure and Suction in Soils, London, Butterworths', pp. 31–37.
- Croney, D., Coleman, J. D. & Black, W. P. M. (1958), Movement and distribution of water in soil in relation to highway design and performance, Technical Report 40, Highw. Res. Bd, Spec.
- Croney, D., Coleman, J. D. & Bridge, P. (1952), The suction of moisture held in soil and other porous materials, Technical Report 24, Road Research Technical Paper.

- Cuisinier, O. & Masrouri, F. (2002), Influence of a suction cycle on the hydromechanical behaviour of a swelling soil, *in* L. Vulliet, B. Schrefler & L. Laloui, eds, 'Environmental Geomechanics', pp. 175–180.
- D4439-15a., A. S. (2015), 'Astm d4439-15a, standard terminology for geosynthetics'.
URL: *www.astm.org*
- Dana, J. & Dana, E. (1892), *System of mineralogy*, Clifford Frondel. Wiley, New York,.
- de Campos, T. M. P. & Carillo, C. W. (1995), Direct shear testing on an unsaturated soil from rio de janeiro, *in* 'Proc. of 1st. Int. Conf. on Unsaturated Soils', Vol. 1, pp. 31–38.
- De Gennaro, V., Canou, J., Dupla, J. C. & Benahmed, N. (2004), 'Influence of loading path on the undrained behaviour of a medium loose sand', *Canadian Geotechnical Journal* **41**(1), 166–180.
- Deer, W. A., Howie, R. A. & Zussman, J. (2013), *An introduction to the rock-forming minerals*, 3rd Edition. London: Mineralogical Society.
- DepV (2009), *Verordnung über Deponien und Langzeitlager (Deponieverordnung - DepV)*, BGBl. I S. 900).
- Desrues, J. (1984), La localisation de la de formation dans les materiaux granulaires, PhD thesis, These de Doctorat es Science, USMG and INPG, Grenoble, France.
- Desrues, J. & Viggiani, G. (2004), 'Strain localization in sand: an overview of the experimental results obtained in grenoble using stereophotogrammetry', *International Journal for Numerical and Analytical Methods in Geomechanics* **28**(4), 279–321.
- di Prisco, C. & posimato, S. (1996), 'Time dependent mechanical behaviour of loose sand.', *Mechanics of cohesive-frictional materials* **17**(1), 45–73.
- Dierickx, W. (1996), Determination of water penetration resistance of geotextiles, *in* 'In: Bhatia, S.K., Suits, L.D. (Eds.), Recent Developments in Geotextile Filters and Prefabricated Drainage Geocomposites. ASTM STP 1281. American Society for Testing and Materials', pp. 65–74.
- Doanh, T., Dubujet, P. & Touron, G. (2010), 'Exploring the undrained induced anisotropy of hostun rf loose sand', *Acta Geotechnica* **5**, 239–256.
- Doanh, T., Finge, Z. & Boucq, S. (2012), 'Effects of previous deviatoric strain histories on the undrained behaviour of hostun rf loose sand', *Geotech Geol Eng.* **30**, 697–712.

- Doanh, T., Finge, Z. & Dubujet, P. (2006), 'Undrained anisotropy of hostun rf loose sand: new experimental investigations', *Canadian Geotechnical Journal* **43**(11), 1195–1212.
- Doanh, T., Ibraim, E. & Matiotti, R. (1997), 'Undrained instability of very loose hostun sand in triaxial compression and extension. part 1: experimental observations', *Mechanics of Cohesive-frictional Materials* **2**, 47–70.
- Donald, I. B. (1956), Shear strength measurements in unsaturated non-cohesive soils with negative pore pressures, *in* 'Proc. 2nd Australia-New Zealand Conf. on Soil Mechanics and Foundation Engineering, Christchurch', pp. 200–205.
- Dong, Q., Liu, L. & Hou, L. (2012), 'Influence of matric suction on shear strength behavior of unsaturated silty sand', *Advanced Materials Research* **446-449**, 1627–1632.
- Dubujet, P. & Doanh, T. (1997), 'Undrained instability of very loose hostun sand in triaxial compression and extension. part 2: theoretical analysis using an elastoplasticity model', *Mechanics of Cohesive-frictional Materials* **2**, 71–92.
- Edlefsen, N. E. & Anderson, A. B. C. (1943), 'Thermodynamics of soil moisture', *Hilgardia* **15**, 31–298.
- Escario, V. (1980), Suction controlled penetration and shear tests, *in* 'Proceedings of the 4th International Conference on Expansive Soils, ASCE, Denver', Vol. II, pp. 781–797.
- Escario, V. & Juca, J. F. T. (1989), Strength and deformation of partly saturated soils, *in* 'Proceedings of the Twelfth International Conference On Soil Mechanics and Foundation Engineering', Vol. 2, pp. 43–46.
- Escario, V. & Saez, J. (1986), 'The shear strength of partly saturated soils', *Gtotechnique* **36**, 453–456.
- Ezaoui, A. & Di Benedetto, H. (2009), 'Experimental measurements of the global anisotropic elastic behaviour of dry hostun sand during triaxial tests, and effect of sample preparation', *Geotechnique* **59**(7), 621–635.
- Fannin, R. J. & Palmeira, E. M. (2002), Soil-geotextile compatibility in filtration, *in* 'Proceedings 7th International Conference on Geosynthetics, Nice (France)', Vol. 3, pp. 853–870.
- Fard, H. S. (2014), Study on the Hydro-Mechanical Behavior of Fiber Reinforced Fine Grained Soils, with Application to the Preservation of Historical Monuments, PhD thesis, Chair of foundation engineering, soil and rock mechanics, Ruhr-Universität Bochum.

- Farouk, A., Lamboj, L. & Kos, J. (2004), 'Influence of matric suction on the shear strength behaviour of unsaturated sand', *Acta Polytechnica* **44** (4)(4), 11–17.
- Feuerharmel, C., Pereira, A., Gehling, W. & Bica, A. (2006), Determination of the shear strength parameters of two unsaturated colluvium soils using the direct shear test, *in* 'Fourth International Conference on Unsaturated Soils Carefree, Arizona, United States', pp. 1181–1190.
- Fisher, R. A. (1926), 'On the capillary forces in an ideal soil; correction of formulae given by w. b. haines', *The Journal of Agricultural Science* **16**(3), 492–505.
- Flavigny, E., Desrues, J. & Palayer, B. (1990), 'Note technique le sable d'hostun rf', *Rev. Francaise Geotechnique* **53**, 67–70.
- Foray, P., Balachowski, L. & Rault, G. (1998), Scale effect in shaft friction due to the localisation of deformations, *in* T. K. et al, ed., 'Centrifuge98', Vol. 1, pp. 211–216.
- Fredlund, D. G. & Morgenstern, N. R. (1977), 'Stress state variables for unsaturated soils', *Journal of Geotechnical Engineering Division, ASCE* **103**(GT5), 447–466.
- Fredlund, D. G. Morgenstern, N. R. & Widger, R. A. (1978), 'Shear strength of unsaturated soil', *Canadian Geotechnical Journal* **15**(3), 313–321.
- Fredlund, D. G., Morgenstern, N. R. & Widger, R. A. (1978), 'The shear strength of unsaturated soils', *Can. Geotech. J.* **15**(3), 313–321.
- Fredlund, D. G. & Rahardjo, H. (1993), *Soil Mechanics for Unsaturated Soils*, JOHN WILEY & SONS, INC.
- Fredlund, D. G. & Xing, A. (1994), 'Equations for the soilwater characteristics curve', *Canadian Geotechnical Journal* **31**(4), 521–532.
- Fredlund, D.G., R. H. & Fredlund, M. (2012), *Unsaturated Soil Mechanics in Engineering Practice*, John Wiley and Sons,.
- Fredlund, D.G., X. A. F. M. D. & Barbour, S. L. (1996), 'The relationship of the unsaturated soil shear strength to the soil-water characteristic curve', *Canadian geotechnical journal* **33**, 440–448.
- Fredlund, M. D., F. D. G. W. G. W. (1997a), Estimation of unsaturated soil properties using a knowledge-based system, *in* 'Proceedings of the Fourth Congress on Computing in Civil Engineering, ASCE, Philadelphia, Pennsylvania,', pp. 501–510.

- Fredlund, M. D., F. D. G. W. G. W. (1997b), Prediction of the soil-water characteristic curve from grain size distribution and volumemass properties, *in* 'In Proceedings of the 3rd Brazilian Symposium on Unsaturated Soils, Rio de Janeiro, Brazil, 2225 April 1997. Freitas Bastos, Rio de Janeiro, Brazil', pp. 13–23.
- Fredlund, M. D., W. G. W. F. D. G. (2002), 'se of the grain-size distribution for estimation of the soil-water characteristic curve', *Canadian Geotechnical Journal* **39**(5), 1103–1117.
- Gallage, C. & Uchimura, T. (2010), 'Effects of dry density and grain size distribution on soil-water characteristic curves of sandy soils', *Soils and Foundations* **50**(1), 161–172.
- Gan, J. K. M. (1986), Direct shear strength testing of unsaturated soils., Master's thesis, M.Sc. thesis, University of Saskatchewan, Saskatoon, SK.
- Gan, J. K. M. & Fredlund, D. G. (1994), Shear strength characteristics of two saprolitic soils from hong kong, *in* 'Proccedings of the Sino-Canadian Symposium on Unsaturated/Expansive Soil, China Institution for Soil Mechanics and Foundation Engineering, CEES, Wuhan, China', pp. 81–107.
- Gan, J. K.-M. & Fredlund, D. G. (1995), Shear strength of two saprolitic soils., *in* 'In: Alonso & Delage (eds.), Unsaturated Soils/Sols Non Satures, A.A. Balkema', Vol. 1, pp. 71–76.
- Gan, J. K.-M. & Fredlund, D. G. (1996), 'Shear strength characteristics of two saprolitic soils.', *Canadian Geotechnical Journal* **33**, 595–609.
- Gan, J. K. M., Fredlund, D. G. & Rahradjo, H. (1988), 'Determination of the shear strength pparameter of an unsaturated soil using direct shear test', *Canadian Geotechnical Journal* **25**, 500–510.
- Garcia, E. F., Gallage, C. P. K. & Uchimura, T. (2007), 'Function of permeable geosynthetics in unsaturated embankments subjected to rainfall infiltration', *Geosynthetics International* **14**(2), 89–99.
- Gay, O., Boutonnier, L., Flavigny, E. & Foray, P. (2003), laboratory characterization of hostun rf sand at very low confining stresses, *in* G. H. D. T. Di Benedetto, H. & C. Sauzeat, eds, 'Deformation Characteristics of Geomaterials / Comportement Des Sols Et Des Roches Tendres'.
- Gennaro, V. D., Canou, J., Dupla, J. C. & Benahmed, N. (2004), 'Influence of loading path on the undrained behavior of a medium sand', *Canadian Geotechnical Journal* **41**, 166–180.

- Giroud, J. P. (1983), 'Geotextile drainage layers for soil consolidation', *Civil Engineering for Practicing and Design Engineers* **2**, 275–295.
- Giroud, J. P. (2010), Development of criteria for geotextile and granular filters, in 'Prestigious Lecture, Proceedings of the 9th International Conference on Geosynthetics, Guarujá, Brazil, May 2010,' , number 1, pp. 45–64.
- Gourc, J., Faure, Y., Rollin, A. & Lafleur, J. (1982), Structural permeability law of geotextiles, in 'Second International Conference on Geotextiles', Vol. 1, pp. 149–154.
- Haines, W. B. (1925), 'Studies in the physical properties of soils: I. mechanical properties concerned in cultivation', *The Journal of Agricultural Science* **15**(2), 178–200.
- Haines, W. B. (1927), 'Studies in the physical properties of soils: Iv. a further contribution to the theory of capillary phenomena in soil', *The Journal of Agricultural Science* **17**(02), 264–290.
- Haines, W. B. (1930), 'The hysteresis effect in capillary properties and the modes of moisture distribution associated therewith', *Journal of Agriculture Science* **20**, 96–105.
- Hamidi, A., Habibagahi, G. & Ajdari, M. (2011), Shear behavior of shiraz silty clay determined using osmotic direct shear box, in S. Jotisankasa, Sawangsuriya & Mairaing, eds, 'Unsaturated Soils: Theory and Practice', pp. 215–219.
- Hammad, W. I. (1991), Modelisation non lineaire et etude experimentale des bandes de cisaillement dans les sables (A non linear modelling and an experimental study of shear bands in sand), PhD thesis, Institut de Mecanique de Grenoble.
- Handoko, L., Dananjaya, H., Yasufuku, N. & Ochihai, H. (2012), Unsaturated hydraulic properties of non-woven geotextile based on a modified capillary test, in '5th European Geosynthetics Congress', Vol. 5, Valencia, pp. 125–131.
- Hanson, J. L., Gilbert, R. B., W. S. G. & Theil, R. S. (2001), Unsaturated interface shear strength properties for nonwoven geotextiles, in 'Proceedings to Geosynthetics 2001, IFAI, Roseville, MN. Conference held in Portland, OR', pp. 135–148.
- Hareb, H. & Doanh, T. (2012), 'Probing into the strain induced anisotropy of hostun rf loose sand', *Granular Matter* **14**, 589–605.
- Hauser, V. (2008), *Evapotranspiration Covers for Landfills and Waste Sites*, CRC Press.

- Hauser, V. L. (2009), 'Evapotranspiration covers for landfills and waste sites', *esource: Engineering and Technology for Sustainable World* **16**(3), 4–16.
- Heitor, A., Rujikiatkamjorn, C. & Indraratna, B. (2013), Behaviour of a compacted silty sand under constant water content shearing, *in* 'Proceedings of the 18th International Conference on Soil Mechanics and Geotechnical Engineering, Paris', pp. 1007–2010.
- Henry, K. S. (1998), The use of geosynthetics to mitigate frost heave in soils, PhD thesis, Civil Engineering Department. University of Washington. Seattle. WA.
- Henry, K. S. & Holtz, R. D. (1997), Capillary rise of water in geotextiles, *in* 'Proceedings of International Symposium on Ground Freezing and Frost Action in Soils', pp. 227–233.
- Henry, K. S. & Holtz, R. D. (1998), 'Measurement of the contact angle of water on geotextile fibers', *Geotechnical Testing Journal* **21**(1), 11–17.
- Henry, K. S. & Holtz, R. D. (2001), 'Geocomposite capillary barriers to reduce frost heave in soils', *Canadian Geotechnical Journal* **38**(4), 678–694.
- Henry, K. S., Stormont, J. C. & Barna, L. (2002), Draft final report geocomposite capillary barrier drain for limiting moisture changes in pavement subgrades and bases, Technical report, Prepared for the IDEA Program Transportation Research Board National Research Council.
- Hilf, J. W. (1956), An investigation of pore-water pressure in compacted cohesive soils, PhD thesis, US Bureau of Reclamation Technical Memorandum 654. University of Colorado.
- Ho, A. F. (2000), Experimental and numerical investigation of infiltration ponding in one-dimensional sand-geotextile columns, Master's thesis, Queens University, Kingston, Ontario, Canada.
- Holtz, R., D. & Kovacs, W., D. (1981*a*), *An Introduction to Geotechnical Engineering*, Prentice Hall.
- Holtz, R. D. & Kovacs, W. D. (1981*b*), *An Introduction to Geotechnical Engineering*, Prentice Hall.
- Holtz, R.D., C. B. & Berg, R. (1997), *Geosynthetic Engineering*, BiTech Publ. Ltd.
- Hormdee, D., Ochiai, H. & Yasufuku, N. (2005), Advanced direct shear testing for collapsible soils with water content and matric suction measurement, *in* 'Site Characterization and Modeling, GeoFrontiers 2005, GSP 138', pp. 1–10.

- Hossain, Md., A. & Yin, J.-H. (2010), 'Behavior of a compacted completely decomposed granite soil from suction controlled direct shear tests', *Journal of Geotechnical and Geoenvironmental Engineering* **136**(1), 189–198.
- Huat, B. B. K., Ali, F. H. & Hashim, S. (2005), 'Modified shear box test apparatus for measuring shear strength of unsaturated residual soil', *American Journal of Applied Sciences. USA: New York.* **2**(9), 1283–1289.
- Ingold, T. S. (1994), *The Geotextiles and Geomembranes Manual.*, Oxford, UK: Elsevier Advanced Technology.
- Iryo, T. & Rowe, R. K. (2003), 'On the hydraulic behavior of unsaturated nonwoven geotextiles', *Geotextiles and Geomembranes* **21**, 381–404.
- Iryo, T. & Rowe, R. K. (2004), 'Numerical study of infiltration into a soilgeotextile column', *Geosynthetics International* **11**(5), 377–389.
- Jafarzadeh, F. & Javaheri, H., S. T. a. M. W. D. (2008), 'Simulation of anisotropic deviatoric response of hostun sand in true triaxial tests', *Computers and Geotechnics* **35**, 703–718.
- Jennings, J. E. B. & Burland, J. B. (1962a), 'Limitations to the use of effective stresses in partly saturated soils', *Géotechnique* **12**(2), 125–144.
- Jennings, J. E. B. & Burland, J. B. (1962b), 'Limitations to the use of effective stresses in partly saturated soils', *Géotechnique* **12**(2), 125–144.
- Jotisankasa, A., Sawangsuriya, A., Booncharoenpanich, P. & Soralump, S. (2012), Influence of kaolin mixture on unsaturated shear strength of decomposed granitic silty sand, in F. D. Claudio Mancuso, Cristina Jommi, ed., 'Unsaturated Soils: Research and Applications', Vol. 1, Springer Link.
- Kamath, Y. K., Dansizer, C. J., Hornby, S. & Weigmann, H. D. (1987), 'Surface wettability scanning of long filaments by a liquid emmbrane method', *Textile Research Journal* **57**, p. 205.
- Karube, D. (1988), New concept of effective stress in unsaturated soil and its proving test, in 'ASTM, Philadelphia, Special Tech. Pub., 977', pp. 269–278.
- Khalili, N. & Khabbaz, M. H. (1998), 'A unique relationship for χ for the determination of the shear strength of unsaturated soils.', *Géotechnique*, **48**(5), 681–688.

- Khire, M. V., Benson, C. H. & Bosscher, P. J. (2000), 'Capillary barriers: Design variables and water balance', *Journal of Geotechnical and Geoenvironmental Engineering* **126**(8), 695–708.
- Kim, B., Shibuya, S., Park, S. & Kato, S. (2013), 'Suction stress and its application on unsaturated direct shear test under constant volume condition', *Engineering Geology* **155**, 10–18.
- Kim, T. (2001), Moisture-induced tensile strength and cohesion in sand, PhD thesis, Dept. of Civil, Environmental and Architectural Engineering, Univ. of Colorado, Boulder, Colo.
- Klute, A. (1986), Water retention: Laboratory methods, *in* 'Methods of Soil Analysis, Part 1, Agronomy Monograph No. 9, American Society of Agronomy-Soil Science of America, 2nd edition', Madison, Wisconsin, USA, pp. 635–662.
- Knight, M. A. & Kotha, S. M. (2001), 'Measurement of geotextile-water characteristic curves using a controlled outflow capillary pressure cell', *Geosynthetics International* **8**(3), 271–282.
- Koerner, R. (2005), *Designing with geosynthetics*, Prentice Hall.
- Koerner, R. M. (2012), *Designing With Geosynthetics*, Xlibris.
- Koerner, R. M. & Soong, T. Y. (1998), 'Analysis and design of veneer cover soils', *Proceedings 6th International Conference on Geosynthetics, Atlanta* **1**, 1–23.
- Kovács, G. (1981), *Seepage Hydraulics.*, Elsevier Science Publishers, Amsterdam.
- Krisdani, H., Rahardjo, H. & Leong, E. (2006), Experimental study of 1-d capillary barrier model using geosynthetic material as the coarse-grained layer, *in* 'Unsaturated Soils', pp. 1683–1694.
- Krisdani, H., Rahardjo, H. & Leong, E. C. (2008a), 'Measurement of geotextilewater charactergeotextiles using capillary rise principle', *Geosynthetics International* **15**(2), 86–94.
- Krisdani, H., Rahardjo, H. & Leong, E.-C. (2008b), 'Measurement of geotextilewater characteristic curve using capillary rise principle', *Geosynthetics International* **15**(2), 86–94.

- Kulkarni, R. U. (2008), A potential technique to determine the unsaturated soil shear strength parameter, Master's thesis, Texas A&M University.
- Kutter, B. L., Abghari, A. & Cheney, J. A. (1988), 'Strength parameters for bearing capacity of sand', *Journal of Geotechnical Engineering* **114**(4), 491–498.
- Lafleur, J., Lebeau, M., Faure, Y. H., Savard, Y. & Y., K. (2000), Influence of matric suction on the drainage performance of polyester geotextiles, *in* 'In Proceedings 53rd Annual Conference of the Canadian Geotechnical Society', pp. 1115–1122.
- Lambe, T. W. & Whitman, R. V. (1969), *Soil Mechanics*, John Wiley and Sons,.
- Lamborn, M. J. (1986), A micromechanical approach to modelling partly saturated soils, Master's thesis, Texas A&M University.
- Lancelot, L., Shahrour, I. & Al Mahmoud, M. (2006), 'Failure and dilatancy properties of sand at relatively low stresses', *Journal of engineering mechanics* **132**(12), 1396–1399.
- Lang, A. R. G. (1967), 'Osmotic coefficients and water potentials of sodium chloride solutions from 0 to 40°C', *Australian Journal of Chemistry - AUST J CHEM* **20**(9), 2017–2023.
- Lee, H. & Wray, W. (1995), Techniques to evaluate soil suction - a vital unsaturated soil water variable, *in* 'Proceedings of First International conference on Unsaturated Soils', number 2, pp. 612–622.
- Lee, I. M., Sung, S. G. & Cho, G. C. (2005), 'Effect of stress state on the unsaturated shear strength of weathered granite', *Canadian Geotechnical Journal*, **42**, 624–631.
- Lee, K. L. & Seed, H. B. (1967), 'Drained strength characteristics of sands', *Journal of Soil Mechanics, ASCE* **93**(6), 117–141.
- Lee, S. J., Lee, S. R. & Kim, Y. S. (2003), 'An approach to estimate unsaturated shear strength using artificial neural network and hyperbolic formulation.', *Computer and Geotechnics* **30**, 489–503.
- Lehmann, P., Staufferb, F., Hinz, C., Dury, O. & Flühler, H. (1998), 'Effect of hysteresis on water flow in a sand column with a fluctuating capillary fringe', *Journal of Contaminant Hydrology* **33**, 81–100.
- Leong, E. C. & Rahardjo, H. (1997), 'Review of soil-water characteristic curve equations', *Journal of Geotechnical and Geoenvironmental Engineering* **123**(12), 1066–1117.

- Leong, E.-C., Tripathy, S. & Rahardjo, H. (2003), 'Total suction measurement of unsaturated soils with a device using the chilled-mirror dew-point technique', *Géotechnique* **53**(2), 173–182.
- Likos, W. J. & Lu, N. (2003), 'Automated humidity system for measuring total suction characteristics of clay', *Geotechnical Testing Journal* **26**(2), 1–12.
- Lima, M. J., Azevedo, M. M., Zornberg, J. G. & Palmeira, E. M. (2016), 'Capillary barriers incorporating non-woven geotextiles', *Environmental Geotechnics* **5**(3), 1–34.
- Lins, Y. (2009), Hydro-mechanical properties of partial saturated sand, PhD thesis, Chair of foundation engineering, soil and rock mechanics, Ruhr-Universität Bochum.
- Lins, Y., Agus, S. S., Tripathy, S. & Schanz, T. (2002), Determination of unsaturated coefficient of permeability for sand, in 'in T. Schanz, ed., "4. Workshop Weimar - Teilgesättigte Böden', Bauhaus-Universität Weimar', pp. 93–99.
- Lins, Y. & Schanz, T. (2005), Determination of hydro-mechanical properties of sand, in T. Schanz, ed., 'Proc. Int. Conf. From Experimental Evidence towards Numerical Modeling of Unsaturated Soils', Vol. 1, Berlin: Springer, Weimar, Germany, pp. 15–32.
- Lloret, A., Villar, M., Sánchez, M., Gens, A., Pintado, X. & Alonso, E. (2003), 'Mechanical behaviour of heavily compacted bentonite under high suction changes', *Géotechnique* **53**(1), 27–40.
- Lorentz, S. A., Durnford, D. S. & Corey, A. (1993), Liquid retention measurement on porous media using a controlled outflow cell, in 'Proceedings of American Society of Agronomy-Crop Science Society of America-Soil Science Society of America 1991 Annual meeting, Denver, Colorado, USA'.
- Lowell, S. & Shields, J. (1984), *Powder Surface Area and Porosity*, Chapman and Hall, New York.
- Lu, N. & Godt, J. (2008), 'Infinite slope stability under steady unsaturated seepage conditions', *Water Resources Research* **44**(11, W11404), 1–13.
- Lu, N., Godt, J. W. & Wu, D. (2010), 'A closed form equation for effective stress in unsaturated soil', *Water Resources Research* **46**(5), W05515.
- Lu, N. & Likos, W. J. (2004), *Unsaturated Soil Mechanics*, Wiley.

- Lu, N. & Likos, W. J. (2006), 'Suction stress characteristic curve for unsaturated soil', *J. Geotech. Geoenviron. Eng.* **132**(2), 131–142.
- Lytton, R. (1995), Keynote address: Foundations and pavements on unsaturated soils, *in* 'Proceedings of the First International Conference on Unsaturated Soils (UNSAT 95)'.
- Marshall, T. J., Holmes, J. W. & Rose, C., W. (1996), *Soil Physics*, Cambridge, UK.
- Matile, L., Berger, R., Wächter, D. & Krebs, R. (2013), 'Characterization of a new heat dissipation matric potential sensor', *Sensors 2013* **13**, 1137–1145.
- Mbonimpa, M., Aubertin, M., Dagenais, A. M., Bussi'ere, B., Julien, M. & Kissiova, M. (2002), Interpretation of field tests to determine the oxygen diffusion and reaction rate coefficients of tailings and soil covers, *in* 'in Proceedings of the 55th Canadian Geotechnical and Joint IAH-CNC and CGS Groundwater Speciality Conferences, Niagara Falls', pp. 147–154.
- McCartney, J. S., Villar, L. F. S. & Zornberg, J. G. (2005), Geosynthetic drainage layers in contact with unsaturated soils, *in* '16th ISSMGE Conference: Geotechnical Engineering in Harmony with the Global Environment. 12-16 September 2005. Osaka, Japan.'
- McCartney, J. S., Villar, L. F. S. & Zornberg, J. G. (2008a), Capillary rise in unsaturated nonwoven geotextiles, *in* 'Proceedings of the First Pan American Geosynthetics Conference and Exhibition-GeoAmericas. 2-5 March 2008, Cancun, Mexico', Vol. CD Rom Publication, Cancun, Mexico.
- McCartney, J. S., Villar, L. F. S. & Zornberg, J. G. (2008b), Nonwoven geotextiles as hydraulic barriers for capillary flow, *in* 'The First Pan American Geosynthetics Conference & Exhibition'.
- McCartney, J. S. & Znidarcic, D. (2010), 'Testing system hydraulic properties of unsaturated nonwoven geotextiles', *Geosynthetics International* **17**(5), 355–363.
- McCartney, J. S. & Zornberg, J. G. (2010), 'Effects of infiltration and evaporation on geosynthetic capillary barrier performance', *canadian Geotechnical Journal* **47**, 1201–1213.
- McGown, A., Andrawes, K. Z. & Kabir, M. H. (1982), Load-extension testing of geotextile confined soil, *in* 'Proceedings of the Second International Conference on Geotextiles , IFAI, Vol. 2, Las Vegas, Nevada, USA, August 1982,' pp. 793–797.

- Miao, L., Liu, S. & Lai, Y. (2002), 'water characteristics and shear strength features of nanyang expansive soil', *Engineering Geology* **65**(4), 261–267.
- Miller, B. (1977), 'Surface characterization of fibres and textiles', *Part II*, eds Schick, MJ, Marcel Dekker, NY p. p. 47.
- Miszkowska, A., Lenart, S. & Koda, E. (2017), 'Changes of permeability of nonwoven geotextiles due to clogging and cyclic water flow in laboratory conditions', *Water* **9**(9), 660.
- Mitchell, J. K. (1993), *Fundamentals of Soil Behavior*, 2nd edition edn, John Wiley and Sons.
- Mohr, O. (1900), 'Welche umstände bedingen die elastizitätsgrenze und den bruch eines materials', *Zeitschrift des Vereines deutscher Ingenieure* **44**, 1–12.
- Mokni, M. (1992), Relations entre deformations en masse et deformations localisees dans les materiaux granulaires, PhD thesis, University of Grenoble, France.
- Mokni, M. & Desrue, J. (1999), 'Strain localisation measurements in undrained plane-strain biaxial tests on hostun rf sand', *Mechanics of cohesive-frictional materials* **4**, 419–441.
- Mokni, M. & Desrues, J. (1998), 'Strain localization measurements in undrained plane-strain biaxial tests on hostun rf sand', *Mech. Cohes.-Frict. Mater.* **4**, 419–441.
- Morris, C. (2000), Unsaturated flow in nonwoven geotextiles, in 'GeoEng', Melbourne, Australia.
- Morris, K. A. & Shepperd, C. M. (1982), 'The role of clay minerals in influencing porosity and permeability characteristics in the bridport sands of wytch farm', *Dorset: Clay Minerals* **17**(1), 41–54.
- Mualem, Y. (1986), Hydraulic conductivity of unsaturated soils: prediction and formulas, in 'in A. Klute, ed., 'Methods of Soil Analysis. Part 1: Physical and Mineralogical Methods', American Society of Agronomy (ASA) and Soil Science Society of America (SSSA), Madison, WI, U.S.A.', pp. 799–823.
- Murray, E. J., a. S. V. (2010), *Unsaturated Soils: A fundamental interpretation of soil behaviour*, Wiley-Blackwell.

- Nahlawi, H., Bouazza, A. & Kodikara, J. (2007a), 'Characterisation of geotextiles water retention using a modified capillary pressure cell', *Geotextiles and Geomembranes* **25**, 186–193.
- Nahlawi, H., Bouazza, A. & Kodikara, J. (2007b), Surface water infiltration in a 1-dimensional soil-geotextile column, *in* B. T. J. Ameratunga & M. Patten, eds, 'Proceedings of the 10th Australia New Zealand Conference on Geo- mechanics', Vol. 1, Brisbane, pp. 368–373.
- Nahlawi, H., Bouazza, A. & Kodikara, J. (2008), Capillary rise in unsaturated nonwoven geotextile, *in* 'Proceedings of the First Pan American Gosynthetics Conference and Exhibition-GeoAmericas. 2-5 March 2008, Cancun, Mexico', pp. 281–289.
- Nam, S., Gutierrez, M., Diplas, P. & Petrie, J. (2011), 'Determination of the shear strength of unsaturated soils using the multistage direct shear test', *Engineering Geology* **122**, 272–280.
- Narasimhan, T. N. (2005), 'Buckingham, 1907: an appreciation.', *Vadose Zone J* **4**, 434–441.
- Neasham, J. W. (1977), The morphology of dispersed clay in sandstone reservoirs and its effect on sandstone shallness, pore space and fluid flow properties., *in* 'Paper SPE 6858, presented at the SPE Annual Technical Conference and Exhibition, Denver, October 912,', Vol. SPE 6858, pp. , 7 pp.
- Nelson, J. & Miller, D. (1992), *Expansive Soils, Problems and Practice in Foundation and Pavement Engineerin*, John Wiley and Sons Inc., New York.
- Nemes, A., Schaap, M., Leij, F. & Wösten, J. (2018), *UNSODA 2.0: Unsaturated Soil Hydraulic Database. Database and program for indirect methods of estimating unsaturated hydraulic properties*, US Salinity Laboratory - ARS - USDA.
- Ng, C. W. W. & Chen, R. (2008), Recompacted, natural and in-situ properties of unsaturated decomposed geomaterials, *in* Huang & Mayne, eds, 'Geotechnical and Geophysical Site Characterization', Taylor & Francis Group, London,.
- Nguyen-Tuan, L. (2014), Coupled Thermo-Hydro-Mechanical Analysis: Experiment and Back Analysis, PhD thesis, Chair of foundation engineering, soil and rock mechanics, Ruhr-Universität Bochum, 49.

- Nishimura, T., Toyota, H., Oh, W. T. & Vanapalli, S. (2007), Evaluation of shear strength parameters of an unsaturated non-plastic silty soil, *in* '60th Canadian Geotechnical Conference, Ottawa 2007,' pp. 1029–1036.
- Oda, M. & Iwashita, K. (1999), *Mechanics of granular materials: an introduction*, Balkema.
- Palmeira, E. M. & Gardoni, M. G. (2000), 'The influence of partial clogging and pressure on the behavior of geotextiles in drainage systems', *Geosynthetics International* **7**, 403–431.
- Park, K. D. & Fleming, I. R. (2006), 'Evaluation of a geosynthetic capillary barrier', *Geotextiles and Geomembranes* **24**, 64–71.
- Peterson, R. F. W. (1988), Interpretation of triaxial compression test results on partially saturated soils. in advanced triaxial, *in* 'In Advanced triaxial testing of soil and rock. American Society for Testing and Materials, Philadelphia, ASTM STP 977,' pp. 512–538.
- Ping, H., MaoSong, H. & DengGao, W. (2014), 'The critical state constitutive model and strain localization for hostun sand', *Applied Mechanics and Materials* **525**, 552–555.
- Pitzer, K. S. & Pelper, J. C. (1984), 'Thermodynamic properties of aqueous sodium chloride solutions', *Journal Phys. Chem. Reference data* **13**(1), 1–102.
- Punmia, B. C. & Jain, A. K. (2005), *Soil Mechanics and Foundations*.
- Purwana, Y. M. & Nikraz, H. (2013), 'The correlation between the cbr and shear strength in unsaturated soil conditions', *International Journal of Transportation Engineering* **1**(3), 211–222.
- Pusch, R. & Yong, R. (2003), 'Water saturation and retention of hydrophilic clay buffer-microstructural aspects', *Applied Clay Science, Elsevier* **23**, 61–68.
- Rassam, D. (2002), 'Variation of evaporative and shear strength parameters along a tailings delta', *Canadian Geotechnical Journal* **39**(1), 32–45.
- Rassam, D. W. & Williams, D. J. (1999), 'A relationship describing the shear strength of unsaturated soils', *Canadian Geotechnical Journal* **36**, 363–368.
- Röchter, L. (2011), Systeme paralleler Scherbänder unter Extension im ebenen Verformungszustand, PhD thesis, Ruhr-Universität Bochum Schriftenreihe Grundbau, Boden- und Felsmechanik Heft 45.
- Reynolds, O. (1885), 'On the dilatancy of media composed of rigid particles in contact, with experimental illustrations.', *Philosophical Magazine. Series 5* **20**(17), 469–481.

- Richards, L. A. (1931), 'Capillary conduction of liquids through porous medium', *J Phy* **1**, 318–333.
- Richards, L. A. (1966), 'A soil salinity sensor of improved design.', *Soil Sci. Soc. Amer. Proc.* **30**, 333–337.
- Richardson, G. (1997), 'Fundamental mistakes in slope design', *Geotechnical Fabrics Report* **15**(2), 15–17.
- Richardson, G. N. & Zhao, A. (2009), Geosynthetic fundamentals in landfill design, in 'Advances in Environmental Geotechnics, Proc. of Int. Symp. on Geoenvironmental Eng. in Hangzhou, China', pp. 275–285.
- Ridley, A. & Wray, W. (1996), Suction measurement: a review of current theory and practices, in A. Tarantino, E. Romero & Y.-J. Cui, eds, 'Proceedings of First International conference on Unsaturated Soils', Vol. 3, pp. 1293–1322.
- Rohm, S. A. & Vilar, O. M. (1995), Shear strength of an unsaturated sandy soil., in 'Unsaturated Soils, ed. Alonso and Delage., Proc. 1st Int. Conf on Unsaturated Soils, Paris, Balkema', Vol. 1, pp. 189–193.
- Rowe, P. W. (1962), 'The stress-dilatancy relation for static equilibrium of an assembly of particles in contact', *Proceedings of the Royal Society of London. Series A, Mathematical and Physical Sciences* **269**(1339), 500–527.
- Rowe, R. K. (1998), Geosynthetics and the minimization of contaminant migration through barrier systems beneath solid waste, in 'Keynote lecture, 6th International Conference on Geosynthetics, 25-29 March, Atlanta, GA.'.
- Rowe, R., K., ed. (2000), *Geotechnical and Geoenvironmental Engineering Handbook*, Springer Science+Business Media, LLC.
- Rushbrook, P. & Pugh, M. (1999), *Solid Waste Landfills in Middle- and Lower Income Countries*, the World Bank Washington, D.C.
- Rutledge, P. (1947), *Review of the cooperative triaxial research program of the War Department, Corps of Engineers (Covering the period Feb. 1940 to May 1944), The Technological Institute, North-Western University, 1944. In: Soil Mechanics Fact Finding Survey, Progress Report: Triaxial Shear Research and Pressure Distribution Studies on Soils, pp 147-178. U.S. Waterw. Exper. Stn, Vicksburg, Miss.*

- Satiya, B. S. (1978), Shear Behavior of Partly Saturated Soils, PhD thesis, Indian Inst. of Technology, Dlihi, India.
- Sawangsurriya, A. (2006), Stiffness-suction-moisture relationship for compacted soils, PhD thesis, The University of Wisconsin-Madison, Madison, Wis.
- Schanz, T. (1998), *Zur Modellierung des mechanischen Verhaltens von Reibungsmaterialien*, Vol. 45, Institut fuer Geotechnik Universität Stuttgart.
- Schanz, T., Agus, S. S. & Tscheschlok, G. (2004), Determination of hydro-mechanical properties of trisoplast, Research Report Bo-015/03, Laboratory of Soil Mechanics, Bauhaus-University Weimar, Weimar, Germany.
- Schanz, T. & Vermeer, P. A. (1996), 'Angles of friction and dilatancy of sand', *Geotechnique* **46**(1), 145–151.
- Scheidegger, A. (1974), *The Physics of Flow Through Porous Media*.
- Schick, P. (2004), 'Scherfestigkeit durch kapillarität in unzementierten ungesättigten bindigen böden', *Bautechnik* **81**(1), 31–37.
- Shahrour, I. & Rezaie, F. (1997), 'An elasto-plastic constitutive relation for the soil-structure interface under cyclic loading', *Computers and Geotechnics* **21**, 21–39.
- Shen, Z. J. (1996), 'Retrospect and prospect of unsaturated soil mechanics', *Advances in Science and Technology of Water Resources* **161**, 1–5.
- Sherard, J. L., D. L. P. & Talbot, J. R. (1984), 'Basic properties of sand and gravel filters', *Journal of Geotechnical Engineering, ASC* **110**(6), 684–700.
- Shimada, K. (1998), 'Effect of matric suction on shear characteristics of unsaturated fraser river sand', *Journal of the Faculty of Environmental Science and Technology* **3**(1), 127–134.
- Shukla, S. & Yin, J. (2006), *Fundamentals of Geosynthetic Engineering*, London: Taylor and Francis/Balkema.
- Siemens, G. & Bathurst, R. J. (2010), 'Numerical parametric investigation of infiltration in one-dimensional sandgeotextile columns', *Geotextiles and Geomembranes* **28**, 460–474.
- Sillers, W. S. (1996), The mathematical representation of the soil-water characteristic curve, Master's thesis, University of Saskatchewan.

- Sillers, W. S. & Fredlund, D. G. (2001), 'Statistical assessment of soil-water characteristic curve models for geotechnical engineering', *Canadian Geotechnical Journal* **38**, 1297–1313.
- Smith, G. N. (1990), *Elements of Soil Mechanics*, 6th edition, BSP Professional Books, Oxford.
- Song, Y.-S. (2014), 'Suction stress in unsaturated sand at different relative densities', *Engineering Geology* **176**, 1–10.
- Southworth, M. S. (1980), An experimental evaluation of the terzaghi criterion for protective filters, Master's thesis, MSc thesis, 1980, Massachusetts Institute of Technology.
- Sposito, G. (1981), *The thermodynamic of soil solution.*, Oxford Clarendon Press. London.
- Sridharan, A. (1968), Some studies on the strength of partly saturated clays, PhD thesis, PhD Thesis, Purdue University, Lafayette, Indiana.
- Sridharan, A. & Nagaraj, H. (1999), 'Absorption water content and liquid limit of soils', *Geotech. Test. J.* **22**(2), 127–133.
- Steinert, B., Melchior, S., Burger, K., Berger, K., T. M. & Miehlich, G. (1997), Design of capillary barriers for capping of landfills and contaminated sites, in H. August, U. Holzlöhner & T. Meggyes, eds, 'Advanced landfill liner systems', Thomas Telford.
- Stoicescu, J. T., Haug, M. D. & Fredlund, D. G. (1998), The soil water characteristics of sand-bentonite mixtures used for liners and covers, in 'Proceeding of the Second International Conference on. Unsaturated Soils. Beijing, China', Vol. 1, pp. 143–148.
- Stormont, J. C., Henry, K. S. & Evans, T. M. (1997), 'Water retention functions of four nonwoven polypropylene geotextiles', *Geosynthetics International* **4** (6)(6), 661–672.
- Stormont, J. C. & Morris, C. E. (2000), Characterization of unsaturated nonwoven geotextiles, in 'Advances in unsaturated geotechnics', Vol. 99, ASCE Geotechnical Special Publication, pp. 153–164.
- Stormont, J. C. & Ramos, R. (2004), 'Characterization of a fiberglass geotextile for unsaturated in-plane water transport', *Geotechnical Testing Journal, ASTM* **27**(2), 1–17.

- Sun, S. & Xu, H. (2007), Determining the shear strength of unsaturated silt, *in* T. Schanz, ed., 'Experimental Unsaturated Soil Mechanics, Springer Proceedings in Physics', Vol. 112, pp. 195–206.
- Tammemagi, H. (1999), *The Waste Crisis*, Oxford University Press,.
- Tamrakar, S. B., Mitachi, T. & Toyosawa, Y. (2007), 'Measurement of soil tensile strength and factors affecting its measurements', *Soils and Foundations* **47**(5), 911–918.
- Tan, S., Chew, S., Ng, C., Loh, S., Karunaratne, G., Delmas, P. & Loke, K. (2001), 'Largescale drainage behavior of composite geotextile and geogrid in residual soil', *Geotextiles and Geomembranes* **19**(3), 163–176.
- Tarantino, A., Ridley, A., M. & Toll, D. G. (2008), 'Field measurement of suction, water content, and water permeability', *Geotechnical and Geological Engineering* **26**(5), 751–782.
- Tatsuoka, F., Goto, S., Tanaka, T., Tani, K. & Kimura, Y. (1997), Particle size effects on bearing capacity of footings on granular material., *in* 'saoka, Adachi and Oka, Editors, Deformation and Progressive Failure in Geomechnics, Pergamon, Nagoya (Japan)'.
- Tekinsoy, M. A., Kayadelan, C., Keskin, M. S. & Soylemaz, M. (2004), 'An equation for predicting shear strength envelope with respect to matric suction', *Computers and Geotechnical* **31**(7), 589–593.
- Terzaghi, K. (1943), *Theoretical Soil Mechanics*, J. Wiley and Sons, inc.
- Thevanayagam, S. (1998), 'Effect of fines and confining stress on undrained shear strength of silty sands', *Journal of Geotechnical and Geoenvironmental Engineering* **124**(6), 479–491.
- Thomson, W. T. (1871), 'On the equilibrium of vapour at a curved surface of liquid', *Philosophical Magazine Series 4* **42**(282), 448–452.
- Toker, N. (2007), Modeling the relation between suction, effective stress and shear strength in partially saturated granular media, PhD thesis, Massachusetts Institute of Technology, USA.
- Toker, N. K. (2002), Improvements and reliability of mit tensiometers and studies on soil moisture characteristic curves, Master's thesis, Massachusetts Institute of Technology, USA.

- Toker, N. K., Germaine, J. T., Sjoblom, K. J. & Culligan, P. J. (2004), 'A new technique for rapid measurement of continuous smc curves', *Geotechnique* **54**(3), 179–186.
- Toll, D. G. (1990), 'A framework for unsaturated soil behaviour', *Géotechnique* **40**(1), 31–44.
- USACE (1953), 'Investigation of filter requirements for undrains', *Tech. Memo., Waterways Experiment Station, Vicksburg* (3-360).
- van Genuchten, M. T. (1980), 'A closed-form equation for predicting the hydraulic conductivity of unsaturated soils', *Soil Science Society of America Journal* **44**, 892–898.
- Vanapalli, S. & Fredlund, D. (2000), Comparison of different procedures to predict unsaturated soil shear strength, *in* 'Advances in Unsaturated Geotechnics', pp. 195–209.
- Vanapalli, S. K., F. D. G. P. D. E. (1996a), 'The relationship between the soil-water characteristic curve and the shear strength of a compacted glacial till', *Geotechnical Testing Journal* **19**(3), 259–268.
- Vanapalli, S. K., F. D. G. P. D. E. C. A. W. (1996b), 'Model for the prediction of shear strength with respect to soil suction', *Canadian Geotechnical Journal* **33**(3), 379–392.
- Vanapalli, S. K. & Lane, J. (2002), A simple technique for determining the shear strength of unsaturated soils using the conventional direct shear apparatus, *in* 'Proceedings of the Second Canadian Specialty Conference on Computer Applications in Geotechnique, April, 2002, Winnipeg', pp. 245–253.
- Vanapalli, S. K., N. M. V. S. R. S. (2008), 'Axis translation and negative water column techniques for suction control', *Geotechnical and Geological Engineering* **26**(6), 645–660.
- Vaunat, J., Romero, E., Marchi, C. & Jommi, C. (2002), Modeling the shear strength of unsaturated soils, *in* C. Mancuso & A. Tarantino, eds, '3rd Intern. Conf. on Unsaturated Soils', Vol. 2, pp. 245–251.
- Vilar, O. M. (2006), 'A simplified procedure to estimate the shear strength envelope of unsaturated soil', *Canadian Geotechnical Journal* **43**, 1088–1095.
- Villar, M. V., Martin, P. L., Gomes.Espina, R. & Ll (2011), Effect of suction and plasticity on the shear strength of sand/silt mixtures, *in* 'Unsaturated Soils, Edited by Antonio Gens, CRC Press', pp. 391–396.

- Wan, R. G. & Guo, P. J. (2004), 'Stress dilatancy and fabric dependencies on sand behavior', *Journal of Engineering Mechanics* **130**(6), 635–645.
- Wheeler, S. J. & Kumar, S. (1992), Development and application of a critical state model for unsaturated soil, *in* 'Proceedings, Wroth Memorial Symposium on Predictive Soil Mechanics, Oxford'.
- White, N. F., Duke, H. R., Sunada, D. K. & T., C. A. (1970), 'Physics of desaturation in porous materials', *Journal of the Irrigation and Drainage Division* **96**(2), 165–191.
- Wilson, G. (1902), Some experiments on conjugate pressures in fine sand, *in* 'Min. Proc. Inst. Civ. Eng.', pp. 208–222.
- Wilson, M. D. & Pittman, E. D. (1977), 'Authigenic clays in sandstones: recognition and influence on reservoir properties and paleoenvironmental analysis.', *J. Sedim. Petrol.* **47**, 3–31.
- Xu, Y. F. (2004), 'Fractal approach to unsaturated shear strength', *J Geotech Geoenviron Eng* **130**(3), 264–273.
- Xu, Y. & Sun, A. (2001), 'Determination of expansive soil strength using a fractal model', *Fractals* **9**(1), 51–60.
- Yang, H., Rahardjo, H., Leong, E. & Fredlund, D. G. (2004), 'Factors affecting drying and wetting soil-water characteristic curves of sandy soils', *Canadian Geotechnical Journal* **41**, 908–922.
- Yu, H.-S. (2000), *Cavity Expansion Methods in Geomechanics*, Springer Netherlands,.
- Zhan, T. & Ng, C. (2006), 'Shear strength characteristics of an unsaturated expansive clay', *Canadian Geotechnical Journal* **43**(7), 751–763.
- Zornberg, J. G., Bouazza, A. & McCartney, J. S. (2010), 'Geosynthetic capillary barriers: current state of knowledge', *Geosynthetics International* **17**(5), 273–300.
- Zornberg, J. G. & Christopher, B. R. (2007), Chapter 37: Geosynthetics., *in* J. W. Delleur, ed., 'The Handbook of Groundwater Engineering, 2nd edition', CRC Press, Taylor & Francis Group, Boca Raton, FL.
- Zornberg, J. G. & McCartney, J. S. (2003), Analysis of monitoring data from the evapotranspirative test covers at the rocky mountain arsenal geotechnical research report, *in* 'US Environmental Protection Agency, Region 8,' p. 227.

Schriftenreihe des Lehrstuhls für Grundbau, Boden- und Felsmechanik der
Ruhr-Universität Bochum

Herausgeber: H.L. Jessberger

- 1 (1979) **Hans Ludwig Jessberger**
Grundbau und Bodenmechanik an der Ruhr-Universität Bochum
- 2 (1978) **Joachim Klein**
Nichtlineares Kriechen von künstlich gefrorenem Emschermergel
- 3 (1979) **Heinz-Joachim Gödecke**
Die Dynamische Intensivverdichtung wenig wasserdurchlässiger Böden
- 4 (1979) **Poul V. Lade**
Three Dimensional Stress-Strain Behaviour and Modeling of Soils
- 5 (1979) **Roland Pusch**
Creep of soils
- 6 (1979) **Norbert Diekmann**
Zeitabhängiges, nichtlineares Spannungs-Verformungsverhalten von gefrorenem Schluff
unter triaxialer Belastung
- 7 (1979) **Rudolf Dörr**
Zeitabhängiges Setzungsverhalten von Gründungen in Schnee, Firn und Eis
der Antarktis am Beispiel der deutschen Georg-von-Neumayer- und Filchner-Station
- 8 (1984) **Ulrich Güttler**
Beurteilung des Steifigkeits- und Nachverdichtungsverhaltens von
ungebundenen Mineralstoffen
- 9 (1986) **Peter Jordan**
Einfluss der Belastungsfrequenz und der partiellen Entwässerungs-
möglichkeiten auf die Verflüssigung von Feinsand
- 10 (1986) **Eugen Makowski**
Modellierung der künstlichen Bodenvereisung im grundwasserdurchströmten
Untergrund mit der Methode der finiten Elemente
- 11 (1986) **Reinhard A. Beine**
Verdichtungswirkung der Fallmasse auf Lastausbreitung in nichtbindigem
Boden bei der Dynamischen Intensivverdichtung
- 12 (1986) **Wolfgang Ebel**
Einfluss des Spannungspfades auf das Spannungs-Verformungsverhalten
von gefrorenem Schluff im Hinblick auf die Berechnung von Gefrierschächten
- 13 (1987) **Uwe Stoffers**
Berechnungen und Zentrifugen-Modellversuche zur Verformungsabhängigkeit
der Ausbaubeanspruchung von Tunnelausbauten in Lockergestein
- 14 (1988) **Gerhard Thiel**
Steifigkeit und Dämpfung von wassergesättigtem Feinsand unter Erdbebenbelastung

- 15 (1991) **Mahmud Thaher**
Tragverhalten von Pfahl-Platten-Gründungen im bindigen Baugrund,
Berechnungsmodelle und Zentrifugen-Modellversuche
- 16 (1992) **Rainer Scherbeck**
Geotechnisches Verhalten mineralischer Deponieabdichtungsschichten
bei ungleichförmiger Verformungswirkung
- 17 (1992) **Martin M. Bizialiele**
Torsional Cyclic Loading Response of a Single Pile in Sand
- 18 (1993) **Michael Kotthaus**
Zum Tragverhalten von horizontal belasteten Pfahlreihen aus langen Pfählen in Sand
- 19 (1993) **Ulrich Mann**
Stofftransport durch mineralische Deponieabdichtungen:
Versuchsmethodik und Berechnungsverfahren
- 20 (1992) **Festschrift anlässlich des 60. Geburtstages von
Prof. Dr.-Ing. H. L. Jessberger**
20 Jahre Grundbau und Bodenmechanik an der Ruhr-Universität Bochum
- 21 (1993) **Stephan Demmert**
Analyse des Emissionsverhaltens einer Kombinationsabdichtung im Rahmen der
Risikobetrachtung von Abfalldeponien
- 22 (1994) **Diethard König**
Beanspruchung von Tunnel- und Schachtausbauten in kohäsionslosem Lockergestein
unter Berücksichtigung der Verformung im Boden
- 23 (1995) **Thomas Neteler**
Bewertungsmodell für die nutzungsbezogene Auswahl von Verfahren zur Altlastensanierung
- 24 (1995) **Ralph Kockel**
Scherfestigkeit von Mischabfall im Hinblick auf die Standsicherheit von Deponien
- 25 (1996) **Jan Laue**
Zur Setzung von Flachfundamenten auf Sand unter wiederholten Lastereignissen
- 26 (1996) **Gunnar Heibroek**
Zur Rissbildung durch Austrocknung in mineralischen Abdichtungsschichten
an der Basis von Deponien
- 27 (1996) **Thomas Siemer**
Zentrifugen-Modellversuche zur dynamischen Wechselwirkung zwischen Bauwerken
und Baugrund infolge stoßartiger Belastung
- 28 (1996) **Viswanadham V. S. Bhamidipati**
Geosynthetic Reinforced Mineral Sealing Layers of Landfills
- 29 (1997) **Frank Trappmann**
Abschätzung von technischem Risiko und Energiebedarf bei Sanierungsmaßnahmen
für Altlasten
- 30 (1997) **André Schürmann**
Zum Erddruck auf unverankerte flexible Verbauwände
- 31 (1997) **Jessberger, H. L. (Herausgeber)**
Environment Geotechnics, Report of ISSMGE Technical Committee TC 5
on Environmental Geotechnics

Herausgeber: Th. Triantafyllidis

- 32 (2000) **Triantafyllidis, Th. (Herausgeber)**
Boden unter fast zyklischer Belastung: Erfahrung und Forschungsergebnisse (Workshop)
- 33 (2002) **Christof Gehle**
Bruch- und Scherverhalten von Gesteinstrennflächen mit dazwischenliegenden Materialbrücken
- 34 (2003) **Andrzej Niemunis**
Extended hypoplastic models for soils
- 35 (2004) **Christiane Hof**
Über das Verpressankertragverhalten unter kalklösendem Kohlensäureangriff
- 36 (2004) **René Schäfer**
Einfluss der Herstellungsmethode auf das Verformungsverhalten von Schlitzwänden in weichen bindigen Böden
- 37 (2005) **Henning Wolf**
Zur Scherfugenbänderung granularer Materialien unter Extensionsbeanspruchung
- 38 (2005) **Torsten Wichtmann**
Explicit accumulation model for non-cohesive soils under cyclic loading
- 39 (2008) **Christoph M. Loreck**
Die Entwicklung des Frischbetondruckes bei der Herstellung von Schlitzwänden
- 40 (2008) **Igor Arsic**
Über die Bettung von Rohrleitungen in Flüssigböden
- 41 (2009) **Anna Arwanitaki**
Über das Kontaktverhalten zwischen einer Zweiphasenschlitzwand und nichtbindigen Böden

Herausgeber: T. Schanz

- 42 (2009) **Yvonne Lins**
Hydro-Mechanical Properties of Partially Saturated Sand
- 43 (2010) **Tom Schanz (Herausgeber)**
Geotechnische Herausforderungen beim Umbau des Emscher-Systems
Beiträge zum RuhrGeo Tag 2010
- 44 (2010) **Jamal Alabdullah**
Testing Unsaturated Soil for Plane Strain Conditions: A New Double-Wall Biaxial Device
- 45 (2011) **Lars Röchter**
Systeme paralleler Scherbänder unter Extension im ebenen Verformungszustand
- 46 (2011) **Yasir Al-Badran**
Volumetric Yielding Behavior of Unsaturated Fine-Grained Soils
- 47 (2011) **Usque ad finem**
Selected research papers
- 48 (2012) **Muhammad Ibrar Khan**
Hydraulic Conductivity of Moderate and Highly Dense Expansive Clays
- 49 (2014) **Long Nguyen-Tuan**
Coupled Thermo-Hydro-Mechanical Analysis: Experimental and Back Analysis
- 50 (2014) **Tom Schanz (Herausgeber)**
Ende des Steinkohlenbergbaus im Ruhrrevier: Realität und Perspektiven für die
Geotechnik Beiträge zum RuhrGeo Tag 2014
- 51 (2014) **Usque ad finem**
Selected research papers
- 52 (2014) **Houman Soleimani Fard**
Study on the Hydro-Mechanical Behaviour of Fiber Reinforced Fine Grained Soils
with Application to the Preservation of Historical Monuments
- 53 (2014) **Wiebke Baille**
Hydro-Mechanical Behavior of Clays - Significance of Mineralogy
- 54 (2014) **Qasim Abdulkarem Jassim Al-Obaidi**
Hydro-Mechanical Behavior of Collapsible Soils
- 55 (2015) **Veselin Zarev**
Model Identification for the Adaption of Numerical Simulation Models - Application
to Mechanized Shield Tunneling
- 56 (2015) **Meisam Goudarzy**
Micro and Macro Mechanical Assessment of Small and Intermediate Strain Properties
of Granular Material
- 57 (2016) **Oliver Detert**
Analyse einer selbstregulierenden interaktiven Membrangründung für Schüttkörper
auf geringtragfähigen Böden
- 58 (2016) **Yang Yang**
Analyses of Heat Transfer and Temperature-induced Behaviour in Geotechnics

- 59 (2016) **Alborz Pourzargar**
Application of suction stress concept to partially saturated compacted soils
- 60 (2017) **Hanna Haase**
Multiscale analysis of clay-polymer composites for Geoenvironmental applications
- 61 (2017) **Kavan Khaledi**
Constitutive modeling of rock salt with application to energy storage caverns
- 62 (2017) **Nina Silvia Müthing**
On the consolidation behavior of fine-grained soils under cyclic loading
- 63 (2017) **Elham Mahmoudi**
Probabilistic analysis of a rock salt cavern with application to energy storage systems
- 64 (2017) **Negar Rahemi**
Evaluation of liquefaction behavior of sandy soils using critical state soil mechanics and instability concept
- 65 (2018) **Chenyang Zhao**
A contribution to modeling of mechanized tunnel excavation
- 66 (2018) **Tom Schanz (Herausgeber)**
Innovationen im Spezialtiefbau und in der Umweltgeotechnik für die Geotechnik Beiträge zum RuhrGeo Tag 2018
- 67 (2019) **Lin Zhi Lang**
Hydro-mechanical behaviour of bentonite-based materials used for disposal of radioactive wastes
- 68 (2019) **Usama Al-Anbaki**
Hydraulic Interaction of Soil and Nonwoven Geotextiles under Unsaturated Conditions

Usama Al-Anbaki

Personal information

Name Al-Anbaki, Usama
Date of Birth 17.04.1980
Email-address usama.al-anbaki@rub.de

Education

- 11.2019 Doctorate: Ruhr-Universität Bochum, Germany.
○ Thesis title: Hydraulic Interaction of Soil and Nonwoven Geotextiles under Unsaturated Condition.
○ Supervisor: Prof. Dr.-Ing. Tom Schanz.
- 06.2006 Master of Science: University of Baghdad (Iraq) (Mark: 74.25%).
○ Title: Three-Dimensional Analysis of Single Pile in Clay by the FEM.
○ Supervisor: Prof. Dr. Omar Al-Farouq Al-Damluji.
- 10.2002 Bachelor of Science: University of Baghdad (Iraq), Civil Engineering (Mark 64.825%, Ranking: 35/125).

Further education

- 4.2015–10.2015 Ruhr-Universität Bochum, Germany
○ Teaching Assistant, Course Title: Problematic soils
- 3.2014-5.2014 Oklahoma University OU, USA
○ Visiting the chair of Prof. -Dr. Gerald Miller

Honors and Awards

1. Scholarship: German Academic Exchange Service (DAAD)
2. Best 10 selected papers for young researchers at 10th International Conference on Geosynthetics

Publications

1. al-Damluji, O.F. and Al-Anbaki, U.S., 2010, Three Dimensional Analysis of Single Pile in Cam-Clay By The Finite Element Method, Al-Handassa, Engineering Journal, College of Engineering, University of Baghdad, Volume 16, No 3, Pp 5699-5723, September 2010.
2. Al-Anbaki, U., König, D., and Schanz, T., Hydro-Mechanical Analysis of Geotextiles under Unsaturated Conditions. Poster, Research Day (2011) Research School - Ruhr-Universität Bochum, Deutschland.
3. Al-Anbaki, U., König, D., Schanz, T., 2012, Determination of water retention curves of a nonwoven polypropylene geotextile”, 2^eme Colloque International sur les Sols Non Saturés - et Environnement (UNSAT Alger 2012)
4. Al-Anbaki, U., König, D., Schanz, T., 2014, Drainage behavior of a cover system consisting of granular soil over nonwoven geotextile layer under unsaturated conditions, 10th International conference on geosynthetics, 21-25 September 2014 Berlin.